Using Electrophysiology to Explore Retinal Function in Autosomal Dominant Optic Atrophy

A thesis submitted to Cardiff University for the degree of
Doctor of Philosophy

By

Enyam Komla Amewuho Morny

School of Optometry and Vision Sciences
Cardiff University

October 2016

Supervisors
Marcela Votruba, Tom Margrain and Alison Binns

SUMMARY

Autosomal dominant optic atrophy (ADOA) is an inherited optic neuropathy due to mutation in the *OPA1* gene. Patients present with bilateral optic nerve head pallor and loss of visual function. Patients also show a reduction in the P50:N95 ratio of the pattern electroretinogram (PERG) and thinning of the retinal nerve fibre layer (RNFL) and macula.

In a mouse model of ADOA, previously generated in this laboratory, the defect first manifested as a dendritic pruning of RGCs, which appeared to be ON-centre specific. Electrophysiological evidence in both humans and the mutant mice showed a reduction in the photopic negative component (PhNR) of the brief flash electroretinogram (ERG). The separation of the photopic ERG into ON- and OFF-pathway components using long-duration monochromatic (red) flash on a rod suppressing blue background, provided an opportunity to assess ON- and OFF-RGC function in ADOA, which had not been previously investigated in humans. This study therefore aimed to assess the effect of ADOA on the red-on blue PhNR-ON and PhNR-OFF components to determine whether the PhNR-ON was a selective marker for ADOA.

In this thesis, a protocol was developed for recording long duration red-on-blue PhNRs from the macula (focal) and entire retina (full-field). A comparison of the retinotopic characteristics of the PhNRs (brief and long-duration) with the N95 of the PERG and the distribution of RGCs in the retina showed that the PhNR was capable of assessing RGC function. Retinal function was then probed in twelve participants with ADOA and sixteen controls using focal and full-field long duration ERG, full-field brief flash ERG and PERG. Retinal structure was also assessed using optical coherence tomography.

In conclusion, this thesis found that the PhNR-ON and PhNR-OFF amplitudes were equally affected with no evidence of a preferential ON-pathway loss.

ACKNOWLEDGEMENTS

Praise to the LORD, the Almighty, the God of all creation;
Who now as then reveals in man His Glory.

This PhD journey for me has been altogether exciting, not because it was smooth sailing, but because it was full of numerous twists and turns as well as high and low points. Its successful completion has been by the amazing and indispensable grace of God, and by the immeasurable support from so many people.

I am particularly grateful to my supervisors Marcela, Tom and Alison. They have been my wise and gracious mentors and dependable guides through this journey. I couldn't have asked for a better deal. Acknowledgements also go to Mr Kishan Patel, who collected some of the electrophysiology data for the study in Chapter 4 under the Cardiff Undergraduate Research Opportunities Programme (CUROP) 2015.

A tonne of gratitude to the Fantastic Flors, my "sister-in-arms" in the "Land of Strangers". *#WWIDWY*? Big-ups go to my colleagues in 2.11, Chris, Seine, Kathy, Sharon, Caroline, Katie, Jimmy, Bert, Rupal and Laura for being good company and loyal subjects for my long experiments. Thanks also to Ashley, Tony and Katie Mortlock, my helpful sounding boards and to Sue Hobbs, the repository of all wisdom and knowledge of the school.

And to Atsufui and Xoese, for not giving up on me and bearing with me the many times I said I'd finish and I didn't. I love you.

TABLE OF CONTENTS

LIST OF FIGURES

LIST OF TABLES

LIST OF ABBREVIATIONS

ANOVA	Analysis of variance
AREDS	Age-related eye disease study
AUC	Area under the curve
CoV	Co-efficient of variation
CS	Contrast sensitivity
DTL	Dawson-Trick-Litzkov
ERG	Electroretinogram
ERP	Early receptor potential
ISCEV	International Society for Clinical Electrophysiology of Vision
LED	Light emitting diode
LGN	Lateral geniculate nucleus
logMAR	Logarithm of the minimum angle of resolution
mfERG	Multifocal electroretinogram
OCT	Optical coherence tomography
OP	Oscillatory potential
PERG	Pattern electroretinogram
PhNR	Photopic negative response
RGC	Retinal ganglion cell
RGCf	Retinal ganglion cell receptive field
RNFL	Retinal nerve fibre layer
ROC	Receiver operating characteristic (curve)
RPE	Retinal pigment epithelium
SD	Standard deviation
SITA	Swedish interactive threshold algorithm
STR	Scotopic threshold response
td	Trolands
VA	Visual acuity
VEP	Visual evoked potential
VFT/VFS	Visual field test/sensitivity

1 CHAPTER ONE – INTRODUCTION

1.1 Introduction to the Thesis

This thesis describes a series of studies using electrophysiology to explore retinal function in healthy participants and participants with autosomal dominant optic atrophy (ADOA), an inherited optic neuropathy caused by mutations in the *OPA1* gene leading ultimately to retinal ganglion cell (RGC) dysfunction or loss. Currently, there is no treatment for this blinding condition however, ongoing research is aimed at establishing early biomarkers for the disease so that treatment options can be introduced in early stages of the disease where the changes can be stopped or potentially reversed.

This thesis is composed of eight chapters. Chapter 1 presents the relevant background information on the healthy eye, ADOA and ocular electrophysiology as well as the main hypotheses, aims and relevance of the PhD. Chapter 2 describes the general methods used in this study, including equipment and the selection of control participants. It also presents a series of studies to develop a suitable protocol for recording the long duration ERG in healthy controls. In Chapter 3, the retinotopic characteristics of the focal long duration ERG developed in chapter 2 are compared to the pattern ERG, a standardised test for RGC function. In Chapter 4, the density profiles of the long duration and brief flash photopic negative response (PhNR) are compared to the published distribution of RGCs in the human retina. Chapters 5 to 7 constitute the main study of this thesis in which twelve participants with ADOA and sixteen age matched controls were recruited. Chapter 5 focuses on the baseline tests (visual acuity, contrast sensitivity, visual fields, colour vision and optical coherence tomography) used to assess the participants. Chapter 6 details their electrophysiological assessment findings while chapter 7 explores the relationship between findings of the baseline and electrophysiological tests. Finally, the general discussion of the thesis, limitations of the study, conclusions and future work are presented in chapter 8.

1.2 Overview of the Retinal Architecture

The human retina is the photosensitive part of the eye (Figure 1.1). It lines the back of the eye and extends from the circular edge of the optic disc to the ora serrata where it is continuous with the epithelial layers of the ciliary body (Remington, 2005; Kolb, 2011). A circular field of approximately 6 mm (~20^{o}) around the fovea is considered the central retina, or macula, while the area beyond this is considered as the peripheral retina (Figure 1.1A) (Kolb, 2011). Anatomically, the macula is defined as the area of the retina where the retinal ganglion cell (RGC) layer is more than one cell thick (Guedes et al., 2003). The fovea is the area of depression in the centre of the macula where cone density is highest. The fovea is about 1.5 mm (5^{o}) in diameter and is used for sharpest acuity and colour vision (Remington, 2005; Kolb, 2011). In the centre of the fovea is the foveal pit, or foveola. It is an area about 0.35 mm (~1^{o}) in diameter containing only cones and no rods (Remington, 2005; Kolb, 2011).

The retina is approximately 0.5 mm thick. A radial section of the human retina reveals that the photoreceptors (rods and cones) lie outermost, against the retinal pigment epithelium and choroid while the RGCs, which are the output neurons of the retina, lie innermost in the retina, closest to vitreous chamber (Figure 1.1B). Light must therefore traverse the thickness of the retina before activating the photoreceptors (Remington, 2005). Typically, the inner or proximal retina refers to the vitreous side of the outer plexiform layer (OPL) while the outer or distal retina refers to the choroidal side of the OPL.

The photoreceptors and RGCs are connected vertically by the bipolar cells, providing a three-step vertical pathway for light signalling through the retina. The horizontal cells, amacrine and interplexiform cells create intra-retinal cross-connections (lateral and vertical), provide feedback information and integrate retinal function. In addition, the retinal architecture is supported by the Müller cells, glial cells which span between the inner limiting membrane and the outer limiting membrane. The outer limiting membrane of the retina is formed from adherens junctions between Müller cells and photoreceptor cell inner segments. The inner limiting membrane of the retina is likewise composed of laterally contacting Müller cell end feet and associated basement membrane constituents.

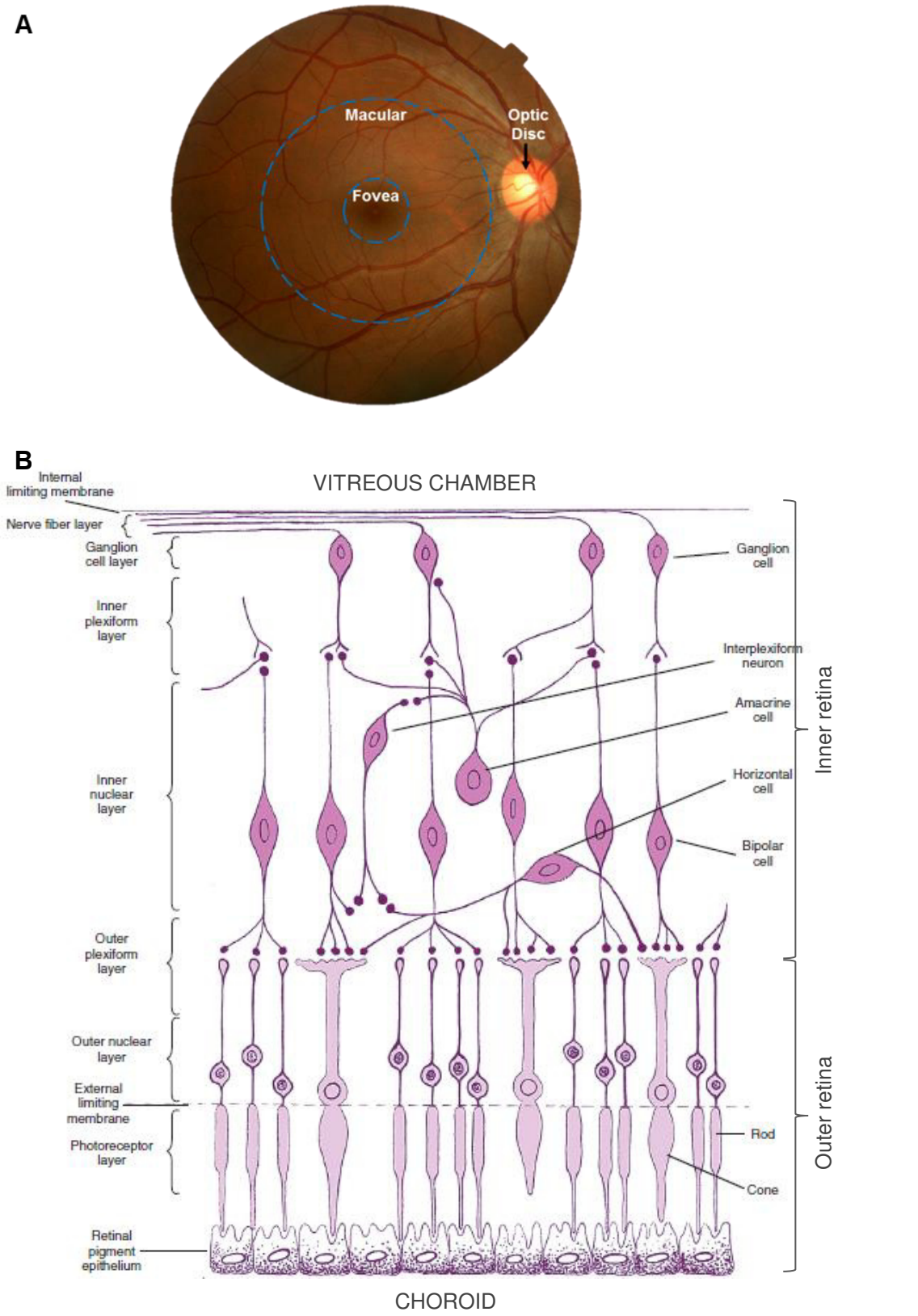

Figure 1.1. (A) A fundus photograph of the retina a study participant. It shows the fovea, macula and optic disc as well as blood vessels coursing from the optic disc. The central retina refers to the macula (outer circular ring) where the retinal ganglion cell layer is more than one cell thick and has a diameter 6 mm (~ 20º). The diameter of the fovea (inner circular ring) is about 1.5 mm (5º). (B) A radial slice through the retina showing the various layers and cells of the retina (Remington, 2005). Typically, inner and outer retina refer to the vitreous and choroidal sides of the outer plexiform layer respectively.

1.2.1 The Photoreceptors

The human retina is made up of rods and three types of cones (Kolb, 2003; Kolb, 2011). There are about 90 - 100 million rods and 4 - 6 million cones (Osterberg, 1935; Curcio et al., 1990). There are no rods in the foveolar, i.e. the central 0.35 mm (1°) area of the fovea (Remington, 2005). Rod density peaks at about 4 - 5 mm (~15 - 18°) from the foveal centre where it is over 150,000 rods/mm^2 and declines to about 40,000 rods/mm^2 towards the periphery. Cone density on the other hand is at its peak of about 200,000 cones/mm^2 at the foveal centre, declines rapidly to about 20,000 cones/mm^2 at 1mm eccentricity and levels off to about 5,000 cones/mm^2 towards the periphery (Osterberg, 1935; Curcio et al., 1990).

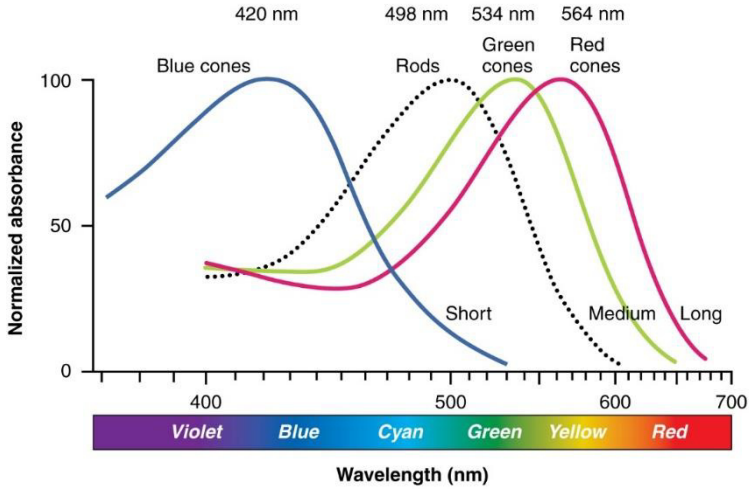

Figure 1.2. Spectral sensitivity curves of the four photoreceptors of the human retina. (Source: https://commons.wikimedia.org/wiki/File:1416_Color_Sensitivity.jpg#/media/File:1416_Color_Sensitivity.jpg)

The rods are highly sensitive to low levels of light and are used for vision under scotopic conditions. They contain the visual pigment rhodopsin (consisting of a protein, opsin, and chromophore, retinal) and are sensitive to blue-green light with peak sensitivity to a wavelength of around 500 nm (Bowmaker and Dartnall, 1980; Bowmaker et al., 1980). The cones are less sensitive to light and are used for vision under photopic conditions. Cone visual pigments contain a different type of opsin to the rod visual pigment, which results in a different spectral sensitivity. The three types of cones are named depending on their sensitivity to different wavelengths; L-cones are maximally sensitive to long

wavelengths of light (peak sensitivity 564nm), M-cones to medium wavelengths of light (peak sensitivity 534nm) and S-cones to short wavelengths (peak sensitivity 420nm) (Figure 2) (Bowmaker and Dartnall, 1980; Bowmaker et al., 1980). The ratio of responses of the three cone types with their overlapping spectral sensitivity curves, and the consequent pathways of connectivity to the brain form the basis of colour perception (Remington, 2005).

1.2.2 The Bipolar Cells

The bipolar cells are the second order neurons in the vertical pathway, transmitting signals from photoreceptors to RGCs. Bipolar cell bodies reside in the inner nuclear layer; their dendrites synapse with photoreceptors in the outer plexiform layer (OPL) and their axon terminals with dendrites of RGCs and amacrine cells in the inner plexiform layer (IPL) (Figure 1.1).

In the human retina, eleven types of bipolar cells have been identified using Golgi staining (Figure 1.3) (Boycott and Wassle, 1991; Kolb, 2003; Wassle, 2004). Only one type of bipolar cell is known to synapse with rods, while the remaining types synapse with cones. Based on their response to light, the bipolar cells are further divided into two groups, depolarising and hyperpolarising bipolar cells. This division gives rise to the ON and OFF parallel pathways in the visual system which are further discussed in section 1.2.4.

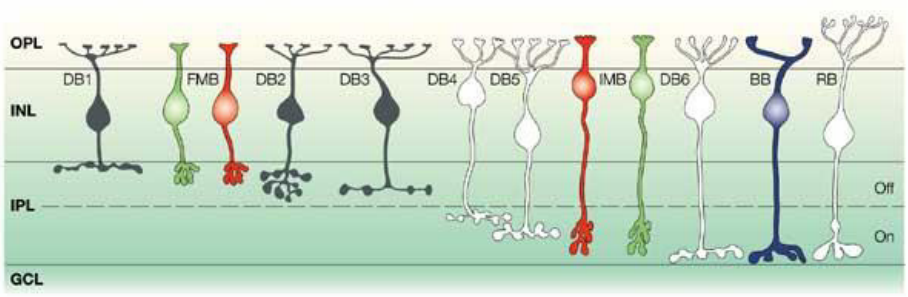

Figure 1.3. Bipolar cell types in the primate retina shown schematically in vertical view. Their axons terminate at different levels in the inner plexiform layer (IPL); OFF cone bipolar cells terminate in the outer half, while ON bipolar cells terminate in the inner half. DB – Diffuse bipolar cells; FMB – flat bipolar cells; IMB – invaginating bipolar cells; BB – blue bipolar cells; RB – rod bipolar cells; OPL – outer plexiform layer; INL – inner nuclear layer; IPL – inner plexiform layer; GCL – ganglion cell layer. (Wassle, 2004)

1.2.3 The Retinal Ganglion Cells

The RGCs are the third order neurons. Their cell bodies are located in the ganglion cell layer (GCL) and receive direct input from the bipolar cells and

amacrine cells (Wassle, 2004). There are approximately 1.2 million RGCs in the human retina (Quigley et al., 1982; Curcio and Allen, 1990). About 50% of the population of RGC bodies are found in the macula (Curcio and Allen, 1990). There are no RGCs in the fovea; their cell bodies are laterally displaced away from the cones they connect to (Curcio and Allen, 1990; Drasdo et al., 2007). The peak density of 32,000 – 38,000 cells/mm^2 therefore occurs in a horizontally oriented elliptical ring about 1 – 2 mm (3 - 5^o) eccentric to the foveal centre (Figure 1.4). Curcio and Allen (1990) report that RGC density is about 15% higher in the nasal retina than at equivalent eccentricities in the temporal retina from 0.4 to 2.0 mm, but from 2 – 4 mm, the nasal and temporal retina have approximately equal densities. Densities along the vertical meridian are equal in the superior and inferior retina from 0.4 – 2.0mm, but from 4 mm eccentricity, the superior retina has 65% higher RGC density than inferior retina.

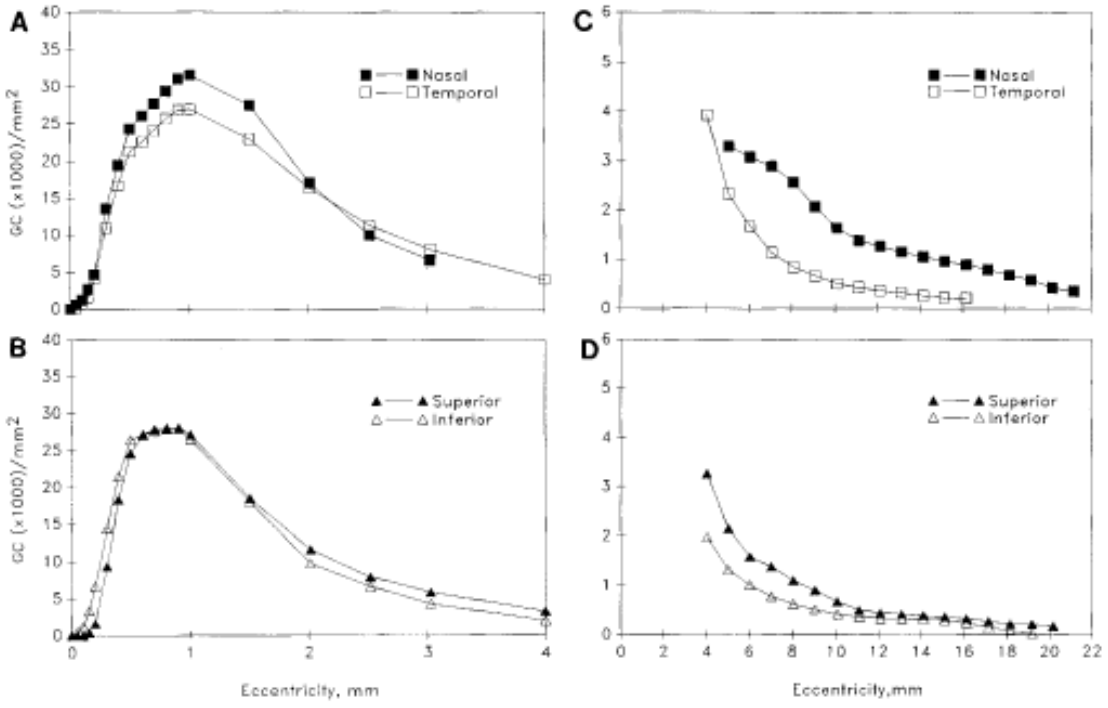

Figure 1.4. Average density of RGC bodies as a function of eccentricity along the horizontal (A, C) and vertical (B, D) meridians of the composite retina. A and B show the central and C, D show peripheral ganglion cell density at appropriate scales. The gap in the nasal curve at 4 mm represent the site of the optic disc. RGC bodies were counted in unstained whole mount retinas of six young normal adults post-mortem (Curcio and Allen, 1990).

Each ganglion cell has a single axon, which emerges from the cell body and turns to run parallel to the inner surface of the retina thus forming the retinal nerve fibre layer (RNFL) (Figure 1.1). The axons take a more or less arcuate

path towards the optic disc where they leave the eye as the optic nerve (Figure 1.5). Axons from the fovea take a direct route towards the temporal rim of the optic disc and form the papillomacular bundle. Approximately 90% of all axons leaving the optic disc eventually terminate in the lateral geniculate body (Figure 1.5); others project to subthalamic areas involved in processes such as the pupillary reflexes and the circadian rhythm (Remington, 2005).

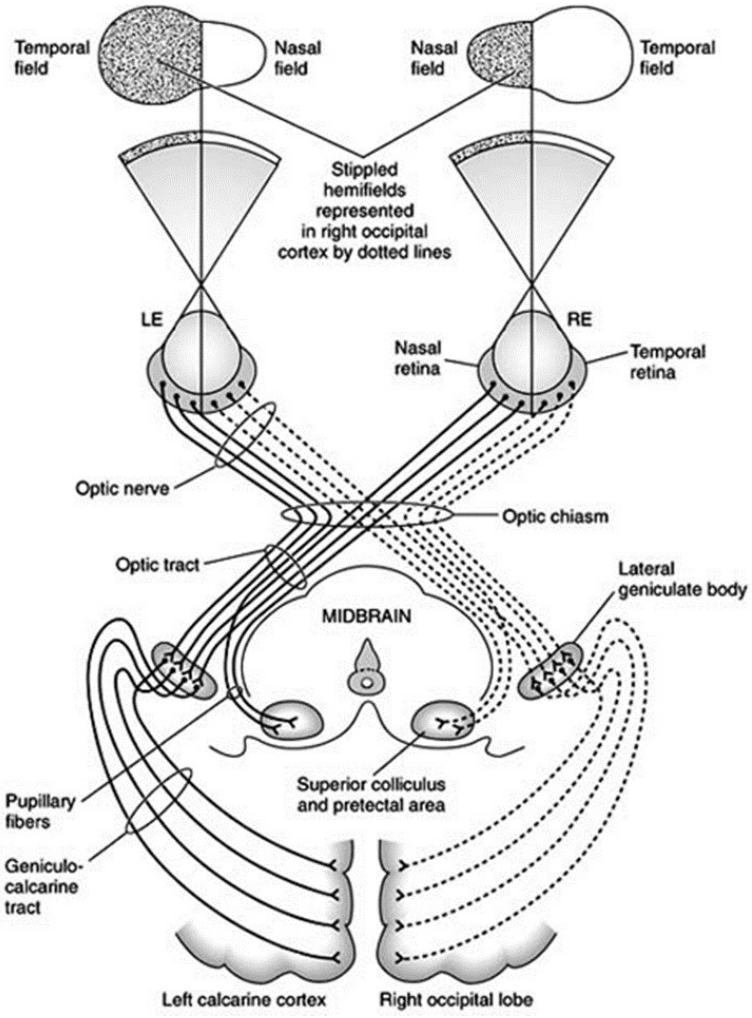

Figure 1.5. The visual pathway. Objects in the nasal field are projected onto the temporal retina and vice versa. The nerve fibres from the nasal retina cross over to join the temporal fibres of the contralateral eye at the chiasm. Approximately 90% of all the nerve fibres in the optic nerve terminate at various layers of the lateral geniculate body. The remaining 10% project to the subthalamic areas of the superior colliculus and pretectal area. The geniculo-calcarine tract is made up of optic radiations projecting from the lateral geniculate body to the cortex in the occipital lobe. (Source: http://www.oculist.net/others/ebook/generalophthal/vaughan/public/co_figures/ch014/ch14fg2.jpg)

There are many types of RGCs in the vertebrate retina with at least 10 – 15 morphological types found in any mammalian retina (Wassle, 2004). Polyak in 1941 identified six types of ganglion cells in primates according to cell body and

dendritic field size, naming them midget, parasol, shrub, small diffuse, garland and giant ganglion cells (Polyak, 1941; Rodieck et al., 1985). Of these six types, the midget and parasol ganglion cells have received the most attention mainly because they together constitute up to 80% of the entire population of RGCs (Rodieck et al., 1985; Watanabe and Rodieck, 1989; Dacey and Petersen, 1992; Dacey, 1993b). Indeed many more RGC types have been identified more recently however, they exist at low densities, ranging from less than 1% to 5% of the total and much of their physiology is yet to be elucidated (Dacey, 2004).

The midget RGCs are also referred to as P-cells and parasol RGCs as M-cells to denote their central projection respectively to the parvocellular and magnocellular layers of the LGN (Leventhal et al., 1981; Perry and Cowey, 1981; Perry and Cowey, 1984; Perry et al., 1984; Rodieck et al., 1985; Dacey et al., 2003; Dacey, 2004). There also exists a third pathway involving the koniocellular (K) layers of the LGN which receives input from the small bistratified RGCs (Hendry and Reid, 2000; Xu et al., 2002; Casagrande et al., 2007). Midget RGCs are identified by their small, dense and monostratified dendritic arbours. They are the most numerous RGC type in the retina constituting about 65-80% of the total number of RGCs in the central retina and about 40-50% in the periphery (Polyak, 1941; Rodieck et al., 1985; Watanabe and Rodieck, 1989; Dacey and Petersen, 1992; Dacey, 1993b). The parasol cells have more extensive dendritic arbours, consisting of relatively thick and frequently branched processes. They make up between 6-10% of RGCs in the central retina increasing to about 8-10% over much of the retina except in the nasal retina where parasols make up 20% or more of the RGC population from eccentricities of 7mm (Silveira and Perry, 1991). Within each group of midget and parasol cells, there is an increase in dendritic field size with eccentricity.

The midget cells with their high sampling density function to preserve visual acuity and transmit chromatic information in the visual pathway. The parasol cells on the other hand respond strongly to achromatic or luminance stimuli, contrast and motion (Dacey, 1996; Dacey, 2004; Callaway, 2005). On the basis of their response to light stimulation, both midget and parasol cells are also grouped into ON-centre (depolarise at light onset) and OFF-centre (depolarise at light offset) varieties.

1.2.4 ON and OFF Pathways of the Retina

Photoreceptors are depolarised in the dark and release a neurotransmitter, glutamate, at the synapse with the bipolar cells. When a photoreceptor absorbs light, the cells hyperpolarise and there is a decrease in the rate of glutamate release, which is detected by two types of bipolar cells with opposing sensitivities to glutamate. ON-bipolar cells (depolarising bipolar cells), depolarise in response to light onset and OFF-bipolar cells (hyperpolarising bipolar cells) hyperpolarise in response to light (or depolarise in response to light cessation). The ON- and OFF- bipolar cells then transmit their signal to their respective ON- and OFF RGCs (Figure 1.6) (Kolb, 2003).

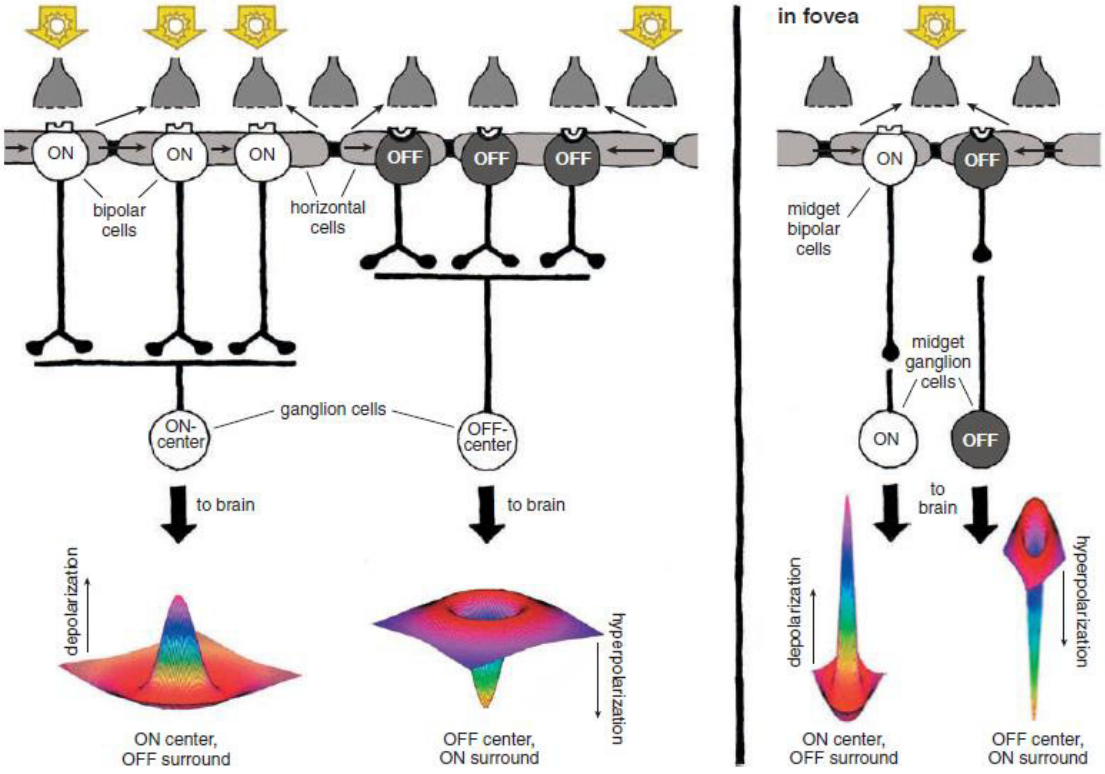

Figure 1.6. A schematic diagram showing the ON and OFF pathways of the human retina. ON-centre ganglion cells are activated when light falls on the centre of their receptive fields, whereas OFF-centre ganglion cells fire in response to light falling on their fields' periphery leaving their centre dark. Horizontal cells convey antagonistic surround signals to bipolar cells and thence to ganglion cells. Ganglion cells have receptive fields, an area in space within which the RGC responds to a light stimulus (Hartline, 1938). RGC receptive fields are modelled as the difference between Gaussian distributions of centre and surround receptive fields, which gives them a so-called "Mexican-hat" shape (see lower section of figure), reflecting their integration of opposing information about centres and surrounds. In the fovea (right), ganglion cells have much narrower receptive fields and each carries information from a single cone. A cone feeds information to two of these midget ganglion cells; at all times each foveal cone transmits either an ON or an OFF signal to the brain. This signal also carries a colour message regarding the type of cone (red or green) it comes from (Kolb 2003).

Cones synapse directly on to either ON-bipolar cells or OFF-bipolar cells which in turn synapse with ON-centre and OFF-centre RGCs respectively. Each L- or M- cone in the central fovea, in contrast with the rest of the retina, connects to two midget ganglion cells, via two midget bipolar cells, so at all times each cone can either transmit a dark-on-light (OFF) signal or a light on-dark (ON) message. The S-cone pathway is mediated by the blue-cone bipolar cells which in turn contact the small bistratified RGCs which exhibit blue ON/yellow OFF responses (Kouyama and Marshak, 1992; Dacey and Lee, 1994; Martin et al., 1997; Calkins, 2001; Szmajda et al., 2008). The bistratified RGCs of the S-cone pathway have two tiers of dendrites which make synaptic connections in two separate strata of the IPL. A bistratified RGC has a major dendritic tier branching in stratum 5 of sublamina *b* and a smaller tier of dendrites in stratum 1 of sublamina *a* (Dacey, 1993a). Its axon projects to the koniocellular layers of the LGN (Martin et al., 1997). The signal that goes to the brain therefore has both spatial and spectral information (Kolb, 2003).

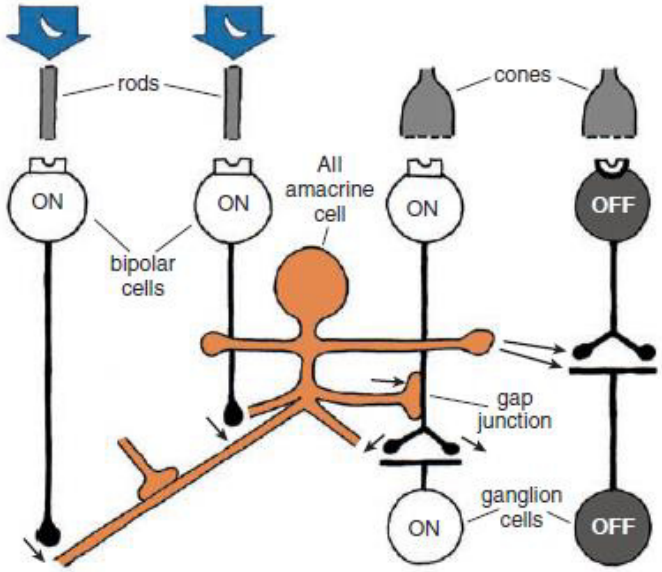

Figure 1.7. The rod pathway. In the rod pathway, rod bipolar cells connect first to the All amacrine cells. The amacrine cells then transmit the information to the ON-bipolar cells of the cone pathway for onward transmission to the ON centre RGCs. The amacrine cells at the same time directly inhibit the OFF-centre RGCs (Kolb, 2003).

Rods, however, contact only rod bipolar cells, which depolarize in response to light stimulation (Rowling, 1987; Kolb, 2003) (Figure 1.7). The rod bipolar cells do not synapse directly with RGCs, instead they synapse with amacrine cells which in turn excite cone-ON bipolar cells, but inhibit cone-OFF bipolar cells in

order to send signals to the RGCs. In addition to this primary rod pathway, two more pathways enable rods to feed into retinal circuits (Euler et al., 2014). The secondary rod pathway involves gap junctions between rods and cones, enabling rod signals to enter the cone pathways in the outer plexiform layer (Tsukamoto et al., 2001; Euler et al., 2014). A tertiary rod pathway has been demonstrated in some mammals: in this pathway, rod terminals make direct basal contacts with some types of OFF-cone bipolar cells (Hack et al., 1999; Sharpe and Stockman, 1999).

1.3 Autosomal Dominant Optic Atrophy

Autosomal Dominant Optic Atrophy (ADOA) is a hereditary optic neuropathy presenting in childhood and characterized by bilateral optic nerve head (ONH) pallor and loss of visual function including reduced visual acuity, paracentral or centro-coecal visual field loss and colour vision defects (Votruba et al., 1998a). The disease is caused primarily by a mutation in the autosomal nuclear gene, *OPA1*, leading to degeneration in the RGCs (Alexander et al., 2000; Delettre et al., 2000). The disease is also known as Kjer's Optic Atrophy and is named after Dr Poul Kjer who described the disease in 19 Danish families in 1959 (Kjer, 1959).

ADOA is one of the primary hereditary optic neuropathies, a group of inherited genetic disorders which all selectively cause the death of the RGCs in the retina. The other primary hereditary optic neuropathies are autosomal recessive optic atrophy, X-linked recessive optic atrophy and the maternally inherited Leber's hereditary optic neuropathy (LHON). ADOA and LHON are the commonest types of hereditary optic neuropathies (Votruba et al., 2003a; Yu-Wai-Man et al., 2009). The common clinical features in these conditions are reduced visual acuity, colour vision defects, central visual field defects and optic disc pallor. Visual loss is typically bilateral, symmetrical and irreversible once RGC loss has occurred (Votruba et al., 2003a; Newman and Biousse, 2004). The common finding of central or centro-coecal scotoma in these conditions is because they preferentially affect the papillomacular nerve fibre bundle.

LHON is characterised by a severe and sudden loss of vision in one eye occurring in the second decade in affected individuals. In nearly all cases, the second eye is affected within six months of onset. LHON is a primary mitochondriopathy, in that it is caused by a point mutation within the mitochondrial genome. Over 95% of LHON pedigrees are known to harbour one of three mitochondrial DNA (mtDNA) point mutations: m.3460G>A, m.11778G>A and m.14484T>C, which all involve genes encoding complex I subunits of the mitochondrial respiratory chain. The mode of transmission is maternal and affected males are more predisposed to lose vision (Yu-Wai-Man et al., 2009).

1.3.1 Prevalence and Epidemiology

The prevalence of ADOA is between 1 in 50,000 in most populations worldwide, to as high as 1 in 8,000 in Sicily, Italy. (Krill et al., 1970; Kjer et al., 1996; Votruba et al., 2003a; Yu-Wai-Man et al., 2010a; Gallus et al., 2012; Lenaers et al., 2012; Chen et al., 2013). In Sicily (Gallus et al., 2012), and in Denmark (Kjer et al., 1996) where the prevalence 1 in 12,000, a founder effect accounts for the high prevalence.

In the United Kingdom, the prevalence of the disease is estimated at 1 in 35,000 with the minimum point prevalence based on molecularly confirmed cases of the disease is approximately 1 in 50,000 (Yu-Wai-Man et al., 2010a). The affected male to female ratio is reported to be 1.06:1 (Yu-Wai-Man et al., 2010a), which confirms earlier reports that males and females are equally affected (Johnston et al., 1979; Votruba et al., 1998a).

1.3.2 Clinical Features

The disease was first described by Batten (1896) and also by Snell (1897), who is generally credited as the first to describe a form of optic atrophy separate from Leber's hereditary optic atrophy (LHON) (Votruba et al., 1998a; Delettre et al., 2002). For many years, clinicians then debated whether all inherited forms of optic atrophy were part of the manifestation spectrum of LHON, as described by Theodore Leber, or whether they were different disease entities. Wolfgang Jaeger in 1954, published genealogical and clinical findings in an extended

German family spanning 5 generations, thereby establishing autosomal dominant optic atrophy as a distinct disease entity (Jaeger, 1954; Fuhrmann et al., 2010). He demonstrated from the pedigree that the disease was inherited as a dominant trait and included male-male transmission, in contrast to LHON where only females transmit the disease (Man et al., 2002; Votruba et al., 2003a). In addition, he pointed out the presence of blue yellow colour vision disturbances in the affected subjects in this family in contrast to the red-green defect typically present in families with LHON (Fuhrmann et al., 2010).

Iverson (1958) also reported congenital optic atrophy in three generations which helped establish a clear autosomal dominant pattern of inheritance of the disease thereby distinguishing it from Leber hereditary optic atrophy (Kelly et al., 2012). However, it was only when the Danish ophthalmologist Kjer described 19 families with autosomal dominant atrophy that the disease was definitively recognised (Kjer, 1959; Delettre et al., 2002).

ADOA is now a well-established clinical entity and clinical diagnosis is based on (1) age and mode of onset, which usually is in childhood and of gradual onset, (2) reduced visual acuity, usually moderate to severe, (3) temporal disc pallor, (4) colour vision defect, usually blue-yellow, (5) centro-coecal scotoma, and (6) an autosomal dominant inheritance pattern established by family history or genetic investigation (Kjer et al., 1996; Votruba et al., 1998a). The positive identification of mutations in the *OPA1* gene (or other implicated genes discussed later in section 1.3.7) may be used to confirm the diagnosis especially in suspected cases of individuals with no family history. It is also important that all other causes of optic neuropathy are excluded. Patients with ADOA, however, show marked intra- and interfamilial variations in clinical features and this is thought to be indicative of the highly variable expression of the *OPA1* gene. The observed wide variation in clinical presentation may be due to allelic heterogeneity, change in disease severity with age and the effects of other modifying genetic and/or environmental factors (Votruba et al., 1998a).

ADOA may also be associated with extra-ocular neurologic features such as deafness, progressive external ophthalmoplegia, muscle cramps, hyper-reflexia, ataxia, stroke or multiple sclerosis-like symptoms. In these cases, the disease is

termed Autosomal Dominant Optic Atrophy Plus (ADOA+) and it is a syndromic form of the disease (Yu-Wai-Man et al., 2010b). Another syndromic form of ADOA associated with cataract is called Dominant Optic Atrophy and Cataract (DOAC), but it occurs rarely (Anikster et al., 2001). This review will focus on the ADOA caused by *OPA1* (non-syndromic form) as the subject of the study.

1.3.2.1 Visual Acuity

The commonest ocular symptom presented in ADOA is blurred vision usually occurring within the first decade. The age of onset is usually reported between 4 and 8 years, however, a later age of onset is not uncommon (Votruba et al., 1998a; Johnston et al., 1999; Yu-Wai-Man et al., 2010a). For example, one study showed a bimodal distribution for the age of onset with peaks at 5 years and between 21 and 30 years. Furthermore, there has been at least one reported case of an original case presenting a late onset acute visual loss at 62 years (Nochez et al., 2009). Late onset cases are thought to reflect cases with sub-clinical symptoms which were not detected until later when the disease progressed (Votruba et al., 1998b; Yu-Wai-Man et al., 2010a).

The decrease in visual acuity is gradual, bilateral and irreversible (Johnston et al., 1979; Votruba et al., 1998a; Johnston et al., 1999; Yu-Wai-Man et al., 2010a). Votruba et al (1998a), in a study of 87 affected individuals from 21 families reported the median best corrected visual acuity (BCVA) was 6/36, while Yu-Wai-Man et al (2010a), recorded ~6/60 as the mean visual acuity in their study of 45 affected individuals from 17 families. However, BCVA in affected individuals covers a wide range from 6/6 to count fingers (Kline and Glaser, 1979; Votruba et al., 1998a; Johnston et al., 1999; Yu-Wai-Man et al., 2010a) and highlights the wide phenotypic variation of the disease. Visual acuity is often symmetrical in the majority of patients, however, there is asymmetry of two lines or more on the Snellen visual acuity in 8 – 17 % of affected individuals (Kline and Glaser, 1979; Votruba et al., 1998a; Yu-Wai-Man et al., 2010a); with a striking example of an individual with VA of 6/9 and 6/60 in the right and left eye respectively (Kline and Glaser, 1979).

Visual acuity generally tends to decline with age although there are considerable intra and inter-familial variations (Votruba et al., 1998a; Johnston

et al., 1999). The visual prognosis in ADOA is comparatively better than in LHON and some affected individuals maintain adequate vision (6/12 or better) for driving (Votruba et al., 1998a; Cohn et al., 2008). Notwithstanding the loss of visual acuity in ADOA, there are cases of individuals with normal BCVA (6/9 or better) in both eyes (Kline and Glaser, 1979; Votruba et al., 1998a; Johnston et al., 1999). For example, Johnston et al (1999), found individuals with normal VA (6/6) in both eyes, but who had mild colour vision defects, temporal or diffuse optic disc pallor and a positive family history of ADOA. In addition, they bore the specific haplotype associated with the disease and were therefore classified as affected with ADOA, but mildly so. These individuals with normal BCVA represented 9% of the number of the study participants with ADOA. Therefore, Johnston et al (1990) recommended that in the context of a family with ADOA, a mild degree of temporal or diffuse pallor of the optic disc and minimal colour vison defects, are highly suggestive of an individual being affected even if the visual acuity is normal.

1.3.2.2 Ocular Motility

Nystagmus is an uncommon finding and if present is seen in individuals with severe visual impairment. For example, Hoyt (1980), found four patients with nystagmus (among 31 ADOA affected patients); none of which had visual acuity better than 20/200. Votruba et al, 1998, examined 87 affected individuals and found only four patients with nystagmus, all of which were horizontal. These patients had visual acuities of 3/60, counting fingers, hand motion and light perception.

1.3.2.3 Optic Nerve Head

A distinctive feature in ADOA is bilateral temporal optic disc pallor (Johnston et al., 1979; Kline and Glaser, 1979; Votruba et al., 1998a; Johnston et al., 1999). The pallor is typically symmetric, wedge-shaped and not commonly associated with the cupping or increased intraocular pressure seen in primary open angle glaucoma (Figure 1.8 A, arrowed) (Votruba et al., 1998b). In some cases however, there is diffuse pallor involving the entire optic nerve head (ONH), while in others the pallor is subtle (Votruba et al., 2003b).

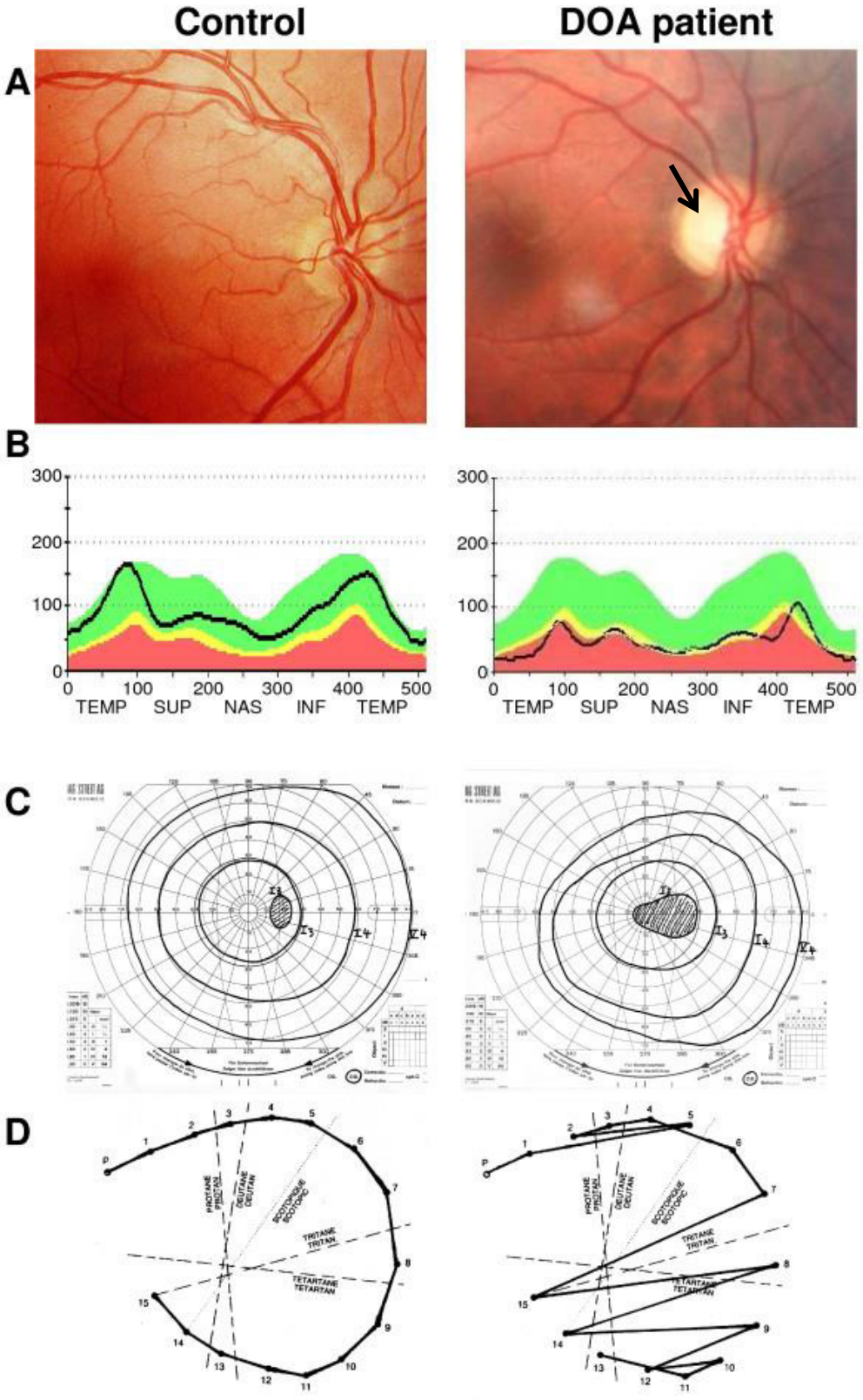

Figure 1.8. Ophthalmologic description of an ADOA patient. Left column displays control eye, right column shows affected eye. (A) Fundus photograph comparing control eye (left) to affected eye (right) showing temporal disc pallor; (B) Optical Coherence Tomography shows the retinal nerve fibre layer (black line) is reduced in DOA; (C) Visual field examination disclosing centro-coecal scotoma in DOA patient, only the blind spot is seen in control patient; (D) Results from a desaturated 15-Hue test presenting tritan defect (blue-yellow axis) in the ADOA patient (Lenaers et al., 2012)

There are also affected individuals who have normal looking optic nerve heads. Generally, best visual acuity is associated with least degree of pallor (Votruba et al., 1998a; Yu-Wai-Man et al., 2010a). However, severity of functional loss is not necessarily reflected in the disc appearance and gross visual field defects may be associated with anything from temporal pallor to complete atrophy of the disc (Votruba et al., 1998a; Yu-Wai-Man et al., 2010a). These differences highlight the clinical heterogeneity in ADOA. Other common optic disc findings include saucerisation, peripapillary atrophy and a cup to disc ratio of > 0.5 (Yu-Wai-Man et al., 2009)

One study found that individuals with ADOA have significantly smaller optic nerve heads than their age matched control counterparts, indicative of a smaller population of axons at birth (Barboni et al., 2010). This feature, however, may be mutation specific since stratification of ONH size by *OPA1* mutation showed that normal sized ONH was associated with two mutations while the smallest size was linked to the ADOA+ phenotype. Thus, mutations in the *OPA1* gene may determine the feature of a smaller optic disc size and this in turn may have relevance for ADOA pathogenesis. Furthermore, *OPA1* gene polymorphic variants may contribute to the normal variability of ONH size in the general population (Barboni et al., 2010).

Histologic examination of the optic nerve by Johnston et al (1979), and Kjer et al, (1983) showed a significant reduction in the retinal nerve fibre layer (RNFL) thickness of affected individuals in comparison to controls (Figure 1.8B). The measurement of circumpapillary RNFL using optical coherence tomography (OCT) in more recent studies confirmed this and showed marked thinning around the optic disc, more pronounced in the temporal quadrant, in affected individuals (Milea et al., 2010; Barboni et al., 2011; Yu-Wai-Man et al., 2011a). These studies showed that the RNFL thickness in patients with ADOA compared to age matched controls, was reduced by about 50 – 60% in the temporal quadrant and about 40 – 50% in the inferior quadrant (Table 1.1). Within the cohort, individuals with ADOA+ phenotypes or severe visual impairment acuity were found to have more marked RNFL thinning.

Table 1.1. RNFL thickness data for *OPA1* patients and normal controls (Yu-Wai-Man et al., 2011a)

Quadrant	Mean RNFL thickness (SD) (μm)				P-valueb
	OPA1 (N=80)	Controls (N=30)	%-age decrease	95% CI	
Average	54.11 (11.98)	98.77 (10.86)	45.2	40.2–50.2	<0.0001
Temporal	33.44 (8.31)	81.60 (14.31)	59.0	53.7–64.4	<0.0001
Inferior	61.84 (18.72)	122.70 (20.14)	49.6	43.0–56.2	<0.0001
Superior	71.00 (21.58)	122.00 (14.86)	41.8	34.9–48.8	<0.0001
Nasal	49.99 (12.76)	67.43 (17.59)	25.9	16.9–34.8	<0.0001

Table 1.2. Comparison of age-related RNFL loss in various studies (Modified from Barboni et al, 2011)

Quadrant	Parikh et al 2007 (n = 187)	Budenz et al 2007 (n = 328)	Sung et al, 2009 (n = 226)	Barboni et al, 2011	
				controls (n = 43)	ADOA (n = 32)
Average	0.16*	0.20*	0.25*	0.30*	0.19 – 0.20*
Temporal	0.20*	NA	0.06*	0.16	0.05 – 0.02
Superior	0.23*	NA	0.34 *	0.26	0.36 – 0.42*
Nasal	0.12	NA	0.24*	0.36*	0.04 – 0.13*
Inferior	0.08	NA	0.36*	0.40*	0.30 – 0.32*

Values are in micrometres per year: NA – not available; * -Significant at $p < 0.05$

Interestingly, the rate of RNFL thinning as a function of age in patients with ADOA (0.19 – 0.20 um/year) was within the range reported for normal individuals in other studies (Table 1.2). Since ADOA was previously reported to be associated with smaller ONH sizes (Barboni et al., 2010), it was hypothesized that the relative deficit in RNFL thickness is established before the second decade of life and the gradual reduction in best corrected visual acuity with age may be a consequence of the superimposed loss of fibres associated with normal ageing.

1.3.2.4 Pupillary Reaction

Another interesting finding is that there is usually no afferent pupillary defect in DOA patients and, if present, it is significantly less marked than the visual deficit would predict. This is similarly the case in LHON suggesting that the melanopsin RGCs, a subpopulation of ganglion cells responsible for pupillary reactions, are largely spared in both diseases (Bremner et al., 2001; Lenaers et al., 2012). Recently, Perganta et al (2013) reported that the pupillary reflex was similarly preserved in a mouse model of ADOA (Perganta et al., 2013).

1.3.2.5 Visual Fields

Central, centro-coecal and paracentral scotomas with sparring of the periphery are the most common field abnormalities in DOA (Figures 1.8C). The scotoma generally affects the central 20 – 30º visual field (Fuhrmann et al., 2010) These findings are consistent with the primary involvement of the papillomacular bundle in this condition. Affected individuals show a spectrum of defects ranging from a small discrete enlargement of the blind spot to a subtotal visual loss (Johnston et al., 1979; Kjer et al., 1996; Votruba et al., 1998b; Johnston et al., 1999; Yu-Wai-Man et al., 2009). In one study, age and duration of disease were correlated with the mean field deviation in the affected patients. In the older patients and those affected for longer the mean deviation diverged from the age matched norm (Votruba et al., 1998a)

1.3.2.6 Colour Vision

The colour vision defect in ADOA is often reported as an acquired blue-yellow loss or tritanopia (Figure 1.8D) (Krill et al., 1971; Hoyt, 1980). A suggested reason for the frequency of tritan defects was that, since the short wavelength sensitive system mediating the blue-yellow channel has fewer cells than the medium and long wavelength sensitive system mediating the red-green channel, a percentage loss of RGCs in the blue-yellow channel was more devastating than an equal percentage loss in the red-green channel (Johnston et al., 1999). However, other studies showed a generalised dyschromatopsia involving both the blue-yellow and red-green axes, with a minority having pure tritanopia (<10%) (Votruba et al., 1998a; Yu-Wai-Man et al., 2009). In one study cohort, there were a number of children with marked protan or protan/deutan deficits who had relatively good visual acuities (Votruba et al., 1998a). The colour vision deficiencies are therefore not confined to the tritan axis, although it is the more severely affected axis (Holder et al., 1998; Johnston et al., 1999).

1.3.3 Syndromic dominant optic atrophy

The syndromic form of ADOA (ADOA+) is associated with extra-ocular features including neurosensory hearing loss, progressive external ophthalmoplegia, ataxia, myopathy and peripheral neuropathy, stroke or multiple sclerosis (Payne et al., 2004; Yu-Wai-Man et al., 2010b). ADOA+ patients usually experience

more severe visual deficits and represent up to 20% of DOA patients with an *OPA1* mutation (Amati-Bonneau et al., 2008; Hudson et al., 2008; Yu-Wai-Man et al., 2010a; Yu-Wai-Man et al., 2010b).

The most prominent manifestation after optic atrophy in these patients is bilateral sensori-neural deafness (occurs in about 60% of cases) beginning in late childhood and early adulthood (Yu-Wai-Man et al., 2010b). Sensori-neural hearing loss ranges from subclinical to severe forms and is associated with a particular *OPA1* mutation; a heterozygous guanine to adenine (G>A) transition in the second nucleotide at codon 445 in the *OPA1* gene, resulting in an arginine-445-to-histidine (R445H) substitution in the GTPase domain (Shimizu et al., 2003; Amati-Bonneau et al., 2005). The combinations of external ophthalmoplegia, ataxia, myopathy or peripheral neuropathy are usually manifest after the third decade of life and are associated with all types of mutations; however, there was an increased risk with missense mutations and with mutations located within the GTPase region (Yu-Wai-Man et al., 2010b).

The mean age of onset of these plus features suggests a chronological pattern: visual failure occurs within the first decade, followed by deafness in late childhood to early adulthood, and then a combination of ataxia, myopathy, peripheral neuropathy and progressive external ophthalmoplegia from the third decade of life onwards (Figure 1.9). Subclinical neurological defects reported in some “pure” ADOA patients also appeared to be age dependent suggesting that multisystem involvement in *OPA1* ADOA may be more pervasive than previously thought, but that the risk of developing clinically overt extra-ocular disease increases with age (Baker et al., 2011).

In the spectrum of ADOA+ phenotypes, a severe early-onset neuromuscular phenotype (hypotonia, delayed motor development, ataxia, dysphagia, and gastrointestinal disability) caused by compound heterozygous mutations in the *OPA1* in two siblings has been described (Schaaf et al., 2011) and there have also been reports of patients presenting extra-ocular features in the absence of visual loss (Yu-Wai-Man et al., 2010b).

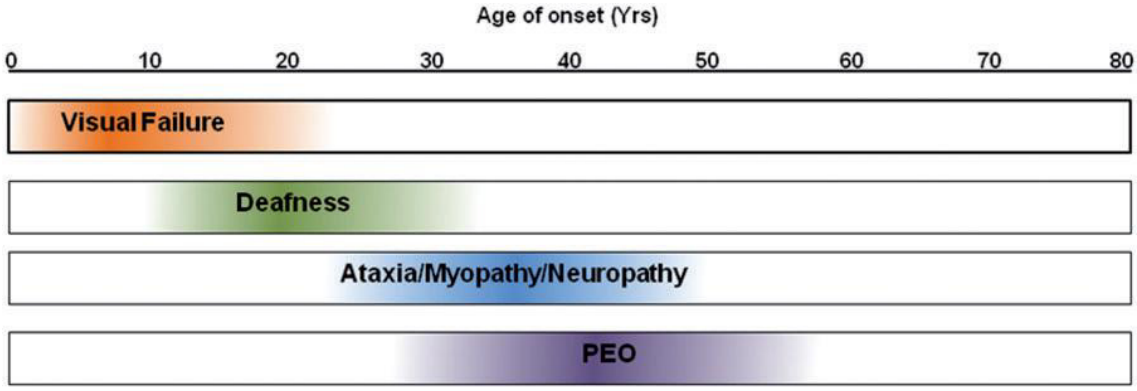

Figure 1.9. Evolution of the major clinical features observed in ADOA+ syndromes. POE – progressive external ophthalmoplegia (Yu-Wai-Man et al., 2010b)

1.3.4 The *OPA1* Gene and its Functions

The *OPA1* gene maps to chromosome 3q28-q29 and comprises 29 exons of spanning more than 100kb genomic DNA of which 28 are coding exons (Alexander et al., 2000; Delettre et al., 2000) (Figure 1.10). The gene encodes eight *OPA1* isoforms resulting from alternate splicing of exons 4, 4b and 5b (Figure 1.11) and the presence of these exons specifies the function of the isoform. By including the alternatively spliced exons 4, 4b, and 5b, the *OPA1* gene contain 31 exons (Delettre et al., 2001; Olichon et al., 2007).

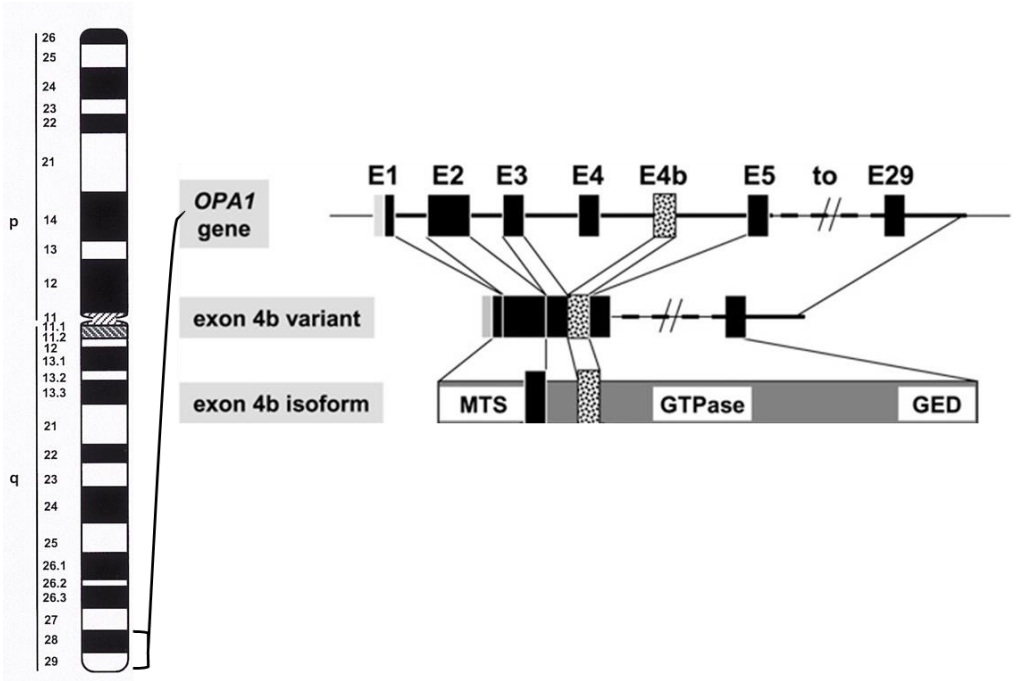

Figure 1.10. A composite diagram depicting human chromosome 3 showing the position of *OPA1* (left) (Delettre et al., 2000) and a schematic representation showing the encoding of *OPA1* (exon 4b isoform) gene (right). (Elachouri et al., 2011) E1 – E29 - *OPA1* exon 1 to exon 29. MTS – Mitochondrial targeting sequence; GED – GTPase effector domain.

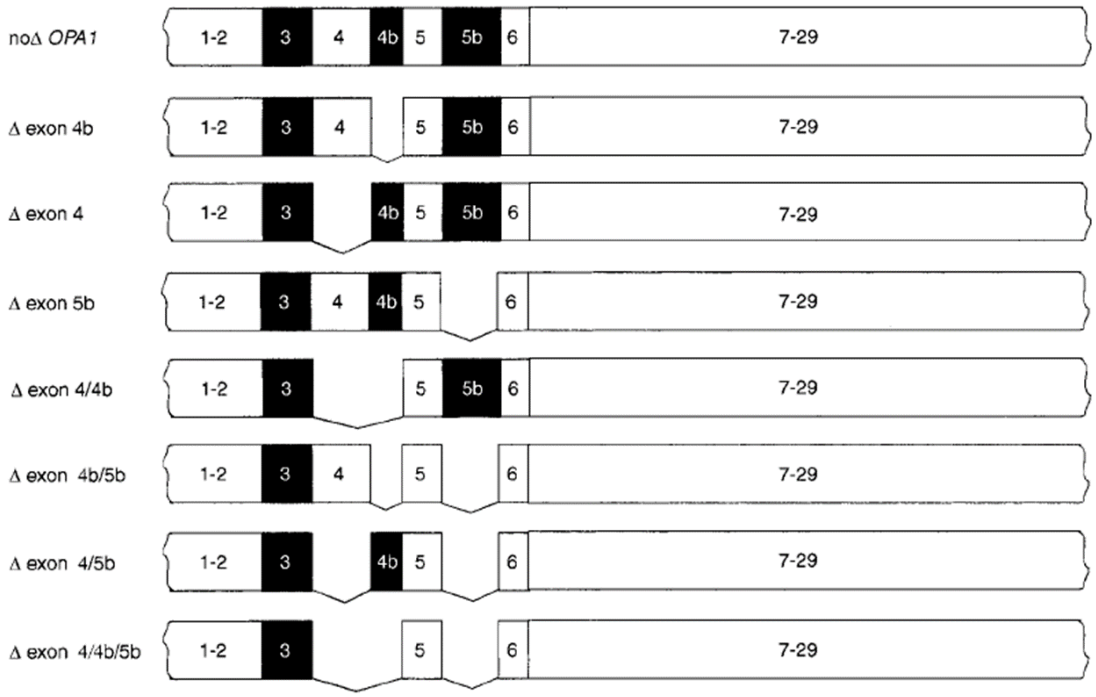

Figure 1.11: Alternative splicing patterns in human *OPA1*. Schematic representation of the 8 alternative transcripts found by RT-PCR. Numbers indicate exons (Delettre et al., 2001).

OPA1 protein is found in many tissues of the body: in the heart, skeletal muscles, liver, testes, the ear, and most abundantly in the brain and retina. In the eye, *OPA1* is present in the cells of the RGC layer, inner and outer plexiform layers and the inner nuclear layer (Aijaz et al., 2004; Pesch et al., 2004; Kamei et al., 2005).

The *OPA1* protein is a dynamin-related guanosine triphosphatase (GTPase) made up of 960 amino acids (Alexander et al., 2000; Delettre et al., 2000; Davies and Votruba, 2006). GTPases are a large family of enzymes that bind and hydrolyse guanosine triphosphate (GTP) to guanosine diphosphate (GDP). Dynamin-related proteins have three characteristic domains, a GTPase domain, a central domain that is conserved among all dynamins, and a GTPase effector domain (GED); and are associated with diverse cellular processes, including the release of transport vesicles, fusion and fission of mitochondria, cell division and resistance to viral infections (Heymann and Hinshaw, 2009). Other examples of dynamin related GTPases are mitofusions and dynramin-related protein-1 (DRP1) (Santel and Fuller 2001; Smirnova et al. 2001; Chen et al. 2003; Olichon et al. 2003).

The *OPA1* protein contains a mitochondrial targeting sequence (MTS), by which it is imported into mitochondria, a GTPase domain, a central dynamin domain, and a GED (Figure 1.10) (Chen and Chan, 2005; Davies and Votruba, 2006). Within the cell, the protein is found in the inner mitochondrial membrane where it is involved in mitochondrial fusion and helps regulate mitochondrial morphology (Chen and Chan, 2005; Fuhrmann et al., 2010). It is also involved in oxidative phosphorylation (OXPHOS) required to produce cellular ATP (Lodi et al., 2004; Lodi et al., 2011). In addition, it plays a protective role by sequestering cytochrome-c within the mitochondrial cristae thereby inhibiting cellular apoptosis (Olichon et al., 2003). There is also evidence that *OPA1*, specifically the exon-4b isoforms influences replication of mitochondrial DNA and is involved in the maintenance of the mitochondrial DNA (Elachouri et al., 2011).

1.3.5 Pathogenesis and Molecular Genetics of ADOA

Most mutations in the *OPA1* gene leads to a haplo-insufficiency situation where the mutated transcripts are degraded by mRNA decay (Alexander et al., 2000; Delettre et al., 2000; Lenaers et al., 2012). This mRNA decay leads to ~50% reduction in the amount of *OPA1* protein produced, thus affecting mitochondrial function. This is thought to result in an insufficient energy supply to the highly energy demanding neurons of the optic nerve, notably the papillomacular bundle, thereby causing blindness by compromising axonal transport in the RGCs (Alexander et al., 2000; Puomila et al., 2005).

There are over 300 mutations of the *OPA1* gene which cause ADOA (http://mitodyn.org/home.php?select_db=*OPA1*, accessed 14/10/2015) and the majority arise in the GTPase and dynamin central regions coded by exons 8 to 24 (Figure 1.12) (Thiselton et al., 2002; Davies et al., 2007; Ferre et al., 2009; Ferre et al., 2015). About 26% of the mutations are missense, 16% lead to frameshift mutations, 14% are nonsense and 6% are deletion or duplication. The different mutations in *OPA1* are not related to the severity of the disease and genotype/phenotype correlations are difficult to infer, however, missense mutations and mutations occurring in the GTPAse domain increase the risk of developing ADOA+ phenotypes in affected individuals (Yu-Wai-Man et al., 2010b; Barboni et al., 2014). In this respect, secondary nuclear genes are

suspected to control the severity of the disease in non-syndromic DOA (Puomila et al., 2005).

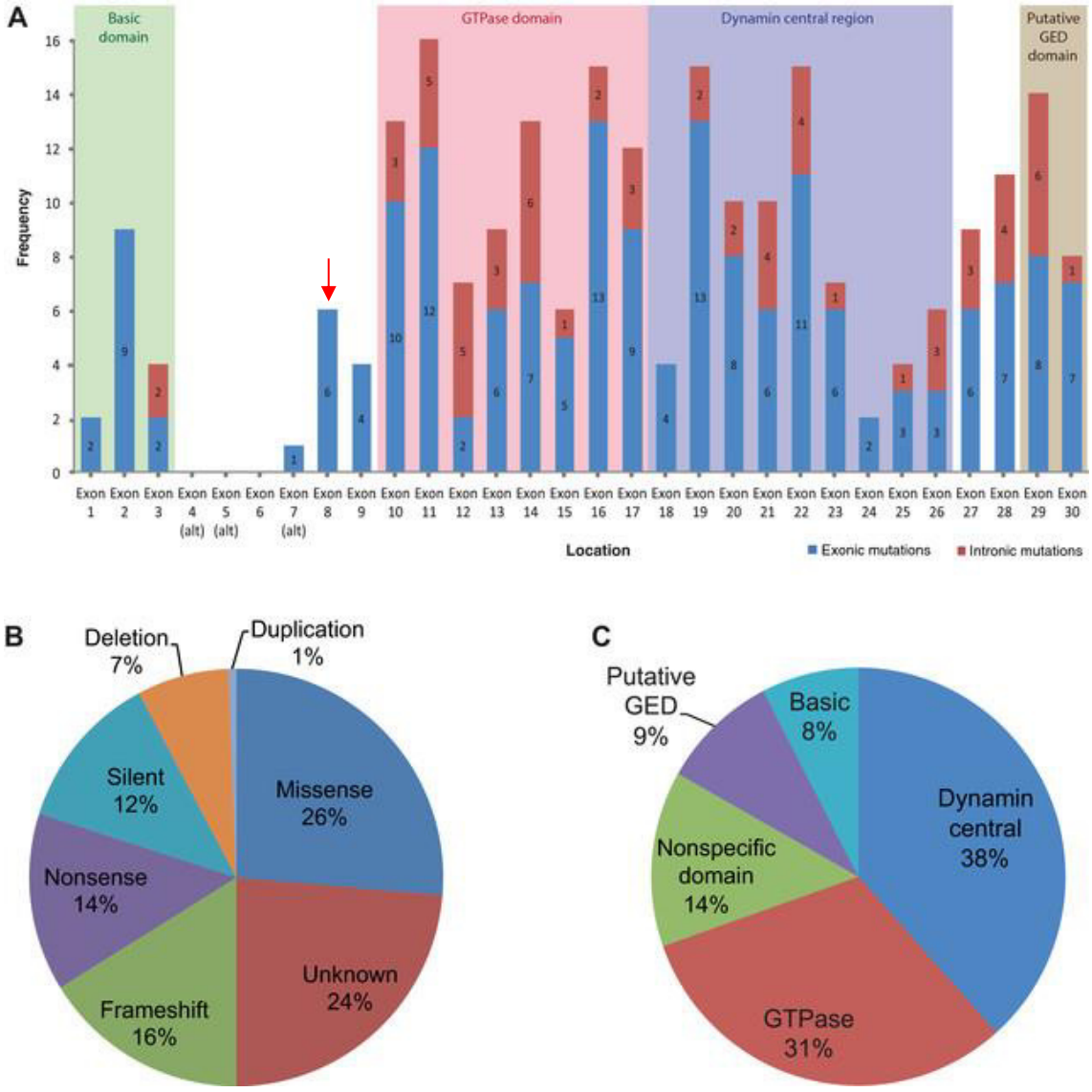

Figure 1.12 Distribution of 233 pathogenic mutations of *OPA1* gene. (A) Exons involved in the variants are shown as blue bars; the variants in the intronic neighbourhood of the exons are shown as red bars. (B) Protein consequence type. (C) Affected domain. Alt - alternative exon; bp - base pairs; GED - GTPase effector domain (Ferre et al., 2015). Red arrow indicates the site of a nonsense mutation in the B6:C3*Opa1*^{Q285STOP} mouse model of ADOA (Davies et al. 2007).

1.3.6 Peculiar Susceptibility of RGCs in ADOA

It is unclear why mutations in *OPA1* leading to ADOA primarily affect the RGCs even though the *OPA1* gene is present in all body tissues (Aijaz et al., 2004; Davies and Votruba, 2006; Sarzi et al., 2012). It is thought that the disease exploits certain peculiar anatomical and physiological constrains of the optic nerve (Yu-Wai-Man et al., 2011b). One such feature is that the axons of RGCs

only acquire a myelin sheath beyond the lamina cribrosa. In the pre-laminar section, the generation and propagation of action potentials are therefore less efficient and require greater energetic input (Carelli et al., 2004; Yu-Wai-Man et al., 2011b). There is therefore a greater accumulation of mitochondria in the pre-laminar (unmyelinated) region than the post-laminar region, creating a differential concentration of mitochondria across the lamina cribrosa (Bristow et al., 2002; Yu Wai Man et al., 2005). The pre-laminar regions of the optic nerve could therefore be viewed as a vulnerable metabolic chokepoint, magnifying the consequences of any impairment in mitochondrial oxidative phosphorylation, however subtle. As the energetic fuelling of RGC in the central retina is further restricted due to the physical constraints imposed by the macula blood vessel organisation, it is hypothesised that ATP synthesis in the RGCs of patients is limited and cannot fulfil the physiological energetic requirements required for long term cell survival due the uncoupling of mitochondrial respiration by the mutation (Alavi et al., 2007; Davies et al., 2007). Interestingly, in two family members with optic atrophy and hearing loss due to a pathogenic *OPA1* mutation, the defect was localised to the terminal unmyelinated portions of the cochlear nerve, which is another cranial nerve marked by a dramatic transition between unmyelinated and myelinated segments (Huang et al., 2009). Furthermore, RGCs are the only neurons of the body that are exposed to the day long stress of light, which generates oxidative species favouring the apoptotic process (Osborne et al., 2008). Therefore, the mitochondrial fragility conferred by *OPA1* mutations together with the photo-oxidative stress could precipitate RGC premature death. Another hypothesis relates to the observation in a mouse model that neuronal tissues and glycolytic muscles on the one hand, and oxidative tissues and the heart, on the other, compensate differently for the loss of mutated *OPA1* transcripts (Sarzi et al., 2012). A common mitochondrial cytochrome oxidase defect is observed in the retina, optic nerve and glycolytic muscle fibres, whereas brain, oxidative muscles and heart are unaffected. In the retina, the cytochrome oxidase defect precedes the onset of visual failure and is thought to contribute to the pathological mechanism leading to RGC death.

1.3.7 Other Loci Associated with Hereditary Optic Atrophy

The first ADOA locus, *OPA1*, located on 3q28 was initially considered unique (Eiberg et al., 1994; Bonneau et al., 1995). However, some ADOA families were

shown to exclude linkage to the *OPA1* locus suggesting genetic heterogeneity of the disease (Seller et al., 1997; Kerrison et al., 1999). Subsequently, additional loci and genes were identified in patients with ADOA phenotypes, but these were associated with different modes of inheritance or syndromic forms (Table 1.3 and 1.4).

Table 1.3. Loci and genes of hereditary optic atrophy. Adapted from Lenaers et al, 2012

Locus	Chromosome	Gene	Mode of Inheritance	Reference
OPA1	3q28-29	*OPA1*	Dominant	(Alexander et al., 2000; Delettre et al., 2000)
OPA2	Xp11.4-p11.21	Unknown	X-linked	(Assink et al., 1997)
OPA3	19q13.2-q13.3	OPA3	Dominant/recessive	(Anikster et al., 2001)
OPA4	18q12.2-q12.3	Unknown	Dominant	(Kerrison et al., 1999)
OPA5	22q12.1-q13.1	Unknown	Dominant	(Barbet et al., 2005)
OPA6	8q21-q22	Unknown	Recessive	(Barbet et al., 2003)
OPA7	11q14.1-q21	TMEM126A	Recessive	(Hanein et al., 2009; Hanein et al., 2013)
OPA8	16q21-q22	Unknown	Dominant	(Carelli et al., 2011)

Table 1.4. Clinical features associated with ADOA caused by mutations in *OPA 1 – 8*. Adapted from Lenaers et al, 2012

Locus	Optic Atrophy	Deafness	Poly neuropathy	Myopathy CPEO	Cardio-myopathy	Cataract
OPA1	+	+/-	+/-	+/-	-	-
OPA2	+	-	-	-	-	-
OPA3	+	-	-	-	-	+
OPA4	+	-	-	-	-	-
OPA5	+	-	-	-	-	-
OPA6	+	-	-	-	-	-
OPA7	+	+/-	-	-	+/-	-
OPA8	+	+/-	-	-	+/-	-

Legend: (+) = systemic; (+/-) = possible; (-) = never reported

OPA4 and OPA5 were mapped to chromosome 18q12.2-q12 and chromosome 22q12.1–q13.1 respectively (Kerrison et al., 1999; Barbet et al., 2005); however, the underlying genes are currently unknown. The phenotype of affected patients with *OPA4* and OPA5 was similar to that of patients harbouring *OPA1* mutations. *OPA3* and TMEM126A (OPA7) are two other genes that have been identified so far. They both encode mitochondrial proteins ubiquitously expressed and associated to the inner mitochondrial membrane. *OPA3* mutations may be inherited in a dominant or recessive pattern while TMEM126A mutations are inherited in a recessive pattern (Reynier et al., 2004; Hanein et al., 2009; Huizing et al., 2010; Hanein et al., 2013).

OPA3 mutations were first identified in Iraqi Jewish families with Type III 3-methylglutaconic aciduria (Costeff syndrome); an autosomal recessive neurodegenerative disorder characterised by optic atrophy, progressive neurodegeneration, increased urinary levels of 3-methylglutaconic acid, and elevated plasma 3-methylglutaric acid levels (Anikster et al., 2001). Pathogenic mutations were subsequently found in two independent French families segregating both optic atrophy and premature cataract in an autosomal-dominant mode of inheritance (ADOAC) (Reynier et al., 2004). However, *OPA3* mutations are likely to be extremely rare, especially in isolated optic atrophy cases; two large scale screening of individuals with hereditary optic atrophy without *OPA1* mutations did not identify any pathogenic *OPA3* mutations (Yu-Wai-Man et al., 2010a; Yu-Wai-Man et al., 2011c).

Mutations in the OPA7 gene cause a non-syndromic autosomal recessive optic atrophy. It has a juvenile onset and it is extremely rare; it has so far been found in only five families, all of Algerian or Moroccan descent (Desir et al., 2012; Hanein et al., 2013). Thus to date, *OPA1* is the major gene responsible for ADOA, accounting for at least of 60 – 70% all the patients, whereas all the other genes or loci only contribute each for less than 1% of the patient cohort (Ferre et al., 2009; Yu-Wai-Man et al., 2010a). The clinical features of the various OPA loci are summarised in Table 1.4.

1.3.8 Current Management

The management of ADOA patients consists in regular ophthalmologic examination, including measurement of visual acuity, colour vision, visual fields and OCT and refraction. In the experience of the author and from anecdotal reports, this provides re-assurance to patients and promotes their psychological wellbeing. To date, no specific treatment exists, but low-vision aids in patients with severely decreased visual acuity can be beneficial (Lenaers et al., 2012). Patients should be registered as visually impaired or severely visually impaired to assist in visual rehabilitation, education and employment. As a general health measure, patients should be strongly advised to avoid smoking and to moderate their alcohol consumption since and smoking and alcohol are associated with an increased risk of visual failure (Yu-Wai-Man et al., 2011b). Genetic counselling should be given to families with ADOA and pregnant women can

request prenatal testing (amniocentesis or chorionic villus sampling) after having been appropriately counselled.

Since the pathogenic mutations in ADOA (and LHON) eventually destabilise complex I resulting in a reduction in ATP synthesis and increased ROS levels, an attractive treatment strategy is to restore the flow of electrons along the mitochondrial respiratory chain by bypassing the blockage occurring at the level of complex I and enabling or maximising the direct shuttling of electrons to complex III. Ubiquinone is an essential carrier that ensures the efficient transfer of electrons along the mitochondrial respiratory chain. Idebenone is a synthetic analogue of ubiquinone and a randomised controlled trial carried out in 85 patients with LHON showed beneficial effects and no adverse drug reactions in the active arm of the cohort on a dose of 900mg/day (Klopstock et al., 2011; Klopstock et al., 2013). Consequently, a pilot study on 7 patients with ADOA was carried out and showed variable improvements in visual acuity and visual field mean defects in 5 patients (Barboni et al., 2013). Idebenone is commercially available under the name Raxone® (Santhera Pharmaceuticals Ltd, Liestal, Switzerland) in 150mg tablets and it is the first medicine to be approved by the European Union for the treatment of visual impairment in adolescents and adult patients with LHON (http://www.santhera.com/index.php?mid=15&vid=&lang=en, accessed 15/10/2015). More research is being carried out on the efficacy and safety of the medicine in the treatment of LHON and ADOA (Yu-Wai-Man et al., 2014).

In the area of developing treatment, near-infrared light (NIR) has been shown to improve mitochondrial function and cellular survival in various models of wound healing, neurodegeneration and methanol-induced retinal toxicity (Desmet et al., 2006). The potential of NIR in rescuing RGC loss is also being tested in a mouse model of ADOA (M Votruba 2015, personal communication, October). An open labelled study of EPI-743, another ubiquinone analogue, for patients with ADOA is under preparation (Yu-Wai-Man et al., 2014). The National Institute for Health Research (NHIR) is spearheading an ambitious translational research programme for rare genetic diseases in the United Kingdom. Inherited optic neuropathies have been selected as one of the priority disease themes. The purpose of the study is to undertake deep phenotyping of patients with

LHON and ADOA to define the natural history of the visual loss and to identify the most sensitive parameters for monitoring disease progression. Importantly, this study will provide useful information on the visual outcome measures that are most likely to reveal a clinically meaningful treatment effect in future clinical trials for pipeline neuroprotective agents.

1.3.9 Mouse Models: What they tell us about *OPA1* in ADOA

Mice are widely used as genetic disease models due to the relative ease of genetic manipulation and high homology to the human genome. The murine retina shows relatively good homology to the human retina, rendering the mouse suitable for modelling a wide range of human visual diseases with a genetic basis (Smith et al., 2002). Three mouse models have so far been published providing insight into the pathophysiology regarding ADOA (Alavi et al., 2007; Davies et al., 2007; Sarzi et al., 2012). However, these models are not perfect because of the range of anatomical limitations in comparing the murine eye to the human eye.

A description of the B6:C3*Opa1*^{Q285STOP} mouse model of ADOA which was developed previously in our laboratory is provided below to highlight the points of interest relevant to this study. A summary of the characteristics of the three ADOA mouse models is provided in Table 1.5.

1.3.9.1 The B6:C3*Opa1*^{Q285STOP} Mouse Model

Davies et al (2007) generated mutant mice carrying an ethylnitrosourea (ENU)-induced mutation in the *Opa1* gene, resulting in a truncated protein. The mutant mouse was generated by screening an ENU-mutagenised DNA archive from C3HeB/FeJ males and selecting a heterozygous nonsense mutation in exon 8 (arrowed in Figure 1.12), which codes for a C–T transition at 1051 base pairs (Q285STOP). This mutation causes protein truncation at the beginning of the dynamin GTPase, close to the location of a number of human disease mutations (c.868C>T (R290 W) and c.869G>T (R290Q) (Ferre et al., 2005; Davies et al., 2007; Williams et al., 2011).

Western blot analysis in heterozygous mutants showed that the mutation resulted in in approximately 50% reduction in *Opa1* protein in the retina and all tissues suggesting that haploinsufficiency underlies the pathophysiological mechanism. The homozygous mutation was embryonic lethal by 13.5 days post-coitum. Fibroblasts taken from the muscle of *Opa1* +/- adult heterozygotes showed an increase in mitochondrial fission and fragmentation compared to wild-type littermates, highlighting the importance of *OPA1* in proper mitochondrial function and morphology. Davies et al (2007) concluded that the *OPA1* GTPase contains crucial information required for the survival of RGCs and that *OPA1* is essential for early embryonic survival.

In addition, electron microscopy revealed the slow onset of optic nerve degeneration starting from 9 months (White et al., 2009); while visual function in heterozygotes demonstrated by optokinetic drum testing and the circadian running wheel was reduced from 12 months (Davies et al., 2007). However, there was no significant change in the number of axons per area optic nerve between wild-type and *Opa1*+/- mice at 6, 9 and 24 months of age to suggest RGC death (White et al., 2009; Williams et al., 2010). Further investigations revealed a selective dendritic pruning in ON-centre RGCs, with no significant changes in the OFF-centre RGCs in mutant mice starting at about 10 months (Figure 1.13) (Williams et al., 2010; Williams et al., 2012). The phase of active dendritic pruning was accompanied by significant changes in synaptic density, synaptic structure and mitochondrial morphology within the synaptic bouton (Williams et al., 2012). These findings imply that synaptic atrophy coincides with or precedes dendritic atrophy, suggesting that dendritic atrophy (and consequently visual dysfunction) may be driven at the level of the synapse. Notably, all these changes occurred in the absence of significant RGC loss and preceded visual loss.

Visual electrophysiology (VEP and ERG) testing in 11 and 13 month old mutant mice showed deficits consistent with RGC dysfunction (Barnard et al., 2011). The a-wave and b-wave of the photopic ERG showed no significant difference between wild-type controls and mutant mice. However, there was a significant reduction in the photopic negative response (PhNR) amplitude, an ERG component known to reflect RGC function (Viswanathan et al., 1999;

Viswanathan et al., 2000; Viswanathan et al., 2001), in mutant mice compared to wild-types (Figure 1.14). (A detailed description of the PhNR is presented in section 1.4.2.5 and 1.4.3.). This electrophysiological finding and the novel finding that ADOA selectively affects the ON-RGCs provided the basis for this project to examine the ON and OFF RGC function separately in affected ADOA patients using electrophysiologic techniques.

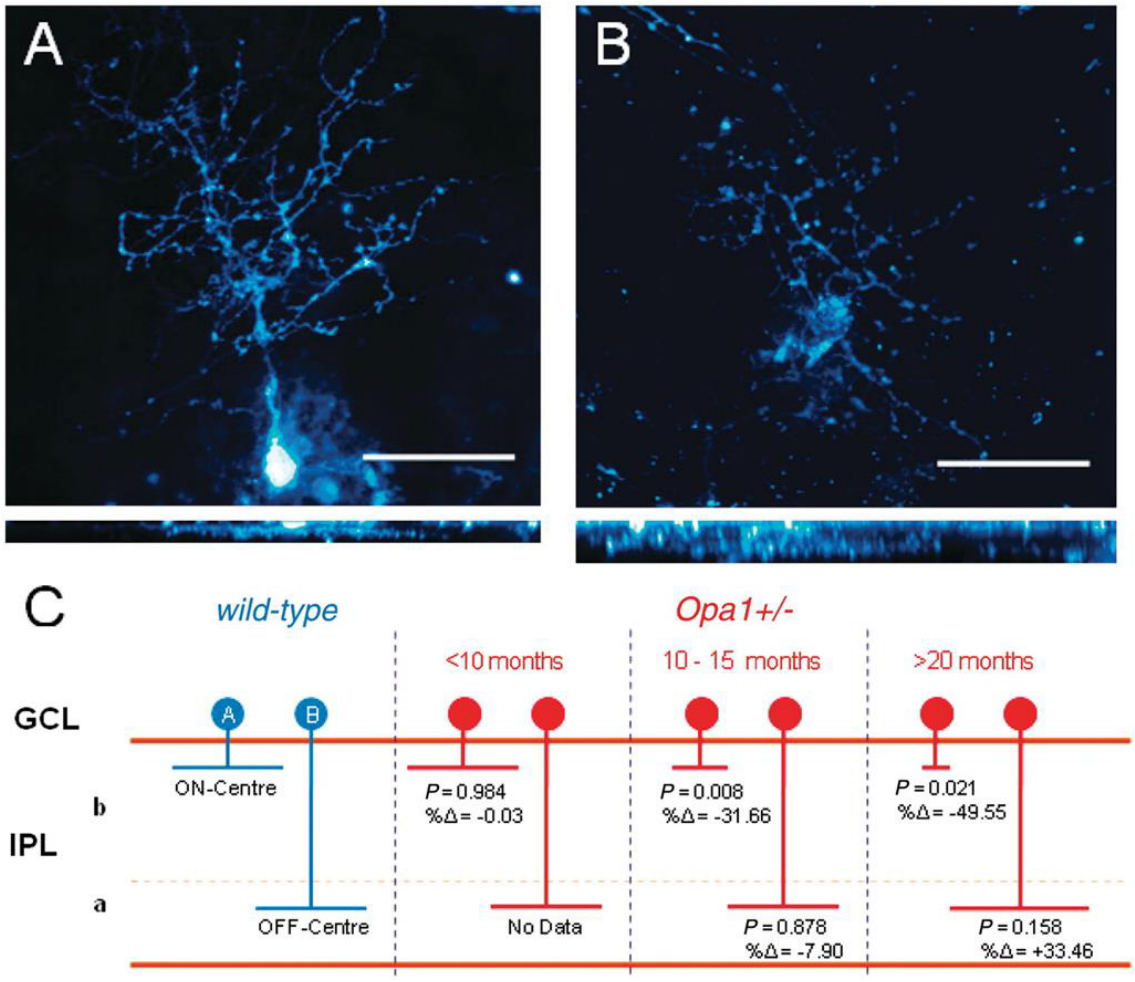

Figure 1.13. Selective dendritic pruning of ON-centre RGCs in *Opa1* deficiency. Examples of ON- and OFF-centre RGCs from an adult (10-month-old) wild-type mouse showing their normal dendritic arbours (A and B respectively). Scale bar = 25 µm. The dendrites of ON-centre RGCs ramify in sublamina b (close to the level of the cell body) and the dendrites of OFF-centre RGCs ramify in sublamina a (close to the inner nuclear layer). Total dendritic length is reduced in the ON-centre RGCs of 10- to 15-month-old and >20-month-old mice (C) while remaining statistically unchanged in OFF-centre RGCs. P = Student's t-test, %Δ = percentage change from wild-type. GCL = ganglion cell layer; IPL = inner plexiform layer (Williams et al., 2010).

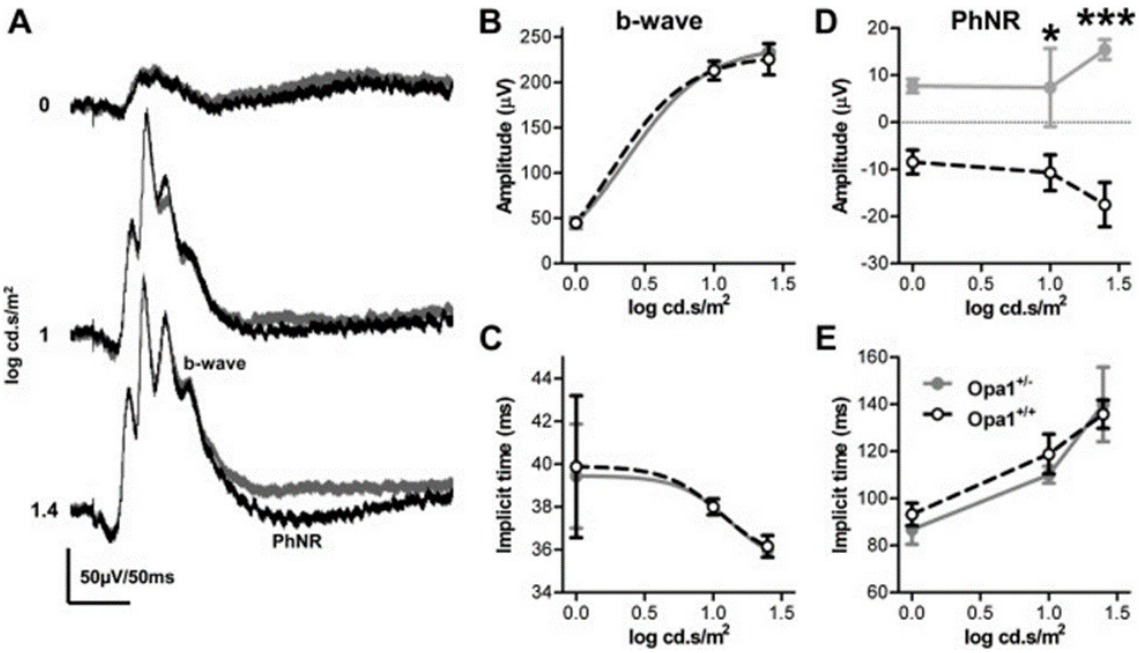

Figure 1.14. Reduction in the photopic negative response amplitude of the light-adapted ERG in *Opa1*$^{+/-}$ mice.Averaged traces for each genotype (n = 5 for both). Stimulus intensity shown on right, values are in log cd.s/m^2. Quantification of (B) amplitude of b-wave, (C) time-to-peak of b-wave, (D) amplitude of PhNR and (E) time-to-peak of PhNR. Plotted values are mean ± SEM, n = 5. * = p < 0.05, *** = p < 0.001: significance of Bonferroni post-tests after repeated measures two-way ANOVA with genotype and stimulus intensity as factors. Wild-type control (*Opa1*+/+) traces and values are shown in black empty symbols, heterozygote mutants (Opa+/-) are in grey/filled symbols (Barnard et al., 2011).

Table 1.5. Comparison of the characteristics of three mouse models of ADOA. Modified from William et al. 2011.

Characteristic	B6:C3-*Opa1*^{Q285STOP} (Davies et al., 2007)	B6:C3-*Opa1*$^{329\text{-}355del}$ (Alavi et al., 2007)	*Opa1*^{delTTAG} (Sarzi et al., 2012)
Mouse type	Strain: C3H:C57B1/6J	Strain: C3H:C57B1/6J	Strain: C57Bl6/J
Mutation	Exon 8; nonsense mutation At DNA level: c. 1051 C>T At protein level: p.Q285X; 50% reduction in protein levels	Intron 10; splice site mutation At DNA Level: c. 1065+5G>A At protein level: p.329-355del; 50% reduction in protein levels	Exon 27; deletion At DNA level: c. 2708-2711 delTTAG At protein level: 25-50% reduction in protein level
Homozygous mutant	Embroyonic lethality <E13.5	Embroyonic lethality ca8.5	Embroyonic lethality <E10.5
Mitochondria	mtDNA copy number: no significant difference compared to wild-type counterparts. Morphology: powdered appearance, increased mitophagy	mtDNA copy number: no significant difference compared to wild-type counterparts. Morphology: disorganised cristae	mtDNA copy number: increased in neuronal tissues, especially optic nerve. Morphology: disorganised cristae, increased mitohpagy
Visual function and electrophysiology	Decreased visual function assessed by OKN and circadian running wheel Reduced PhNR amplitude	Decrease in VEP amplitude No significant change in ERG even in aged mice	Increased latency in VEP No significant reduction in VEP amplitude No significant changes in ERG
ERG stimulus	Full-field white flash on white background. Flash duration = 4 msec; Flash luminance = 0.0, 1.0, 1.4 log cd.s/m^2; Background = 30 cd/m^2 (Barnard et al., 2011)	Full-field white flash on white background. Flash duration = Not given; Flash luminance = -2.0, -1.0, 0.0, 1.0 log cd.s/m^2; Background = 30 cd/m^2 (Jaissle et al., 2001)	Not given
Plus phenotype	Increased transfer arousal, longer freezing periods, decreased locomotor activity No COX-SDH ragged red fibres, no hearing loss	Abnormal clutching reflex, tremor, decreased locomotor activity, lighter weight, less body fat than wild-type, no COX-SDH ragged red fibres, no hearing loss	Encephalomyopathy, Ataxia, Peripheral neuropathy, Cardiomyopathy, Severe hearing loss, Premature ageing
Optic nerve	Demyelination, myelin clumping, watery degeneration, no axon loss	Demyelination; disorganisation, swollen and distorted axons, complete loss of large axons, significant loss of small axons	Demyelination, myelin vacuolisation, swollen axons
RGC population and morphology	Dendritic atrophy of ON-centre RGC with age No significant difference in population	Reduction with age starting at 13 months	Reduction with age starting at 16 months
ON-/OFF-RGC lamination examined	Yes	No	No

1.4 Ocular Electrophysiology

Electrophysiologic techniques provide a valuable objective non-invasive means of assessing the integrity of the visual pathway. The electroretinogram (ERG), the electro-oculogram (EOG) and the visual evoked potential (VEP) are the most commonly used types in clinical practice (Weisinger et al., 1996; Wolpert and Tsang, 2011). The ERG provides an objective assessment of retinal function whereas the EOG evaluates the function of the retinal pigment epithelium-photoreceptor complex. The VEP evaluates the pathway to the striate cortex (Weisinger et al., 1996). Other electrophysiologic techniques include the electromyogram for the assessment of the extra-ocular muscles and the electronystagmography, for measurement of nystagmus and eye movements (http://www.iscev.org/standards/proceduresguide.html, accessed 22/08/2016).

Two important characteristics make electrophysiologic techniques different from others; they are both functional and objective. Many ocular tests such as angiography, ultrasonography and OCT are objective, but provide structural information rather than functional, and some, such as perimetry and contrast sensitivity test are functional, but not objective (Movassat, 2012). Clinical electrophysiological testing became practical in the middle of the twentieth century, but a wide variety of procedures were used by different laboratories to elicit responses. Comparing data among research or clinical reports was therefore very difficult and this impeded both clinical care and the interpretation of clinical research. The International Society of Clinical Electrophysiology of Vision (ISCEV) was founded in 1961 in recognition of the need for standardisation of these techniques and since 1989, ISCEV has published standards for clinical electrophysiological techniques (Marmor and Zrenner, 2006). This review focuses on the ERG which was the electrophysiological technique used in this thesis.

1.4.1 The Electroretinogram

The term “electroretinogram” refers to a number of electrodiagnostic waveforms or techniques that test retinal function (Figure 1.15). The different ERG types are produced by manipulating the stimulus and testing conditions in order to

investigate different cell types, layers or areas of the retina (Wolpert and Tsang, 2011). A single flash of light evokes a transient ERG (Figure 1.15, A – C, E) while a flickering stimulus (e.g. 30 Hz) evokes a flicker or steady state ERG Figure 1.15F). A patterned stimulus can also be used to evoke a pattern ERG (discussed later in section 1.4.3). In all cases, electrodes placed on the cornea or conjunctiva and around the orbit record changes in the electrical potential of the eye in response to specific (light) stimuli (Weisinger et al., 1996).

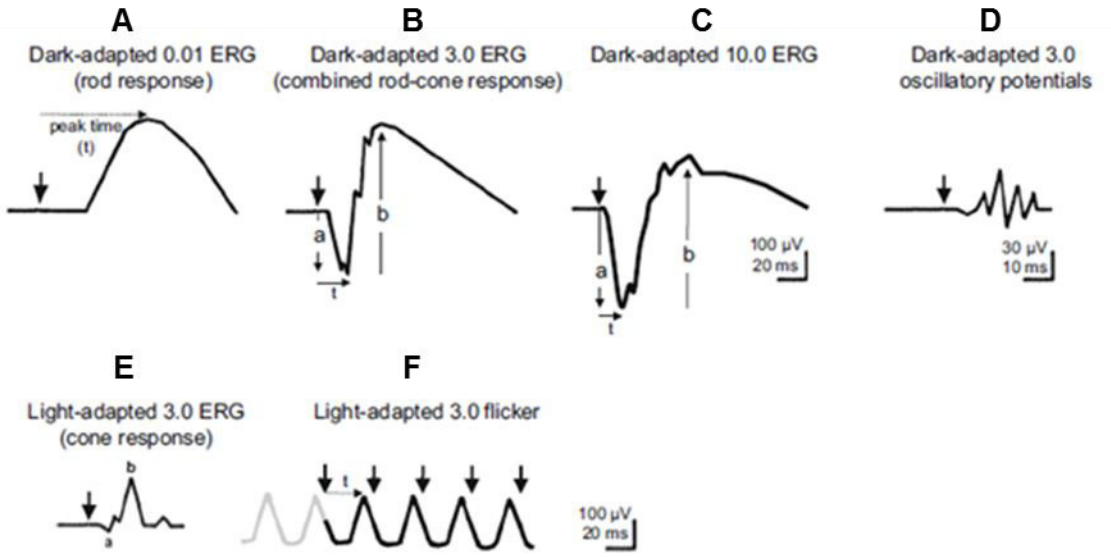

Figure 1.15. Diagram of the six basic ERGs defined by the ISCEV Standard. Bold arrowheads indicate the stimulus flash; solid arrows illustrate a-wave and b-wave amplitudes dotted arrows exemplify how to measure time-to-peak (t or time-to-peak). The headings describe the stimulus (and response) names by their state of light adaptation and the flash strength in photopic cd.s/m^2 (McCulloch et al., 2015).

1.4.2 The Flash Electroretinogram

The flash ERG is a recording of the summed potential changes generated by the retina in response to a single flash of light (Figure 1.16) (Fishman, 2001). This retinal potential can be recorded in all vertebrates and in many invertebrates, e.g. Drosophila, however, the waveforms for each species are different (Fishman, 2001; Wolpert and Tsang, 2011). Different waveforms are also produced under different recording conditions (e.g. photopic or scotopic) and stimulus parameters (e.g. frequency of stimulation, wavelength, luminance, duration and size of stimulus). The focus of this review is on the human ERG elicited under photopic conditions.

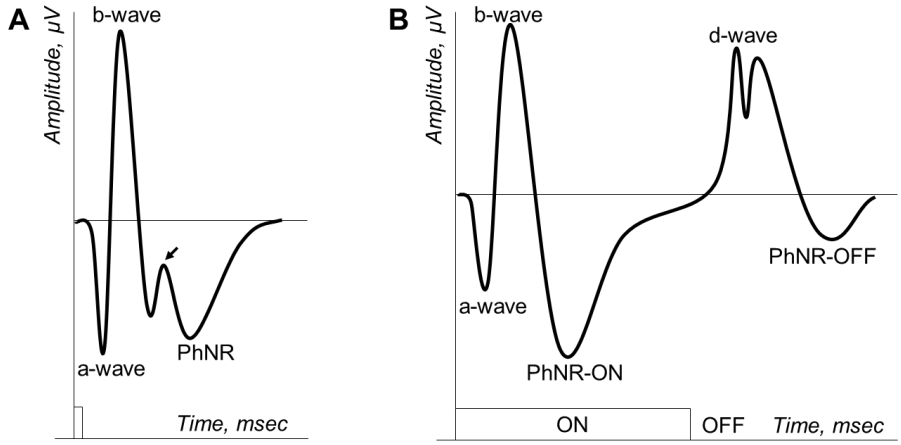

Figure 1.16 Representative full-field ERGs showing the recorded response to (A) a brief flash and (B) a long duration flash. In response to the long duration flash, the ERG is separated into ON and OFF components as indicated on the time axis. The positive going wave interrupting the descending limb of the b-wave arrowed in A is the i-wave. Diagrams are not to scale.

The major components of the photopic ERG in humans are shown in Figure 1.16. A brief flash ERG comprises the a-wave, b-wave and photopic negative response (PhNR). In addition to these, other components can be identified on the ERG by manipulating experimental recording conditions. These components include the early receptor potential and c-wave (not shown, both best recorded under dark adapted condition in response to a bright flash), the oscillatory potentials (seen as wavelets riding on the ascending limb of the b-wave in Figure 1.15B) and the i-wave (arrowed in Figure 1.16A) (Perlman, 2001). The d-wave is a component seen only in long duration ERGs (Figure 1.16B) (Perlman, 2001). The PhNR is also separated into the PhNR-ON and PhNR-OFF using a long duration flash (Viswanathan et al., 1999).

The words “brief” or “short” and “long” are arbitrary qualifiers used by electrophysiologists to refer to stimulus durations in relation to the temporal integration time of photoreceptors. The integration time refers to the time within which a photoreceptor summates or collects a sample of photons while producing a single response (Warrant, 1999; Kolloniatis and Luu, 2007). For rods it is about 100 msec while for cones it is 10-15 msec (Kolloniatis and Luu, 2007). Brief flashes (shorter than the photoreceptor integration time) produce a combined response from the ON and OFF pathways of the retina while long duration flashes (>100ms) separate the ERG into ON and OFF components (Sieving, 1993; Kondo et al., 2000; Sustar et al., 2006). In this thesis, the terms

"brief ERG" and "long ERG" will be used in reference to ERGs obtained with brief and long duration flashes respectively.

The ERG components are evaluated by measuring both amplitude and timing characteristics (Figure 1.17). The latency is the time from the onset of the stimulus until the beginning of the response and the time-to-peak is the time from the onset of the light stimulus until the peak amplitude response. The amplitude is the vertical displacement of the response from a given baseline at a given time, although commonly, the term refers to the maximum displacement measured at the time-to-peak (Weisinger et al., 1996; Fishman, 2001).

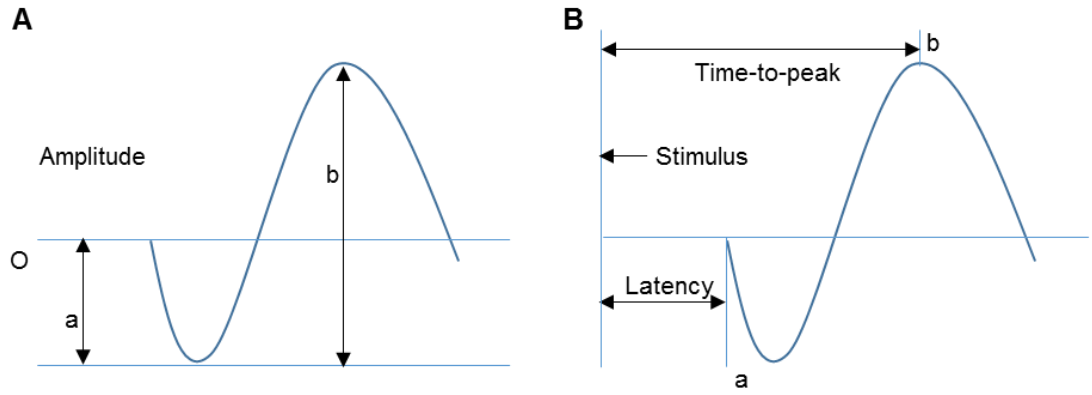

Figure 1.17. Methods of measuring ERG waveform amplitudes (A) and time relationships (B). The b-wave amplitude is measured from trough of a-wave to peak of b-wave, O, while a-wave is measured from baseline. Latency of response refers to time from stimulus onset to beginning of the waveform (illustrated for a-wave), while time-to-peak (b-wave response illustrated) is measured from stimulus onset to peak of the subcomponent (Fishman, 2001).

Three types of flash ERGs can be further identified according to the area of the retina being tested. The first is the full-field ERG, where the entire retina is illuminated and the second is the focal ERG, where a localised area of the retina (often the macula) is illuminated. The components and cellular origins of the full field and focal ERG are similar and can therefore be subjected to the same analysis (Kondo et al., 2008a). Nevertheless, there are distinct characteristics in their waveforms which reflect the areas of the retina being assessed. These distinctions will be discussed later in Chapter 4 where full-field and focal ERGs are compared. "Full-field" and "focal" ERGs will be qualified appropriately throughout this thesis.

The third type of flash ERG is the multifocal ERG which comprises many local ERG responses recorded quasi-simultaneously (Figure 1.18) (Sutter and Tran, 1992; Hood et al., 2012). The recording technique, waveform and components of the multifocal ERG are distinct and will not be further discussed in this review. The interested reader may, however, refer to the following for further details (Sutter, 2000; Hood et al., 2002; Harrison et al., 2006).

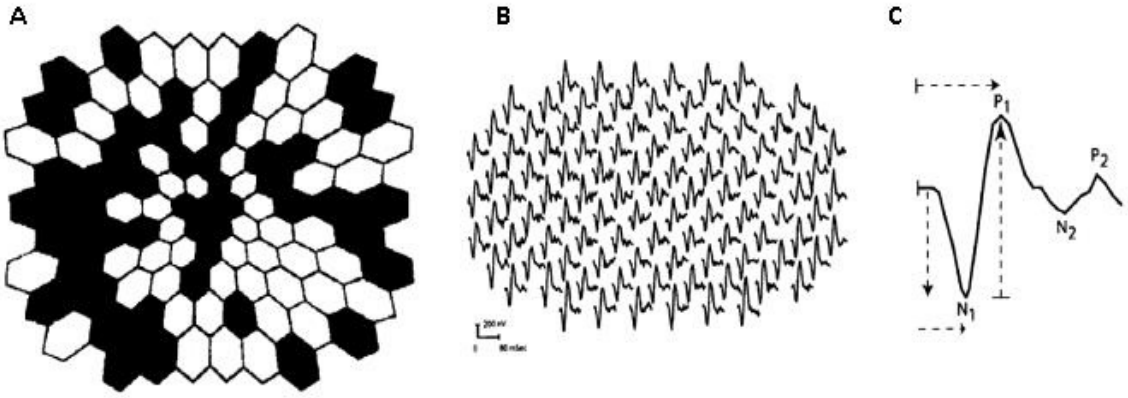

Figure 1.18. The multi-focal ERG. (A) Representative hexagonal mfERG stimulus array with 103 elements, half of which are illuminated at any one time; (B) Diagram of an mfERG response. (C) Sample of a single mfERG trace showing the designation of the major components and the recommended method of measuring the amplitude and time-to-peak. Adapted from Holder et al (2012).

1.4.2.1 Origins of the ERG Components

The flash ERG is the most commonly performed and the best understood electroretinographic test. Understanding the retinal sources of its components is fundamental to interpreting the results obtained using this technique. The components of the ERG are formed by the summation of the active retinal elements at any given moment after the stimulus onset (Granit, 1933; Frishman, 2006; Wolpert and Tsang, 2011). Several approaches have been used over the years to determine the origins of ERG components (Frishman, 2006). During current source-density analysis, microelectrodes are used to identify the retinal layer from which the electrical signals originate (Heynen and van Norren, 1985; Baker et al., 1988; Xu and Karwoski, 1994; Xu and Karwoski, 1995; Xu and Karwoski, 1997; Karwoski and Xu, 1999). Alternatively, pharmacological agents may be used to block synapse between the retinal layers to isolate the origin of the signal (Hood et al., 1999; Viswanathan et al., 1999; Luo and Frishman, 2011). In humans, the effect of diseases known to affect specific populations of retinal neurons on the ERG subcomponents provides further evidence for their

origin (Viswanathan et al., 2001; Miyata et al., 2007; Kondo et al., 2008b) as does the change in the ERG waveform under different adaptation and stimulus conditions (Robson and Frishman, 1998).

Granit's classic analysis in 1933 of the scotopic transient ERG in the rod-dominated cat retina demonstrated that the long ERG consisted of three processes, called PI, PII and PIII (Figure 1.19). He recorded the ERG from the anaesthetised cat using corneal electrodes and observed the gradual removal of the different components as the level of anaesthesia was deepened. The Roman numerals designated the order in which the different components disappeared.

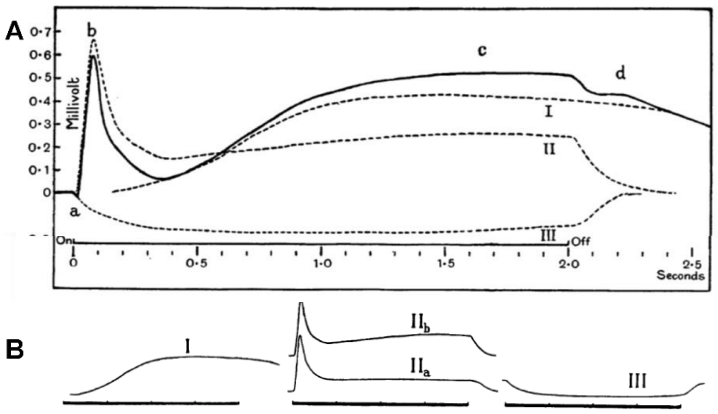

Figure 1.19. Granit's component analysis of the ERG of a cat to a 2-sec light stimulus. (A) Composite diagram showing the processes I, II and III (broken lines) that give rise to the a-. b-, c- and d-waves. (B) Shows the individual traces of the three fundamental processes that combine to make the ERG. Adapted from Granit (1933)

The PI component is a slow, corneal-positive wave; PII is also a corneal-positive wave that rises relatively fast to peak amplitude and then recovers to an intermediate potential while the light is stimulus is still on. The last component P-III, which was the most resistant to the level of anaesthesia, is a cornea-negative wave that develops faster than the other two and remains as a negative potential for as long as the light stimulus is on. He showed that the ERG signal was a composite of these PI, PII and PIII processes, which dominated the ERG at different times giving rise to the c-, b- and a-waves respectively (Granit, 1933; Perlman, 2001). Granit's component analysis has been modified slightly over the years, but remains the basis for understanding the ERG.

1.4.2.2 The a-wave

The a-wave is the first negative deflection seen on a conventional electroretinogram (Figure 1.16). Its appearance is dependent on the state of adaptation of the eye and the intensity of the stimulus. The a-wave is best seen with bright stimuli ($\geq$ 10 cd.s/m^2) in the dark-adapted eye, in which case it contains both rod and cone responses when using a white flash (Frishman, 2006; McCulloch et al., 2015). However, only the first 10 – 12 msec of the a-wave reflect photoreceptor activity (Hood and Birch, 1993; Marmor et al., 2004); the remaining part of the wave contains additional contributions from post-receptoral cells (see later discussion in this section). Under both dark and light adapted conditions, the a-wave is truncated by the rise of the b-wave (Frishman, 2006).

Granit's PIII component can be divided into two components: a fast PIII and a slow PIII (Murakami and Kaneko, 1966). The a-wave is shaped by the leading edge of Granit's fast PIII component. ERG recordings with intra-retinal microelectrodes in animals point to the photoreceptor layers as the origin of the fast PIII (and therefore the a-wave) (Brown and Wiesel, 1961a; Brown and Wiesel, 1961b; Brown, 1968). Further evidence was provided by studies clamping the inner retinal circulation (Brown et al., 1965; Brown, 1968). Since the inner layers of the neural retina are supplied by the retinal vasculature and the photoreceptors by the choroidal plexus, clamping the retinal circulation suppressed electrical activity proximal to the photoreceptors resulting in the removal of the b-wave while leaving the a-wave intact.

Pharmacological dissection has confirmed the photoreceptoral origins of the a-wave, but has also revealed post-receptoral contributions (Sillman et al., 1969; Bush and Sieving, 1994). L-glutamate is the neurotransmitter of the photoreceptors as well as the bipolar cells in all vertebrate retinas (Massey, 1990). Therefore, exposing the retina to agonists or antagonists of L-glutamate, can effectively block synaptic transmission from the photoreceptors and isolate the contribution of the photoreceptors to the ERG.

Aspartate, a known agonist for glutamate, in high concentrations blocks transmission from photoreceptors to bipolar cells owing to accumulation of

excess glutamate in the extracellular space. ERGs recorded after injection of aspartate show the b-wave is removed while the a-wave remains, providing further evidence for the photoreceptoral origins of the a-wave (Sillman et al., 1969). L-2-amino-4-phosphonobutyric acid (APB), is a more specific agonist which blocks metabotrophic transmission and hence eliminates light-evoked responses of depolarizing (ON) bipolar cells and thus the more proximal ON pathway contributions (Slaughter and Miller, 1981). In contrast, cis-2,3-piperidine dicarboxylic acid (PDA) is a specific glutamate antagonist which blocks major ionotropic glutamate receptors in the retina and hence eliminates signal transmission to hyperpolarizing (OFF) bipolar cells and horizontal cells as well as amacrine and ganglion cells in both ON and OFF pathways (Slaughter and Miller, 1983).

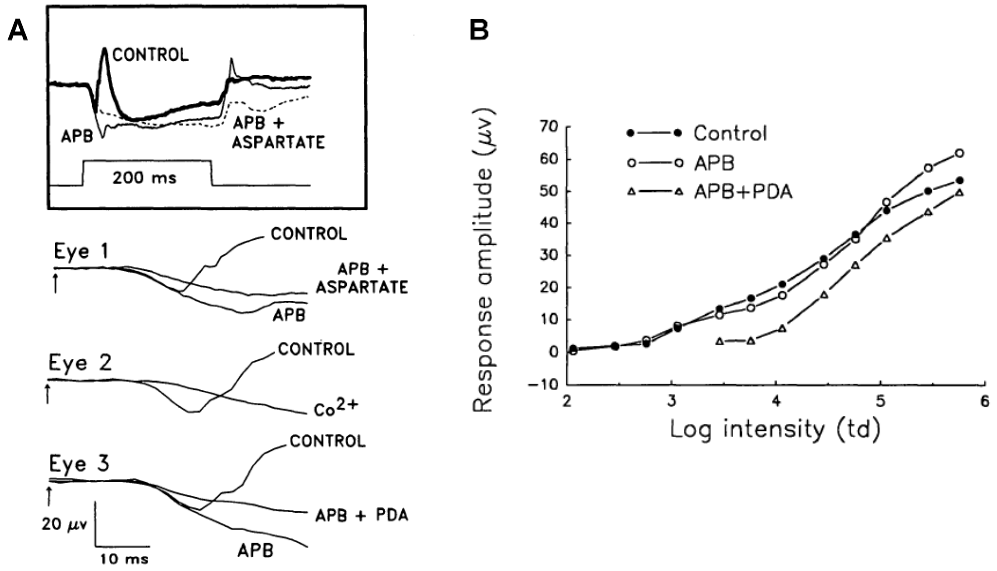

Figure 1.20. Post-receptoral contributions to the a-wave of the macaque ERG. (A) Comparison of the effects of aspartate and cobalt to the effect of APB and APB+PDA on the photopic ERG a-wave of three different eyes of two monkeys. The inset at the top shows 400ms traces of eye#1 to the 200ms stimulus of 2.01 log cd/m^2 on a steady background of 1.33 cd/m^2. The bottom three traces show the first 40ms after flash onset (indicated by arrow) to the same stimulus. (B) Stimulus response function (V log I plot) of the photopic a-wave of the macaque measured at times corresponding to the a-wave peak in the control responses (solid circles). Amplitudes after APB (open circles) and after APB+PDA (triangles) were measured at the same time as the trough of the control a-waves measures at the same stimulus intensity. In this figure, as in part A, APB has no effect on the a-wave amplitude. In contrast, PDA reduced the amplitude (Bush and Sieving, 1994).

Using these agents, Bush and Sieving (1994) showed that the amplitude of the a-wave in a macaque retina was reduced by a combination of PDA and APB, but not APB alone (Figure 1.20A). The reduction in a-wave amplitude with the addition of PDA (APB+PDA in eye 3) showed that post-receptoral PDA

sensitive components (OFF-bipolar cells, horizontal cells, amacrine and RGCs) contributing to the a-wave were removed. When the effects of APB + PDA on the photopic a-wave were evaluated over a wide range of stimulus strengths, the proportion of the response due to post-receptoral cells declined from about 50% at the lower luminance to about 25% at the highest luminance where the a-wave was saturated (Figure 1.20B).

The slow component of the PIII cannot be identified in a regular ERG response due to the large amplitude positive PI wave. However, by separating the retina from the pigment epithelium, PI can be eliminated and by exposing the retina to drugs, such as aspartic acid, that block synaptic transmission from the photoreceptors to the neurons in the inner nuclear layer, the PIII component can be isolated and studied (Witkovsky et al., 1975). Measurements of the extracellular concentration of potassium ions and of the isolated PIII component of the ERG at different retinal depths reveal the involvement of retinal glial (Müller) cells in the generation of the slow PIII. The Müller cells are highly permeable to potassium ions. Therefore, the reduction in the extracellular concentration of potassium ions in the photoreceptor layer, due to light absorption in the photoreceptors, elicits changes in the trans-membrane potential of the Müller cells and is expressed as the slow P-III component of the ERG (Perlman, 2001). This slow PIII process contributes to the shape of the c-wave.

1.4.2.3 The b-wave and oscillatory potentials

The largest component of the flash ERG is the cornea-positive b-wave (Figure 1.16). It is dominated by Granit's PII component (Figure 1.19). It follows immediately after the a-wave. It is a very sensitive component and can be recorded at low luminances approximating perceptual threshold (Frishman et al., 1996). The b-wave appears within 25 to 35 msec in photopic conditions and 40 to 60-ms in scotopic conditions, peaking about 40 to 80 msec later. The b-wave amplitude appears large under scotopic conditions because there is little a-wave present to oppose its actions, but it achieves a maximum when recorded under dark adapted conditions to a bright flash (i.e. mixed rod and cone response). Often the b-wave will have several low-amplitude oscillatory waves, called oscillatory potentials evident on the rising edge especially when a

series of bright flashes are presented to the dark adapted eye (Asi and Perlman, 1992; Janaky et al., 1996; Wachtmeister, 1998; McCulloch et al., 2015). Oscillatory potentials are thought to arise from feedback mechanisms in the inner retina, most likely generated by amacrine cells (Wachtmeister, 1998; Rangaswamy et al., 2006).

In the brief ERG, the b-wave is a summed response arising from the ON and OFF bipolar cells (Sieving, 1993; Sustar et al., 2006). Some earlier studies had also implicated the Müller cells in the generation of the b-wave (Miller and Dowling, 1970; Heynen and van Norren, 1985), but later evidence showed that the b-wave was relatively unaffected when barium ions were administered to block Müller cell activity in the frog and rabbit retina (Xu and Karwoski, 1994). In contrast, administration of APB, a glutamate known to eliminate the ON-bipolar cell response, was shown to extinguish the b-wave in the mudpuppy and salamander (Stockton and Slaughter, 1989). Therefore, although Müller cell activity may contribute to the b-wave, it is now generally accepted that the b-wave directly reflects the activity of the ON-bipolar cells (Xu and Karwoski, 1994; Stockton and Slaughter, 1989).

1.4.2.4 The d-wave

The d-wave is a positive potential in the ERG at light offset in the photopic ERG (Figure 1.16B). The d-wave is not normally found with short duration stimuli; it is observed only when the ON and OFF retinal responses are separated using light stimuli of relatively long duration (>100ms). In the photopic ERG elicited by brief flashes, the d-wave is merged with the b-wave (Sieving, 1993; Sustar et al., 2006).

Current source density analysis of the d-wave in frog retina shows it originates primarily from the hyperpolarising (OFF) bipolar cells with a small contribution from photoreceptors (Sieving, 1993; Sieving et al., 1994; Xu and Karwoski, 1995). The d-wave was reduced or eliminated in monkey retina by the injection of PDA or kynurenic acid (KYN), which both block responses of OFF bipolar cells as well as horizontal cells and inner retinal amacrine and ganglion cells (Figure 1.21) (Sieving, 1993). The effect of PDA was not replicated by blocking

inner retinal cells with N-methyl-D-aspartate (NMDA), confirming the role of the OFF bipolar cells.

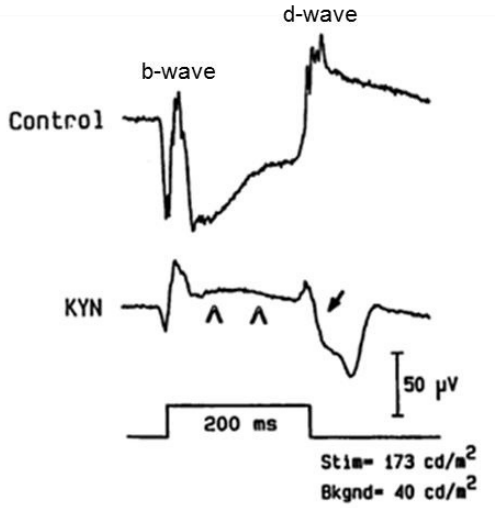

Figure 1.21. Reduction of the d-wave by kynurenic acid (KYN) in a monkey photopic ERG elicited with 200 msec flash. KYN blocks OFF pathway, elevates the plateau (arrow heads) and causes a negative waveform swing at stimulus termination (Sieving, 1993)

1.4.2.5 The Photopic Negative Response (PhNR)

The PhNR is a slow negative potential seen after the b-wave in a normal photopic ERG for a brief flash (Figure 1.16A). For a long duration flash, the PhNR is seen again as a negative going potential after the d-wave (Figure 1.16B). Here, the PhNR which follows the b-wave is termed as the PhNR-ON and represents an on-response of RGCs during stimulus onset; the PhNR-OFF refers to the PhNR seen after the d-wave and represents an off-response of RGCs to stimulus offset (Viswanathan et al., 1999; Kondo et al., 2008a).

The PhNR was named and fully described by Viswanathan et al (1999) although Spileers et al (1993) had reported observing it as a new negative cone response evoked by brief red LED flashes in human subjects. Spileers et al (1993) called their new cornea-negative response the photopic threshold response (PTR), hypothesising that it was an analogue to the scotopic threshold response (Sieving et al., 1986; Sieving and Nino, 1988; Wakabayashi and Sieving, 1988; Frishman et al., 1993). Viswanathan et al (1999) on the other hand, conducted a more detailed experiment on macaque monkeys using red LED flashes on a rod saturating blue background. They explored the characteristics of the PhNR to various luminance levels, flash durations,

induced glaucoma and pharmacological agents and subsequently implicated the RGCs and their axons as the major contributors to the PhNR in monkey and human retina.

The PhNR to brief and long duration stimuli were both eliminated in the macaque monkey by intravitreal injection of tetrodotoxin (TTX), a drug which blocks sodium dependent action potentials that occur in all RGC and some amacrine cells (Figure 1.22). The PhNRs were also significantly reduced in monkeys with laser induced experimental glaucoma that destroys RGCs (Viswanathan et al., 1999; Rangaswamy et al., 2007).

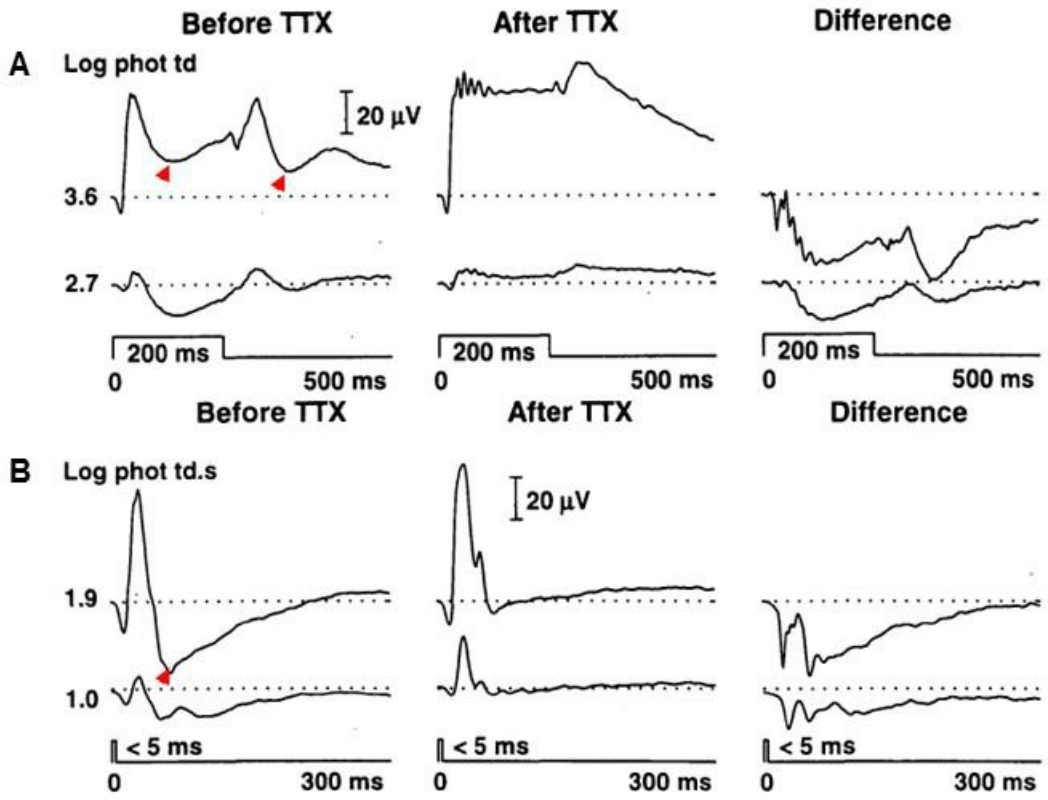

Figure 1.22. ERG responses in a monkey to 200ms stimuli (A) and 5ms flash (B) before (left column) and after (middle column) intravitreal injection of TTX in the same eye. The difference ERG (right) was obtained by subtracting the ERG after TTX (B) from the control (A). The PhNRs are indicated by red arrowheads (Viswanathan et al., 1999).

Later studies also showed that the PhNR was significantly reduced in human patients with primary open glaucoma (Colotto et al., 2000; Viswanathan et al., 2001; Gotoh et al., 2004; Machida et al., 2008b; North et al., 2010; Horn et al., 2011; Kremers et al., 2012; Pangeni et al., 2012; Preiser et al., 2013), and in other ocular diseases known to cause RGC or optic nerve dysfunction (Gotoh et

al., 2004; Rangaswamy et al., 2004; Chen et al., 2006; Kizawa et al., 2006; Ueno et al., 2006a; Chen et al., 2008; Matsumoto et al., 2009; Matsumoto et al., 2011; Moon et al., 2011; Nakamura et al., 2011b; Wang et al., 2012; Morny et al., 2015).

These observations strongly implicate RGC spiking activity in the generation of the PhNR. Furthermore, in intra-retinal microelectrode recordings in cats, local signals of the same time course as the PhNR were largest in and around the optic nerve head indicating RGC axon involvement in generating the PhNR. However, the disruption of the PhNR by Ba^{2+} in cats, indicates that there is also glial involvement in mediating the generation of the response (Viswanathan and Frishman, 1997). Additionally, the PhNR was reduced in EAST Syndrome (epilepsy, ataxia, sensorineural deafness and renal tubulopathy syndrome) patients with known mutations of the KCNJ10 gene, a condition in which the primary K^+ channels of the Muller cells are impaired (Thompson et al., 2011).

There is also evidence suggesting that the generators of the PhNR are species dependent. While the PhNR in humans, monkeys and cats, originates from the spiking activity of RGCs and their axons (Viswanathan et al., 1999; Viswanathan et al., 2001; Hood et al., 2002), the PhNR in rodents is believed to receive significant input from the amacrine cells (Bui and Fortune, 2004; Miura et al., 2009; Smith et al., 2014), although both are TTX-sensitive inner retina neurons. This is thought to be due to the greater proportion of amacrine cells in rodents than in primates (Bui and Fortune, 2004; Machida et al., 2008a; Miura et al., 2009). Section 1.4.3 discusses the characteristics of the PhNR in more detail.

1.4.3 The Characteristics of the PhNR

As with other components of the ERG, the amplitude and time-to-peak are the data typically analysed for the PhNR (Fishman, 2001; Movassat, 2012). These are both affected by factors such as luminance, duration and spectral composition of the stimulus flash as well as the background on which the flash is presented (Viswanathan et al., 1999; Colotto et al., 2000; Viswanathan et al., 2001; Sustar et al., 2006; Rangaswamy et al., 2007; Mortlock et al., 2010; Binns et al., 2011). In addition, for long duration stimuli (>100ms), the photopic ERG

waveform is separated into ON and OFF components, while for brief flashes (<10ms) the ON and OFF responses overlap as seen in figure 6 (Sieving, 1993; Viswanathan et al., 1999; Sustar et al., 2006). Additional factors affecting the PhNR, especially the amplitude, include age of the subject, area of the retina stimulated (full field or focal) and the type of electrodes used in the recording (Viswanathan et al., 2001; Mortlock et al., 2010; Machida et al., 2011).

In both animal and human trials, the time-to-peak of the PhNR has been difficult to pinpoint owing to the broad trough of the PhNR which impedes accurate assessment of the most negative point in the trough. In addition, a small positive potential that occurs in the falling phase of the b-wave or just after it, especially in the brief PhNR, called the i-wave (Figure 1.16 and 1.23), often interferes with the PhNR under certain luminance conditions (Viswanathan et al., 1999; Viswanathan et al., 2001; Rangaswamy et al., 2007; Sustar et al., 2009; Machida, 2012). Horn et al (2011), has also recently described a similar potential on the falling phase of the d-wave, calling it the i_{off}-wave. This makes it difficult to accurately determination the amplitude of the responses as well.

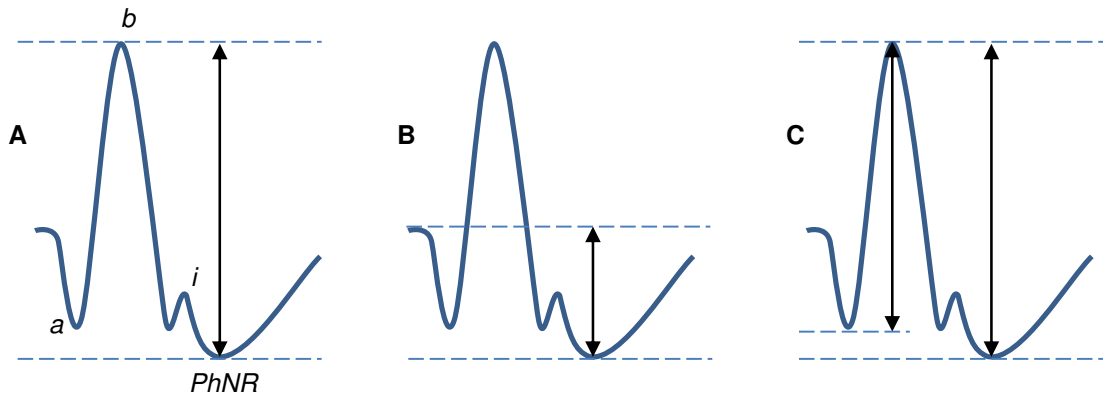

Figure 1.23. Different techniques used in measuring PhNR amplitude ; (A) peak to trough; (B) pre-stimulus baseline to trough; (C) b-wave amplitude to PhNR amplitude ratio. The letters a, b and i represent the a-, b- and i-waves respectively.

As yet, the International Society for Clinical Electrophysiology of Vision (ISCEV) does not have a standard protocol for recording or analysing the PhNR. Various investigators have thus used different combinations of stimulus and background parameters as well as measuring techniques in an attempt to find the optimal parameters for quantifying the PhNR (for example (Viswanathan et al., 1999;

Colotto et al., 2000; Drasdo et al., 2001; Rangaswamy et al., 2007; Binns et al., 2011). Notwithstanding this, three common techniques have been used by various studies in measuring the PhNR amplitude. These are (i) from peak of b-wave to the trough of the PhNR, (ii) from pre-stimulus baseline to PhNR trough, or (iii) from either peak of b-wave or pre-stimulus baseline to a fixed time point in order to overcome the influence of the i-wave (Figure 1.23).

The ratio of the b-wave to the PhNR amplitude has also been used as a potentially less variable means of PhNR assessment and Mortlock et al (2010) reported that the ratio of b-wave to PhNR amplitude showed the lowest level of inter-individual, inter-session and inter-ocular variability of all the measurement techniques. Measurements taken from the pre-stimulus baseline were found to have the highest coefficient of variation (CoV), as well as the poorest inter-session and inter-ocular repeatability, whether the measurement was taken to the trough or to a fixed time-point. In contrast, measurements taken from the peak of the b-wave to either the trough or the fixed time-point had a much improved CoV, comparable with and often better than the a- and b-waves (Colotto et al., 2000; Fortune et al., 2004; Mortlock et al., 2010). However, peak-to-trough measurements of the PhNR may be confounded by the influence of the b-wave amplitude on the measured PhNR and thus require careful analysis for accurate interpretation (Mortlock et al., 2010; Binns et al., 2011). The influence of recording parameters and demographic factors on the PhNR are discussed in the following subsections.

1.4.3.1 Effect of Stimulus Duration

For a series of brief flashes of increasing duration, but equal luminance, Kondo et al (2008) found that time-to-peak of focal PhNR in macaque increased over a limited range and then stabilised (Figure 1.24). For a fixed luminance of 55 phot cd/m^2, the time-to-peak was approximately 75ms for a 5ms flash. This became longer with increasing stimulus durations and reached a maximum time-to-peak of 110ms for a 50ms flash (Figure 12A, red dashed vertical lines). Further increases in the stimulus duration did not change the time-to-peak of the PhNR, but resulted in the separation of the waveform into ON- and OFF-responses. The gradual increase in the time-to-peak of the PhNR most likely resulted from an increase in stimulus energy and the increase in the midpoint of the stimulus.

The amplitude of the focal PhNR also increased with increasing stimulus durations when the stimulus durations were shorter than 30 to 50ms. This increase in the amplitude is most likely due to the increase in the stimulus energy (Figure 1.24B). Further increases in the stimulus duration led to a slight decrease in the PhNR amplitude and the emergence of the d-wave and the PhNR-OFF. This is similar to the b-wave response to increasing stimulus duration described by Sustar et al (2006). They reported that the b-wave amplitude reached its peak value with a 10ms flash and decreased with longer duration flashes. From 25 to 200ms flash duration the b-wave amplitude did not change significantly.

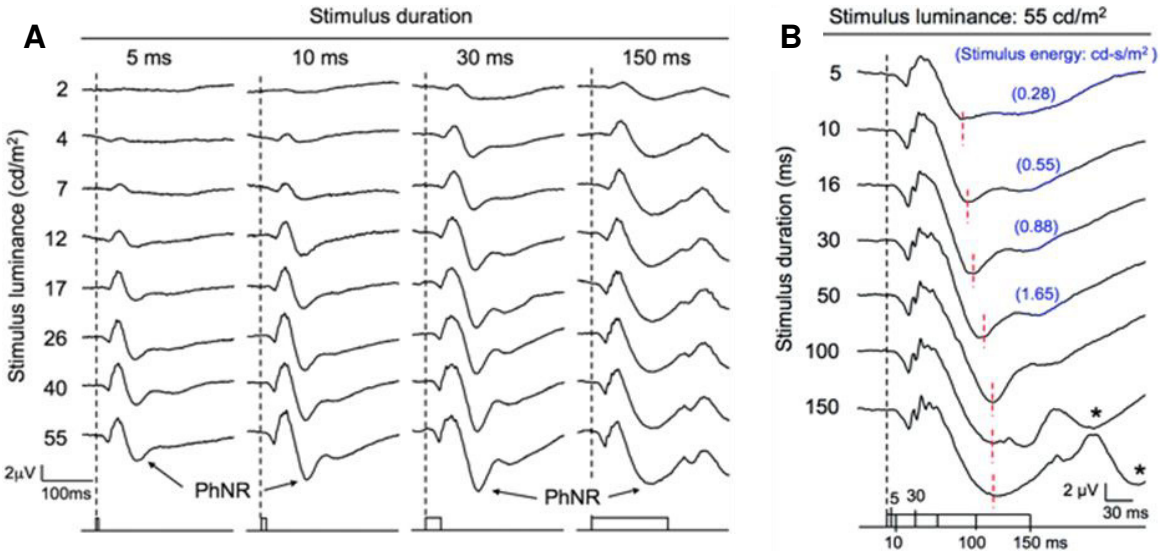

Figure 1.24. (A) Representative focal ERGs elicited from a rhesus monkey by different stimulus luminances (2–55 phot cd/m2) and different stimulus durations (5, 10, 30, and 150 ms). The amplitude of PhNR increases with increasing stimulus duration and luminance. (B) Effect of stimulus duration on the focal PhNR showing representative focal ERGs elicited by different stimulus durations (5-150ms) for a constant stimulus luminance of 55 phot cd/m^2. Vertical dotted line: peak of the PhNR. The asterisks (*) represent the PhNR-OFF, which appears only when the ERG is separated into ON- and OFF components by long duration flashes (100 and 150ms). The values of stimulus energy (cd.s/m^2) are also indicated for brief flashes of 5 to 30ms (Kondo et al., 2008a).

For long duration flashes, it is not clear what the effect of increasing stimulus duration has on the time-to-peak of the PhNR-OFF. The PhNR-OFF time-to-peak was reported to be about 114 – 117 $\pm$10 msec by Viswanathan et al (1999). However, in their study and in others (Rangaswamy et al., 2007; Horn et al., 2011) the waveform and timing characteristics of the off-response varied considerably, making accurate measurements of the PhNR-OFF problematic.

1.4.3.2 The Effect of Stimulus luminance

Generally, increasing stimulus luminance leads to an increase in the amplitude and a decrease in the time-to-peak of ERG components. The change in the amplitude and time-to-peak continues till maximum amplitude or minimum time-to-peak is reached and further increases in the stimulus lead to no significant changes in the response. At this point, the response is said to be saturated and it is particularly notable in photopic ERGs (Fishman, 2001). Some subcomponents (e.g. the photopic b-wave), however, show a reduction in the amplitude to further increases in stimulus luminance. This is the so called photopic-hill phenomenon (Wali and Leguire, 1992; Kondo et al., 2000). Under scotopic conditions, the saturation point is not as notable because the amplitude and time-to-peak of components continue to increase and decrease respectively beyond the "saturation point" as cone elements become active in response to the higher luminance. The saturation point therefore becomes the threshold at which cone elements are activated (Fishman, 2001).

The increase in PhNR amplitude in response to stimulus luminance is depicted in Figure 1.25, taken from the Viswanathan et al (1999) study. It shows increases in the amplitude of the PhNR for both the brief and long duration stimulus in a full field ERG. Viswanathan et al (1999) also reported a decrease in the time-to-peak with increasing stimulus luminance. The brief PhNR amplitude plateaus at about 2.0 log phot td beyond which the amplitude begins decrease (Viswanathan et al., 2001; Chen et al., 2006; Rangaswamy et al., 2007; Miyata et al., 2008; Sustar et al., 2009; Binns et al., 2011). The relationship between the stimulus strength and the response can be described by stimulus-response functions (S/R functions) and Binns et al (2010) have showed that the amplitude-response data for brief flashes of low to moderate luminance can be fitted to a generalised Naka-Rushton function (Figure 1.26).

The generalised Naka–Rushton function: $V = \frac{Vmax * I^n}{(I^n + K^n)}$, is a sigmoidal curve, where V = response amplitude; Vmax = the maximum amplitude; I = stimulus intensity; K = the semi-saturation constant i.e. the stimulus intensity at which the amplitude is at a half of Vmax; and n = an exponent describing the slope of the function, at the point where stimulus strength = the exponent, K. The function

has been shown to describe the increase in b-wave amplitude with increasing stimulus intensity (Binns et al., 2011). This reportedly provides a good fit to data across a range of intensities, although the relationship breaks down at high intensities for both light and dark-adapted b-waves.

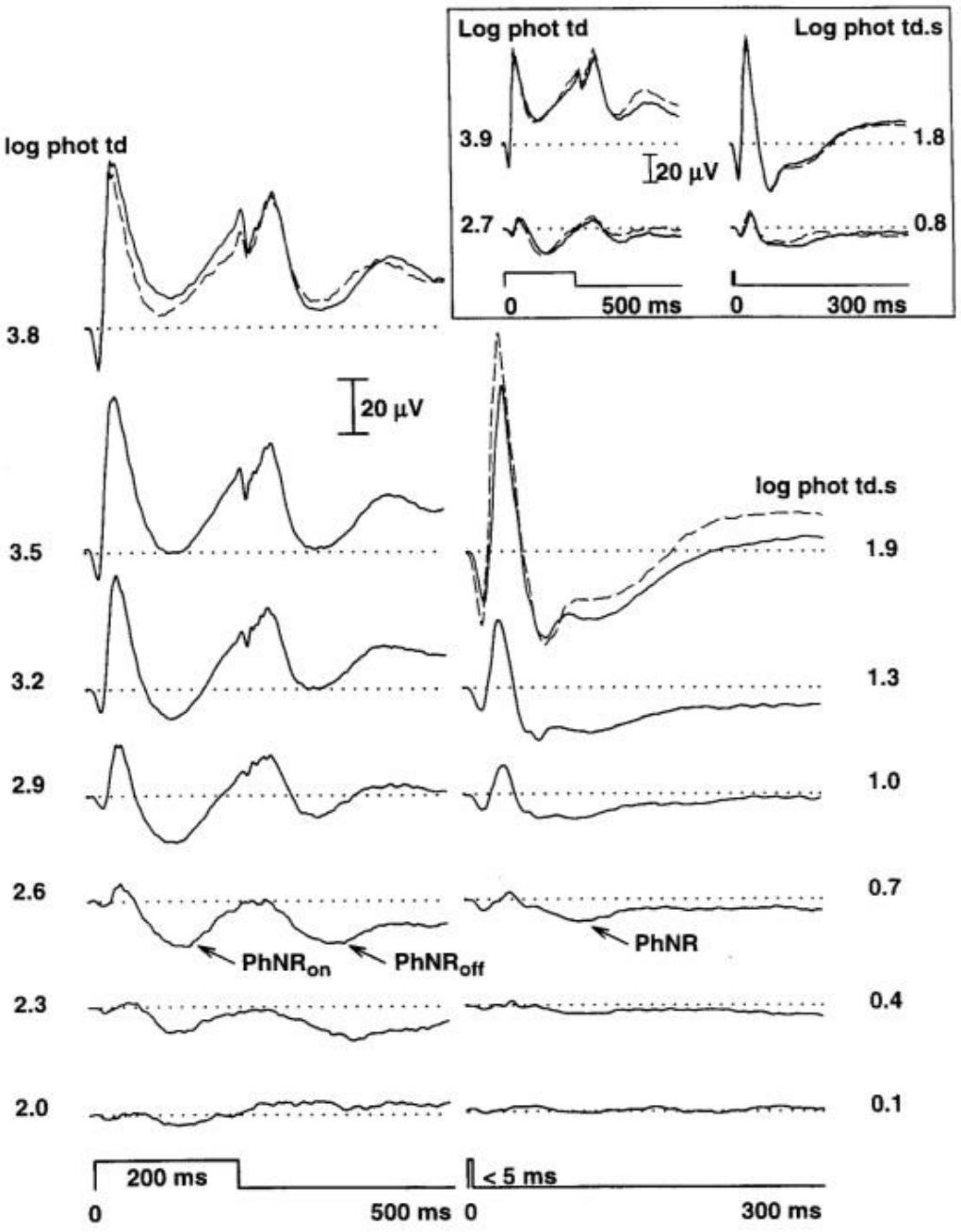

Figure 1.25. ERG responses to a series of long duration (left) and brief (right) red stimuli of increasing luminance on a rod saturating blue background showing the PhNR in macaque monkeys (arrowed) (Viswanthan et al., 1999)

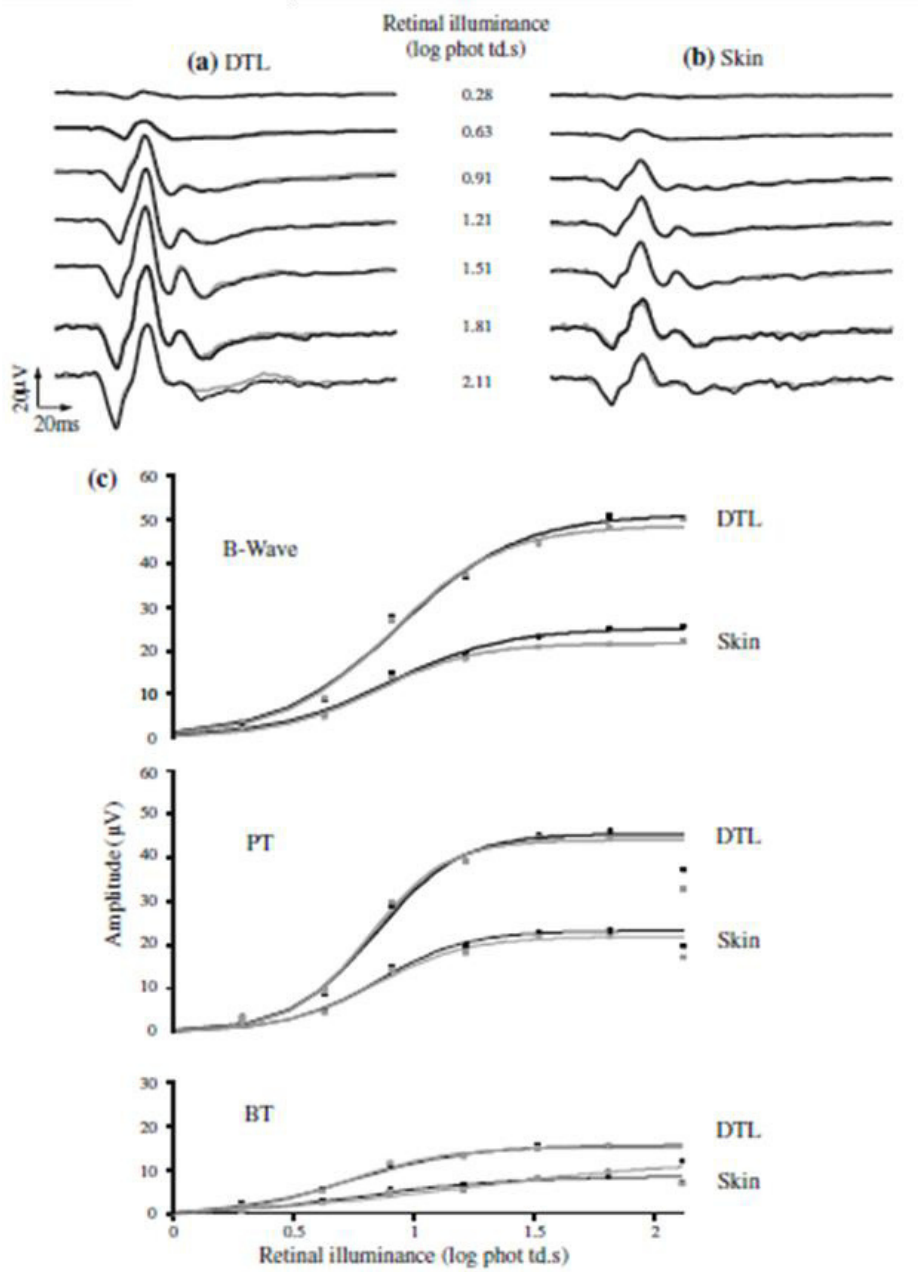

Figure 1.26. Sample ERGs recorded from a subject using DTL (a) and skin (b) active electrodes. RE data are shown in black and LE in grey. Panel (c) shows the amplitudes of the b-wave and PhNR-ON (PT and BT) plotted as a function of stimulus intensity, with best fitting Naka-Rushton function. PT amplitudes are measured from peak of b-wave to trough of PhNR and BT amplitudes are measured from baseline to trough. Note the decrease in amplitude in PhNR amplitude beyond 2 log phot td.s (Binns et al., 2011)

The amplitude of the PhNR-OFF has, however, been more difficult to characterise because of difficulties encountered in measuring it (Viswanathan et al., 2001; Rangaswamy et al., 2007). Notwithstanding, Horn et al (2011) reported a general increase in the PhNR-OFF amplitude in response to increasing stimulus luminance (Figure 1.27). They showed that both in normal subjects and glaucoma patients, the PhNR-OFF amplitude increased as stimulus luminance was increased, although the amplitude for glaucoma

patients at each level was significantly lower than for controls (p=<0.001). They could not demonstrate saturation of the PhNR-OFF since only three intensities (40, 60 and 80 cd/m^2) were tested. Nevertheless, their results confirm that the PhNR-OFF amplitude increases with stimulus luminance as has been observed in other studies (Viswanathan et al., 1999; Viswanathan et al., 2001; Rangaswamy et al., 2007)

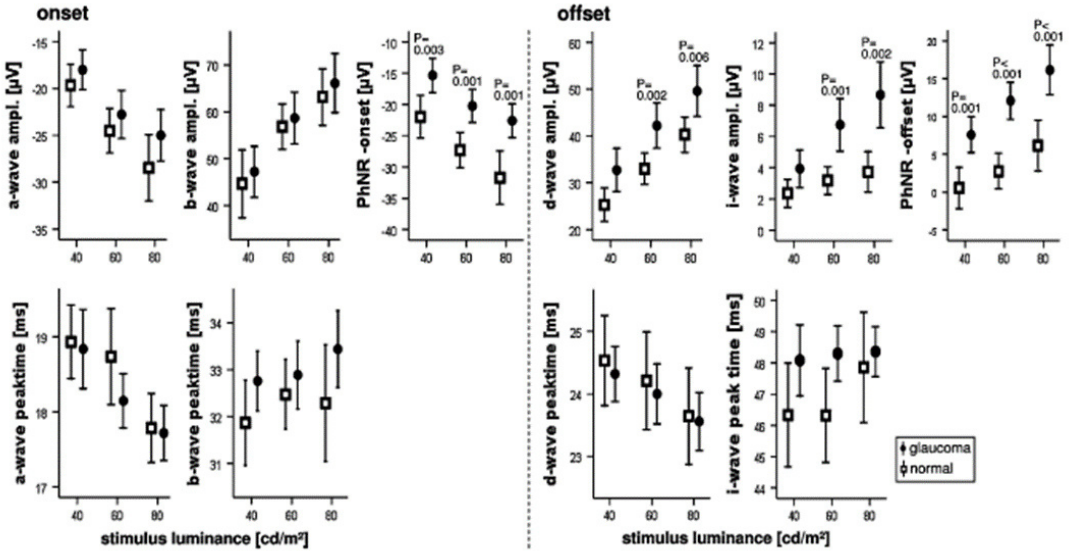

Figure 1.27. Plot of amplitudes (top row) and time-to-peak (bottom row) of long duration ERG components as a function of stimulus luminance in 12 controls (open symbols) and 12 glaucoma patients (closed symbols). Analysis of repeated measurements indicated significant dependence (p < 0.001) of all amplitudes and of the a- and d-wave time-to-peak on stimulus luminance. (Horn et al., 2011).

1.4.3.3 The Effect of Stimulus and Background Colour (Wavelength)

ISCEV recommends that cone ERGs be recorded using white-flash stimuli on a white background light ("white-on-white") (McCulloch et al., 2015). However, studies have suggested that this may not be the most appropriate stimulus for eliciting the PhNR (Viswanathan et al., 1999; Rangaswamy et al., 2007; Sustar et al., 2009). Viswanathan et al (1999) who published the first study on the PhNR, used red-flash stimuli on a rod saturating blue background ("red-on-blue") to record the PhNR. While this has widely been adopted as a recording protocol (Rangaswamy et al., 2004; Kondo et al., 2008a; Tamada et al., 2009; Mortlock et al., 2010; Binns et al., 2011), some other studies have investigated the effect of other stimulus wavelength on the PhNR.

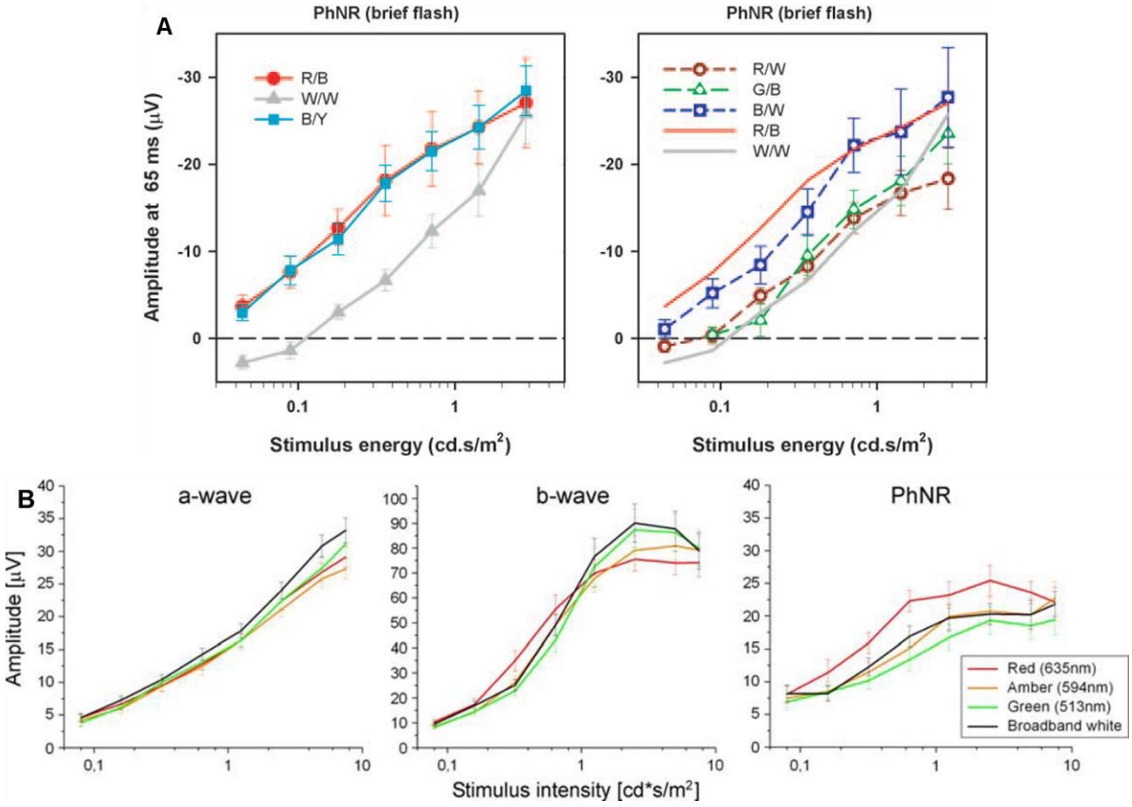

Figure 1.28. ERG amplitude response to increasing luminance of stimuli of different wavelengths. (A) Results from Rangaswamy et al (2007) showing mean PhNR amplitude as a function of stimulus luminance for red on blue, white-on-white and blue on yellow (left) and for red on white, green on blue and blue on white (right). Red on blue and white on white have been superimposed on the right plot for comparison. (B) Intensity-response functions of the a-wave, b-wave and PhNR for different stimulus wavelengths recorded from control subjects. Red flash on blue background (red line) produces significantly higher PhNR amplitudes across the range except for the lowest and highest intensities. From Sustar et al. (2009).

Rangaswamy et al (2007) conducted an experiment on macaque monkeys to determine the wavelength of stimulus and background that best isolate the PhNR and maximise amplitude. They compared a combination of red, white, blue and green flashes on scotopically matched white, blue and yellow backgrounds. For every colour combination, the PhNR amplitude increased as stimulus luminance was increased, though in case of white on white and green on blue, the PhNR was not evident until the stimulus luminance was considerably greater than was needed for the other colours (Figure 1.28A, right). Consequently, they found that red on blue and blue on yellow were generally the most effective stimuli. For these colour combinations, the PhNR amplitude rose steadily and nearly linearly with the logarithm of stimulus luminance (i.e. much less rapidly than in direct proportion to stimulus luminance) over the whole range of luminance studied (Figure 1.28, left). However, selective pharmacological inhibition of inner retinal activities using

TTX and PDA after TTX, showed the PhNR elicited by the red on blue stimulus to be less contaminated by other negative potentials also from the inner retina (presumably from horizontal cells). In other words, red-on-blue stimuli elicit a PhNR with more RGC responses i.e. a larger signal was generated, than the other colours, especially in the low and intermediate stimulus range. (Rangaswamy et al., 2007)

Sustar et al (2009) corroborated the results of Rangaswamy et al (2007) in a similar study on human subjects using different coloured stimuli (4msec flashes) of varying stimulus luminance (0.08 to 7.5 cd.s/m^2) on a steady rod saturating blue background. They observed that the red on blue stimulus produced the highest PhNR amplitude for brief flashes (4msec) of luminance up to 2.5 cd.s/m^2 after which they observed a dip in the amplitude (Figure 1.28B). Their findings further revealed that the PhNR amplitude to a red stimulus was significantly correlated to the pattern ERG amplitude (especially the N95 component) and visual field defects in glaucoma patients. (Sustar et al., 2009)

Kremers et al (2012) have however suggested that when both the stimulus and background are specified in photopic photometric terms (i.e. if stimulus and background luminance for different wavelengths are matched photopically), all chromatic combinations produce a similar amplitude PhNR, except for a blue flash on an orange background, which gives a larger response. The authors of previous studies into the spectral sensitivity of the PhNR have mainly used different stimuli at a fixed scotopic background luminance (Rangaswamy et al., 2007; Sustar et al., 2009). However, Kremers et al. (2012) assessed the spectral sensitivity of the PhNR by presenting coloured flashes of varying luminance on different coloured backgrounds of varying luminance (which were photopically matched to each other i.e. 10, 25, 50, 100 and 250 cd/m^2). They found that the largest PhNR amplitude in normal subjects was produced by a 458 nm (blue) flash on a 591 nm (amber) background. They attributed this to possible contribution from S-cone or rod-driven responses. In addition, the best stimulus condition used to separate the PhNR of normal subjects and glaucoma patients was a 1 cd.s/m^2 458 nm flash on a 10 cd/m^2 591 nm background (Kremers et al., 2012).

This reflects the findings of Drasdo et al (2001), who also found that a stimulus designed to elicit an S-cone response gave a better separation in PhNR amplitude between controls and people with glaucoma than a red on blue protocol (Drasdo et al., 2001). Kremers et al (2012), state however, that their stimulus composition of a short wavelength flash (to which rods are sensitive) on a long wavelength background (which desensitise L- and M-cones) may have introduced rod driven responses into the data; as such the PhNR amplitude observed would not be an entirely cone driven response. In addition, the effectiveness of this stimulus in distinguishing between normal and glaucomatous eyes, measured using the area under the receiver operating characteristic (ROC) curve, was 0.81; a value lower than the results (> 0.90) in other studies using a red on blue stimulus (Viswanathan et al., 1999; Sustar et al., 2009)

The above discussion confirms that the PhNR can be elicited by a brief flash using various combinations of stimuli and background colours. However, the red on blue stimulus remains the best for eliciting a truly cone dominated PhNR.

1.4.3.4 Effect of Age

In an experiment on normal human subjects, Viswanathan et al (2001) found the PhNR time-to-peak averaged by age-group (subjects aged 20 – 80+ years) in response to a 6ms flash (1.7 log td.s), showed a slight increase in time-to-peak with age (Figure 1.29). This increase was however not significant. Furthermore, they observed a decrease in the PhNR amplitude with age in both controls and participants with POAG. The correlation was however not significant. Miyata (2007) also did not observe a significant correlation between PhNR amplitude and age for controls subjects and for ADOA patients.

It therefore appears that while there is a tendency towards a decrease in amplitude with age both in healthy controls and in participants with RGC dysfunction, the correlation is not significant.

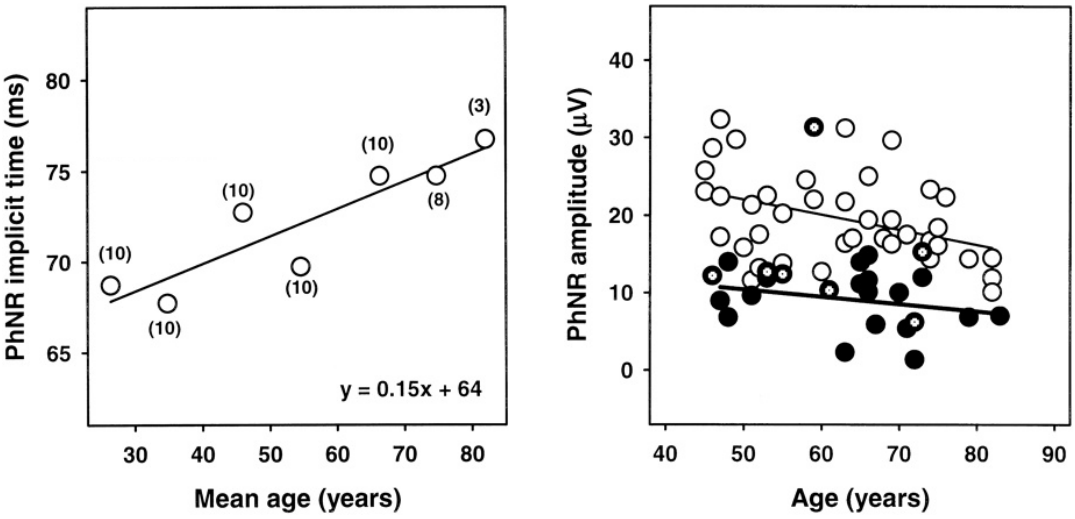

Figure 1.29. (Left) PhNR times-to-peak for a 1.7 log phot td.s flash of group averaged responses of normal subjects in age bins (number in each bin indicated in brackets) plotted as a function of mean age in each bin. The straight line represents the best-fitting linear regression line. (Right) PhNR amplitudes for the same flash intensity for all primary open angle glaucoma patients (filled symbols), suspects (filled circles with centre dot) and control subjects (open symbols) in the same age range plotted as a function of age. The thick (bottom) and thin (top) lines represent the best fitting linear regressions through the patient ($r = -0.24$, $p<0.07$) and control ($r = 0.26$, $p < 0.3$) data respectively. Note the correlation was not statistically significant (Viswanathan et al., 2001).

1.4.3.5 Comparing Full Field PhNR to Focal PhNR

The full field ERG reflects the function of the entire retina. Studies have noted, however, that the full field ERG is not as effective in detecting defects when assessing diseases that affect localised areas of the retina, for example, in early stage glaucoma and macular degeneration (Tamada et al., 2009; Machida, 2012). In these circumstances a focal ERG is more sensitive than the full field ERG. In a focal ERG, a spot of light (of a given size) is directed towards the area of interest on the retina and responses are recorded from that discrete area. In order to ensure that the responses are focal, the effect of stray light generating responses from the peripheral retina are minimised or eliminated by using a desensitising background or surround (Brindley and Westheimer, 1965; Colotto et al., 2000; Kondo et al., 2008a).

A number of studies show that the focal PhNR is produced by the same inner retinal neurons as the full field PhNR (Kondo et al., 2008a; Kurimoto et al., 2009). Figure 1.30 shows that the effect of TTX on the focal PhNR is similar to that of the full field PhNR (compare to Figure 1.22). In addition, the changes in the waveform in response to stimulus parameters such as duration, luminance

and wavelength are similar for the focal and full field PhNR. The focal PhNR, however, has comparatively lower amplitudes due to the smaller retinal area it assesses. Nevertheless, the focal PhNR is found to be more sensitive than the full field PhNR in detecting localised RGC defects (Tamada et al., 2009; Machida et al., 2011; Morny et al., 2015).

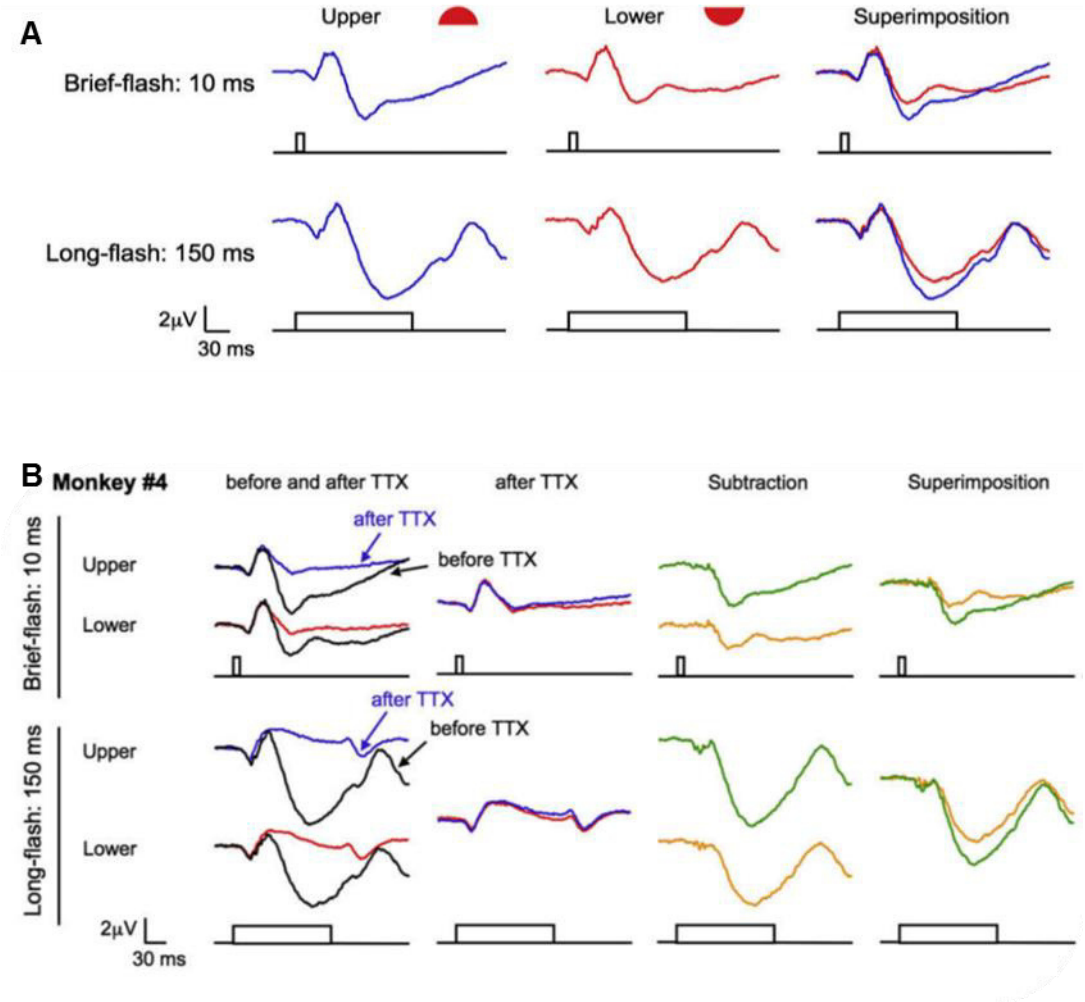

Figure 1.30. Focal macular ERG. A) Representative focal macular ERGs recorded from the superior and inferior macular areas in a rhesus monkey to brief (upper traces) and long duration (lower) traces. (B) Shows the effect on the traces after TTX. (Kurimoto et al., 2009)

Tamada et al. (2009) for example, found that in eyes with central visual field defects (in which other areas of the visual field remained unaffected) only the focal PhNR amplitudes were significantly reduced; the full field PhNRs were not significantly different from those of control eyes (Tamada et al., 2009). Machida et al. (2011) compared the focal and full-field ERGs of glaucoma patients at different stages of the disease progression and found that in early to intermediate glaucoma, the sensitivity of using PhNR amplitude (peak to trough)

to detect glaucoma was 88 - 93% for the focal ERG compared to 38 – 59% for the-full field ERG. These therefore showed the focal ERG has a higher diagnostic ability in detecting early and intermediate glaucoma than the full field ERG.

Another advantage of the focal PhNR is that the stimulus size and shape can be modified and this can allow for comparison between different areas of the retina background (Seiple et al., 1986; Colotto et al., 2000; Kurimoto et al., 2009; Machida et al., 2011). For example, in the experiment by Kurimoto et al (2008) focal ERGs were recorded from the superior and inferior macular as well as the nasal and temporal macular using a semi-circular stimulus in five rhesus monkeys (Figure 1.30). Their findings revealed that the superior macular PhNR amplitude was 27% and 23 % greater than the inferior macular PhNR amplitude for brief and long duration stimuli respectively (Figure 1.30A). The nasal macula produced a response which was 27% and 25% greater than the temporal macular for brief and long duration stimuli respectively (Kurimoto et al., 2009). These asymmetries were, however, eliminated after intravitreal injection of TTX; in contrast the superior-inferior and nasal-temporal asymmetries remained in the TTX sensitive components (shown in Figure 1.30B as the subtracted component). These observations showed that the asymmetries were caused by TTX sensitive spiking activities of inner retinal neurons (Kurimoto et al., 2009). Their findings are in agreement with histological studies into monkey (Perry and Cowey, 1985) and human (Curcio and Allen, 1990) retina which report the RGC density to be higher in the superior and nasal retinas compared to the inferior and temporal retinas respectively.

1.4.4 The Pattern ERG (PERG)

The pattern electroretinogram (PERG) is a mass response from the retina evoked by pattern stimulation (e.g. checkerboard or grating) of constant luminance. (Bach et al., 2013). It is usually recorded from the macula and provides information about RGC function. Consequently the PERG is used extensively in the assessment of disease that are associated with loss of RGC function (Holder, 2001; Bach and Poloschek, 2013; Vincent et al., 2013)

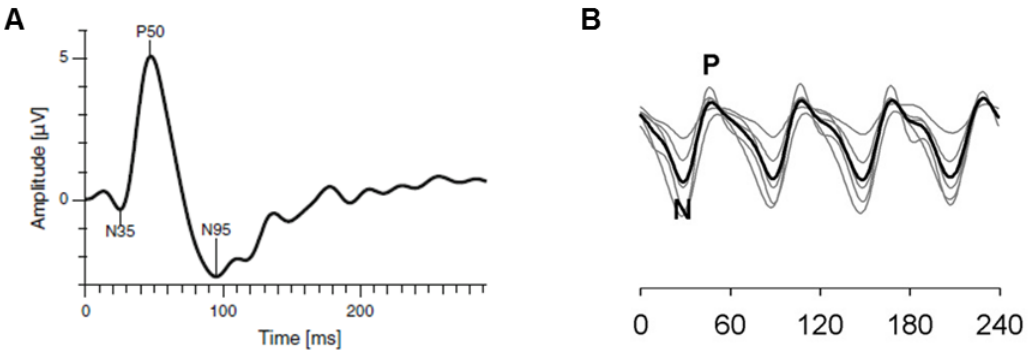

Figure 1.31. Representative diagrams of the PERG. (A) transient PERG recorded at 2Hz (4rps) and (B) steady state PERG recorded at 8.3 Hz (16 rps). Adapted from (Bach et al., 2013)

The waveform of the PERG is determined by the temporal frequency of the stimulus patterned stimulus (Figure 1.31). A transient PERG is recorded to stimulus frequencies ≤4 reversals per second (rps) (equal to 2 Hz) and the steady state PERG is recorded to stimulus frequencies ≥8 repetitions per second (rps) (4 Hz). The transient PERG comprises an initial negative component with a time-to-peak of approximately 35ms (N35), followed at 45-60ms by a much larger positive component (P50) and a large negative component at 90-100ms (N95) (Figure 1.31A). The steady state PERG produces a sinusoidal response (Figure 1.31B) and it may be measured either directly from peak (P) to trough (N) or by assessing the second harmonic of the signal using a fast Fourier transform.

The ISCEV standard PERG is a transient response, recorded to abrupt contrast reversal of a black and white checker-board pattern with central fixation. This is the PERG employed in this study and will be the focus of this review.

1.4.4.1 Origins of the PERG

When a subject gazes at a reversing pattern such as a checker-board with an equal number of light and dark patches, the total quantity of light entering the eye (luminance) remains constant as the pattern reverses, but in the region of the retinal image, there are repetitive local changes (ON/OFF) in illumination (Bach and Hoffmann, 2006). That is, the region of the retina stimulated by a square that goes from dark to bright, will produce an ON-response while the adjacent region stimulated by a bright to dark square will produce an OFF

response. A pattern reversal stimulus will then elicit responses from bright and dark patches that are of the same magnitude, but have a different sign. When recorded from a corneal electrode, which averages across the entire retina, linear responses will cancel out. Remarkably however, any imbalance between the two responses will not cancel out and will therefore be revealed. The imbalance between the two responses is due to nonlinear properties of the underlying neural substrate such as a response with a strong ON component, but no OFF component, a generator with a very rapid adaptation or a response from the interaction of neighbouring bright and dark patches (border contrast). Thus while the flash ERG is evoked by solely by changes in stimulus luminance, the PERG is evoked by changes in stimulus contrast as well. The PERG thus contains a luminance (retinal illuminance) response and a pattern specific response (Drasdo et al., 1987; Bach and Hoffmann, 2006).

The retinal origins of the PERG have been investigated using current-source density analysis (Sieving and Steinberg, 1987; Baker et al., 1988), pharmacological interventions (Viswanathan et al., 2000; Luo and Frishman, 2011), pathophysiological conditions in animals (Mafei and Fiorentini, 1981; Maffei et al., 1985) and humans (Harrison et al., 1987; Holder, 1997; Holder et al., 1998) and the assessment of the parameter dependencies of the electrophysiological response (Drasdo et al., 1987; Thompson and Drasdo, 1989; Thompson and Drasdo, 1994). These all show a fairly consistent picture that the N95 component of the PERG is a contrast related component generated by RGCs. The P50 is in part RGC derived, but also has origins distal to the ganglion cells (Viswanathan et al., 2000; Holder, 2001; Luo and Frishman, 2011).

1.4.4.2 Recording the PERG

PERGs are small signals, typically around 2-8µV across a normal population, making PERG recording more challenging than standard flash ERGs. The stimulus for the ISCEV standard PERG is a black and white reversing checkerboard. The width of the individual checks (check size) is 0.8º (+0.2º) and the mean width of the stimulus field is 15º (+3º). It is not necessary to use a square field, but it is important that there are equal number of white and black

patches. Otherwise the PERG signal is contaminated with a luminance response (Bach and Hoffmann, 2006).

The contrast between black and white squares should be at least 80% and the mean luminance for the white areas should be greater than 80 cd/m^2. PERG signals are affected by optical blur and as such electrodes which degrade the optical image cannot be used (e.g. contact lens electrodes); fibre, foil or loop electrodes are recommended in this case. PERGs are recorded with pupils natural pupils and participants should also wear their appropriate spectacle correction where required (Bach et al., 2013).

1.4.5 Electrophysiological Findings in ADOA

Visual electrophysiological findings provide additional evidence for the primary loss of RGCs and the sparing of the outer retinal layers in ADOA. The pattern visual evoked cortical potentials (PVEP) are often absent or when recordable, have reduced amplitudes and delayed latencies (Berninger et al., 1991; Holder et al., 1998; Reis et al., 2013). The multifocal VEP is also abnormal especially in the central field. The PERG shows an abnormal P50:N95 ratio and a reduction in the amplitude of the N95 waveform consistent with GCL dysfunction. The amplitude of the P50 component may also be reduced, but this is not a consistent feature in ADOA patients (Berninger et al., 1991; Holder et al., 1998).

The standard flash ERG is normal in patients with ADOA, except in severe cases suggesting sparing of or a minimum impact on the photoreceptors and bipolar cells in most patients (Johnston et al., 1979; Holder et al., 1998; Granse et al., 2003). The multifocal ERG amplitudes have also been reported to be normal (Granse et al., 2003), however, another study (Reis et al., 2013) reported a reduction in amplitudes.

Following the discovery of the PhNR (Viswanathan et al., 1999), one study looked at the brief PhNR elicited with a white on white stimulus in humans and reported a significant reduction in the PhNR amplitude in participants with ADOA (Miyata et al., 2007). They also reported a reduction in oscillatory potentials. In the mouse model developed previously in our laboratory, the

PhNR was shown to be selectively attenuated in mutant mice with relative sparing of the a-wave and b-wave (see section 1.3.9). Altogether, the electrophysiological findings in ADOA point to RGC dysfunction affecting the central retina. A summary of the electrophysiological findings in ADOA from the various studies are provided in Table 1.6.

Table 1.6. Summary of electrophysiological findings from previous studies

Study	Flash ERG	Pattern ERG	Multifocal ERG	Flash VEP	Patten VEP	Multifocal VEP
Berninger et al., 1991	NA	Normal P50, reduced N95	NA	NA	Reduced amplitudes in severe patients only	NA
Granse et al., 2003	Normal	NA	Normal	NA	NA	Reduced amplitudes in central field
Miyata et al., 2007	Selective reduction in PhNR and OP amplitude in patients	NA	NA	NA	NA	NA
Holder et al., 2008	NA	Reduced N95 amplitude, N9:P50 ratio, reduced P50 in some patients	NA	Normal	Absent and if present, reduced amplitudes and delayed latencies	NA
Reis et al., 2013		Reduced N95 and P50 amplitude	Reduced amplitudes		Reduced amplitude, increased *time-to-peak*	Reduced amplitudes in central ring

NA = Not applicable

1.5 Rationale of the Study

ADOA is a progressive inherited optic neuropathy characterised by childhood onset, optic atrophy, a central to centro-coecal visual field loss and colour vision loss (Votruba et al., 1998). The disease is caused by mutations in the *OPA1* gene which affect mitochondrial integrity and function. The mutations lead to the death or loss of RGCs eventually resulting in visual loss (Alexander et al., 2000; Delettre et al., 2000).

The PhNR is a negative going potential occurring immediately after the b-wave in a brief flash cone ERG, and in a long duration flash ERG, it is seen again after the d-wave. The PhNR elicited by a red on blue stimulus can be used to assess RGC function. Using a long duration flash, the PhNR is separated into ON and OFF components which can be used to separately investigate the ON and OFF pathways.

In the only study to have evaluated the PhNR in humans with ADOA, significant reductions in amplitude have been reported in the small (n=8) sample (Miyata et al., 2007), but no comparative or longitudinal data are available. Although these results highlight the diagnostic potential of the PhNR in ADOA, they used a brief white flash to evoke a full field PhNR, which provides a poor signal to noise ratio compared to a red on blue flash, and cannot distinguish ON and OFF components. A recent study in a mouse model shows that the ON-centre RGCs, but not the OFF-centre RGCs, are preferentially affected early in the disease process prior to visual loss (Williams et al, 2010). This finding therefore needs to be investigated in humans with ADOA and deserves full exploration.

In addition, reports on the use of idebenone in LHON have been encouraging (Klopstock et al., 2011). Pharmacological trials and gene therapy rescue in a mutant mouse model of ADOA, B6;C3-*Opa1*^{Q285STOP} (Davies et al., 2007) are currently underway and if successful, these will lead the way to human therapeutic trials. It is therefore essential to detect and quantify early human disease and monitor subtle changes in status due to therapy with suitable, relevant biomarkers and end-points.

1.6 Hypothesis

On the basis of the above, it was hypothesised that

1. a selective reduction in the ON ganglion cell response (PhNR-ON) in humans should be diagnostic for ADOA and seen very early in the disease and
2. the PhNR-ON amplitude, and specifically the ratio of PhNR-ON to PhNR-OFF (PhNR-ON:PhNR-OFF), will decrease as the disease progresses.

1.7 Aims of the Study

The primary aim of this thesis was to assess the effect of *OPA1* mutation causing ADOA on the ON and OFF pathway of the retina in individuals affected by the disease using a long duration ERG elicited by a red on blue stimulus. The specific objectives of this study were

1. to optimise an electrophysiological protocol for recording the focal and full-field PhNR ON and PhNR OFF components using a long duration red flash on a rod suppressing blue background (red on blue stimulus) in healthy participants
2. to record focal and full-field long duration ERGs using a red on blue stimulus as well as pattern reversal ERGs and full-field brief flash ERGs in participants with ADOA and to compare them to recordings from controls.
3. to record and compare baseline measures which will include visual acuity, contrast sensitivity, colour vision, perimetry, and optical coherence tomography (OCT) in participants and in controls.
4. to determine and compare the diagnostic potential of the red on blue long duration PhNRs and other electrophysiological tests used in previous studies (i.e. the PERG and brief flash PhNR)
5. to assess the relationship between the long duration PhNRs and other clinical tests of the retina (i.e. visual acuity, contrast sensitivity, visual field sensitivity and optical coherence tomography).

2 CHAPTER TWO – ELECTROPHYSIOLOGICAL PROTOCOL DEVELOPMENT

2.1 Introduction

The overall aim of this project was to explore retinal function of patients with ADOA using electrophysiology. The ocular electrophysiology methods used in this study were the focal and full-field long duration flash ERG, the full-field brief flash ERG and the PERG.

As there was no published standard protocol for recording the PhNR-ON and PhNR-OFF, a pilot project was carried out in healthy controls to develop a suitable protocol for measuring these components. The protocol for recording the full-field brief ERG was adopted from an earlier study conducted in the same laboratory (Mortlock et al., 2010) and is described later in Chapter 5. The PERG recording protocol was as recommended by ISCEV and is described later in Chapter 3. This chapter describes the general methods and ERG recording equipment used throughout the study as well as experiments conducted to determine an appropriate protocol for measuring the focal PhNR-ON and PhNR-OFF components. Specific methods used in the different experiments will be described under their respective sections.

2.2 General Methods

2.2.1 Participants

All participants recruited as controls at the protocol development stage were healthy adults recruited from students and staff of the School of Optometry and Vision Sciences, Cardiff University as well as their friends and family. Inclusion criteria were best corrected visual acuity of 0.1 logMAR or better in the test eye, clear ocular media ($\leq$ Grade 2, LOCS-III (Chylack et al., 1993)), a normal retinal appearance and normal colour vision. Exclusion criteria were history of ocular disease or systemic disease known to affect visual function. The study conformed to the Declaration of Helsinki and was approved by the National Health Service (NHS) Research Ethics Committee for Wales (REC Reference

02/9/001) as well as the ethics committees of the School of Optometry and Vision Sciences, Cardiff University. All participants provided their written consent after receiving a participant information sheet and having the opportunity to ask questions.

2.2.2 Light Stimulator

Flash stimuli and light backgrounds for focal and full-field long duration ERGs were generated by a modified light emitting diode (LED) miniature Ganzfeld stimulator (Figure 2.1A) (CH Electronics, Bromley, Kent, UK). (Details of the modification to the stimulator are provided in section 2.2.3). The stimulator head contained blue (469 nm), green (521 nm), amber (597 nm) and red (660 nm) LEDs. The luminance of each LED was controlled by an analogue dial on the control box. The dial had a minimum setting of 0 and maximum of 1000. The relative spectral profiles and the photometric properties of the LEDs are provided in Figure 2.2A and Table 2.1 respectively and the luminances of the LEDs in response to the dial settings are plotted in Figure 2.2B.

Focal stimulation was produced by mounting the modified miniature Ganzfeld LED tube into the middle of a light box (44 cm x 44 cm x 10 cm) such that the circular stimulus subtended 20^{o} diameter at a viewing distance of 15.6cm (Figure 2.1B and C). The face of the light box (towards the viewer) was made of transparent Perspex covered on the back with diffuser sheet. The focal stimulus was thus in the plane of the face of the light box. A strip of white LEDs (colour temperature > 7000K) lined the inside of the box and the LEDs were passed through a blue filter (Lee Filter 068 Sky Blue; peak transmission of ~75% for wavelengths 425 – 450 nm; Lee Filters, Hampshire, UK) to produce a blue surround background needed to desensitise the peripheral retina and minimise or eliminate the effect of stray light. (The spectral profile of the net output of blue surround is shown in Figure 2.2). Luminance of the surround was controlled by a variable voltage dial (Figure 2.1B). A pair of cross hairs centred in the middle of the stimulus served as the fixation target. Full-field ERGs were recorded by holding the stimulator head directly to the eye (Figure 2.1D). All the equipment used in this project met the ISCEV recording requirements (Marmor et al., 2009).

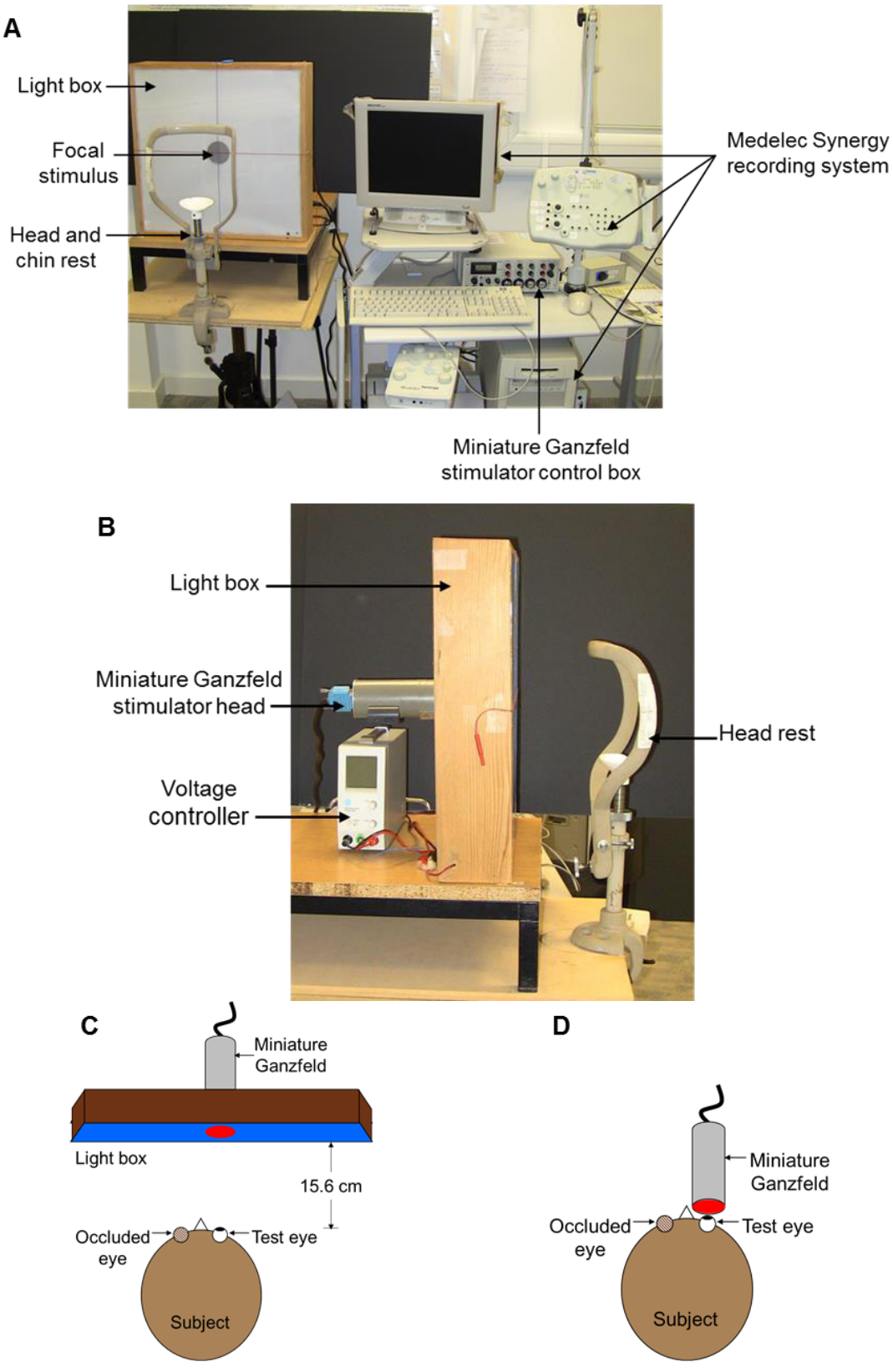

Figure 2.1. A photograph showing the equipment used for recording the focal ERGs. (A) Front view. (B) Side view of the light box with the miniature Ganzfeld stimulator head in place. The voltage controller controls the luminance of the LEDs in the light box. (C) Cartoon showing the positions of the participant and the focal stimulus when recording focal ERGs. (D) Position of the miniature Ganzfeld held directly to the eye when recording full field ERGs. Note that the rod saturating blue background was on constantly with the flashing red stimulus superimposed on the blue background.

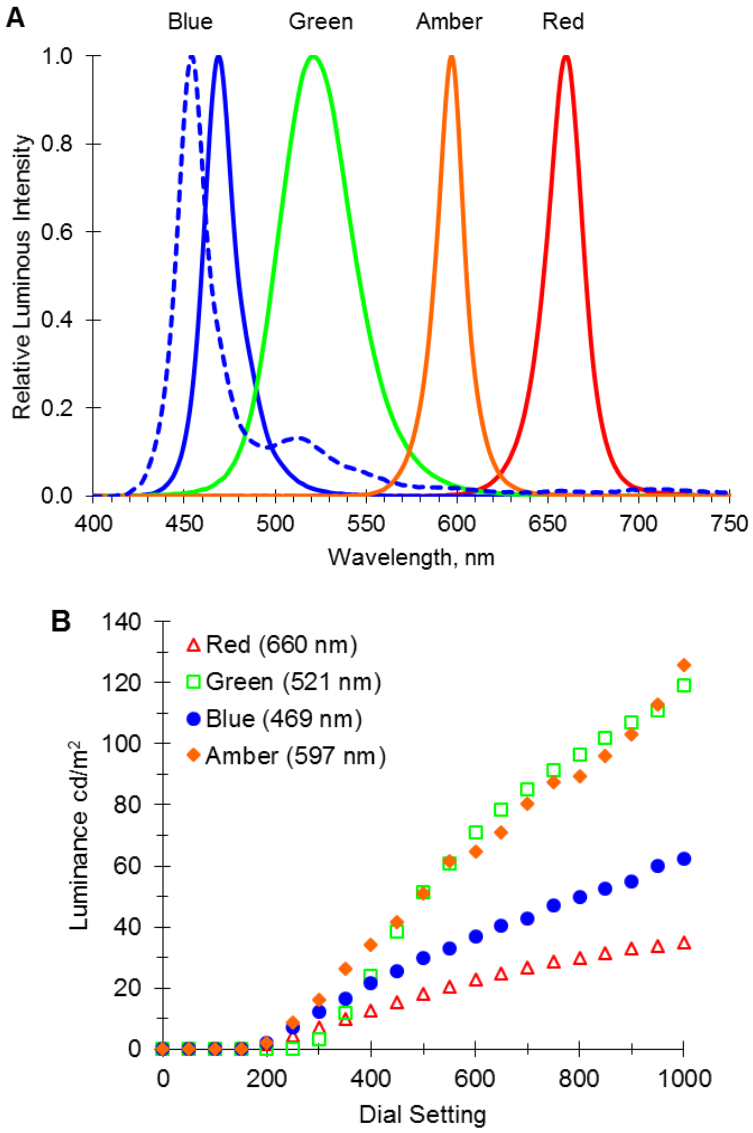

Figure 2.2. (A) Relative spectral profiles of light sources used in this study measured using a spectro-radiometer (Specbos 1201, Horiba Jobin Yvon, Middlesex, UK). The spectra of the LEDs are shown in thick lines and that of the blue desensitising background is shown as a dashed blue line. (B) Graph showing the changes in luminance of the four LEDs in the miniature Ganzfeld to the dial settings from 0 (minimum) to 1000 (maximum). Luminances were measured using Minolta CS-100 (Konica Minolta, Osaka, Japan) on 21/02/2013.

Table 2.1. Photometric properties of light sources used in the study.

LED	Peak wavelength, nm	FWHM	Chromaticity Coordinates		Colour Purity, %
			x	y	
Red	660	23.20	0.71	0.28	97.65
Blue	469	20.30	0.12	0.09	96.25
Green	521	47.20	0.79	0.68	71.40
Amber	597	17.70	0.60	0.40	99.70
Blue surround	454	19.80	0.16	0.12	81.50
Amber surround	615	94.00	0.59	0.40	97.50

FWHM = Full width at half maximum

2.2.3 Calibration of equipment

In the pilot study, all stimuli and background lights were calibrated using an LS-110 spot photometer (Konica Minolta, Osaka, Japan). In experiments conducted after the pilot study, an ILT 1700 Research Radiometer with Y#29295/R#1032 luminance detector (model SED033, Able Instruments and Controls, Reading, UK) was used, because of its better performance at measuring very brief flashes. The computer monitor used for pattern ERG recordings was calibrated with a spot photometer (LS-110; Konica Minolta, Osaka, Japan) which is recommended by ISCEV for measuring the luminance of a small area (Brigell et al., 2003). The wavelengths of the light sources were measured using a Specbos 1201 spectro-radiometer (Horiba Jobin Yvon, Middlesex, UK)

At the start of the study, it was noticed that the maximum luminance produced by the red LED in the miniature Ganzfeld stimulator was 35 cd/m^2 when it was set up for focal ERG recording (Figure 2.2B). This was lower than required for the study. In order to increase the luminance of the red LED for recording focal ERGs, the stimulator was modified as follows. A hemispherical diffusion cap, which was originally fitted to the miniature Ganzfeld stimulator, was found to be responsible for attenuating the luminance of the LEDs. It was therefore removed and replaced with a series of white diffusion sheets (Lee Filters: 216 white diffusion, 250 ½ white diffusion and 251 ¼ white diffusion; Lee Filters, Hampshire, UK) which produced a relatively homogenous plane surface without sacrificing luminance. The diffusers were introduced at different stages during the pilot study. The LEDs were re-calibrated after each change (i.e. dial settings were changed) to ensure the required luminances were obtained. The dial settings, corresponding luminance and dates are provided in Appendix I. This modified configuration of the miniature Ganzfeld stimulator was also used to record the full field ERG (i.e. the plane diffuser system was maintained). A transparent Perspex cover was fitted over the stimulator head to keep the diffusing sheets in place when the stimulator was in the hand-held mode.

In addition, the different coloured LEDs took different amounts of time to attain a stable luminance after they had been switched on. The “warm-up” times for the various LEDs were measured (Table 2.2) and a 30-minute time allowance was made before starting ERG recordings.

Table 2.2. Minimum warm-up time for LEDs in miniature Ganzfeld stimulator

LED	Red	Green	Blue	Amber
Minimum warm up time, mins	20	10	10	30

2.2.4 Electrodes

In this study, ERGs were recorded monocularly with Dawson-Trick-Litzow (DTL) fibre electrodes (Unimed Electrode Supplies, Surrey, UK) as active (in the test eye) and contralateral reference (in the occluded non-test eye) electrodes. This configuration improves signal to noise ratio (Coupland, 2006; Bach et al., 2013).

When using DTL electrodes, the placement of the fibre is a key consideration as it affects response amplitudes (Smith and Lamb, 1997; Hebert et al., 1999). In this study, the DTL fibre was placed in the lower fornix of each eye and the loose end fastened using medical tape at the inner canthus (Blenderm, Viasys Healthcare Ltd, Warwick, UK). Although this method produces about a 30% reduction in amplitude of signals as compared to placing the DTL on top of the lower lid margin in apposition to the cornea, the former produces more repeatable signals that are less contaminated by blinks and eye movement artefacts (Hebert et al., 1999). A silver-silver chloride 9-mm diameter, touch-proof skin electrode (Viasys Healthcare Ltd, Warwick, UK), placed at the mid-frontal forehead was used as the ground electrode.

2.2.5 Electronic recording system

Signals were digitally averaged and bandpass filtered from 1 to 100 Hz (unless otherwise indicated) using a Medelec Synergy system (Oxford Instruments PLC, Surrey, UK). The sampling rate was 1 KHz. Signals were recorded in blocks of 10 - 20 responses, with a total of 40 – 60 averaged per trace. Four to eight traces were obtained for each stimulus condition. The traces were superimposed on each other and visually inspected to confirm signal repeatability and averaged off-line into a single trace containing 160 – 300 averages. An automatic artefact rejection system removed signals contaminated by large eye movements and blinks.

2.2.6 Procedures

At least one eye (test eye) of the subject was dilated with one drop of 1% Tropicamide. While the subject waited for mydriasis (20 – 30minutes), the miniature Ganzfeld stimulator was turned on for the LEDs to warm-up. The subject's forehead was scrubbed with gel (Nuprep, D.O. Waver and Co, Aurora, CO) in order to reduce the impedance. The electrode cup for the ground electrode was filled with electrolyte gel (Teca, Pleasantville, NY) and then attached with surgical tape (Blenderm, EM, St. Paul, MN) to the mid-frontal forehead. The DTL electrodes was attached to their holders and placed in the lower fornix of each eye; the holder and the free end of the fibre were secured with surgical tape at the outer canthus and nose respectively. All leads from the electrodes were secured to the nape, with enough allowance for head movements.

When the test eye was fully dilated, the electrodes were plugged into the Medelec Synergy system. The resistances of the electrodes were checked to ensure each was below 4kΩ. The participant was then seated in front of the stimulus (which had been allowed to warm-up for 30 mins) and pre-adapted for a minimum of 5 minutes prior to testing. If subjects complained of irritations or discomfort with the DTL that interfered with the recordings, a drop of 0.5% Proxymethacaine was administered in each eye to ease the discomfort.

2.2.7 Signal Analysis

The ERGs were exported into a Microsoft Excel 2013 spreadsheet and Fourier analysed offline to remove high frequency signals above 50Hz. Fourier analysis was based on the approach by Stroud (1986). The cut-off frequency was determined from a visual inspection of the power spectrum plot which showed that most of the power was concentrated in the first 20 harmonics and had levelled off at 25 harmonics (50Hz) (see Appendix VI). The amplitude of the a-wave was measured from baseline to trough, and the b-wave amplitude was measured from the trough of the a-wave to the peak of the b-wave as recommended by ISCEV (Marmor et al., 2009). The PhNR-ON was measured from peak of b-wave to the negative trough immediately following the b-wave. The d-wave was measured from the time point of stimulus offset to the first

maximum peak (Sustar et al., 2006; Horn et al., 2011). The PhNR-OFF was measured from the peak of d-wave to the most negative trough immediately after the d-wave (Horn et al., 2011) (Figure 2.3). The peaks and troughs of the components were identified objectively within a predefined time window using Microsoft Excel 2013.

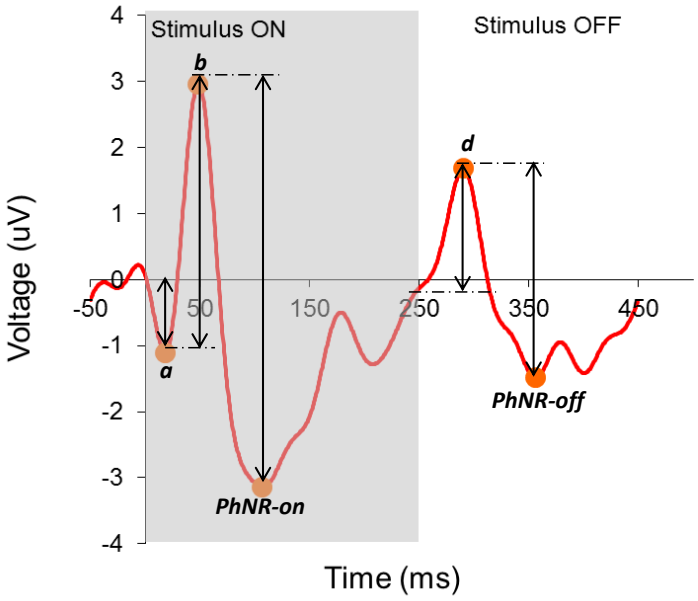

Figure 2.3. A representative diagram of a focal long duration ERG recorded from one participant. It shows the various ERG components and how they were measured. a = a-wave; b = b-wave d = d-wave

2.3 Experiment 1: Determining Stimulus Duration

2.3.1 Introduction

The waveform of the ERG changes with stimulus duration. In a brief flash ERG (<50ms), the ON- and OFF responses are superimposed while for longer duration stimuli, the responses are separated (Evers and Gouras, 1986; Sieving, 1993; Kondo et al., 2008a). In these studies, the OFF responses were clearly separated when stimulus duration was 100ms or greater. Stimulus duration also affected both amplitude and time-to-peak of the ERG components. For example, in a study using macaque monkeys, Kondo et al (2008) observed that the b-wave and PhNR amplitudes of the focal ERG increased with duration up to about 50msec and then decreased just as the d-wave (OFF responses) began to emerge. They also found that the time-to-peak of the PhNR, increased from 75 msec for a 5 msec flash to 110 msec when the stimulus duration was

50 msec. Further increases in the stimulus duration did not change the time-to-peak significantly.

The purpose of this experiment was therefore to study the effect of stimulus duration on the focal PhNR in human subjects and to select the optimum stimulus duration for the main study. A red stimulus spot on a blue illuminated background was used because it has been reported that this colour combination is most effective in eliciting large PhNRs especially at weak to moderate stimulus intensities (Viswanathan et al., 2001; Rangaswamy et al., 2007).

2.3.2 Methods

Three healthy participants were recruited for this experiment and prepared as described in section 2.2.6 above.

A 20^{o} diameter red flash stimulus (55 cd/m^2) on a blue rod-suppressing background (100 scot cd/m^2), was generated by the miniature Ganzfeld stimulator. The flash and background luminance used in this study were based on values reported as being optimal for eliciting the focal PhNR in macaque (Kondo et al., 2008a). The luminance of the blue surround from the light box was calibrated to provide the same scotopic luminance as the blue LED in the miniature Ganzfeld stimulator. The stimulus duration was increased from 50 to 250 msec in 50 msec steps on a 500 msec time base. The stimulus repetition rate was fixed at 2 Hz. An additional ERG with a flash duration of 500 msec and 1 Hz frequency on a 1 sec time base was recorded from one participant. A minimum of 180 responses were averaged for each major trace. Signals were analysed as described in section 2.2.7. The ERGs of the three individuals were inspected to look for qualitative changes in waveform with an increase in stimulus duration. Time-to-peak and amplitudes were also plotted as a function of stimulus duration.

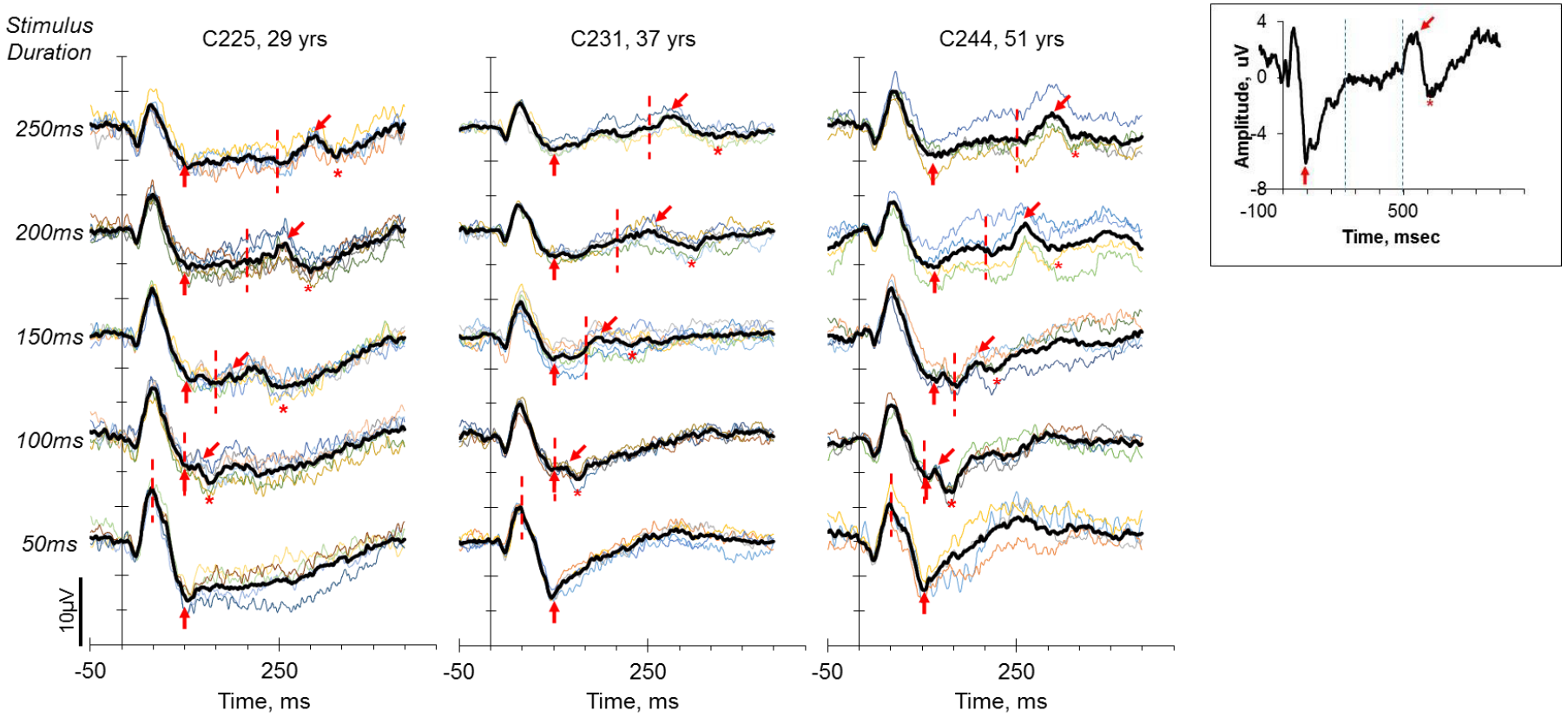

Figure 2.4. The effect of increasing stimulus duration on the ERG components is shown for three participants in this study. The red vertical dashed lines represent the point of stimulus offset. Red upward arrows show the PhNR-ON, the down arrow and asterisks show the d-wave and PhNR-OFF components respectively. Right inset shows the ERG recorded from one participant (C231) using a 500msec flash on a 1sec sweep duration.

2.3.3 Results

Figure 2.4 shows the focal ERGs of the three participants in response to different stimulus durations of 50 to 250 msec. As stimulus duration increased, the waveform was separated into ON and OFF components corresponding to the on and off phases of the stimulus respectively. The ON component consisted of the a-wave, b-wave and PhNR-ON. The OFF components consisting of the d-wave (red downward arrow) and PhNR-OFF component (asterisks) began to emerge when stimulus duration reached 100msec.

However, the traces recorded using stimulus duration of 200 and 250 msec showed the d-wave and the PhNR-OFF more clearly separated from the ON-responses. It can also be observed that when stimulus duration was 250 msec, the traces appeared level off between 200 and 250msec. This was checked with a 500msec flash which showed that the ON responses returned to baseline by 250msec (Figure 2.4 inset).

The mean amplitude of the b-wave and PhNR-ON decreased with stimulus duration and approached a plateau with the 250msec flash (Figure 2.5). The d-wave and PhNR-OFF on the other hand increased in amplitude and also approached a plateau with the 250msec flash.

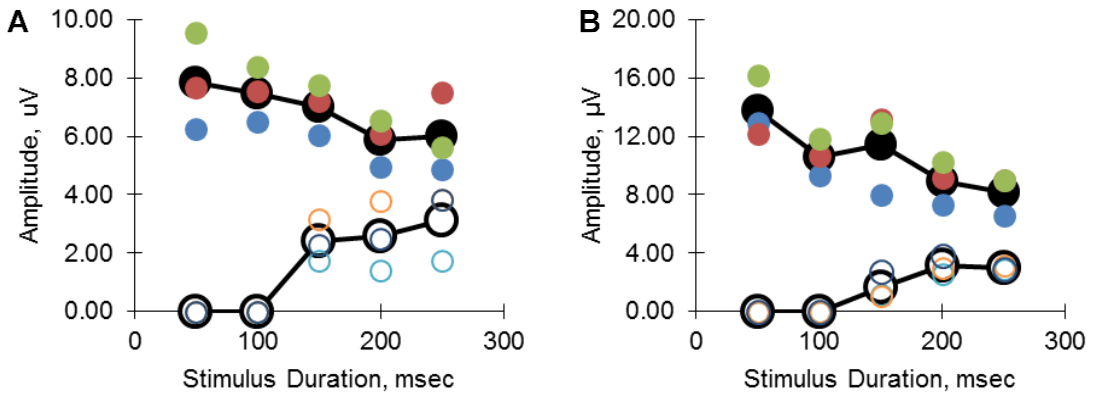

Figure 2.5. Effect of stimulus duration on (A) b-wave (filled dots) and d-wave (open dots) amplitudes and (B) PhNR-ON (filled circles) and PhNR-OFF (open dots) amplitudes. The black dots represent the mean and the coloured dots are for individuals

2.3.4 Discussion

The results show a progressive separation of the ON and OFF responses with increasing stimulus duration. However, distinct d-wave and PhNR-OFF components were seen with the 200 and 250msec flash duration in this study. This is similar to findings reported in focal ERGs obtained from macaque using similar recording parameters (Kondo et al., 2008a).

The effect of stimulus duration on the b-wave and d-wave amplitude was similar to reports from other studies investigating the full-field ERG (Evers and Gouras, 1986; Sieving, 1993; Sustar et al., 2006). In this study, the decreasing PhNR-ON amplitude and the increasing PhNR-OFF amplitude which mimicked the behaviour of the b-wave and d-wave respectively, also approached a plateau with the 250msec duration. This is important as it signifies the complete separation of the ON and OFF components when the plateau is reached. This was confirmed by the return of the ON components to baseline within 250 msec when the 500msec flash was used.

2.3.5 Conclusion

In conclusion, the 250 msec stimulus flash duration was selected for the main study since it produced optimal delineation of the PhNR-ON and PhNR-OFF components of the focal ERG. In addition, it was the same stimulus duration used by Colotto et al (2000) to study the focal PhNR-ON and PhNR-OFF components.

2.4 Experiment 2: Determining Stimulus Luminance

2.4.1 Introduction

The amplitudes of ERG waveforms vary as a function of stimulus luminance and the increase is not always monotonic. For example the b-wave of the brief flash ERG initially increases in amplitude with increasing stimulus luminance, but after reaching a peak at a luminance of about 0.5 – 0.86 log cd.s/m^2, it gradually declines creating the so called photopic hill (Wali and Leguire, 1992; Binns et al., 2011). The b-wave amplitude of long duration flash on the other

hand reaches a plateau at higher luminances without decreasing whereas the d-wave exhibits the photopic hill phenomenon (Kondo et al., 2000).

In order to determine the effect of stimulus intensity on the focal PhNR waveform, and to optimise experimental parameters, a second set of experiments was undertaken. Previous investigators (Kondo et al., 2008a), determined that 55 cd/m^2 maximised the focal PhNR signal in monkeys and did not produce stray light. As such, this experiment investigated the intensity response relationship for the focal PhNRs for a range of luminances from 2 – 55 cd/m^2.

2.4.2 Methods

The stimulus set up was as described in section 2.3.2, but in this study the stimulus duration was fixed at 250ms, while the luminance was varied from 2 – 55 phot cd/m^2 (Table 2.3). Three subjects (2 males, age 29 and 24 years; 1 female, age = 37 years) were recruited for this experiment and prepared as described in section 2.2.6. A minimum of 180 responses were averaged for each major trace. The recording equipment and procedures for preparing the participants are described in section 2.2. The ERG amplitudes were measured as described previously in 2.2.7. The amplitudes of the ERG sub components were plotted against flash luminance for each individual. The mean amplitudes were however, normalised and plotted as a function of the luminance.

Table 2.3. Luminance and dial settings used in this study.

Luminance, cd/m^2	2	4	7	12	17	26	40	55
Dial Setting	198	230	272	339	412	556	772	989

2.4.3 Results

Generally, all the ERG components increased in amplitude and became more prominent with increasing stimulus luminance (Figure 2.6 and 2 7). The PhNR-ON and PhNR-OFF were discerned in two subjects (C245 and C247) from 4 cd/m^2 and upwards and were visible in all three subjects from 7 cd/m^2 (shown by red arrows in Figure 2.6)

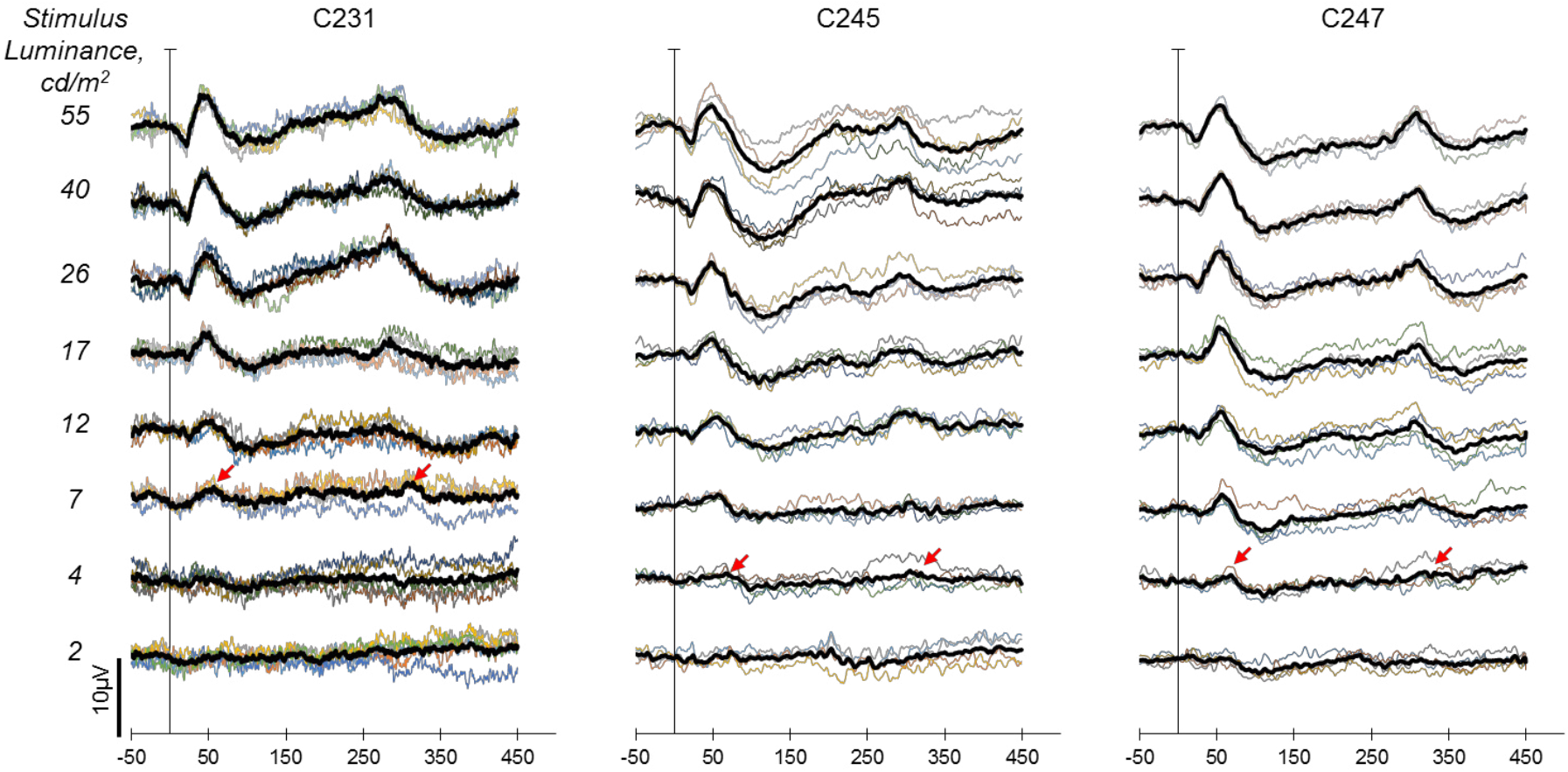

Figure 2.6. ERGs of three control participants showing the effect of luminance on the focal long duration ERG. Thick black traces are averaged traces of the light coloured individual traces. All traces band-passed at 1-100 Hz except traces for C231 (bandpass = 1 – 1KHz). The PhNR-ON and PhNR-OFF components (red arrows) were first discernible in participants C245 and C247 at 4cd/m2 and later in participant C231 at 7cd/m^2.

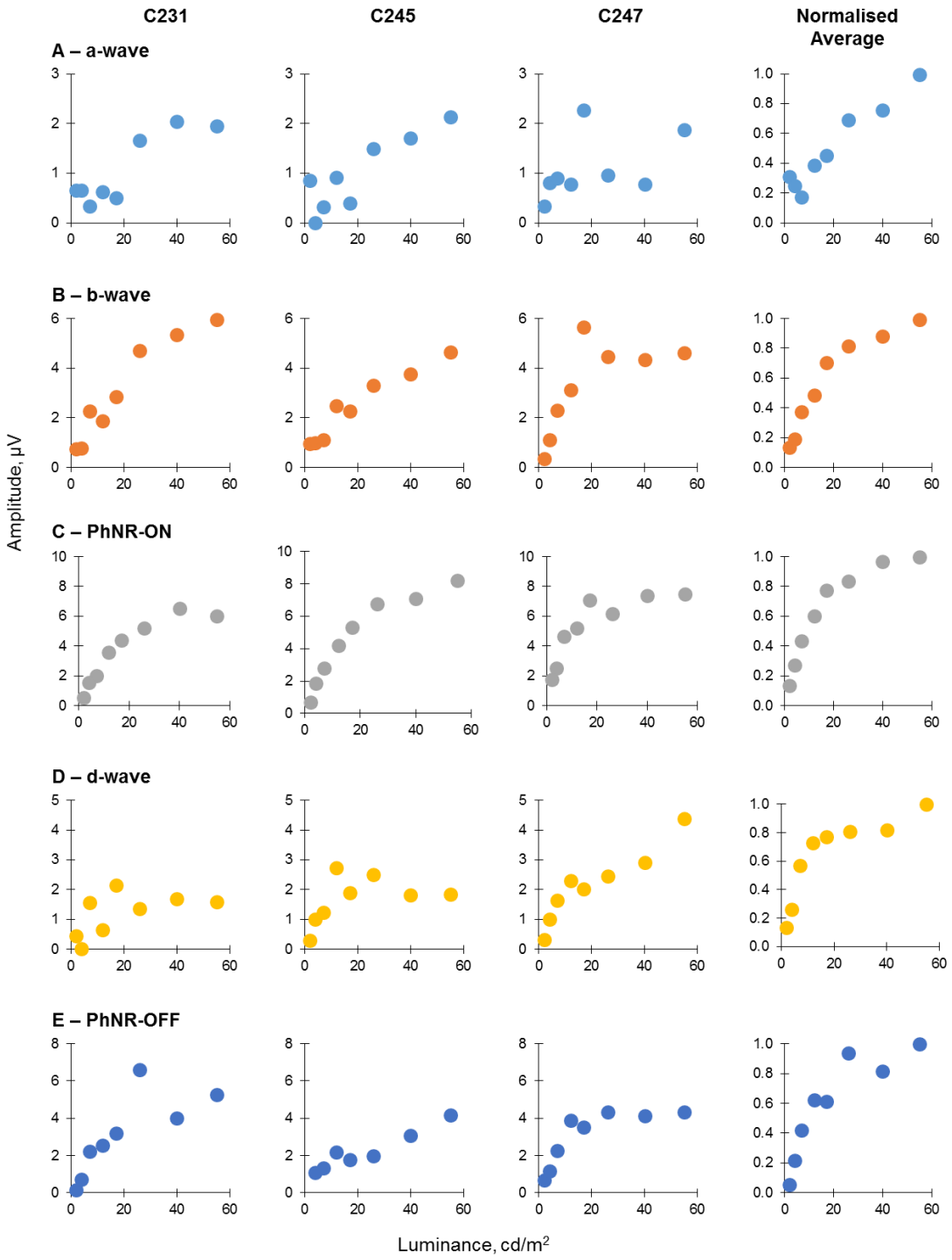

Figure 2.7. Plot of stimulus luminance (x-axis) against amplitude (y-axis)for the traces shown in Figure 2.6 (above). The plot on the extreme right represents the normalised averaged amplitudes of the corresponding components for the three participants.

The mean amplitude of the a-wave showed a linear increase with stimulus luminance whilst the mean amplitudes of the b-wave, PhNR-ON, d-wave and PhNR-OFF increased steadily from the lowest luminance and tapered off towards the highest tested luminance (Figure 2.7). The response of d-wave amplitude to luminance was different in all three subjects, however, when the

data were normalised and averaged (extreme right), the plot showed an increase in amplitude with luminance. The PhNR-OFF showed a general increase in amplitude with luminance for all three subjects.

2.4.4 Discussion

This experiment set out to determine the optimum stimulus luminance for isolation of the PhNR-ON and PhNR-OFF using a red-on-blue stimulus. The results indicate that the PhNR-ON and PhNR-OFF, as well as the b- and d-wave amplitudes increased with stimulus luminance and approached a plateau at the higher luminances. The a-wave, however, did not show any such plateauing effect over the luminance range tested. The greatest amplitude was obtained for all waveforms with the most luminous stimulus, 55 cd/m^2. A similar behaviour of the a- and b-wave was reported by Kondo et al (2000) for a full-field ERG. They also showed that the d-wave exhibited a photopic hill phenomenon i.e. with increasing stimulus luminance, the d-wave amplitude increased to a maximum and then decreased. This was not observed in this study with the d-wave over the recorded luminance range. Examination of the PhNR-ON and PhNR-OFF luminance-response curves in Figure 2.7 indicates that still larger PhNRs may be obtained with still higher stimulus intensities i.e. the function has not saturated even at the highest luminance used. However, it was reported that using focal stimulation with luminances >55 cd/m^2 may be contaminated by peripheral stray light (Kondo et al., 2008a). Furthermore, equipment limitations prevented the delivery of higher luminances. The 55 cd/m^2 was therefore selected as optimal luminance, similar to the luminance reported by Kondo et al (2008).

2.4.5 Conclusion

The focal PhNR-ON and PhNR-OFF are optimally elicited using a red flash of luminance 55cd/m^2 on a blue background with luminance 100 scot cd/m^2.

2.5 Experiment 3: Determining optimal stimulus and background colours (wavelengths)

2.5.1 Introduction

The ISCEV standard recommends using a white flash on a white desensitising background for clinical full-field flash ERG. However, various studies investigating the PhNR have used different combinations of stimulus and background colours and popular among these is the red flash on blue background. Previous studies have shown that red flashes on a rod saturating blue background gives higher amplitude responses than other combinations of chromatic or achromatic stimuli (Viswanathan et al., 1999; Viswanathan et al., 2001; Rangaswamy et al., 2007; Sustar et al., 2009). Rangaswamy et al (2007) and Sustar et al (2009) posit that the amplitude of the PhNR elicited by stimuli of different colours depends not only on the strength of the stimulus, but also on the specificity of each coloured stimulus for a single type of cone and the effectiveness of the rod-saturating background in adapting the cones that are activated. As such combinations of monochromatic light, which are more specific for a single cone type and induce the least spectral antagonism are best for eliciting the PhNR. A red-on-blue is thus effective because the red stimulus selectively stimulates the L-cones while the blue background selectively adapts the rods and S-cones.

Some studies into ADOA suggest that the S-cone pathway is more affected by the disease than the L and M cones (Holder et al., 1998; Johnston et al., 1999) while others suggest the disease has no preference for any particular cone pathway (Votruba et al., 1998a; Reis et al., 2013). An S-cone dominated ERG may also be elicited using a blue-on-amber stimulus (Gouras et al., 1993; Arden et al., 1999; Vincent et al., 2013). This experiment was therefore conducted to investigate the effect of different combination of stimulus and background wavelength on the human focal ERG and to optimise parameters for the main study.

2.5.2 Methods

The experiment was conducted using the equipment and methods described in section 2.3.2. However, the flash duration was fixed at 250 msec. In addition,

different combinations of stimulus flash and background wavelengths were recorded and are described in Table 2.4

Table 2.4. Flash and background parameters

Flash (Peak wavelength)	Photopic Luminance, cd/m^2 (Dial Setting)	Background (Peak wavelength)	Scotopic Luminance, scot cd/m^2
Red (660nm)	55	Blue (469nm)	100
Amber (597nm)	55	Blue (469nm)	100
Green (521nm)	55	Blue (469nm)	100
Blue (469nm)	55	Amber (597nm)	52
Blue (469nm)	55	Green (521nm)	100
Red (660nm)	55	Amber (597nm)	52
Green (521nm)	55	Amber (597nm)	52
Blue (469nm)	55	Amber (597nm)	104
Blue (469nm)	55	Amber (597nm)	115

For simplicity, luminance values have been rounded up to nearest whole number

The initial aim of this experiment was to record ERGs using flashes with a luminance of 55cd/m^2 on backgrounds with a luminance of 100 scot cd/m^2. However, the maximum photopic luminance produced by the amber LED was 300 cd/m^2 which equates to 52 scot cd/m^2 (= 2000 scot td for 7mm pupil), assuming light emitted was monochromatic at a wavelength of 597nm. This sufficiently produced the luminance required to suppress the rods (Aguilar and Stiles, 1954) and ERGs on amber backgrounds were recorded at this setting. In this set of experiments, five healthy participants (3 females and 2 males; aged 22 - 26) were recruited for this experiment. However, data for two participants were not included in the results. One participant (C222) complained of discomfort from the glare of the stimulus lights and as such she often squinted and made small eye movements during the experiment which made the ERGs unreliable. In the case of the second participant (C246), a complete dataset was not available.

Due to the limitation of the amber LED in the miniature Ganzfeld stimulator, two attempts were made to increase the amber background to at least 100 scot cd/m^2. In the first attempt, a projector system was employed to increase the amber background luminance to 100 scot cd/m^2. An amber filter (LEE Golden Amber) was fitted to a projector which was then used to floodlight the viewing surface of the light box. The projector was mounted on a stand and placed about 1.5m behind and to the side of the participant (i.e. when participant was seated for recordings). The projector was then angled in such a way that the

participants were not in the way of the projected beam. This method was successful in increasing the amber background to 600 cd/m^2 (= 104 scot cd/m^2). ERGs were recorded in two female participants (C258 and C259).

In the second attempt, an amber filter (LEE Golden Amber) was fitted to an LED lamp. The lamp was placed on top of the light box and angled down so that the beam of the LED flood lit the viewing surface of the light box. This configuration was successful in increasing the luminance of the amber background to 665 cd/m^2 (115 scot cd/m^2). ERGs were recorded from 2 additional healthy participants (C226 and C332).

2.5.3 Results

The ERGs obtained with the different stimuli combinations are shown in Figure 2.8. The waveforms of the ERGs produced by the red, green and amber flashes on the rod-saturating blue background were similar. The ON pathway (a-wave, b-wave and PhNR-ON) and OFF pathway (d-wave and PhNR-OFF) responses were easily discernible in with these stimuli.

The ERG waveforms produced by the blue-on-amber and blue-on-green stimuli were similar to each other, but different from the others (Figure 2.8, column 4 and 5). The red-on-amber and green-on-amber ERGs, recorded from one individual, did not show discernible components (Figure 2.8 inset) and were not repeated for the other participants.

Further ERGs were collected from two participants (C258 and C259) using the projector system to increase the luminance of the amber background to above 100 scot cd/m^2. However, the hum of the projector generated a lot of electrical noise and so this aspect of the experiment was discontinued (Figure 2.9). The second configuration, which used the external LED lamp to increase the luminance of the amber background, produced noise levels lower than the noise levels associated with the projector in the two participants tested (Figure 2.10).

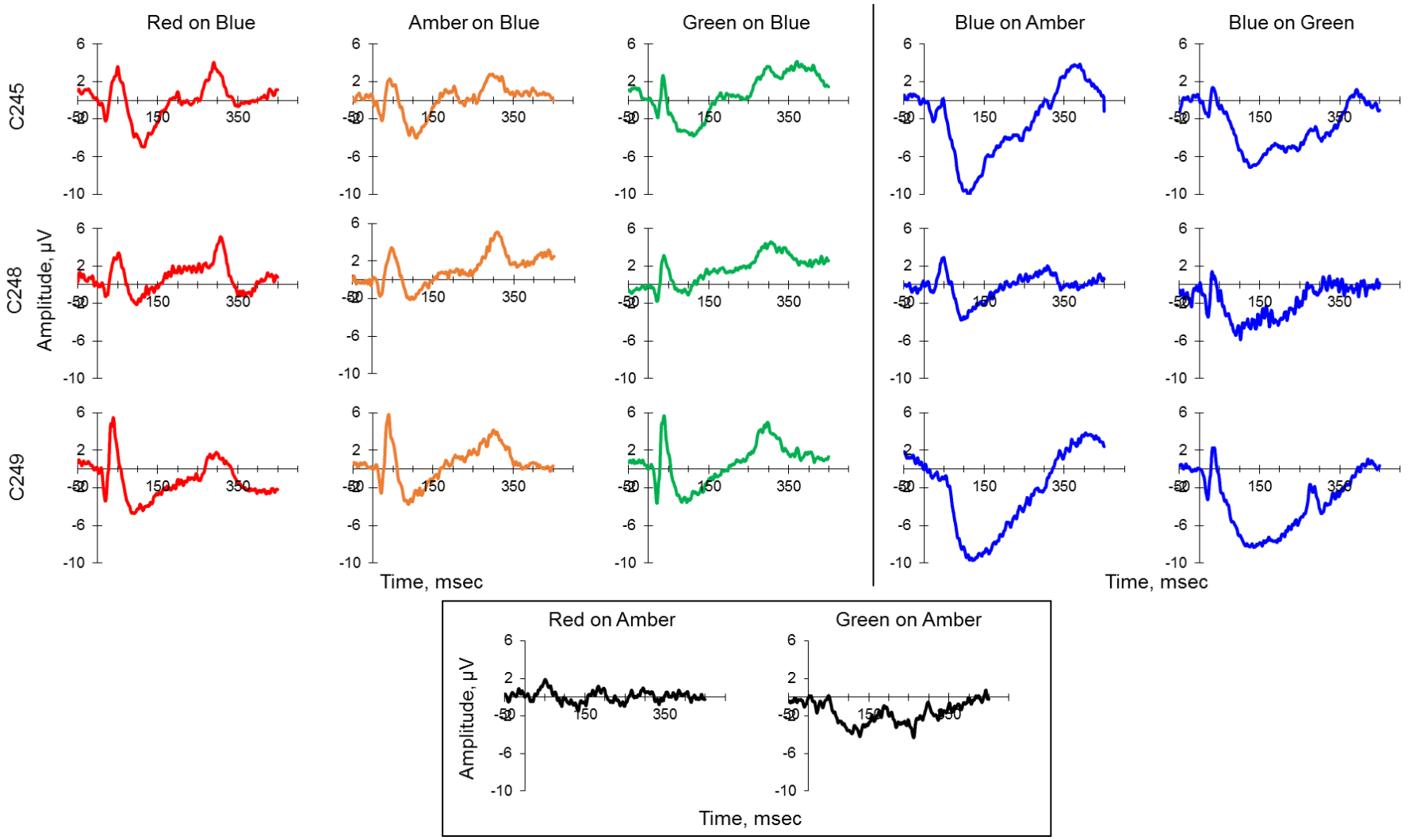

Figure 2.8. Focal ERGs recorded from 3 participants C245, C248 and C249 using different combinations of flash and background colours. The luminance for all flashes was 55 cd/m^2. The luminances of the blue and green backgrounds were 100 scot cd/m^2 and that of the amber was 52 scot cd/m^2

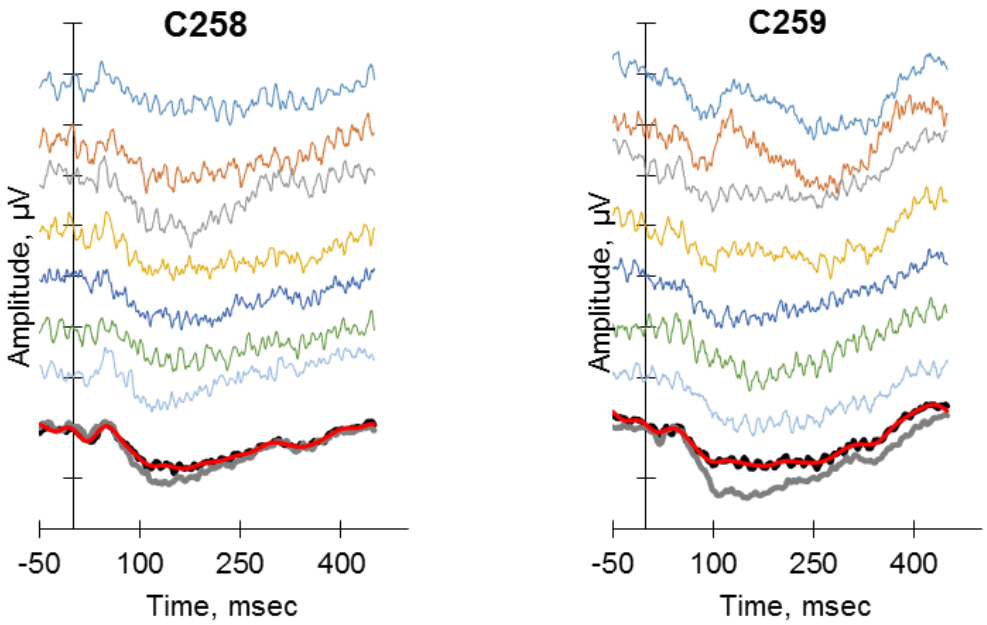

Figure 2.9. Focal ERGs recorded with blue flash (55 cd/m^2) on an amber background (104 cd/m^2) in two participants A and B. The ERGs were recorded in blocks of 45 to 60 responses (thin coloured lines) and averaged offline (thick black line). The projector created a lot of electrical noise (seen in the thin upper traces). The red line represents the averaged ERG after using Fourier analysis to remove high frequency noise (above 30Hz). The thick grey lines are focal blue on amber ERGs recorded from the same participants with the projector switched off (i.e. the amber background now reduced to 52 scot cd/m^2)

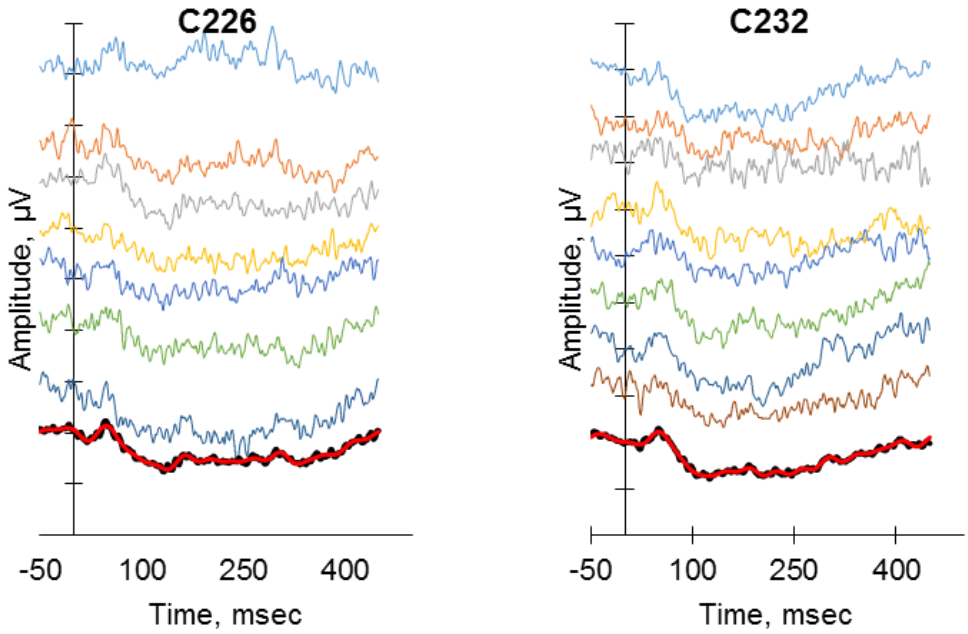

Figure 2.10. Focal ERGs recorded with blue flash (55 cd/m^2) on an amber background (115 scot cd/m^2) in two participants C226 and C232. The ERGs were recorded in blocks of 45 to 60 responses (thin coloured lines) and averaged offline (thick black line). The red line represents the averaged ERG after using Fourier analysis to remove high frequency noise (above 30Hz).

2.5.4 Discussion

The results showed that focal PhNR-ON and PhNR-OFF responses can be obtained using red, amber or green flashes on a rod saturating blue background. These assumed to be dominated by responses from the L and M pathway (Rangaswamy et al. 2007).

It was also possible to record an S-cone dominated focal ERG with a blue flash on an amber or green background. These focal ERGs produced large PhNR-ON components with little or no obvious PhNR-OFF responses since the S-cone pathway does not exhibit OFF-responses. These ERGs are believed to be dominated by S-pathway responses (Arden et al., 1999). The results in this study were also qualitatively similar to S-cone ERGs recorded using a silent substitution method (Drasdo et al., 2001).

2.5.5 Conclusion

The optimal wavelength combination for eliciting an L and M pathway dominated ERG is the red flash on a rod saturating blue background. The optimal wavelength combination for eliciting an S-pathway dominated ERG is the blue flash on an amber background.

2.6 Experiment 4: Comparison of ERGs Recorded from the Central, Nasal and Temporal Macula

2.6.1 Introduction

Previous studies show that there are regional variations in the amplitude and time-to-peak of the PhNR recorded across the macular area (Kurimoto et al., 2009; Nakamura et al., 2011a). In addition, it has been shown that the PhNR amplitude is well correlated with the average RNFL (Horn et al., 2011). These suggest that the PhNR amplitude would reflect the anatomical loss of retinal neurons induced by disease.

In people with ADOA, the optic atrophy is often more prominent in the temporal disc and studies show that the retinal nerve fibre layer in affected individuals is more severely affected in the temporal quadrant as well. It may therefore prove

to be diagnostically beneficial to compare responses from different retinal locations. An exploratory study was therefore conducted to record focal ERGs from the central, nasal and temporal retina in order to investigate the retinotopic distribution of responses in healthy participants.

2.6.2 Methods

Focal ERGs were recorded from the central, nasal and temporal retina from three participants (two males, age = 24 and 26; one female, age 26). The stimulus configuration was as described in section 2.3.2, using a stimulus duration of 250msec, and the luminance of 55 cd/m^2. To record from the central retina, the participant was asked to fixate on the cross hairs in the middle of the stimulus (Figure 2.11). An additional marker was positioned on the left and another on the right side of the stimulus field so that they were horizontally aligned to the centre of the red target.

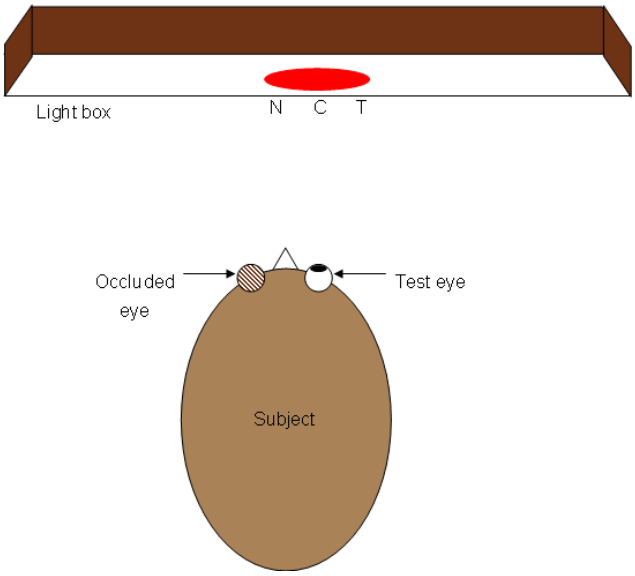

Figure 2.11. An illustration of a subject looking at the stimulus. Focal ERGs are recorded from the central, nasal and temporal retina when the subjects fixate at C, N and T respectively.

To record from the nasal retina, the participant was asked to assume the primary position of gaze and the screen moved laterally till the marker on the nasal side of the participant's field of view (N) was aligned to the participant's line of sight. To record from the temporal retina, the screen was moved in the opposite direction until the temporal target relative to the participant's visual field (T) was aligned to the participant's line of sight. Amplitudes and times-to-

peak were measured as described in section 2.2.7. The means of the amplitudes and times-to-peak of the PhNR recorded from the three locations were calculated and compared.

2.6.3 Results

Figure 2.12 shows the ERG waveforms for the tested areas and Table 2.5 displays data showing amplitude and times-to-peak for the ERG components. The results show that in all three subjects, the largest PhNR-ON amplitudes were recorded in the central macula (average = 7.30, SD = 2.29) followed by the temporal macula (average = 6.33, SD = 2.12) and then the nasal macular (average = 6.01, SD = 1.40) in descending order.

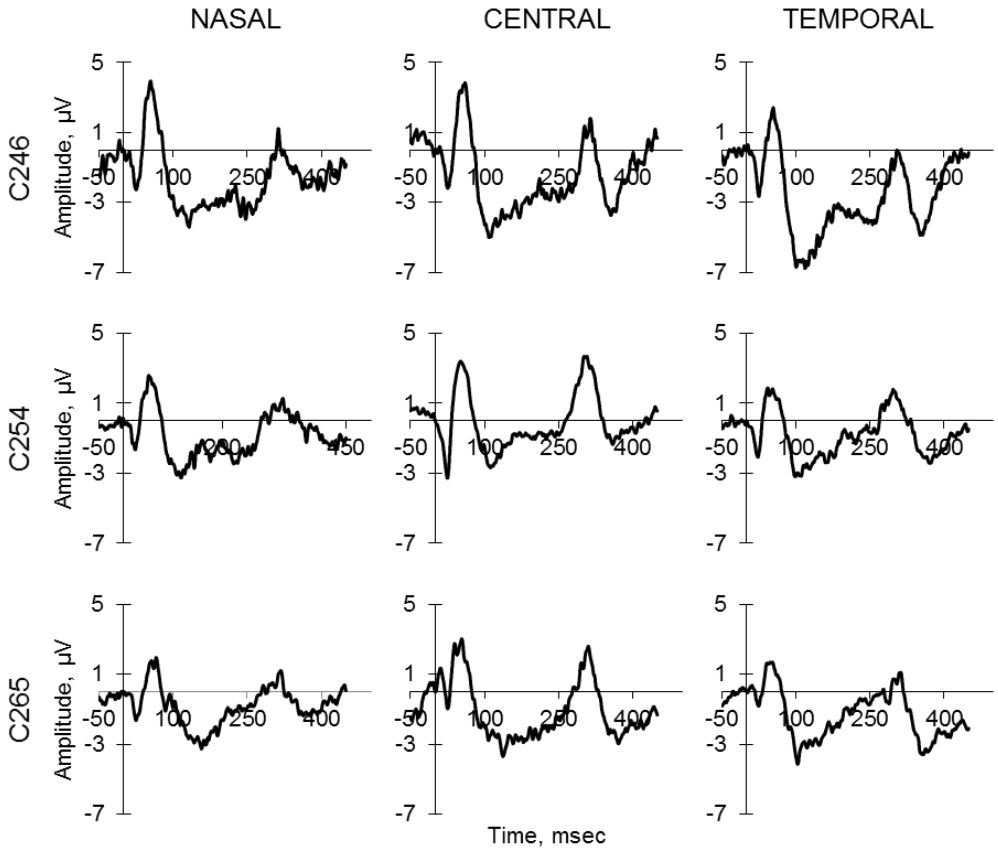

Figure 2.12. Focal ERGs from 3 subjects taken from nasal, central and temporal macular regions (left to right)

A similar pattern was recorded for the PhNR-OFF with central macular being the largest (average = 5.43, SD = 1.29), followed by the temporal macula (average = 4.12, SD = 0.21) and the nasal being the least (average = 1.9 SD = 0.50). It could not be reliably determined whether these differences in amplitude

between the three locations were statistically significant due to the limited number of participants in this study (n = 3).

Table 2.5. Amplitude and time-to-peak of focal ERG components from nasal, central and temporal macular areas

COMPONENT	Par't	NASAL		CENTRAL		TEMPORAL	
		Amp, µV	Time, msec	Amp, µV	Time, msec	Amp, µV	Time, msec
a-wave	C246	1.95	23.00	2.81	25.00	1.97	25.00
	C254	1.08	22.00	2.49	20.50	1.21	19.50
	C265	1.29	27.00	0.68	19.00	0.55	17.50
	Avg	**1.44**	**24.00**	**1.99**	**21.50**	**1.24**	**20.67**
	SD	**0.45**	**2.65**	**1.15**	**3.12**	**0.71**	**3.88**
	CoV	**31.26**	**11.02**	**57.76**	**14.52**	**57.10**	**18.79**
b-wave	C246	5.41	56.50	6.27	56.00	3.92	55.00
	C254	3.73	54.00	5.92	53.50	3.38	52.00
	C265	3.11	57.50	2.63	52.50	1.89	52.50
	Avg	**4.08**	**56.00**	**4.94**	**54.00**	**3.06**	**53.17**
	SD	**1.19**	**1.80**	**2.01**	**1.80**	**1.05**	**1.61**
	CoV	**29.24**	**3.22**	**40.60**	**3.34**	**34.22**	**3.02**
PhNR-ON	C246	7.50	125.00	9.94	104.00	8.78	114.00
	C254	5.83	115.50	6.17	115.50	5.27	110.50
	C265	4.71	150.50	5.80	136.50	4.96	104.00
	Avg	**6.01**	**130.33**	**7.30**	**118.67**	**6.33**	**109.50**
	SD	**1.40**	**18.10**	**2.29**	**16.48**	**2.12**	**5.07**
	CoV	**23.35**	**13.89**	**31.33**	**13.89**	**33.52**	**4.63**
d-wave	C246	3.69	64.00	5.03	57.00	3.83	56.00
	C254	2.57	53.50	4.11	57.00	2.14	45.00
	C265	1.76	59.50	3.70	58.50	0.94	57.00
	Avg	**2.67**	**59.00**	**4.28**	**57.50**	**2.30**	**52.67**
	SD	**0.97**	**5.27**	**0.68**	**0.87**	**1.45**	**6.66**
	CoV	**36.32**	**8.93**	**15.94**	**1.51**	**63.05**	**12.64**
PhNR-OFF	C246	2.26	129.00	6.92	102.50	4.37	103.50
	C254	1.33	116.00	4.64	106.00	3.99	114.50
	C265	2.11	121.00	4.72	121.00	4.00	107.00
	Avg	**1.90**	**122.00**	**5.43**	**109.83**	**4.12**	**108.33**
	SD	**0.50**	**6.56**	**1.29**	**9.83**	**0.21**	**5.62**
	CoV	**26.47**	**5.37**	**23.85**	**8.95**	**5.17**	**5.19**

Table 2.5 also shows that the times-to-peak of the PhNR-ON and PhNR-OFF recorded from the nasal macula are the longest (average = 130 msec, SD =

18.10 and 122 msec, SD = 6.56 respectively) compared to the central (ON: 118.67 msec; OFF: 109.83 msec) and temporal areas (109.50 msec; OFF: 108.33 msec).

2.6.4 Discussion

These experiments showed that the focal PhNR-ON and –OFF can be measured from the central, nasal and temporal retina. It can be seen from the results that there are regional variations in the amplitudes and times-to-peak of the PhNRs. However, unlike published reports which show the nasal macula produces larger PhNR amplitudes than the temporal macula (Kurimoto et al., 2009; Nakamura et al., 2011a), the results for this experiment showed that the temporal macula had greater amplitudes that the nasal macula. This could be due to the size of the stimulus in relation to the dimensions of the retina.

The horizontal distance between the fovea and the temporal edge of the optic nerve head is about two disc diameters, equivalent to about 12º visual angle (Quigley et al., 1990; Remington, 2005). The optic nerve head is approximately 6º in diameter (Jonas et al., 1992). This means that when the patient positions the eye for recording the nasal retina, the 20º stimulus overlaps the optic nerve head (Figure 2.13).

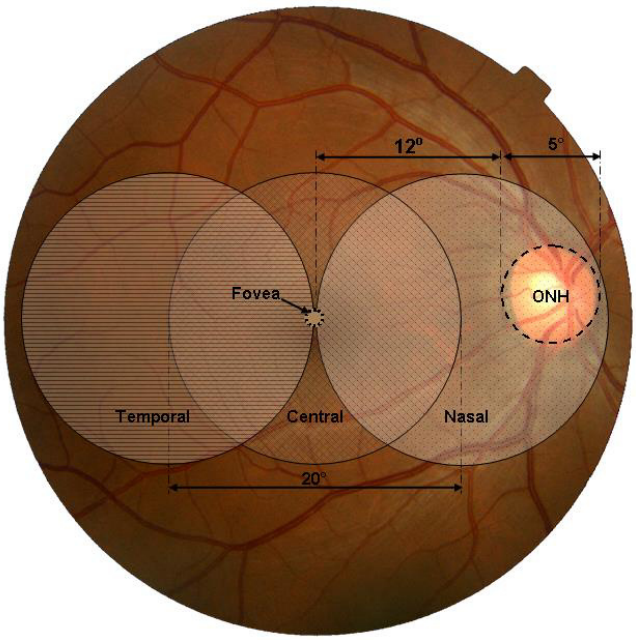

Figure 2.13 Diagram showing the positions of the image of the stimulus on the retina during tests. Diagram is not to scale

Since the optic nerve head is insensitive to light, it leads to a loss in signal. The percentage of signal lost can be calculated as follows:

$$\frac{area\ of\ optic\ nerve\ head}{area\ of\ stimulus} * 100\%$$

$$= \frac{(3.0^2)\pi}{(10.0^2)\pi} * 100\% \qquad = 9.0\ \%$$

In the case of the PhNR-ON, the amplitude in temporal macula was ~5% greater than in the nasal macula while for the PhNR-OFF, the amplitude in the temporal macula was more than 100% greater than the nasal macula. The percentage loss in signal in the nasal macula due to the presence of the ONH could therefore not completely explain the results obtained in this study. Since the number of participants in this study was small, a later study involving a larger sample size was conducted in Chapter 3 to further explore the observation made in this study.

2.6.5 Conclusion

The PhNR-ON and PhNR-OFF can be recorded from the central, nasal and temporal macula.

3 CHAPTER THREE – A COMPARISON OF THE RETINOTOPIC CHARACTERISTICS OF THE PATTERN ERG AND FOCAL ERG

3.1 Introduction

The retinal ganglion cells (RGCs) are thought to give rise to the photopic negative response (PhNR) component of the flash ERG (Viswanathan et al., 1999; Viswanathan et al., 2000; Viswanathan et al., 2001) and the N95 component of the pattern ERG (PERG) (Arden et al., 1982; Thompson and Drasdo, 1994; Luo and Frishman, 2011). The amplitudes of both components are reduced in diseases affecting RGC function as well as following pharmacological blockade of inner retinal function (Viswanathan et al., 1999; Colotto et al., 2000; Viswanathan et al., 2000; Rangaswamy et al., 2004; Luo and Frishman, 2011; Preiser et al., 2013). Although the PhNR and PERG are both electrophysiological responses known to contain RGC contributions, the PhNR is elicited by changes in luminance (Viswanathan et al., 1999; Viswanathan et al., 2000; Rangaswamy et al., 2007; Sustar et al., 2009) while the PERG is generated by changes in contrast (Drasdo et al., 1987; Porciatti, 1987; Thompson and Drasdo, 1989; Thompson and Drasdo, 1994). The purpose of this study, therefore, was to compare the retinotopic characteristics of these two responses recorded from the central, nasal and temporal macula in the same individuals.

Furthermore, in the previous pilot study (section 2.6), it was observed that the PhNR amplitudes in the temporal macula were larger than the amplitudes recorded from the nasal macula, contrary to previous reports (Kurimoto et al., 2009). Since there were only three participants in the previous pilot study, it was not possible to reliably determine whether the results were significant. This present study, which involved a larger number of healthy participants, therefore provided the opportunity to more reliably determine the veracity of the findings in the previous pilot study.

3.2 Methods

3.2.1 Participants

Eighteen healthy participants were recruited as previously described in section 2.2.1

3.2.2 ERG Recording

Long duration focal ERGs were recorded using the equipment and procedures previously described in 2.2.2 – 2.2.6. The focal ERGs were recorded in response to a 20º diameter red flash (peak wavelength 664nm, 250msec, 55 cd/m^2, 2Hz) on a rod saturating blue background (454nm, 100 scot cd/m^2).

Transient PERGs were generated at 4 reversals per second on a computer monitor at 98% contrast. The screen was masked with a black opaque cardboard with a 13 x 13 cm square cut-out at the centre so that it produced a 20º x 20º field at a viewing distance of 36 cm. The size of the individual check elements was 1º. Signals were digitally averaged and bandpass filtered from 1 - 100 Hz, at a sampling rate of 1 kHz using the electronic recording system and methods described in section 2.2.5.

The PERG was always recorded first with normal pupils. Participants wore their corrective prescriptions where required (Bach et al., 2013). After the PERG recordings, at least one pupil (the test eye) was dilated using 1% Tropicamide in order to record the focal ERGs. The PERGs and focal ERGs were recorded from the central, nasal and temporal macula of the participants. To record the PERG from the central macula, the participant was asked to fixate on a red target located in the centre of the PERG stimulus field. An additional marker was positioned on the left and another on the right side of the stimulus field so that they were horizontally aligned to the central red target. To record from the nasal retina, the participant was asked to assume the primary position of gaze and the screen moved laterally till the marker on the nasal side of the participant's field of view was aligned to the participant's line of sight. To record from the temporal retina, the screen was moved in the opposite direction until the temporal target (relative to the participant's visual field) was aligned to the

participant's line of sight. In the case of the focal ERGs, the procedures described in section 2.6.2 were employed.

3.2.3 Signal Analysis

The ERGs were exported into a Microsoft Excel 2013 spreadsheet and Fourier analysed offline to remove high frequency signals above 30 Hz and 50 Hz for the PERG and focal ERGs respectively. Fourier analysis was based on the approach by Stroud (1986). The cut-off frequency for the PERG was determined from a visual inspection of the power spectrum plot, which showed that most of the power was concentrated in the first 10 harmonics (20 Hz) and had levelled off to a minimum at 15 harmonics (30Hz). The cut-off for the focal ERG was similarly determined; the power was concentrated in the first 20 harmonics (40 Hz) and had levelled off to a minimum at 25 Hz (50 Hz) (see Appendix VI for the power spectrum plots).

The amplitude and time-to-peak of the P50 and N95 of the PERG were measured as recommended by ISCEV (Bach et al., 2013). The P50 amplitude was measured from the trough of the N35 to the peak of P50. The N95 was measured from the peak of P50 to the trough of N95. In the focal ERGs, the a-wave and b-wave were measured as recommended by ISCEV (McCulloch et al., 2015). The d-wave was measured from the time point of stimulus offset to the first maximum peak. The PhNR-ON amplitude was measured from peak of b-wave to a fixed time point in the trough of the PhNR-ON while the PhNR-OFF was measured from peak of d-wave to the a fixed time point in the trough of the PhNR-OFF. The fixed time points were determined by finding the times-to-peak of the PhNR-ON and PhNR-OFF components of the group-averaged trace for each location (Table 3.1). This method was adopted from the study by Mortlock et al (2010). All peaks and troughs of the other sub components were identified objectively as described in section 2.2.7. The ERGs recorded from the different locations were also inspected to look for qualitative changes in waveform. In order to account for the loss in signal in ERGs recorded from the nasal macula due to the presence of the optic nerve head in that location (assuming an angular radius of 3.5^{o} (Curcio and Allen, 1990)), the nasal ERGs were multiplied by a factor of 1.11 for PERGs and 1.14 for focal ERGs.

Table 3.1. Fixed time points at which amplitudes of focal long duration PhNRs were measured

Location	PhNR-ON, msec	PhNR-OFF, msec
Central	105	361
Nasal	120	397
Temporal	104	361

3.2.4 Statistical Analysis

The distribution of the ERG data was checked for normality using the Shapiro-Wilk test. Where data were normally distributed, comparisons between ERGs recorded from the central, nasal and temporal macula from participants were conducted using one-way repeated measures analysis of variance (ANOVA) with Bonferonni adjustment for multiple comparisons; otherwise a Friedman test (with post-hoc Wilcoxon Signed Ranked tests for post-hoc pairwise comparisons) was conducted. Differences between the locations were considered significant when $p < 0.05$. The relationship between PhNRs of the focal ERG and the N95 of the PERG were explored using regression analysis. Relationships were considered significant when $p < 0.05$.

3.3 Results

3.3.1 Comparison of Central, Nasal and Temporal Macula ERGs

Transient pattern ERGs and focal flash ERG were recorded successfully from all three retinal locations in 18 healthy participants aged between 20 and 61 years (mean $\pm$ SD = 31 $\pm$ 12 years) (Figure 3.1). The PERGs were characterised by a prominent positive peak, the P50, followed by a negative potential, the N95 (Figure 3.1A). The waveforms of the PERGs from the nasal macula were different to those from the central and temporal macula. In the nasal PERG, the descending limb of the P50 which usually continues uninterrupted into the trough of the N95 was interrupted by a positive going wave at a time point near the trough of the N95 (Figure 3.1A, arrowed in middle column). This also caused the most negative point of the N95 component to be displaced towards a later time-to-peak close to 150 msec. As this was out of the known normal range for the component, the nasal N95 was instead measured from P50 peak to the first trough before the interrupting positive wave.

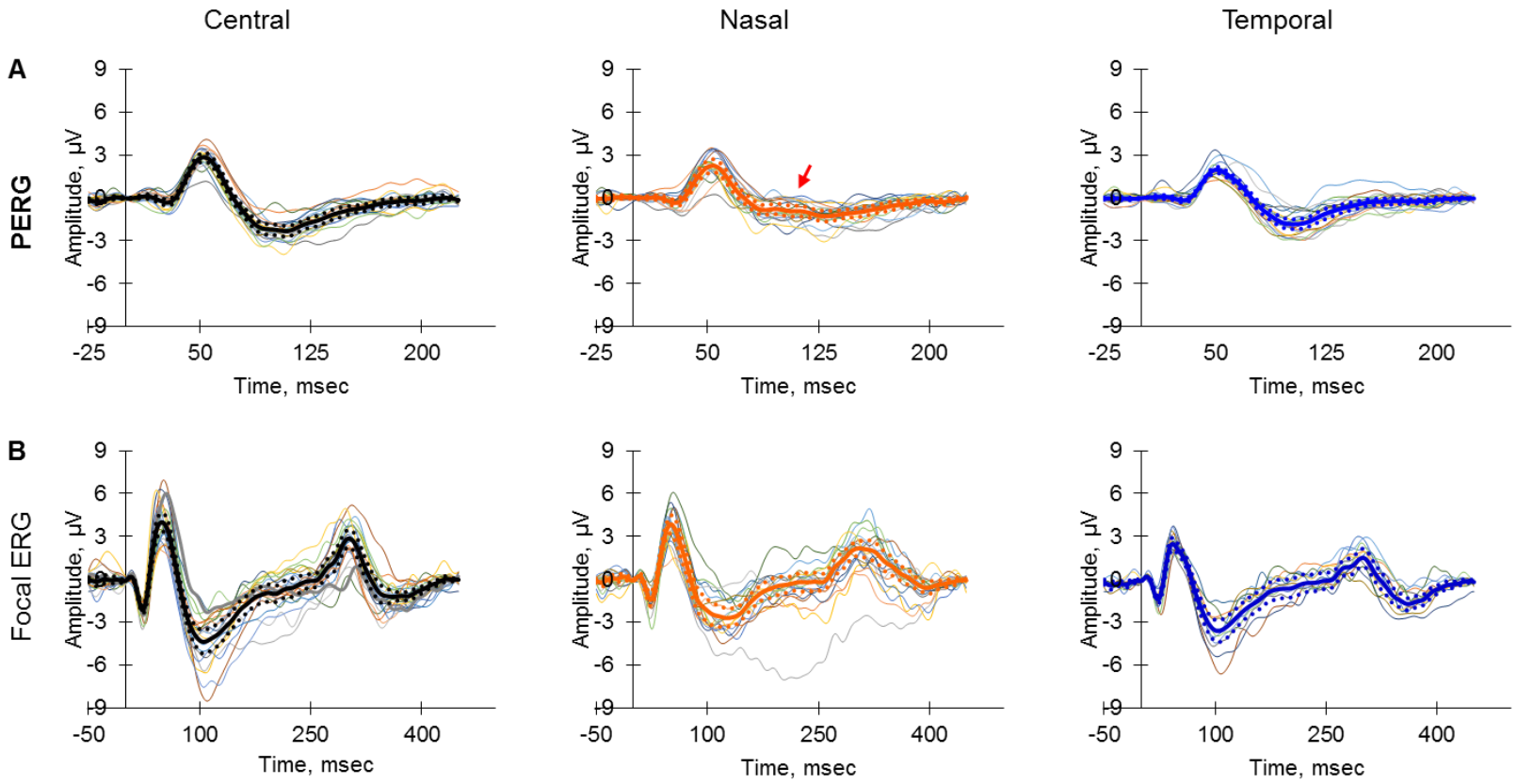

Figure 3.1. The PERGs (A) and long duration focal ERGs (B) recorded from the central, nasal and temporal macula of participants. Thin coloured lines represent the traces from individual participants. Thick lines represent the group averaged traces in the various locations. Dotted lines represent the 95% confidence interval. The red arrow in nasal PERG shows the positive wave interrupting the N95 trough.

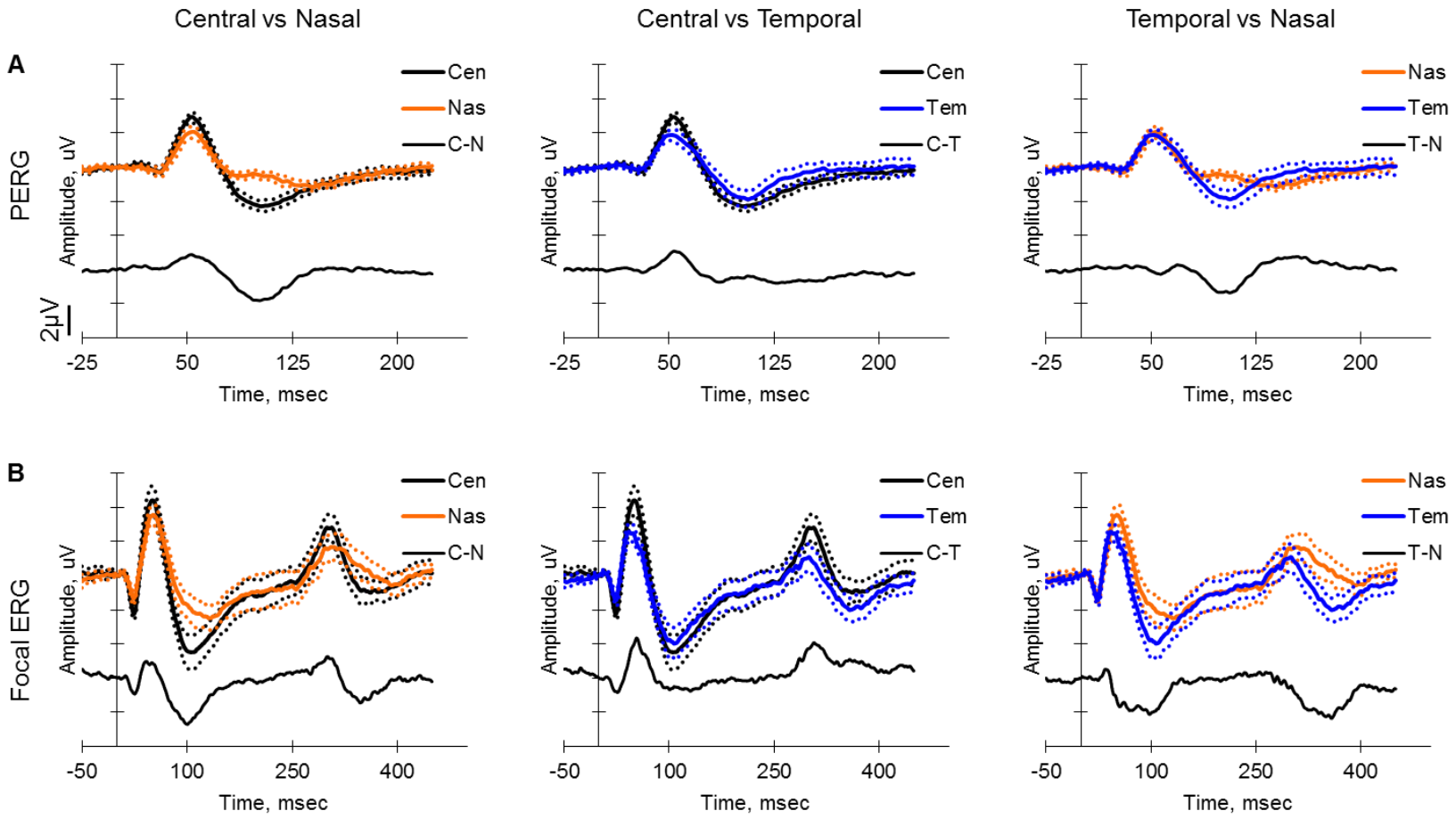

Figure 3.2. Group-averaged traces from the three locations. Comparison between (A) central and nasal retina; (B) central and temporal retina; and (C) temporal and nasal retina. The single trace at the bottom of each comparison is the difference ERG between each pair the two locations. Dashed lines represent the 95% confidence intervals.

The focal ERG was characterised by the a-wave, b-wave, PhNR-ON, d-wave and PhNR-OFF (Figure 3.1B). Once again, the traces from the nasal macula were different from those from the central and temporal retina. The trough of the PhNR-ON and the peak of the d-wave were broader than their central and temporal counterparts. Figure 3.2A shows pairwise comparisons of the group averaged PERGs from the three locations. The difference ERGs, obtained by subtracting one ERG from the other, showed that differences between the nasal and the central/temporal PERGs were more prominent in N95 components while the differences between the central and temporal PERGs were more prominent in the positive components.

A repeated measures ANOVA showed that there were significant differences in the P50 and N95 amplitudes depending on the location from which they were recorded (Table 3.2). Post hoc tests using Bonferroni correction showed that the central P50 and N95 amplitudes were significantly greater than their counterparts recorded from the nasal and temporal retina. The nasal P50 amplitude was significantly greater than the temporal P50, however, the N95 amplitudes of the nasal and temporal macula were not statistically different. The contradiction between the differences observed in the graphs and the results from the statistical analysis is addressed in the discussion. The times-to-peak of the P50 and N95 components did not show a significant difference between the three locations.

In Figure 3.2B, pairwise comparisons were made between the ERGs recorded from the three locations and the differences between them were highlighted by the difference ERGs. The difference ERGs were obtained by subtracting one ERG from the other (see legend of Figure 3.2). The differences between the nasal and the central/temporal focal ERGs were more prominent in their negative components while the differences between the central and temporal focal ERGs were more prominent in their positive components. The b-wave and d-wave amplitudes were significantly greater in the nasal than in the temporal macula. However, there were no significant differences in the a-wave, PhNR-ON or PhNR-OFF amplitudes between the nasal and temporal macula.

Table 3.2. Statistical comparisons of central, nasal and temporal macula ERG components

Component		Central	Nasal	Temporal	p-value
P50	A, µV	3.34 ±0.81	2.83 ±0.60	2.29 ±0.52	Significant ($p < 0.0001$; $P.Eta^2 = 0.72$) Pairwise: Cen > Nas > Tem (all significant at $p \leq 0.0050$)
	T, msec	53.08 ±3.11	53.65 ±4.46	52.06 ±3.89	Not significant† χ^2 (2) = 3.09; p = 0.2138
N95	A, µV	5.39 ±0.92	3.59 ±0.98	4.02 ±0.85	Significant ($p < 0.0001$; $P.Eta^2 = 0.85$) Pairwise: Cen > Nas ($p < 0.0001$); Cen > Tem ($p < 0.0001$)
	T, msec	102.31 ±7.06	95.61 ±9.41	103.26 ±6.40	Not significant ($p = 0.0636$; $P.Eta^2 = 0.29$)
a-wave	A, µV	2.17 ±0.60	1.38 ±0.70	1.34 ±0.66	Significant ($p = 0.0001$) Pairwise: Cen > Nas ($p<0.0001$); Cen > Tem ($p < 0.0001$)
	T, msec	23.56 +1.79	23.06 ±1.57	22.63 ±1.50	Not significant† χ^2 (2) = 3.70; p = 0.1569
b-wave	A, µV	6.56 ±1.59	5.14 ±1.25	4.01 0.92	Significant $p < 0.0001$; $P.Eta^2 = 0.77$ Pairwise: Cen > Nas > Tem (all significant at $p < 0.0010$)
	T, msec	49.13 ±4.79	50.13 ±3.86	43.06 3.75	Significant† χ^2 (2) = 27.09; $p < 0.0001$ Pairwise: Cen > Tem (p= 0.0003); Nas > Tem (p = 0.0002)
PhNR-ON	A, µV	8.68 ±2.50	6.18 ±1.66	6.19 ±1.64	Significant $p < 0.0001$; $P.Eta^2 = 0.77$ Pairwise: Cen > Nas ($p < 0.0001$); Cen > Tem (p = 0.0000)
	T, msec	105.31 ±6.84	120.69 14.10	103.44 ±5.70	Significant ($p < 0.0001$; $P.Eta^2 = 0.70$) Pairwise: Nas > Cen (p = 0.0029); Nas > Tem ($p < 0.0001$)
d-wave	A, µV	3.09 ±0.88	2.66 ±0.79	1.70 ±0.78	Significant ($p < 0.0001$; $P.Eta^2 = 0.78$) Cen > Nas > Tem (all significant at $p < 0.0500$)
	T, msec	302.06 ±5.36	306.34 ±9.35	298.94 ±4.77	Significant (p = 0.0066; $P.Eta^2 = 0.47$) Pairwise: Cen > Tem (0.0454); Nas > Tem (p = 0.0050)
PhNR-OFF	A, µV	4.21 ±1.29	2.90 ±1.29	3.34 ±1.10	Significant (p = 0.0073; $P.Eta^2 = 46$) Pairwise: Cen > Nas (p = 0.0057); Cen > Tem (p = 0.0188)
	T, msec	367.89 ±19.44	401.28 ±22.13	360.66 ±13.32	Significant ($p < 0.0001$; Peta2 = 0.71) Pairwise: Nas > Cen (p = 0.0004); Nas > Tem (p = 0.0002)

† - Data not normally distributed and Friedman test was used

3.3.2 Relationship between the N95 and PhNR components

The relationship between the long duration focal PhNRs and the N95 component were explored using regression analysis. Scatter plots of the

relationship are shown in Figure 3.3. Generally, the focal PhNR-ON amplitude demonstrated a positive trend with the N95 amplitude in all locations, however, the regression coefficients were low ($R^2 < 0.2$) and not significant ($p > 0.05$) (Table 3.3). The focal PhNR-OFF amplitude on the other hand showed a positive trend with the N95 amplitude in the central and temporal macula, but a negative trend in the nasal macula. The relationships once again were not significant.

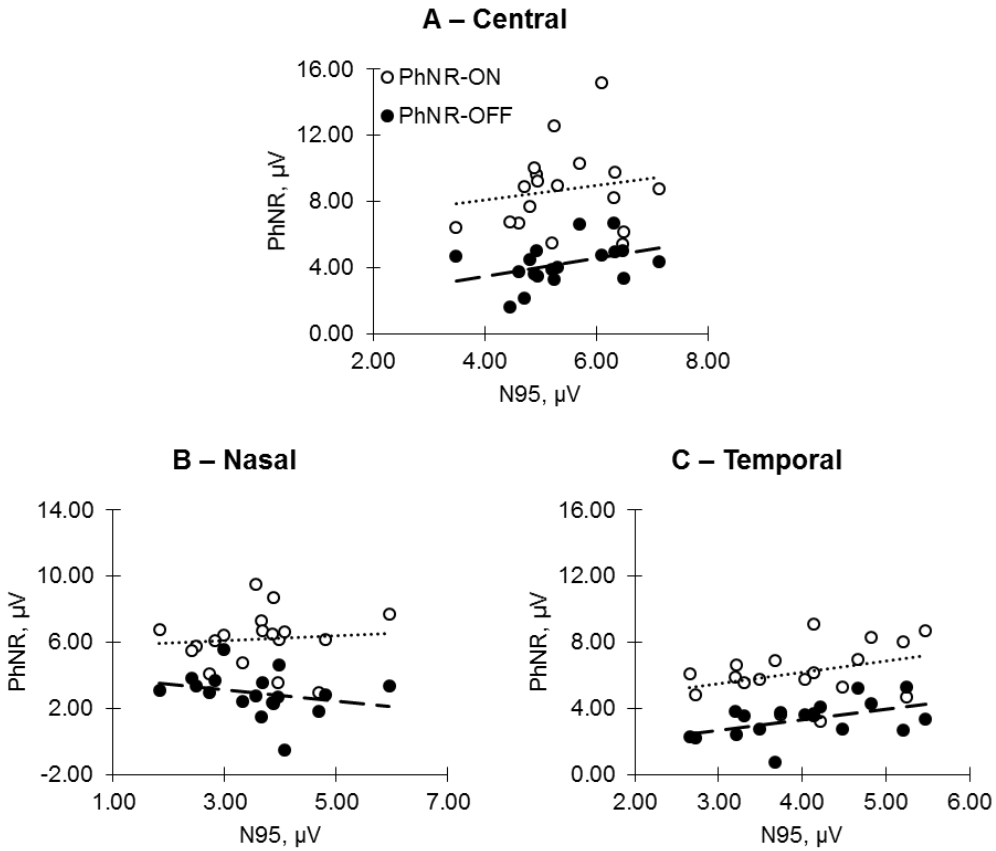

Figure 3.3. Scatter plots showing the relationship of the N95 (x-axis) amplitude with the PhNR-ON and PhNR-OFF amplitudes (y-axis) recorded (A) central, (B) nasal and (C) temporal macula of participants. The legend in A applies to B and C. The graphs are scaled equally. The equation of the regression lines are provided in Table 3.3.

Table 3.3. Results of regression analysis of the PhNR components (y/dependent variable) and the N95 (x/independent variable) in the various locations.

Location	Dependent Component	Equation	R^2	p-value
Central	PhNR-ON	y = 0.4339x + 6.3455	0.0255	0.5246
	PhNR-OFF	y = 0.5498x + 1.2482	0.1546	0.1076
Nasal	PhNR-ON	y = 0.1555x + 5.6177	0.0085	0.7133
	PhNR-OFF	y = -0.3450x + 4.1408	0.0687	0.2954
Temporal	PhNR-ON	y = 0.6868x + 3.4242	0.1273	0.1450
	PhNR-OFF	y = 0.641x + 0.7628	0.2437	0.0827

3.4 Discussion

In this study, the retinotopic characteristics of the PERG and the long duration focal ERG in response to a red on blue stimulus in three retinal locations were compared in healthy participants. This study found that the positive going components of both the PERG (P50) and focal ERG (b-wave and d-wave) were greater in the nasal macula than in the temporal macula. This was similar to the findings in the previous pilot study (section 2.6.3). The P50 is in part derived from the RGCs, but also has origins distal to the RGCs, most likely the bipolar cells and photoreceptors (Arden et al., 1982; Holder, 1997; Holder, 2001; Holder et al., 2009; Luo and Frishman, 2011). The b-wave and d-wave are derived from the ON and OFF bipolar cells respectively (Brown, 1968; Evers and Gouras, 1986; Sieving et al., 1994; Ueno et al., 2006b). Given that the nasal macula has a greater photoreceptor density, and by implication a greater bipolar cell density, than in the temporal macula (Curcio et al., 1990), the results for the positive components were expected.

However, this was not the case for the negative going components (N95 of the PERG, a-wave, PhNR-ON and PhNR-OFF for the long duration ERG). The mean amplitudes recorded for these parameters (except the a-wave) were larger in the temporal macula than in the nasal macula (Table 3.2). This was similar to the results from the pilot study (section 2.6.3). However, the differences in amplitude between the nasal and temporal macula for these parameters were not significant.

The N95 and the PhNRs are primarily derived from the RGCs (Viswanathan et al., 1999; Viswanathan et al., 2000; Holder, 2001; Luo and Frishman, 2011) and RGC density is significantly greater in the nasal retina than in the temporal retina (Curcio and Allen, 1990; Silveira and Perry, 1991; Drasdo et al., 2007). The lack of statistical differences in the N95, PhNR-ON and PhNR-OFF amplitudes recorded from the nasal and temporal macula could thus be due to a number of factors. The PERG and focal ERG traces from the nasal macula were different in waveform compared to those from the central and temporal retina. In the PERG, the difference could possibly be due to the luminance imbalance caused by the presence of the ONH when the nasal retina was stimulated. Symmetry between light and dark areas of the PERG stimulus is

mandatory in generating the PERG signal (Bach et al., 2013). The overlap of the symmetric square patterns over the asymmetric oval ONH in the nasal retina would result in an asymmetry between light and dark areas. During pattern reversal a luminance component may thus be generated which could have contaminated the PERG signal and thus explain the interrupted N95 component observed in nasal retinal PERGs.

The difference in waveform of the nasal focal ERG could be due to the intrusion of components associated with the optic nerve head (Sutter and Bearse Jr, 1999). Sutter and Bearse (1999) reported the presence of an optic nerve head contribution to the ERG which varied with distance from the optic nerve head. The 20° stimulus completely overlapped the optic nerve head when recordings were made from the nasal macula. The contribution of the optic nerve head component would thus be maximal in the recordings from the nasal macula and minimal in the recordings from the temporal macula.

A number of studies have sought to establish the relationship between the N95 of the PERG and the PhNR of the flash ERG in glaucoma patients since both components reflect RGC activity (Colotto et al., 2000; North et al., 2010; Preiser et al., 2013). They found that the N95 amplitude was significantly correlated with the brief flash red-on-blue PhNR amplitude (North et al. 2010; Preiser et al. 2013) and the uniform field white-on-white PhNR-ON of the focal ERG (Colotto et al. 2000). The findings of these studies were consistent with the concept that the two parameters share similar retinal origins, which are the RGCs. In this study however, there was neither a significant relationship between the PhNR-ON and the N95 nor the PhNR-OFF and the N95 amplitudes in healthy participants.

Although the results of this study appear to stand in contrast to the earlier findings, Preiser et al (2013) also showed that there was no significant correlation between the PhNR to b-wave ratio (PhNR ratio; defined as the PhNR amplitude divided by the b-wave amplitude) and the $N95_{0.8}$ to $N95_{16}$ ratio (N95 ratio; defined as the N95 amplitude generated by a 0.8° check size divided by the N95 amplitude generated by a 16° check size). They proposed that the significant correlation between the “raw” amplitudes of the PhNR and N95 may

be due to “trivial” factors like eye size or electrode position, which vary between eyes, but are common to the two measures. Calculation of the ratios, cancels these trivial factors out, leaving no significant correlation between individual PhNR ratio and PERG ratio values. They therefore suggested that lack of correlation between the PhNR and PERG ratios was because the two measures either tapped into different disease mechanisms or measured different RGC populations.

If this was true to some degree, then a linear combination of the two measures should be a better discriminator for the presence of glaucoma. Their test of the hypothesis using receiver operating characteristics (ROC) curve, showed that the area under the curve (AUC) of the combined PhNR-and PERG ratios rose to 0.90 in comparison to that of the independent PhNR-ratio (0.80) and N95 ratio (0.79) (Preiser et al., 2013). The results in this study in healthy participants may therefore support the proposal by Preiser et al (2013) that the PhNR and N95 arise from different classes of RGCs.

Furthermore, as noted in the introduction, the focal ERG is produced in response to changes in stimulus luminance (Viswanathan et al., 1999; Viswanathan et al., 2000; Rangaswamy et al., 2007; Sustar et al., 2009) while the PERG is produced in response to changes in stimulus contrast (Drasdo et al., 1987; Porciatti, 1987; Thompson and Drasdo, 1989; Thompson and Drasdo, 1994). The lack of correlation between the focal PhNR and the PERG may therefore be due to the different functional properties of RGCs that generate the responses. Additionally, since ERGs are affected by stimulus and background colour (Viswanathan et al., 1999; Rangaswamy et al., 2007; Sustar et al., 2009), the results in this study could be explained by differences in chromatic contents of the stimuli used to generate the PhNR (red on blue) and the PERG (black and white checkerboard). This is clinically relevant as it suggests that the PhNRs elicited by a long duration red on blue stimulus and the N95 component of the PERG provide different information about macula function.

3.5 Conclusion

This study suggested that the focal PhNRs of the ERG elicited by a long duration red-on-blue stimulus and N95 of the PERG share some similar retinotopic characteristics, supporting previous reports that the PhNR and N95 may share similar cellular origins. However, the N95 of the PERG was not significantly correlated with the PhNR-ON and –OFF parameters, suggesting that the PERG and the focal ERGs do not have identical generators and are providing distinct clinical information. This study also suggested that apart from regional RGC density, there are other factors (e.g. proximity to the ONH) which affect the amplitude and time-to-peak of the PhNRs and N95 components in the temporal and nasal retina.

4 CHAPTER FOUR – THE RELATIONSHIP BETWEEN RETINAL GANGLION CELL DISTRIBUTION AND THE PHOTOPIC NEGATIVE RESPONSE

4.1 Introduction

The retinal ganglion cells (RGC) and their receptive fields (RGCf) are most densely packed in the centre of the retina and become increasingly sparse towards the retinal periphery (Curcio and Allen, 1990; Watson, 2014). RGCs also exhibit central-peripheral asymmetries in other properties such as cell size, axon length and size, dendritic field size, receptive field size, convergence to first and second order neurons, peak sensitivity, contrast sensitivity and contrast gain (Perry et al., 1984; Rodieck et al., 1985; Drasdo et al., 1987; Watanabe and Rodieck, 1989; Dacey and Petersen, 1992; Dacey, 1993a; Dacey, 1993b; Croner and Kaplan, 1995; Lee, 1996; Yamada et al., 1996; Lee et al., 1998; Dacey et al., 2000). These properties of the RGCs predict that RGC function depends on eccentricity. As such, an ERG component reflecting activity of the RGCs will be expected to exhibit properties that conform to known characteristics of RGCs.

The photopic negative response (PhNR) is a negative going wave seen after the b-wave in a brief flash photopic (cone) ERG (Viswanathan et al., 1999; Viswanathan et al., 2000). When a long-duration flash is used to evoke the ERG, the PhNR is seen once after the b-wave (PhNR-ON) and again as a negative going wave after the d-wave (PhNR-OFF). These components are thought to reflect the activity of the ON- and OFF- pathways (Rangaswamy et al., 2007; Luo and Frishman, 2011). The PhNR, particularly when elicited by a red flash on a rod saturating blue background, is believed to primarily originate from spiking activity in RGCs and their axons with contributions from amacrine cells and possible involvement of associated glial cells/astrocytes of the retina (Viswanathan et al., 1999; Viswanathan et al., 2000; Frishman, 2006; Rangaswamy et al., 2007). In line with this theory, the PhNR amplitude is selectively reduced in retinal diseases affecting the RGC and/or optic nerve with relative sparing of the a-wave and b-wave, both of which are components from the outer retina (Colotto et al., 2000; Gotoh et al., 2004; Machida et al., 2004;

Ueno et al., 2006a; Miyata et al., 2007; North et al., 2010; Nakamura et al., 2011b; Morny et al., 2015).

The amplitude of an ERG is directly proportional to the area of stimulation and to the number of stimulated neurons (Errico et al., 1990; Murray et al., 2004). The response density of an ERG component can be calculated by dividing the amplitude of the response by the area from which it was recorded (Brindley and Westheimer, 1965; Errico et al., 1990; Sutter and Tran, 1992; Kondo et al., 1998; Sutter and Bearse Jr, 1999). A response density profile can thus be created by calculating the response densities at different retinal eccentricities. The response density profile can then be matched to the topographical density profile of a class of retinal neurons of interest to determine the relationship between the response and the distribution of the neuron. If the number of neurons thought to produce a particular ERG component in a specified area is known, it follows that the response of a single neuron can be computed by dividing the amplitude by the number of neurons in that area.

The following were therefore hypothesised.

1. The amplitudes of the PhNRs will increase with increasing stimulus sizes
2. The change in the response densities of the brief and long-duration PhNR with eccentricity would reflect the change in RGC receptive field density (i.e. the number of receptive fields per degree squared).
3. The PhNR per RGC would increase from central to peripheral retina in consonance with known characteristics of RGCs that are directly linked to its functional output (e.g. cell size, dendritic field size, receptive field size).

The separation of the ON and OFF components of the ERG using a long duration red flash on a blue saturated background (Viswanathan et al., 1999; Rangaswamy et al., 2007) provided an opportunity to determine the relationship between the response densities of the PhNR-ON and PhNR-OFF components and the receptive field densities of the ON- and OFF-RGCs. In addition, the brief flash PhNR elicited by a red on blue stimulus, which is optimal for assessing combined RGC function (Rangaswamy et al., 2007; Sustar et al., 2009) enabled a determination of the relationship between the brief flash PhNR

and the general RGC density profile. The aim of this study therefore was to determine the relationship between the long duration and brief flash PhNRs and the distribution of RGCs across the retina using a red on blue stimulus of increasing area. In addition, it was sought to estimate the responses of single RGCs as a function of eccentricity on the basis of ERG recordings.

A previous study by Errico et al (1990), qualitatively showed a close match between the density profile of a negative going wave seen after the b-wave, which they referred to as “PIII”, and a previously published density profile for cones (Osterberg, 1935). Errico et al therefore attributed the origins of their PIII component to the cones. However, this negative wave has now been established as the PhNR-ON component, a signal attributed to the activities of the ON-centre RGCs (Viswanathan et al., 1999; Viswanathan et al., 2000; Kondo et al., 2008a; Luo and Frishman, 2011). This therefore warrants further investigation. Errico et al (1990) may have erroneously attributed the PIII with cones rather than RGCs because the receptive field topographies of cones and RGCs are qualitatively similar; they peak at the centre and decrease rapidly towards the periphery (Osterberg, 1935; Curcio and Allen, 1990; Curcio et al., 1990; Drasdo et al., 2007).

Furthermore, since the discovery of the PhNR in 1999 by Viswanathan et al (1999), its response characteristics as a function of various stimulus parameters (e.g. luminance, duration, wavelength, etc.) have been reported with the aim of standardising its use in measuring RGC function (Rangaswamy et al., 2007; Miyata et al., 2008; Kurimoto et al., 2009; Sustar et al., 2009). These studies employed either focal stimuli of different sizes or full-field stimuli using brief or long duration flashes. A systematic study of the response characteristics of the PhNR amplitude to varying stimulus sizes, which has not yet been reported, will therefore be relevant to the standardisation of the PhNR recording protocol.

4.2 Methods

4.2.1 Participants

All participants were recruited from among staff and students of the School of Optometry and Vision Sciences, Cardiff University, as well as their friends and families. The study conformed to the Declaration of Helsinki and was approved by the ethics committee of the School. All participants provided their written consent after receiving a participant information sheet and having the opportunity to ask questions. All participants had a corrected visual acuity of 0.1 logMAR or better with normal visual fields, and were aged between 18 and 50 years. Six participants were recruited for Experiment 1 and 16 for Experiment 2.

All ERGs and baseline tests in Experiment 1 were recorded by the author (EM). All ERGs and baseline tests in Experiment 2 (except for 3 participants) were recorded by a second year optometry student (KP) under the supervision of the author under the Cardiff Undergraduate Research Opportunities Programme (CUROP). Preliminary results of the project were presented as a poster at the CUROP 2015 exhibition.

4.2.2 ERG Recording and Participant Setup

All ERGs responses were elicited using a modified miniature Ganzfeld LED stimulator and recorded on a Medelec Synergy system. The equipment and procedure for recording the ERGs are described in detail in section 2.2.2 – 2.2.6).

ERGs were recorded using DTL fibre active electrodes and the pupils of participants were dilated in at least one eye using 1% tropicamide to a minimum of 7mm.

4.2.3 Experiment 1: Long duration ERGs

Focal long duration ERGs were recorded using a red circular stimulus (peak wavelength 660 nm, 250 ms, 50 cd/m^2, 2 Hz) on a rod saturating blue background (peak wavelength 469 nm, 100 scot cd/m^2). A desensitising blue background (peak wavelength 454 nm, 140 scot cd/m^2) was used to minimised the effect of stray light (details in section 2). The angular diameters of the focal

stimulus were 5.5º, 10º, 15º, 20º, 30º, 45º and 60º (Figure 4.1); they were obtained by varying the viewing distance (Table 4.1). The stimulus sizes were chosen to address one of the objectives of this study, i.e. to compare focal ERGs recorded with different sized stimuli. As such, stimulus sizes that had been commonly used to record focal ERGs in previous studies by other laboratories (5º, 10º and 15º (Kondo et al., 2008a; Machida et al., 2008b)) and from this laboratory (20º and 30º) were selected. The stimulus size was then increased in 15º steps to obtain the 45º and 60º stimuli. Further increments beyond 60º could not be obtained, as the focal stimuli could not be placed closer than to the observer without touching the observer's nose. The areas of the circular stimuli are shown in Table 4.1. A full-field long duration ERG was recorded by holding the modified miniature Ganzfeld directly to the eye. For the purpose of calculation, the angular diameter of the full-field stimulus was assumed to be 110º. The focal stimuli were centred on the fovea by asking the participant to fixate at the intersection of a pair of cross-hairs centred in the middle of the stimulus.

4.2.4 Experiment 2: Brief flash ERGs

Focal brief flash ERGs were recorded using the same setup as in Experiment 1 except for the following changes. The duration, luminance and frequency of the red flash were 5 msec, 0.28 cd.s/m^2 and 4 Hz respectively. The angular diameters of the stimulus were 5º, 10º, 15º, 20º, 30º and 60º; they were obtained by varying the viewing distance (Table 4.1). The 45º stimulus was discontinued after Experiment 1 as it did not provide additional information. The full-field ERG was recorded by holding the miniature Ganzfeld directly to the eye as in Experiment 1.

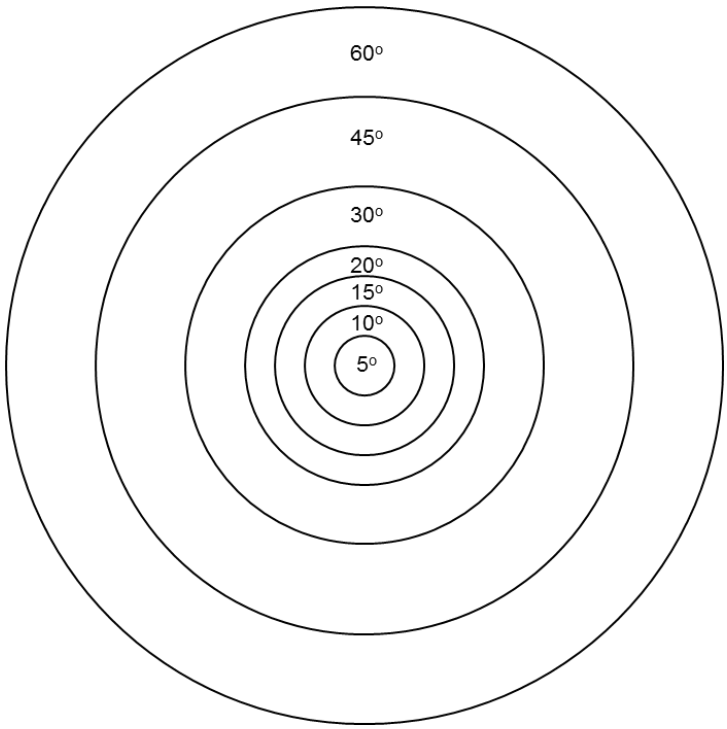

Figure 4.1. A schematic diagram of the stimulus sizes used in this study. Each circular stimulus was centred on the fovea. The numbers are the angular diameters the stimuli.

Table 4.1. Dimensions of the stimulus sizes used in the study

Stimulus Angular Size (Diameter), deg	Viewing distance, cm	Stimulus Angular Area, deg^2	Annulus Area, deg^2	Eccentricity (Midpoint of Annulus), deg
5	66.42	19.63	19.63	1.25
(5.5)	(60.37)	(23.76)	(23.76)	(1.38)
10	33.15	78.54	58.90 (54.78)	3.75 (3.88)
15	22.03	176.71	98.17	6.25
20	16.45	314.16	137.44	8.75
30	10.82	668.37	392.70	12.50
(45)	7.00	(1590.43)	(883.57)	(18.75)
60	5.02	2788.95	2120.58 (1237.00)	22.50 (26.25)
110	NA	9464.83	6675.88	42.50

Values in brackets apply to long duration stimulus used in Experiment 1. NA – not applicable. NB – The area of the optic nerve head (38.48 deg^2; assuming a diameter of 7° and beginning at 11° from the fovea (Watson, 2014)) has been subtracted from angular areas of stimuli $\geq$30°

To compute the response density of components as a function of eccentricity, the following approach was adopted. The arithmetic difference in amplitude between two successive stimulus sizes was divided by the area of the annulus created by the said two stimulus sizes. For example, to find the amplitude of responses in the 10° annulus, the amplitudes of components in the 5° area were subtracted from the amplitudes of their respective counterparts produced by the

10º stimulus. This was then plotted as a function of the midpoint (in deg) of the annulus (distance between the inner and outer circle). The areas of the annuli and their midpoints (eccentricity) are shown in Table 4.1.

For simplicity, stimulus sizes are referred to by their angular diameters (e.g. 5.5º, 10º, etc.) rather than by their areas. The annuli are referred to by the diameter of the larger (outer) circle. For example, the 20º annulus is the annulus with an inner diameter of 10º and an outer diameter of 20º.

4.2.5 Signal Analysis

The ERGs were Fourier analysed to remove high frequency signals above 50Hz as described in section 2.2.7. The PhNR-ON (PhNR in Experiment 2) amplitude was measured from the peak of the b-wave to the trough of the PhNR. The PhNR-OFF was measured from the d-wave peak to the PhNR-OFF trough. An additional positive potential was observed immediately following stimulus off-set in ERGs produced by stimuli larger than 30º (arrowed in Figure 4.3). In these cases, the PhNR-OFF was measured from the second positive since its time-to-peak corresponded to the d-wave in the smaller stimulus ERGs.

4.2.6 Distribution of RGCs and their Receptive Fields

Every RGC has a receptive field, an area in space within which the RGC responds to a light stimulus (Hartline, 1938; Barlow, 1953; Kuffler, 1953; Wassle et al., 1983; Lennie, 2003; Spillmann, 2014). The distribution of RGCs and their receptive fields are therefore expected to be similar. However, RGC bodies within the central zone (up to ~4 mm (15º) eccentricity) are centrifugally displaced from their receptive fields due to the length of the laterally connecting Henle fibres and the oblique pathway through the bipolar cells (Curcio and Allen, 1990; Drasdo et al., 2007). The peak density of RGCs therefore occurs not at the foveal centre, but at a point 1 – 2 mm (3.5º – 5º) away from it and the local density of receptive fields in the central retina does not reflect the local density of RGC bodies (Curcio and Allen, 1990; Drasdo et al., 2007). By implication, the response to a stimulus of a given size is determined by the number of receptive fields covered by the stimulus, and not necessarily by the

number of RGCs in that specific area. Thus in this study, the PhNR density is compared to that of the RGCf.

In this study, a formula by Watson (2014) was used in calculating RGCf field density (in deg^2) as a function of eccentricity (in deg) in the human retina (Equation 1).

$$d_{gf}(r,k) = d_{gf}(0) * \left[a_k\left(1+\frac{r}{r_{2,k}}\right)^{-2} + (1-a_k)\exp\left(-\frac{r}{r_{e,k}}\right)\right]$$

Equation 1

where $d_{gf}(r, k)$ is the density of RGCfs at eccentricity, r, in degrees along meridian, k; $d_{gf}(0)$ is the density of receptive fields at the centre of the fovea (33,163.2 RGCf/deg^2), a_k is the weighting function of the first term, r_2 is the eccentricity at which RGC receptive field density is reduced by a factor of 4 (and spacing is doubled) and $r_{e,k}$ is the scale factor by the index k. The values of the constants are provided in Table 4.2.

Table 4.2. The values of constants for Equation 1 in four meridians (Watson, 2014)

Meridian (k)*	a	r_2	r_e
Temporal	0.9851	1.058	22.14
Superior	0.9935	1.035	16.35
Nasal	0.9729	1.084	7.633
Inferior	0.9960	0.9932	12.13

* Meridians refer to visual field locations

This formula is based on histologic data by Curcio and Allen (1990) and Drasdo et al (2007), and on a method of converting retinal dimensions in millimetres to visual angle in degrees using a wide angle schematic eye (Drasdo and Fowler, 1974). The formula provides RGCf densities for each of four meridians. Since a circular stimulus centred on the fovea was used in this study, the mean density of the four meridians was calculated and used to plot Figure 4.2A. Note that the meridians refer to visual field locations (not retinal locations) and thus the blind spot appears in the temporal meridian. In the data provided by Watson (2014), the blind spot was 7^o wide and started at an eccentricity of 11^o in the temporal meridian and thus the RGCfs in this area (blind spot) was zero. Accordingly, the area of the blind spot (38.48 deg^2) was subtracted from the areas covered by

stimuli greater than 20º. The mean cumulative counts of RGCf as a function of eccentricity (Figure 4.2B), was calculated by integrating the mean density at eccentricity, *r*, (using the trapezoid rule) and multiplying this by 2πr to account for the increasing area, as required by Watson (2014).

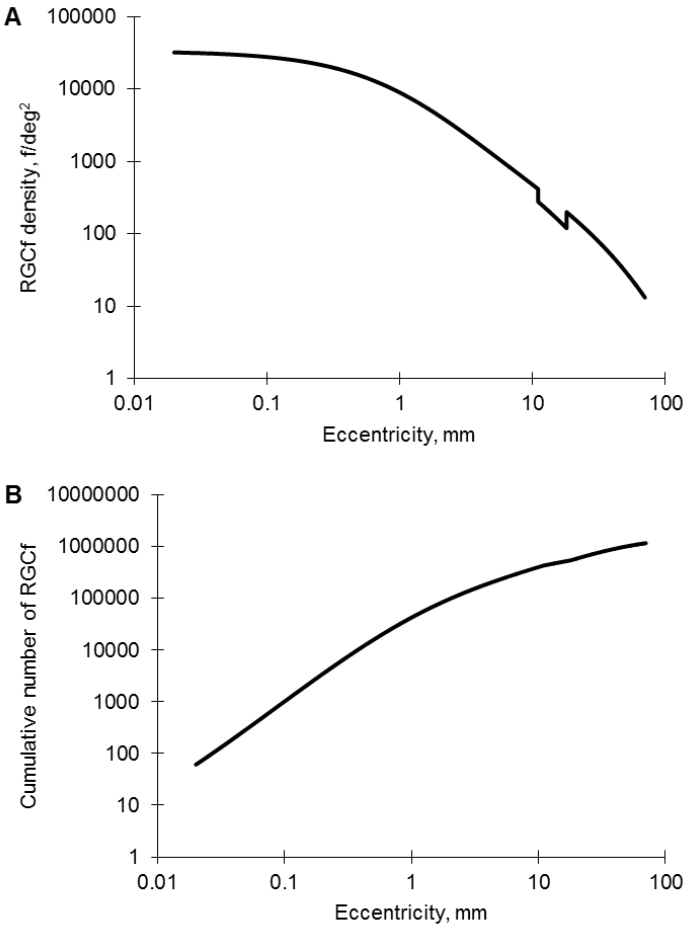

Figure 4.2. (A) Mean density of midget ganglion cell receptive fields as a function of eccentricity computed from the formula provided by Watson (2014). The "valley" in the curve corresponds to the blind spot. (B) Cumulative number of midget ganglion cell receptive fields as a function of eccentricity. Graphs are plotted on a log scale.

For the long duration stimulus, the densities and cumulative counts of the receptive fields of ON and OFF RGCs were required in order to compare them respectively to the PhNR-ON and PhNR-OFF parameters. For this, the distributions of ON and OFF cells of all RGC types were needed. As there are many different RGC types in the retina, the two major morphological types, the midget and parasol RGCs, were chosen. A third group, which was called "others" was added to include all the other RGCs in the retina. Computations regarding the midget RGCs, which constitute the most numerous type of RGCs,

were based on the published results of Dacey (1993) and Drasdo (2007) in which mRGCs make up ~90% of the population of RGCs near the fovea reducing to ~40% in retinal periphery. Calculations for ON and OFF mRGCs were based on the ratio of ON:OFF mRGCs from 0 – 5° = 1:1; from 5 – 25° = 1:1 to 1:1.69; and beyond 25° = 1:1.69 (Drasdo et al., 2007). Explicit details of the distribution of the parasol RGCs (pRGCs) in humans were not available in the searched literature. Therefore, they were assumed to constitute 10% of the RGC population at all eccentricities based on the 8 – 12% reported by Silveiro et al (2004) for macaque. The ON:OFF ratio of parasol RGCs was then computed to be 0.4:0.6 based on the dendritic field size differences between ON and OFF pRGCs (Dacey and Petersen, 1992). The proportion of RGCs in the "others" group was calculated by subtracting the sum of the midget and parasol RGCs from the total number of RGCs at each eccentricity. The ON:OFF ratio for the others group was assumed to be 1:1. (Please see Appendix II for the calculation tables).

4.2.7 Statistical Analysis

The changes in response density and response per RGC with eccentricity as well as the relationship between the PhNR density and the RGCf density were determined by linear regression. Comparisons were considered significant when $p < 0.05$. As the sample size was less than 30, 95% confidence intervals were calculated using the Student's t-distribution (Altman, 1991).

4.3 Results

4.3.1 Participants

In Experiment 1, six participants made up of four females and two males, were recruited. They were aged between 24 and 37 years (average 29.33 $\pm$ 4.23 years). In Experiment 2, sixteen participants aged between 21 and 50 years (average 27.5 $\pm$ 6.88 years) and comprising seven females and nine males were recruited. Two participants from Experiment 1 were included in Experiment 2. Data for the oldest participant were excluded because the age fell two standard deviations outside the mean of the data set. Data for five more participants were excluded for the following reasons:

1. The ERG amplitudes did not increase systematically with increasing stimulus size and participant was not available for re-test (n =1)
2. incomplete data set for all tested sizes (n = 2)
3. systematic difference in waveform due to poor fixation, drift or decompensated heterophoria at near (n = 2)

4.3.2 Experiment 1

The traces from individual participants are shown in Figure 4.3A. All the ERGs recorded with the various stimulus sizes, with the exception of the 5.5° stimulus, had clearly identifiable a-wave, b-wave, PhNR-ON, d-wave and PhNR-OFF components in all participants. The components were not clearly identifiable in two of the participants in the 5.5° ERG. The average value of the amplitudes of the components determined for the remaining four participants were therefore assigned to these two participants and used for analysis. This was done so that the amplitude difference between for the 5.5° and 10° stimuli could be calculated.

The group-averaged traces (Figure 4.3A) and the mean amplitudes of components as a function of eccentricity (Figure 4.4A, Table 4.3) demonstrated that the amplitudes of the ERG components increased with the stimulus size. The mean time-to-peak, however, appeared to decrease slightly except for the PhNR-OFF (Figure 4.4B).

The group-averaged ERGs for each stimulus size were normalised to their respective b-wave amplitudes to allow for comparison of the waveforms (Figure 4.3B). The waveforms of the normalised ERGs in response to the smaller stimulus sizes (5.5° – 30°) were different from those in response to the larger sizes (45° – full-field). The proportion of the PhNR-ON and PhNR-OFF amplitude was greater in the ERGs of the smaller stimulus sizes than in the larger stimulus sizes. A ledge on the rising limb of the d-wave (arrowed), first seen on the 15° ERGs become progressively prominent and developed into a separate peak in the 60° and full-field ERGs.

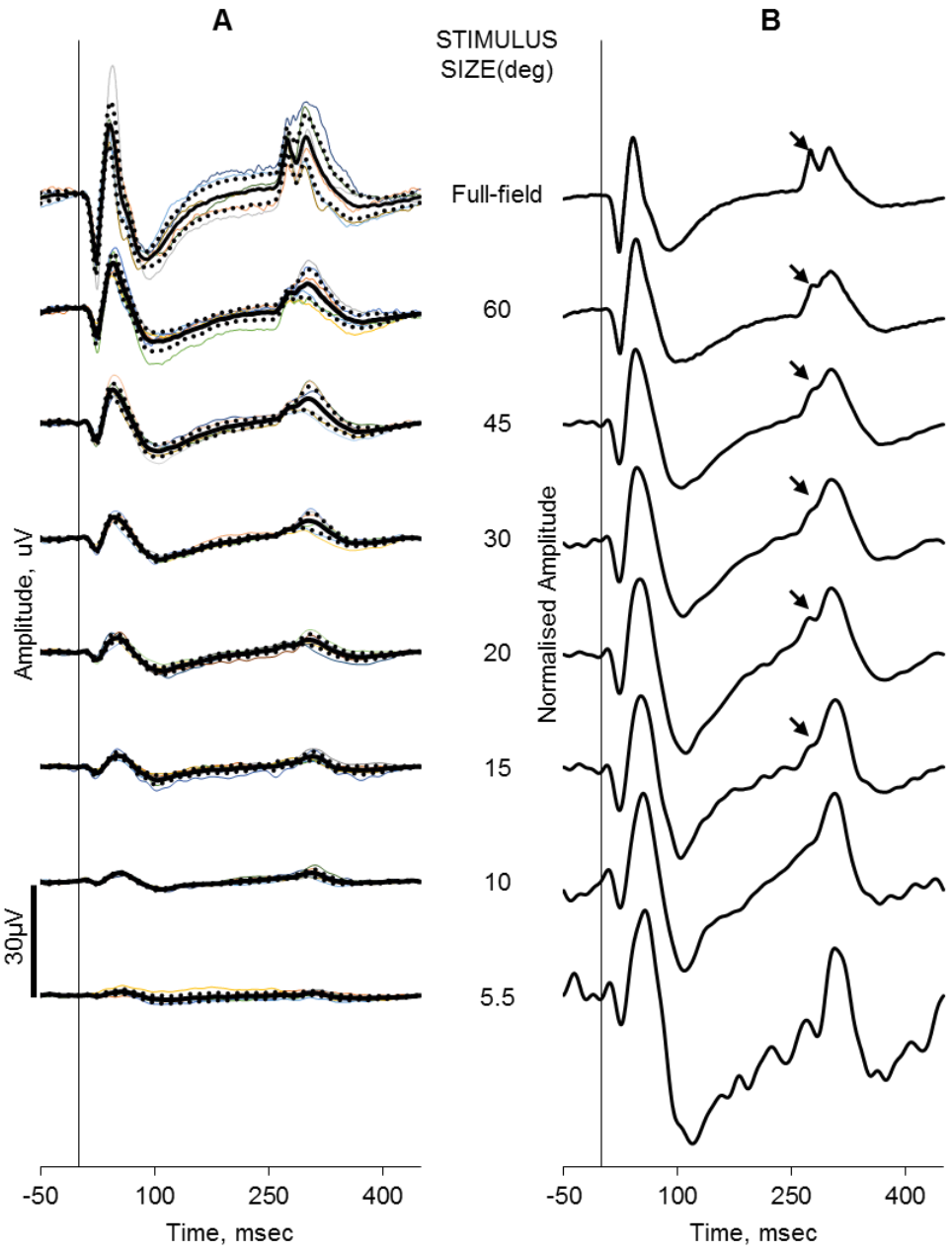

Figure 4.3. (A) Group-averaged long duration ERGs (thick black lines) recorded from participants in response to increasing stimulus size (bottom to top). Thin coloured lines are the individual traces and dotted lines show the 95% confidence interval. (B) The same group-averaged ERGs for each stimulus size which have been normalised to their respective b-wave amplitudes. Arrows indicate an emerging additional positive peak on rising phase of the d-wave.

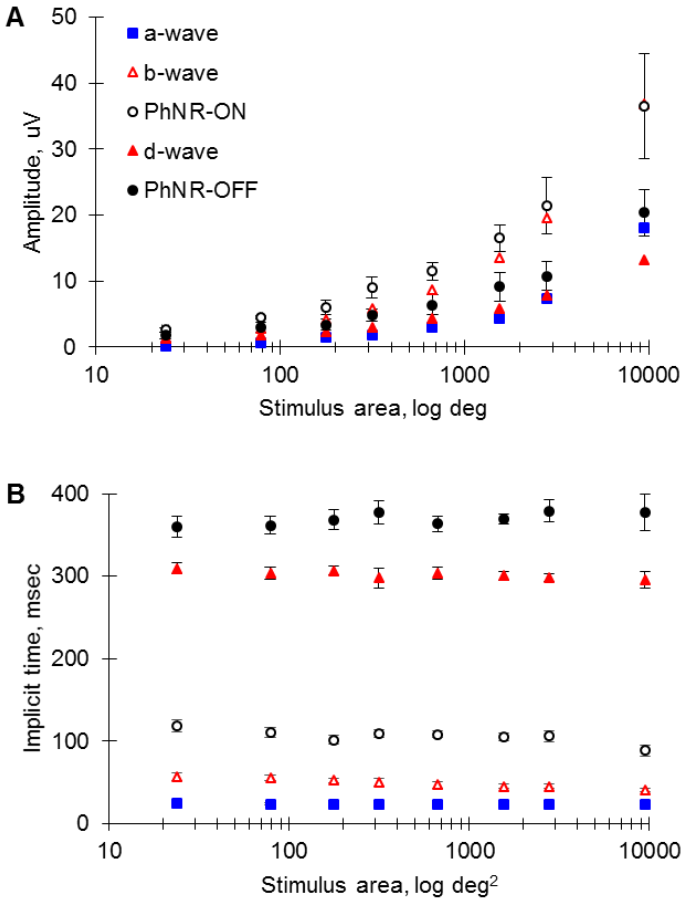

Figure 4.4. (A) Amplitudes of components of the long duration ERG as a function of stimulus area. For clarity, error bars are shown for only the PhNR-ON and PhNR-OFF. B – Time-to-peak of the long duration ERG components. The legend in A applies to B. Error bars represent 95% confidence intervals.

Table 4.3. Mean values of amplitudes and times-to-peak of ERG components recorded for the different stimulus sizes.

Stim Size, deg	a-wave		b-wave		PhNR-ON		d-wave		PhNR-OFF	
	Amp, µV	Time, msec	Amp, µV	Time, msec	Amp, µV	Time, msec	Amp, µV	Time, msec	Amp, µV	Time, msec
5.5	0.35 ±0.12	25.13 ±6.33	1.31 ±0.30	56.75 ±3.71	2.61 ±0.27	118.4 ±9.7	1.31 ±0.49	309.5 ±9.4	1.77 ±0.39	359.3 ±18.4
10	0.69 ±0.43	23.92 ±1.36	2.86 ±0.52	55.50 ±2.85	4.50 ±0.41	110.5 ±5.6	1.89 ±0.70	303.8 ±7.1	3.03 ±1.00	361.8 ±11.0
15	1.46 ±0.59	23.58 ±1.36	4.23 ±0.69	52.25 ±2.21	6.02 ±1.38	101.5 ±5.5	2.41 ±1.03	306.5 ±5.3	3.41 ±1.09	368.5 11.6
20	1.89 ±0.80	23.33 ±0.88	5.93 ±1.31	49.75 ±4.63	9.00 ±2.04	109.3 ±4.7	3.08 ±2.16	297.7 ±12.0	4.88 ±1.12	377.0 ±13.7
30	3.08 ±0.80	22.92 ±0.58	8.77 ±1.52	46.92 ±4.22	11.50 ±1.66	108.0 ±4.2	4.40 ±2.16	304.0 ±7.1	6.42 ±1.80	363.3 ±9.2
45	4.41 ±1.36	23.08 ±0.58	13.52 ±3.12	45.17 ±2.94	16.53 ±2.52	105.0 ±5.1	5.92 ±3.62	300.7 ±5.5	9.15 ±2.70	368.8 ±6.0
60	7.43 ±2.74	23.67 ±0.26	19.60 ±5.59	45.00 ±2.51	21.47 ±5.29	105.9 ±6.4	7.88 ±3.50	298.3 ±4.5	10.79 ±2.72	378.8 ±13.5
110	18.12 ±4.48	22.83 ±0.82	36.87 ±11.43	41.25 ±9.44	36.57 ±9.96	88.5 ±6.9	13.16 ±4.53	295.5 ±9.4	20.38 ±4.44	377.5 ±21.8

Values are given as mean ± standard deviation.

The response density plot in Figure 4.5A showed that both PhNR-ON and PhNR-OFF were maximal at the fovea and decreased towards the periphery. The density plots of the PhNR-ON and PhNR-OFF were qualitatively similar to that of the ON (blue dashed line) and OFF (grey-dashed lines) RGCf densities respectively. A cone density plot derived from the data provided by Curcio et al (1990) is also shown as a dashed orange line in Figure 4.5A. It may be seen that although cone density drops with eccentricity, the profile unlike that of the RCGf profile, deviates from that of the PhNR data from an eccentricity of about 4°.

Linear regression analysis showed a strong relationship between the PhNR-ON and ON-RGCf ($R^2 = 0.99$, $p < 0.0001$) and between the PhNR-OFF and OFF-RGCf ($R^2 = 0.99$, $p < 0.0001$) (Figure 4.5B). The response per RGC (response in annulus/number of RGCf in annulus) of the PhNR-ON and PhNR-OFF both showed a significant increase with eccentricity (PhNR-ON: $R^2 = 0.89$, $p = 0.0001$; PhNR-OFF: $R^2 = 0.50$, $p = 0.0489$) (Figure 4.5C). The mean values of the response density and response per cell are reported in Table 4.4.

Table 4.4. Mean values of the response density and response per RGC of the PhNR-ON and PhNR-OFF as a function of eccentricity.

Eccentricity, deg	Response Density, $\mu V/deg^2$ ($x10^{-2}$)		Response per RCG, $\mu V/RGC$ ($x10^{-5}$)		RGCf Density	
	PhNR-ON	PhNR-OFF	PhNR-ON	PhNR-OFF	ON-RGCf	OFF-RGCf
1.38	11.00 ±1.15	7.45 ±1.58	3.98 ±0.42	2.60 ±0.55	3180.99	3310.83
3.88	3.45 ±0.85	2.35 ±1.25	4.05 ±0.10	2.63 ±1.40	871.95	907.54
6.25	1.55 ±1.11	0.74 ±0.34	3.61 ±2.45	1.58 ±0.73	444.08	473.64
8.75	2.17 ±1.34	1.07 ±0.13	8.43 ±5.20	3.61 ±0.45	270.70	302.59
12.50	0.85 ±0.33	0.52 ±0.26	7.18 ±2.80	3.53 ±1.77	102.97	121.91
18.75	0.57 ±0.27	0.31 ±0.14	9.22 ±4.42	3.55 ±1.55	81.45	105.96
26.25	0.40 ±0.31	0.13 ±0.06	9.99 ±7.66	2.15 ±1.01	45.19	62.24
42.50	0.23 ±0.09	0.14 ±0.06	14.01 ±5.82	5.90 ±2.55	18.46	24.31

Values are given in mean ± standard deviation. NB – the RGC receptive field (RGCf) density provided in the last two columns were derived using formulas from Watson 2014.

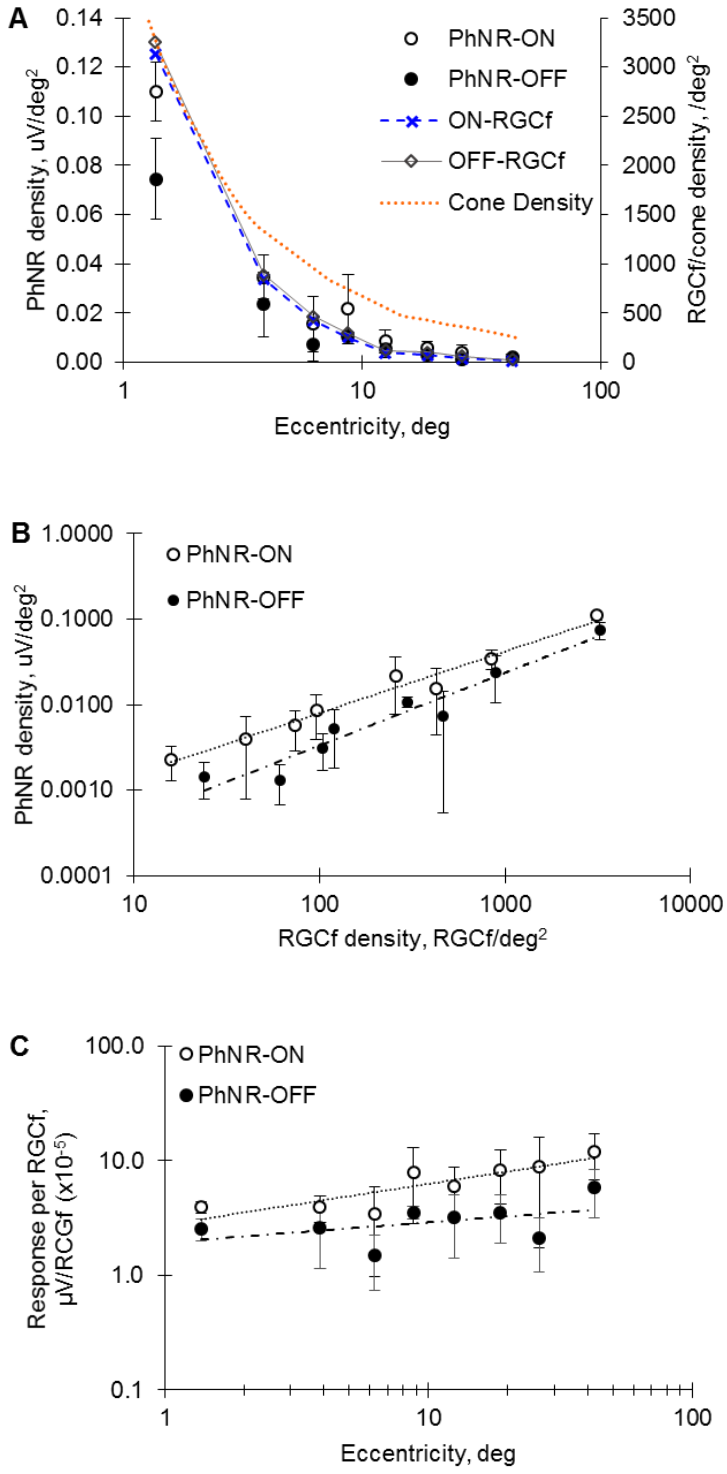

Figure 4.5. (A) Amplitude densities of the PhNR-ON and PhNR-OFF components as a function of eccentricity. For comparison, the receptive field densities of ON-RGCs (ON-RGCf) and OFF-RGCs (OFF-RGCf) plotted from the data provided by Watson (2014) are shown as blue and grey dashed lines respectively. Cone densities plotted from Curcio et al (1990) are also shown as the orange dotted line. (B) Linear regression analysis of PhNR density and RGCf density. The equation for the PhNR-ON line is y = 3.0 x 10-5x + 0.0046; R^2 = 0.99, p < 0.0001. The equation for the PhNR-OFF line is y = 2.0 x 10-5x + 0.0011; R^2 = 0.99, p < 0.0001. (C) Estimated response of the PhNR-ON and PhNR-OFF contributed by each ON-RGC and OFF-RGC respectively as a function of eccentricity. The equation of the PhNR-ON line is y = 0.25x + 3.7161; R^2 = 0.86, p = 0.0001. The equation of the PhNR-OFF line is y = 0.07x + 2.1377; R^2 = 0.50, p = 0.0486. Error bars represent 95% confidence intervals.

4.3.3 Experiment 2

The traces of the brief flash ERGs from individual participants are shown in Figure 4.6A. All the ERGs recorded with the various stimulus sizes had clearly identifiable a-wave, b-wave and PhNR components. The amplitudes of all the components increased with stimulus area (Figure 4.7A, Table 4.5) while the time-to-peak for the components, except the a-wave, decreased (Figure 4.7B). The waveforms of the normalised brief flash ERGs were similar for all stimulus sizes except for the full-field, which had a positive going component interrupting the descending limb of the b-wave (the i-wave, arrowed) (Figure 4.6B). Similar to observations made in the long duration ERG, the proportion of the PhNR amplitude to the b-wave amplitude reduced as stimulus area increased.

As observed in the long duration PhNRs, the brief PhNR density was maximal at the fovea and declined rapidly towards the periphery (Figure 4.8A). The results nearly overlap with Watson's data in Figure 4.8A. Once again, the cone density profile shows poor overlap with the PhNR density profile (Figure 4.8A). Linear regression analysis demonstrated a strong relationship between the two quantities ($R^2 = 1.00$, $p < 0.0001$) (Figure 4.8B). The calculated response per RGC increased with eccentricity as previously observed for the long duration PhNRs. The mean values of the density and response per RGC of the PhNR are provided in Table 4.6.

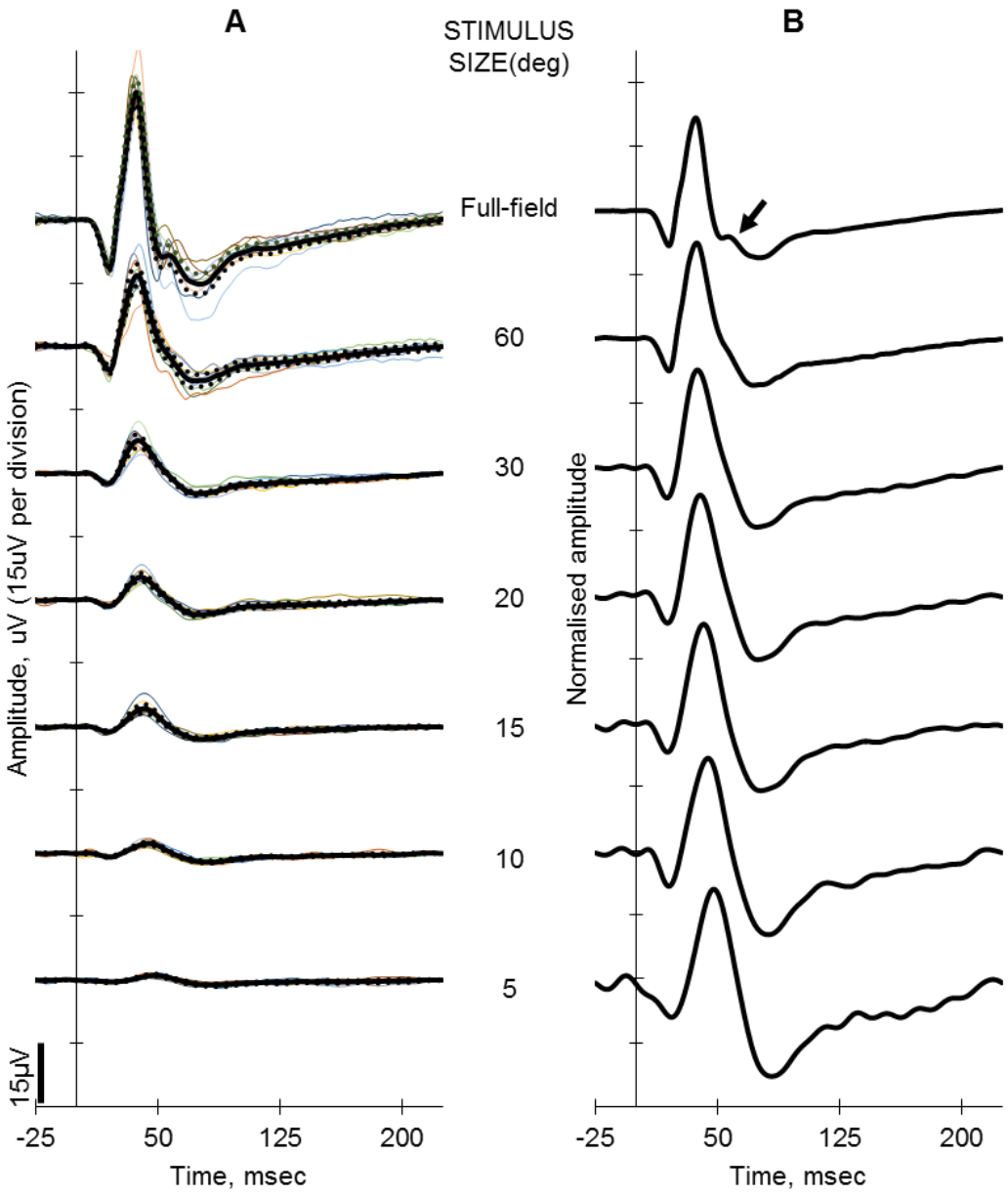

Figure 4.6. (A) Group-averaged brief flash ERGs (thick black lines) recorded from participants in response to increasing stimulus size (bottom to top). Thin coloured lines are the individual traces and dotted lines show the 95% confidence interval. (B) The same group-averaged ERGs for each stimulus size which have been normalised to their respective b-wave amplitudes. Arrow indicates the positive wavelet (i-wave) on the falling phase of the b-wave.

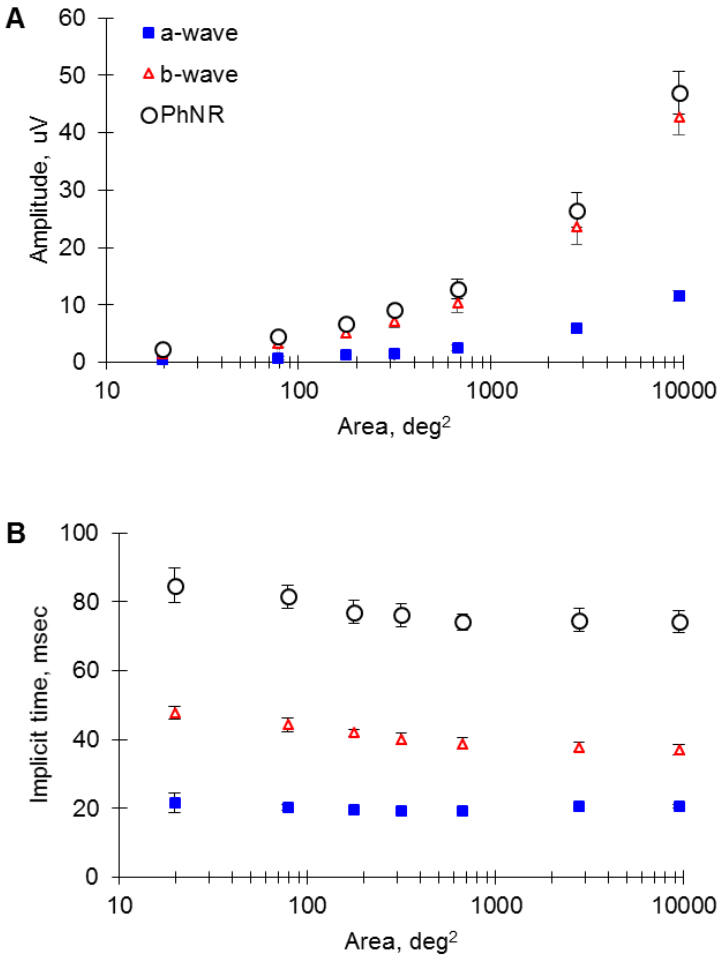

Figure 4.7. (A) The amplitudes of the brief flash a-wave, b-wave and PhNR plotted as a function of the log of stimulus area. (B) Time-to-peak of the components plotted as a function of the stimulus area. The legend in A applies to B. Error bars represent 95% confidence intervals.

Table 4.5. Mean values of amplitudes and times-to-peak of brief flash ERG component recorded for the different stimulus sizes.

Stimulus Size, deg	a-wave		b-wave		PhNR	
	Amp, µV	Time, msec	Amp, µV	Time, msec	Amp, µV	Time, msec
5	0.59 ±0.34	21.63 ±3.91	1.59 ±0.48	47.80 ±2.71	2.38 ±0.51	84.65 ±7.08
10	0.78 ±0.46	20.25 ±1.38	3.24 ±0.95	44.30 ±2.93	4.46 ±0.70	81.53 ±4.73
15	1.28 ±0.61	19.58 ±0.80	5.14 ±1.22	42.03 ±1.41	6.81 ±1.03	77.00 ±4.76
20	1.44 ±0.59	19.35 ±0.64	7.12 ±1.59	40.15 ±2.19	9.25 ±1.17	76.08 ±4.77
30	2.54 ±0.62	19.15 ±0.69	10.39 ±2.54	38.73 ±2.34	12.75 ±2.41	74.13 ±3.16
60	5.97 ±1.32	20.60 ±0.68	23.62 ±4.22	37.83 ±1.80	26.51 ±4.18	74.68 ±4.71
110	11.60 ±1.38	20.65 ±0.98	42.78 ±4.52	37.03 ±1.92	46.92 ±5.27	74.30 ±4.40

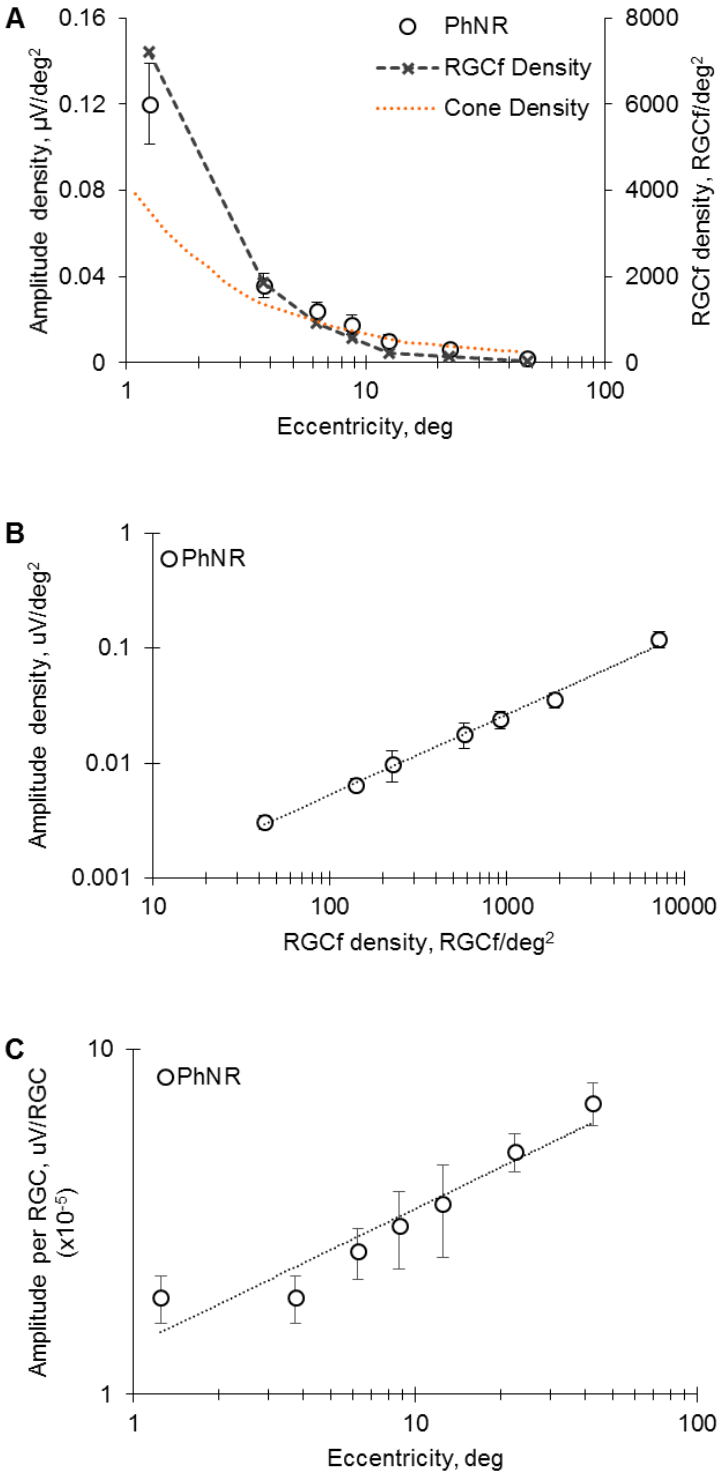

Figure 4.8. (A) Amplitude density of the brief flash PhNR plotted as a function of eccentricity. For comparison, RGCf density plotted from the data provided by Watson 2014 is shown as the grey dashed line and cone density plotted from Curcio 1990 is shown the orange dotted line. (B) Linear regression analysis of the PhNR density and RGCf density. The equation of the line is $y = 2.0*10^{-5}x + 0.0059$, $R^2 = 0.9965$, $p < 0.0001$. (C) Estimated PhNR amplitude contributed by each RGC as a function of eccentricity. The equation of the regression line (dotted line) is given by $y = 0.128x + 1.8062$, $R^2 = 0.98$, $p < 0.0001$. Error bars represent 95% confidence intervals.

Table 4.6. Mean values of the response density and response per RGC of the brief flash PhNR as a function of eccentricity.

Eccentricity, deg	Response Density, μV/deg^2 (x10^{-2})	Response per RCG, μV/RGC (x10^{-5})	RGCf Density
1.25	12.01 ±2.63	1.91 ±0.42	7211.95
3.75	3.56 ±0.77	1.90 ±0.41	1857.47
6.25	2.39 ±0.57	2.60 ±0.61	917.72
8.75	1.77 ±0.63	3.09 ±1.09	573.29
12.50	0.99 ±0.42	3.56 ±1.51	224.88
22.50	0.65 ±0.11	5.06 ±0.90	139.60
42.50	0.31 ±0.06	7.01 ±1.39	42.77

Values are given in mean ± standardard deviation. NB – the RGC receptive field (RGCf) density provided in the last two columns were derived using formulas from Watson 2014.

4.4 Discussion

4.4.1 Changes to ERG Components with Stimulus Size

This study demonstrated that all the ERG components of the long duration and brief flash ERG increased in amplitude with increasing stimulus area. This is because the cumulative count of the retinal cells from which these components arise increases with retinal area (Osterberg, 1935; Curcio and Allen, 1990; Curcio et al., 1990; Drasdo et al., 2007). Previous studies have reported a similar increase in the amplitudes of other ERG components (a-wave, b-wave, d-wave, flicker ERG) with stimulus size as more neurons are stimulated (Seiple et al., 1988; Errico et al., 1990; Junghardt et al., 1993; Murray et al., 2004; Jacob et al., 2015). However, the extent of increase was not uniform across ERG components (Brindley and Westheimer, 1965; Errico et al., 1990). This lack of uniformity was reflected in this study and demonstrated by the changes in the waveform and ratios of the ERG components to each other with increasing stimulus area. This may be explained by the changes in the relative proportions of retinal cells which occur with increasing eccentricity (Curcio and Allen, 1990; Curcio et al., 1990; Kolb, 2003; Drasdo et al., 2007; Kolb, 2011). For example, in Figure 4.3B, the increase of the b-wave, a bipolar cell response, in proportion to the PhNR-ON (or brief PhNR in Figure 4.6B), which arises from the RGCs may be explained by the increasing proportion of the

bipolar cells to RGCs (or decreasing proportion of RGCs to bipolar cells) with eccentricity. This suggests that individual variation in the topography of retinal cells in the normal population contributes to the inter-individual variability in ERG recordings.

In the long duration ERGs, the emergence of two distinct positive peaks after stimulus offset in the 60^{o} and full-field ERGs, not seen in the ERGs produced by smaller stimuli, was notable. These peaks are often seen in full-field long duration ERGs (Sieving et al., 1994; Viswanathan et al., 1999; Sustar et al., 2006; Ueno et al., 2006b; Horn et al., 2011). Pharmacological evidence attributes the first positive peak to the depolarisation of OFF-bipolar cells after stimulus offset while the second positive peak is attributed to depolarisation of cones after stimulus offset (Sieving et al., 1994; Ueno et al., 2006b). As the timing of the d-wave peak of the smaller stimuli (5.5^{o} – 45^{o}) more closely matched the timing of the second peak in the larger stimuli (60^{o} and full-field), it suggested that the cellular origins of the focal d-wave and those of the full-field d-wave (i.e. the first peak) were not the same; the focal d-wave may be dominated more by cone responses than OFF-bipolar cells. This implies that the cellular contributions to the focal ERG components are not the same for full-field ERGs. In other words, the focal ERG is not necessarily a scaled down version of the full-field ERG.

It was further observed that the times-to-peak of the ERG components generally tended to decrease with increasing stimulus sizes. The exceptions were the a-wave time-to-peak which appeared constant and the PhNR-OFF which appeared to increase. The decrease in the time-to-peak of the ERG components could be due to increasing amplitude of the ERG components and convergence of first order neurons onto second and third order neurons; however, the exact mechanism could not be ascertained. It was also not clear why the PhNR-OFF peak time showed an increase with stimulus size, however, it appeared the additional positive peak after stimulus offset seen to emerge as the stimulus size got bigger (Figure 4.3B) may have contributed to this.

4.4.2 PhNR Density and Retinal Eccentricity

Another key finding in this study was the strong relationship between the distribution of the response densities of the PhNRs (PhNR-ON, PhNR-OFF and brief PhNR) and the reported RGCf density (Watson, 2014) with increasing eccentricity. The mean densities of all the PhNRs were highest at the fovea and declined with eccentricity similar to the pattern reported for the RGCf. This result in itself is insufficient to link the PhNR to the RGCs since it is possible to obtain similarly strong relationships between the RGCf density and the other photopic ERG components. This is essentially because the neurons eliciting these responses are all denser in the central than peripheral retina. In fact, Errico et al (1990), compared the density profile of the negative going so-called "PIII" following the b-wave (now identified as the PhNR-ON) to cone density profile and erroneously attributed the component to cones. However, the results in Figure 4.5A and 4.8A, showed that the cone density profile derived from data from Curcio et al (1990), unlike the RGCf profile, was a poor fit for the long and brief PhNRs density profiles. This deviation lends support to the notion that the PhNR primarily arises from RGCs rather than cone photoreceptors. Furthermore, pharmacological evidence and diseases that selectively impinge on RGC function show that the PhNR is essentially an RGC response (Viswanathan et al., 1999; Viswanathan et al., 2000; Gotoh et al., 2004; Rangaswamy et al., 2004; Ueno et al., 2006a; Miyata et al., 2007; Machida et al., 2008b; North et al., 2010).

Finally, this study attempted to estimate the PhNR amplitude produced by a single RGC on the basis of ERG recordings. The results suggested that the response of an RGC increases with eccentricity. In the long duration ERG, the ON-RGC response (PhNR-ON) showed about a threefold increase from approximately 4 x 10^{-5}µV per cell at the fovea to 14 x 10^{-5}uV per cell in the periphery, while the OFF-RGC response (PhNR-OFF) per cell for the PhNR-OFF showed a twofold increase from approximately 3 x 10^{-5}µV per cell to 6 x 10^{-5}µV per cell. The brief PhNR (assumed to be the response from the total RGC population) showed about a threefold increase from 2 x 10^{-5}µV to 7 x 10^{-5} µV.

The increase in response per cell with eccentricity, may be directly related to the increase in the dendritic field and/or cell size of the RGCs which also increases with eccentricity (Rodieck et al., 1985; Watanabe and Rodieck, 1989; Silveira and Perry, 1991; Dacey and Petersen, 1992; Dacey, 1993b; Yamada et al., 1996). For the range of eccentricities examined in this study (i.e. 1^{o} – 45^{o} ~ 0.3 mm – 12 mm), morphometric data from previous studies showed that the soma sizes of midget and parasol ganglion cells each increase approximately by a factor of two (Rodieck et al., 1985; Watanabe and Rodieck, 1989). Dendritic field diameter, on the other hand, increases about 20 to 40 fold for midget ganglion cells and 10 fold for parasol ganglion cells (Rodieck et al., 1985; Watanabe and Rodieck, 1989; Dacey and Petersen, 1992; Dacey, 1993b). The increase in PhNR amplitude per RGC with eccentricity therefore appears to be more closely related to soma size than to dendritic field size.

Although the increase in response per cell was statistically significant, the graphs (Figure 4.5C and 4.8C) showed considerable variations between individuals suggesting that large differences may exist in the output of cells among individuals. While this may be the case, it is possible that some of the variation in the data may be an artefact of the method of calculation used in this study as explained below. There are wide variations in the topography of RGCs in the normal population (Curcio and Allen, 1990; Drasdo et al., 2007). These variations are closely linked to the axial length and size of the eye, which both vary in the normal population (Grosvenor, 2007; Read et al., 2008; Hashemi et al., 2012). In this study, these individual variations in RGC distribution were not accounted for. Instead the mean values of RGC distribution reported by one study were used. In Experiment 1, the dichotomy of ON and OFF RGCs in addition to the low number of participants could therefore artificially increase the variability. A similar argument would apply in Experiment 2, however, the effect of the artefact is expected to be less since the ON/OFF dichotomy was avoided and a larger sample size was used.

Another possible explanation for the observed increase in the response per cell with eccentricity is related to the generation of the PhNR component. The RGCs are considered as the primary generators of the PhNR, however, there is evidence to show that the photoreceptors, amacrine cells, Muller and other glial

cells contribute to the PhNR amplitude (Bush and Sieving, 1994; Viswanathan et al., 1999; Machida et al., 2008a; Luo and Frishman, 2011; Thompson et al., 2011). Therefore, it may well be that all RGCs generate the same magnitude of response regardless of location, but that the larger amplitudes recorded with the larger stimuli (from which response per cell was highest) may have been boosted by other eccentricity based factors such as increasing convergence (e.g. more photoreceptors than RGCs) and lateral interaction of RGCs. This study was however, not designed to assess the impact of these confounding factors and further research is required to address them. Nevertheless, as previously mentioned, RGCs exhibit central to peripheral asymmetries in both structure and function. The findings from this study therefore appear to be in consonance with this characteristic of RGCs.

4.4.3 PhNR-ON and PhNR-OFF Asymmetry

With regards to the long duration ERG, the mean amplitude of the PhNR-ON was larger than that of the PhNR-OFF for all the stimulus sizes tested (Table 4.3). The PhNR-ON amplitude was ~50% greater than the PhNR-OFF amplitude for the 5.5º and 10º stimulus sizes. For the remaining sizes, the PhNR-ON amplitude was 75 – 100% greater than the PhNR-OFF amplitude. Ganglion cell counts in the human retina, however, show that ON- and OFF-centre RGCs are equal up to 5º eccentricity, from which point OFF-centre RGCs gradually outnumber ON-centre RGCs (ON: OFF ratio from 0 – 5º = 1:1; from 5 – 25º = 1:1 to 1:1.69; and beyond 25º = 1:1.69) (Dacey, 1993b; Drasdo et al., 2007) (See also Table II.4 in Appendix II). Since ERG responses are proportional to cell numbers, this appears to contradict the fact that there are more OFF-centre RGCs than ON-centre RGCs in the human retina (Dacey, 1993b; Drasdo et al., 2007). It may, however, be argued that ON-centre RGCs have certain larger anatomical features (e.g. soma size, dendritic field, axon diameter) (Dacey and Petersen, 1992; Dacey, 1993b) and larger physiological responses (Chichilnisky and Kalmar, 2002; Maturana et al., 2014) than their OFF-centre counterparts that predict greater electrophysiological responses from ON-centre RGCs. Yet, the anatomical and functional data from the above listed previous studies predict ON-OFF asymmetries of 10 – 50% in favour of ON-centre RGCs. Since the asymmetries in this study exceed this prediction, other factors have to be considered and are addressed later in this section.

The results from this study further suggested that the PhNR-ON amplitude per cell was ~50% larger than the PhNR-OFF for the 5.5 and 10º annuli (computed from Table 4.4). However, for annuli ≥15º the PhNR-ON response per cell was larger by 100% or more than the PhNR-OFF response. In comparison, anatomical data shows that soma sizes of human ON midget ganglion cells are no more than 10% greater than that of their OFF midget counterparts (Dacey, 1993b). (Data for parasol ganglion cell not available, but expected to be similar). The dendritic fields of human ON-centre parasol and midget cells are 30-50% larger in diameter than their OFF-centre counterparts (Dacey and Petersen, 1992). As noted previously, the known anatomical and/or functional differences between ON- and OFF-centre RGCs may therefore not account completely for the larger asymmetry in the PhNR-ON to PhNR-OFF response per cell at eccentricities greater than 5º.

It is presently difficult to account for the larger asymmetry recorded between the PhNR-ON and –OFF recorded in this study in comparison to the known anatomical and functional asymmetry between ON and OFF-centre RGCs. A possible factor however, may be related to the generation of the PhNR-ON and PhNR-OFF components. As mentioned earlier, other retinal cells apart from the RGCs are known to contribute to the components. It is possible that these non-RGC cells do not contribute equally to the PhNR-ON and PhNR-OFF components thus enhancing the asymmetries in the PhNR-ON and PhNR-OFF components.

4.4.4 Clinical and Research Implications

The findings of this study have clinical and research implications. Currently, ISCEV recommends the full-field brief ERG as the standard for clinical use. This study, however, suggests that the use of the full-field stimulus may not be the best since the degree to which the PhNR amplitude is reduced is dependent on the location of the lesion. The functional loss in peripheral RGCs would have a greater impact on the PhNR amplitude than a functional loss of similar magnitude in the central RGCs. In other words, retinal lesions affecting the central RGCs need to be large or extensive to produce significant reductions in the full-field PhNR amplitudes. This has been noted in other studies (Tamada et

al., 2009; Machida et al., 2011; Kiszkielis et al., 2012). ERGs should therefore be recorded with consideration to the locus of the disease.

4.5 Conclusion

This study showed that the PhNR of the brief flash ERG, as well as the PhNR ON and PhNR-OFF of the long duration ERG, increased in amplitude with increasing stimulus area reflecting the number of RGCs stimulated. The strong relationship between PhNR density and RGCf density supports previous findings that the PhNR reflects activity of RGCs and that it is possible to use ERG PhNR recordings to determine RGC distribution within the retina. Finally, this study suggests that the contribution of a single RGC to the PhNR amplitude depends on its eccentricity as well as its morphological and intrinsic physiological characteristics.

5 CHAPTER FIVE – ELECTROPHYSIOLOGICAL ASSESSMENT OF RETINAL FUNCTION IN AUTOSOMAL DOMINANT OPTIC ATROPHY – I: GENERAL METHODOLOGY AND RESULTS OF BASELINE TESTS

5.1 Preamble

The next three chapters (Chapters 5 – 7) constitute the main study of this PhD. This chapter reiterates the rationale and aims of the main study. The participant selection criteria, general methodology and results of baseline tests (i.e. visual acuity, contrast sensitivity, visual field sensitivity, peripapillary retinal nerve fibre layer thickness and macula thickness) are also described. In Chapter 6, the results of the electrophysiological assessment are presented and discussed. Finally, the correlations between the baseline tests and the electrophysiological assessments are presented and discussed in Chapter 7. Part of the data presented in Chapters 5 and 6 have been published (see Morny, et al., 2015 in Appendix VI

5.2 Introduction

Autosomal dominant optic atrophy (ADOA) is a hereditary optic neuropathy presenting in the first or second decade of life and characterised by bilateral optic nerve head pallor and loss of visual function including reduced visual acuity, centro-coecal visual field loss and colour vision defects (Votruba et al., 1998a; Votruba et al., 1998b; Votruba et al., 2003b; Newman and Biousse, 2004; Yu-Wai-Man et al., 2009). It is the commonest hereditary optic neuropathy with a prevalence between 1 in 50,000 to 1 in 8,000 (Krill et al., 1970; Kjer et al., 1996; Votruba et al., 2003a; Yu-Wai-Man et al., 2010a; Gallus et al., 2012; Lenaers et al., 2012). ADOA is caused primarily by mutations in the autosomal nuclear gene, *OPA1* (Alexander et al., 2000; Delettre et al., 2000; Ferre et al., 2005; Ferre et al., 2009; Yu-Wai-Man et al., 2010a), a key player in

mitochondrial dynamics, controlling mitochondrial fusion, amongst other key roles.

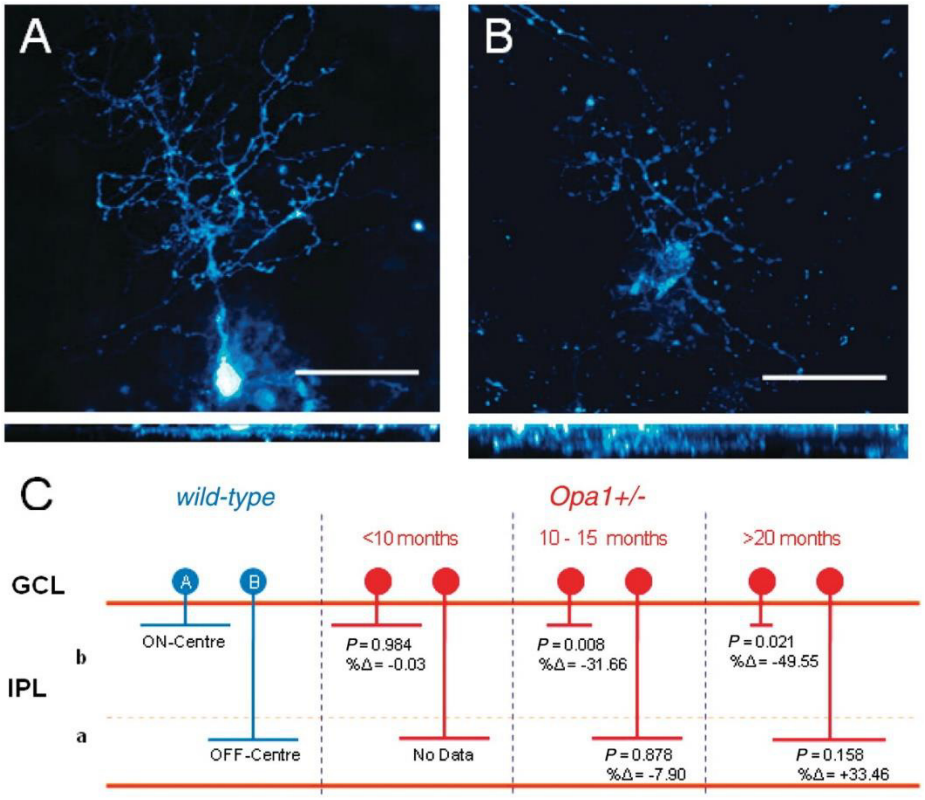

Figure 5.1. Selective dendritic pruning of ON-centre RGCs in Opa1 deficiency. Examples of ON- and OFF-centre RGCs from an adult (10-month-old) wild-type mouse showing their normal dendritic arbours (A and B respectively). Scale bar = 25 µm. The dendrites of ON-centre RGCs ramify in sublamina b (close to the level of the cell body) and the dendrites of OFF-centre RGCs ramify in sublamina a (close to the inner nuclear layer). Total dendritic length is reduced in the ON-centre RGCs of 10- to 15-month-old and >20-month-old mice (C) while remaining statistically unchanged in OFF-centre RGCs. P = Student's t-test, %Δ = percentage change from wild-type. GCL = ganglion cell layer; IPL = inner plexiform layer (Williams et al. 2010). (This figure is the same as Figure 1.13)

Histopathological studies in humans (Johnston et al., 1979; Kjer et al., 1983) and mouse models (Alavi et al., 2007; Davies et al., 2007; Williams et al., 2010; Sarzi et al., 2012) show that ADOA is principally characterised by the degeneration of the retinal ganglion cells (RGC). In a mouse model of ADOA, previously generated in our laboratory of this (Davies et al., 2007), the defect was first evident as a dendritic pruning of RGCs in B6:C3-*Opa1*^{Q285STOP} *Opa1* mutant mouse which appears to be ON-centre specific (Williams et al., 2010; Williams et al., 2012). The mean dendritic field area and mean dendritic length was reduced in ON-centre RGCs, but not OFF-centre RGCs, of 10- to 20-month mutant mice compared with age-matched wild-type controls (Figure 5.1). This selective vulnerability of ON-centre RGCs may reflect their higher energy demands in comparison to their OFF-centre counterparts, since *OPA1*

mutations are thought to curtail mitochondrial energy output (Williams et al., 2010; Williams et al., 2012). This new finding has, however, not been investigated in humans with ADOA.

The functional integrity of RGCs can be evaluated by assessing the photopic negative response (PhNR) of the flash ERG. The PhNR is a negative potential seen after the b-wave in a photopic ERG elicited by a brief flash. The PhNR is believed to originate from spiking activity in RGCs and their axons, with contributions from amacrine cells and associated glial cells like the astrocytes and Muller cells (Viswanathan et al., 1999; Viswanathan et al., 2000; Viswanathan et al., 2001; Rangaswamy et al., 2007; Thompson et al., 2011). When a long duration flash (>50 msec) is used to evoke the ERG, the PhNR is seen once after the b-wave (PhNR-ON) and again as a negative going potential after the d-wave (PhNR-OFF).

The brief flash PhNR is attenuated in patients with ADOA (Miyata et al., 2007) and in the *Opa1*^{Q285STOP} mutant mouse (Barnard et al., 2011). In the mouse model, the defect is seen prior to reduction in optokinetic visual acuity and to dendritic pruning which suggests that retinal connectivity may be affected before currently identifiable morphological abnormalities occur (Williams et al., 2012). Miyata et al (2007) and Barnard et al (2011) highlight the diagnostic potential of the PhNR in ADOA, however, the investigators used a brief white flash (broadband stimulus) to evoke the PhNR, which provides a poor signal to noise ratio compared to monochromatic stimuli (Rangaswamy et al., 2007), and cannot distinguish ON and OFF components (Viswanathan et al., 1999; Sustar et al., 2006; Rangaswamy et al., 2007). Furthermore, the studies elicited full-field (global) PhNRs which, in contrast to the focal PhNR, are less sensitive in detecting focal retinal lesions such as those seen in early to moderate glaucoma (Tamada et al., 2009; Machida et al., 2011).

Clearly, the delineation of the PhNR-ON and PhNR-OFF components by long duration red flash provides an opportunity to test the functional integrity of these two classes of RGCs in ADOA. In addition, the use of a focal ERG, rather than the full field ERG might be more appropriate in ADOA given the focal nature of the abnormality (Votruba et al., 1998a). It is possible that the focal PhNR-ON

deficit could serve as a bio-marker for the early onset of ADOA. If such early changes in RGC function are reversible, they need to be defined as markers for targeted therapies in any forthcoming therapeutic trials.

The main aim of this study, therefore, was to assess the effect of ADOA on the PhNR-ON and PhNR-OFF components elicited using focal and full-field long duration red flashes on a rod supressing blue background. On the basis of the evidence in mice, it was hypothesised that a selective reduction of the PhNR-ON in humans would be seen early in the disease with a progressive decrease in the PhNR-ON amplitude as the disease progressed. Hence, the ratio of the PhNR-ON to PhNR-OFF would also decrease with disease progression.

The specific objectives and their respective hypotheses are presented below.

1. To record focal long duration ERGs and PERGs from the central, nasal and temporal macula in order to assess regional differences in the focal PhNRs and PERG components between and within the ADOA and control cohorts.

   Hypotheses: In healthy individuals, RGC density is greatest in the central macula and in addition, greater in the nasal macula than in the temporal macula at equal eccentricities. This led to the hypothesis that in controls, the amplitudes of the focal PhNRs and N95 would be greatest in the central macula, followed by the nasal macula and least in the temporal macula.

   ADOA is typically characterised by central and centrocoecal scotomas. This supported the hypothesis that a greater difference in ERG parameters between participants with ADOA and controls would be seen in the central and nasal macula than in the temporal macula. A further hypothesis was that, as the disease progressed in participants with ADOA, the PhNR and N95 amplitudes would decrease more in the central and nasal macula than in the temporal macula, resulting in the loss of the asymmetry between the locations (found in controls) or a reversal of this asymmetry (i.e. focal PhNR and N95 amplitudes would be

greater in the temporal than in the central and nasal macula) in the ADOA cohort. This would be clinically useful since the temporal macula of an individual could serve the control.

2. To compare the focal long duration ERG to the full-field long duration ERG which have been recorded using the same stimulus parameters.

   Hypothesis: The distribution of RGCs in the normal retina is densest in the macula and progressively sparse with increasing eccentricity. In Chapter 4, the results showed that the contribution of the PhNR-ON and –OFF components to the long duration ERG decreased with increasing eccentricity. It was therefore hypothesised that there would be a greater contribution of PhNR-ON and –OFF components in the focal ERG than in the full-field ERG. In addition, it was hypothesised that the amplitude loss of the PhNRs in the focal ERG would be greater than in the full-field ERG due to the localised/centro-coecal nature of visual field defects in ADOA.

3. To compare the diagnostic potential of the long duration PhNR to responses which have previously been shown to be affected by ADOA; the full-field brief flash PhNR (Miyata et al., 2007; Barnard et al., 2011) and the N95 amplitude of the pattern electroretinogram (PERG) (Holder et al., 1998),

   Hypothesis: It was hypothesised that the diagnostic power of the long duration PhNRs would be similar to that of the brief flash PhNR and the N95 of the PERG as all of these responses reflect the spiking activity of the RGCs (Viswanathan et al., 1999; Viswanathan et al., 2000; Luo and Frishman, 2011).

4. To assess the effect of ADOA on retinal thickness measured using the OCT.

   Hypothesis: A reduction in the retinal thickness especially of the inner retina was predicted in ADOA

5. To assess the relationship between the results of the electrophysiological, psychophysical and structural tests obtained in this study.

   Hypothesis: It was hypothesised that tests that provide similar information about the retina would be well correlated e.g. RGC layer thickness and PhNR amplitude.

6. To assess the effect of age on the electrophysiological parameters measured in this study in ADOA and controls.

   Hypothesis: Previous studies have shown that the rate of RGC loss with age appears constant in both ADOA and controls (Barboni et al., 2011). However, it has also been suggested that individuals with ADOA may have a reduced complement of RGCs from birth (Barboni et al., 2010). It was therefore hypothesised that due to the reduced redundancy of neurones in ADOA, the age related changes would have a greater effect on function in participants with ADOA than in controls. This is important since previous attempts to correlate disease severity (visual dysfunction using VA) with age have been equivocal. Some studies (Berninger et al. 1991; Yu-Wai-Man et al. 2010a; Reis et al. 2013) have reported a progressive visual loss with age, while other studies (Votruba et al. 1998a; Cohn et al. 2008; Almind et al. 2012; Ronnback et al. 2013) did not find a significant change in VA with age.

5.3 Methods

5.3.1 Ethical Approval

This cross-sectional study had a multi-centre ethics approval from the National Health Service Research Ethics Committee for Wales. The study was carried out mainly at the School of Optometry and Vision Sciences, Cardiff University, Cardiff (Cardiff site), however, a second site was later set up at the Division of Optometry and Visual Science, City University, London (City site). Ethical approval was therefore obtained from the ethics committees of the School of

Optometry and Vision Sciences, Cardiff University, and the Division of Optometry and Visual Science, City University, London. All participants provided their written consent after receiving a participant information sheet and having the opportunity to ask questions. This study conformed to the Declaration of Helsinki.

5.3.2 Sample Size and Power Calculations

Miyata et al (2007) observed a difference in PhNR amplitude of 13.3µV between people with ADOA and healthy controls and a standard deviation of 9µV within healthy controls. Hence the computed standardised difference was 1.48. Using the nomogram provided by Altman (Altman, 1991), to detect this difference with 80% power at a significance level of 0.05 required a total sample size of 14 participants (7 per group) (See Appendix III).

This sample size was small and as a substantial body of data was collected requiring a full day of attendance, the aim was to recruit as many participants as possible. The additional participants allowed the sample size requirements to be met in the case of incomplete datasets or participant dropout.

5.3.3 Inclusion and Exclusion Criteria

The inclusion and exclusion criteria used to select participants with ADOA and controls for this study are summarised in Table 5.1 and 5.2.

Table 5.1. Inclusion criteria for participants

CRITERION	ADOA	CONTROLS
Age	Adults 18 years and above	Same as for ADOA
Gender	Male and female	Same as for ADOA
Visual acuity	Better than or equal to 2.0 logMAR (1/100 Snellen) in better seeing eye	Better than or equal to 0.1 logMAR (6/7.5 Snellen) in better seeing eye
Mutation	*OPA1* mutation confirmed or member of family with confirmed *OPA1* mutation	Not applicable

Table 5.2. Exclusion criteria for participants

CRITERION	ADOA	CONTROLS
Medications	Medications that affect visual function	Medications that affect visual function
Pre-existing systemic condition	Photosensitive epilepsy and any systemic disease affecting vision (e.g. uncontrolled diabetes)	Photosensitive epilepsy and any systemic disease affecting vision (e.g. uncontrolled diabetes)
Pre-existing ocular condition	Significant ocular conditions except ADOA (e.g. glaucoma, age related macular degeneration with 1 or more risk factors on Age Related Eye Disease Study (AREDS) Scale (Ferris et al., 2005))	Significant ocular conditions (e.g. glaucoma, age related macular degeneration with 1 or more risk factors on Age Related Eye Disease Study (AREDS) Scale (Ferris et al., 2005))

5.3.4 Participant Recruitment

Twelve participants from six families with documented *OPA1* mutations (Table 5.4) and sixteen healthy age matched controls were recruited for the study. All participants with ADOA, except Patient 1021, were recruited from a database of patients nationwide who had been formally diagnosed by a single consultant ophthalmologist (MV). Participants were first contacted over the telephone in cases where a telephone number was available. A recruitment letter and participant information sheet were then sent out if the participant showed interest. In cases where a telephone contact was not available, the letters were sent out to the last known address of the participants.

Patient 1021 contacted this research group and agreed to participate in the study after he had been diagnosed with subclinical ADOA by a different consultant ophthalmologist at a different facility. Patient 1021 had been diagnosed after his 8 year old daughter was diagnosed with classical signs of ADOA. Genetic testing at the same facility confirmed he and his daughter both carried the same *OPA1* mutation. The data from the five members of Family E were first obtained at the City Site, however, two members (1018 and 1020) later travelled to Cardiff to re-record their ERGs.

The participants who acted as controls were recruited from staff and students of the School of Optometry and Vision Sciences, including their friends and family. All the data from controls were obtained at the Cardiff Site.

5.3.5 Visual Acuity

The best corrected visual acuity (BCVA) of participants was recorded monocularly using an ETDRS chart at 4m (Ferris et al., 1982; Ferris and Bailey, 1996). The distance was reduced when necessary. The ETDRS charts are based on the design principles of Bailey and Lovie (Bailey and Lovie, 1976) and are the recommended standard in clinical research (Ferris and Bailey, 1996). Patients were encouraged to guess letters they could not see clearly until they made three or more errors on a line (Carkeet, 2001; Elliot, 2007). In all cases, the right eye was assessed before the left eye.

5.3.6 Contrast Sensitivity

Contrast sensitivity (CS) was measured monocularly using the Pelli-Robson CS chart at 1m (Pelli et al., 1988; Elliot, 2006; Elliot, 2007). The mean luminance of the chart was 477 cd/m^2 and participants wore their habitual distance correction as required for this test.

5.3.7 Autorefraction

Refraction was assessed objectively for each eye using an auto-refractor (KR-7500 Auto-kerato-refractometer, Topcon, Tokyo). At least three individual objective refractions for each eye were obtained and mean sphero-cylinder refraction was recorded.

5.3.8 Visual field Assessment

Visual field sensitivity (VFS) was assessed using the 24-2 SITA fast protocol of the Humphrey Visual Analyser (24-2 SITA-FAST, Humphrey Visual Field Analyser, Carl Zeiss Meditec, Inc., Dublin, CA, USA). This protocol assesses VFS 24^o either side of the fovea and provides the mean deviation scores, in decibels (dB) on a 54 point grid (Figure 5.2). However, only the 16 points on the total deviation plot (boxed area of Figure 5.2) corresponding to an 18^o x 18^o area on the retina were used for the analysis described in this study. The total deviation score at each point on the visual field test report is expressed on a logarithmic scale (10dB = 1 log unit). Therefore, to calculate the mean deviation (i.e. average of the total deviation scores) of the 16 locations, total deviation scores were first converted into a linear scale and averaged (Hood and Kardon,

2007; Hood et al., 2009). The mean deviation value was then obtained by converting the linear average back to a dB value.

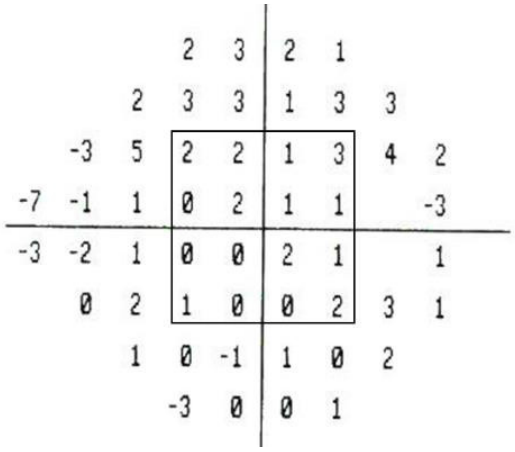

Figure 5.2. The total deviation plot of one of the control participants in this study. The mean deviation of visual field sensitivity was calculated from the central 16 points (boxed area).

5.3.9 Colour Vision

Colour vision was assessed monocularly using the L'Anthony desaturated D15 (DS-D15) test. All colour vison tests were performed in a light box with artificial daylight bulb of illumination 615 Lux (Artificial Daylight Bulb, 20 W, Thorn). The order in which the coloured caps were arranged was recorded on the D-15 score sheet to determine the axis of confusion as recommended (Elliot, 2007). The pass criterion was a circular diagram and no more than a single transformation between adjacent caps (Birch, 2008).

5.3.10 Imaging

OCT images were obtained using a Topcon 3D-1000 OCT machine (Topcon Medical Systems, Inc., Tokyo, Japan) at the Cardiff site and a Topcon 3D-2000 machine (Topcon Medical Systems, Inc., Tokyo, Japan) at the City University site. Cube scans (6mm x 6 mm = 512 horizontal x 128 vertical scans) were recorded from both optic nerve head and macula of participants. These were exported and analysed offline using the Iowa Reference Algorithm OCT Explorer Version 3.6 (Garvin et al., 2008; Garvin et al., 2009; Lee et al., 2010).

The OCT Explorer is able to analyse scans from the Topcon 3D OCT which are recorded in an *.fds format. This setting was not activated on the Topcon at the

London site at the time the OCT images were recorded for this study. Attempts were made to segment the images from City using an alternative third party software (ImageJ), however, this proved unsuccessful. As such only the images recorded from the Cardiff site (n = 6) could be used in this analysis.

5.3.11 Image Segmentation and Analysis

The Iowa Reference Algorithm OCT Explorer, hereafter referred to as "OCT Explorer", is a suite of algorithms for quantitative analysis of human and murine 3-D retinal OCT images. The OCT Explorer is compatible with OCT image data obtained from all widely-available clinical OCT machines including Heidelberg Spectralis and Topcon 1000 and 2000. The OCT Explorer is capable of automatically identifying up to 11 surfaces on retinal images as well as providing thickness and volume measurements for each identified layer (Figure 5.3).

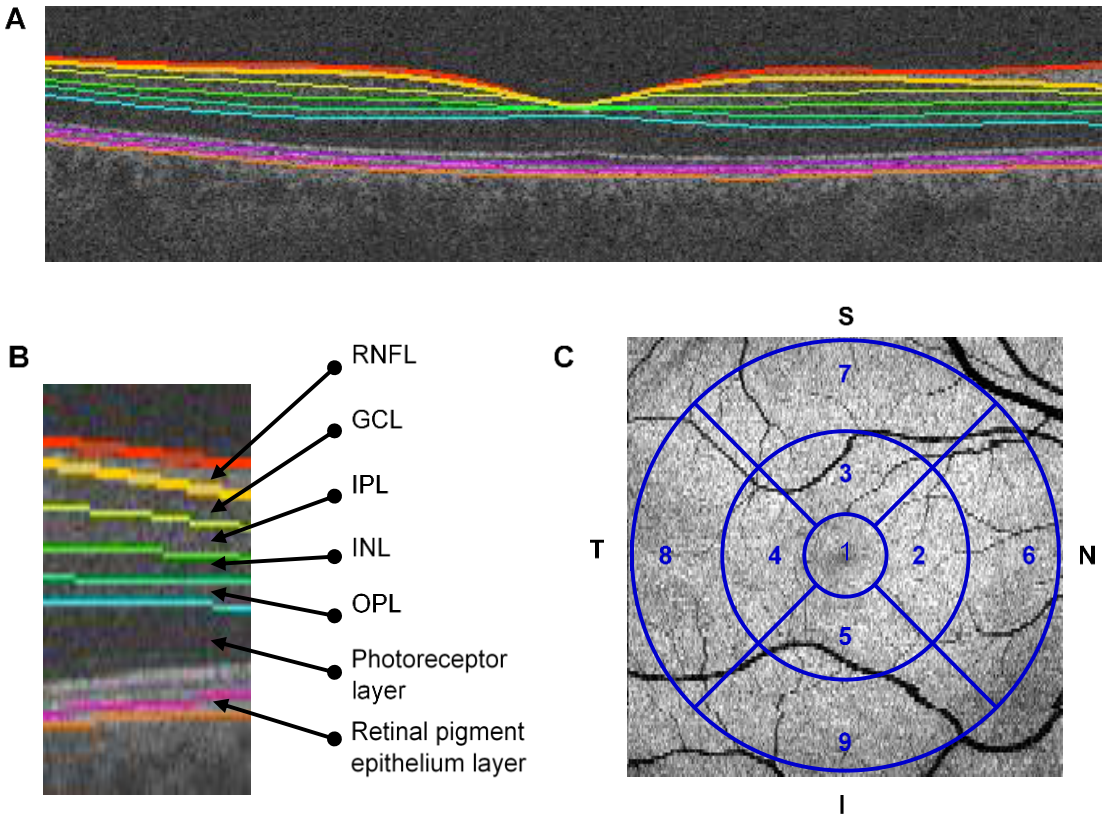

Figure 5.3. (A) A screenshot of the macula of a participant in this study showing the layers segmented by the OCT Explorer (coloured lines). (B) An enlarged section of the macula in (A) above showing the labelled layers. (C) The enface view of the macula. The macula was divided into three circular zones using an ETDRS grid (superimposed). The diameters of the circles (innermost to outermost) are 1, 3 and 6mm. S – superior, N – nasal, I – inferior, T - temporal

In this study, macula scans were segmented into the nine layers: retinal nerve fibre layer (RNFL), ganglion cell layer (GCL), inner plexiform layer (IPL), inner nuclear layer (INL), outer plexiform layer (OPL), photoreceptor layer and retinal pigment epithelium (RPE) (Figure 5.3B). Each layer was then divided into nine sectors using the Early Treatment Diabetic Retinopathy Study (ETDRS) grid. The mean thickness was calculated for each sector. Measurements from the innermost ring for RNFL and GCL were not included in the analysis since RGCs and their cell bodies in this area are displaced centrifugally.

The thickness of the peripapillary RNFL was measured using a circular scan (1.73mm diameter) centred on the optic nerve head (Figure 5.4). The circle was divided into four quadrants to assess the superior, temporal, inferior and nasal quadrants.

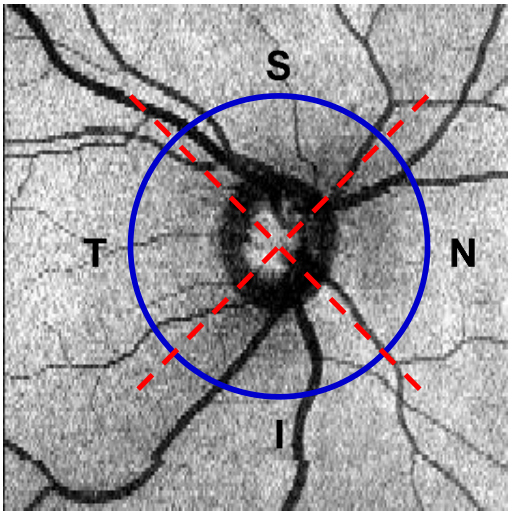

Figure 5.4. A screenshot of the optic nerve head (right eye) of a control participant as seen on the OCT Explorer. The peripapillary thickness was measured along the blue circle and divided into quadrants as shown by the red dashed lines. S – superior, N – nasal, I – inferior, T - temporal

5.3.12 Electroretinography

All ERGs were recorded monocularly using DTL fibre electrodes as the active electrode (Unimed Electrode Supplies, Ltd, Surrey, UK) and contralateral reference electrode. The DTL fibre was placed in the lower fornix to maximise stability during recording and the loose end fastened using medical tape at the inner canthus (Blenderm, Viasys Healthcare Ltd., Warwick, UK). A silver-silver chloride 10mm diameter touch-proof skin electrode (Unimed Electrode Supplies, Ltd, Surrey, UK), placed at the mid-frontal forehead position was used

as ground electrode. (The procedure for preparing participants for ERG recordings and the details of the equipment for recording the focal ERG have been presented in section 2.2.2 – 2.2.6)

All ERG responses were obtained using an evoked potential monitoring system (Medelec EP, Oxford Instruments PLC, Surrey, UK [Cardiff site]; Espion, Diagnosys LLC, Cambridge, UK [City site]). Responses were bandpass filtered from 1 – 100 Hz and digitally averaged. Signals were recorded in blocks of 10 - 20 responses, with a total of 40 – 60 averaged per trace. Between 4 and 6 traces were obtained for each stimulus condition. The traces were superimposed to confirm signal repeatability and averaged off-line into a single averaged trace containing 160 – 300 responses. An automatic artefact rejection system removed signals contaminated by large eye movements and blinks.

Transient PERG stimuli (4 reversals per second; check size = 1^o) were generated on a computer monitor at 98% contrast. The screen was masked with a black opaque cardboard with a 13 x 13 cm square cut-out at the centre so that it produced a 20^o x 20^o field at a viewing distance of 36cm.

Long duration ERGs were recorded at both sites using a red flash stimulus (peak output 660nm, 250msec duration, 55 cd/m^2, 2Hz) on a rod saturating blue background (peak output 469nm, 80 scot cd/m^2) produced by a hand-held miniature Ganzfeld light emitting diode (LED) stimulator (CH Electronics, Kent, UK). Focal stimulation was produced by mounting the miniature Ganzfeld LED tube into the middle of a light box (44 cm x 44 cm x 10 cm) such that the circular stimulus subtended 20^o diameter at a viewing distance of 15.6 cm. In order to minimise the effect of stray light stimulating the peripheral retina, the light box contained a strip of white LEDs (Super Bright InGan) passed through a blue filter (Lee Filter 068 Sky Blue, Lee Filters, Hampshire, UK) to produce a desensitising blue surround of 140 scot cd/m^2 (field size = 109^o x 109^o field). The stimulus configuration for recording from the central, nasal and temporal macula was described in section 2.6.2. To test the central macula, the participant fixated on the cross hairs in the middle of the stimulus; to test the nasal macula, the stimulus was moved temporally until the nasal edge of the stimulus was aligned to the participant's line of sight gaze; to record from the

temporal macula, the procedure for nasal macula was reversed. Full-field ERGs were recorded by holding the stimulator head, fitted with a diffusing cap, directly to the eye.

Full-field brief (flash) ERGs were elicited at the Cardiff site by a Ganzfeld stimulator (GS2000, LACE Elettronica, Italy) presenting a xenon flash stimulus (1.51 cd.s/m^2, 300 µsec maximum flash duration, 4Hz). Filters were used to obtain a red stimulus (Lee Filter “Terry Red”, Lee Filters, Hampshire, UK, transmittance <5% at wavelengths shorter than 575 nm, and above 85% from 625–700 nm) over a continuous rod saturating 64 scot cd/m^2 blue background (Schott Glass filter BG28, Schott AG, Mainz, Germany, peak transmittance 454 nm).

All ERGs were recorded by the same investigator using the same protocol at both sites. PERGs were always recorded first and as recommended, with natural pupils and appropriate near refractive correction when necessary (Bach et al., 2013). Pupils were then dilated using 1% tropicamide to a minimum of 7mm and flash ERGs were recorded in the following order: focal long-duration, full-field long duration and full-field brief flash ERG. The entire session for collecting data from each participant was between 4 – 5 hours including breaks which were incorporated to relieve fatigue. The recording protocol is provided in Appendix IV.

The long duration ERGs (focal and full-field) were generated by the same miniature Ganzfeld LED stimulator at both sites. However, the computer monitor for generating the PERG stimuli and the stimulator for the full-field brief flash available at the City site were different. They produced waveforms which were different to the ones obtained at the Cardiff site. As such, these recordings were not analysed.

All stimulus backgrounds were of sufficient scotopic illuminance (> 2000 scot td) to saturate the rods (Aguilar and Stiles, 1954). All stimuli were calibrated using an ILT 1700 radiometer with SED033/Y/R luminance detector (Able Instruments and Controls, Reading, UK) assuming a 7 mm pupil with no correction for the

Stiles-Crawford effect. The wavelength of the light sources was measured using a Specbos 1201 spectro-radiometer (Horiba Jobin Yvon Ltd, Middlesex, UK).

5.3.13 Signal Analysis

The method for measuring the amplitude of the various ERG sub-components is described in Figure 5.5. PERGs and focal ERGs were Fourier analysed to remove high frequency noise above 30Hz and 50Hz respectively.

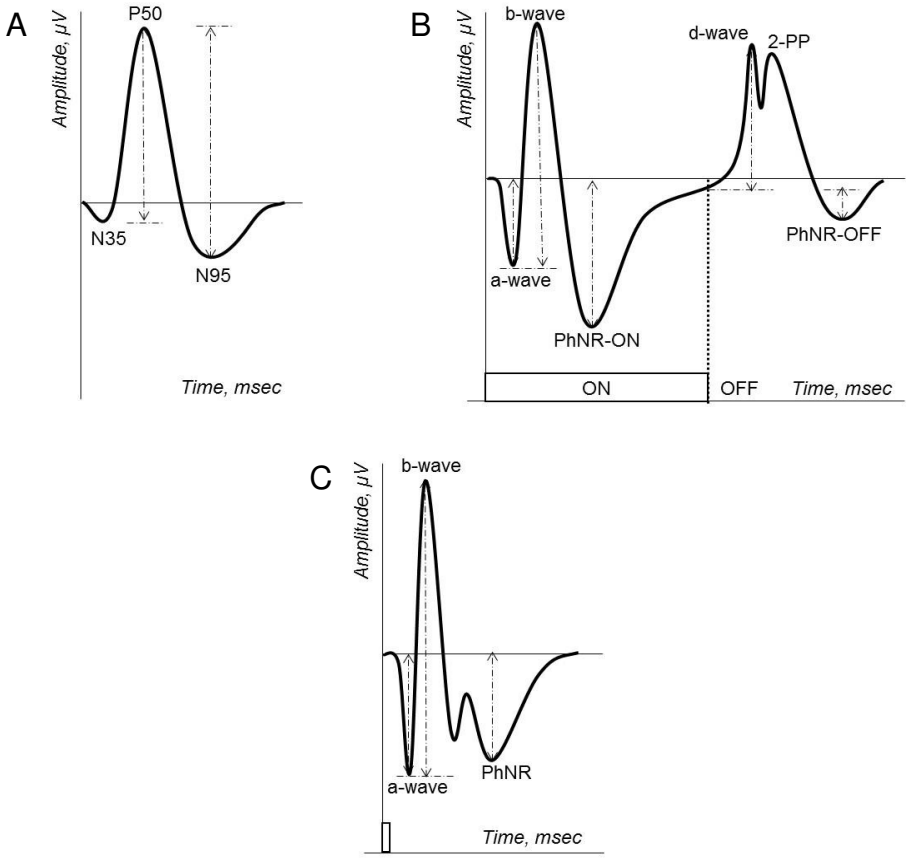

Figure 5.5. Representative traces of the (A) PERG, (B) full-field long-duration ERG and (C) full-field brief flash ERGs showing their components and how their amplitudes were measured (double headed arrows). The amplitudes of the P50, N95 (A) and b-wave (B-C) were measured as recommended by the International Society of Clinical Electrophysiology of Vision (ISCEV) (Marmor et al., 2009; Bach et al., 2013). The a-wave was measured from the point of light onset to the trough of the a-wave while the d-wave amplitude was measured from the point of light offset to the peak of the d-wave. The PhNR-ON (PhNR in brief flash) and PhNR-OFF amplitudes were measured from the voltage at stimulus onset and offset respectively to a fixed time point in their respective troughs (see main text for details). The focal long duration ERG had the same profile as the full-field long duration except that in the focal ERG there was only one prominent positive peak after light offset, the d-wave.

The PhNR-ON (PhNR for brief flash ERG) and PhNR-OFF amplitudes were measured from the voltage at stimulus onset and offset respectively to a fixed time point in their respective troughs. When determining the most appropriate

fixed time point at which to measure the PhNR-ON and PhNR-OFF responses, the group averaged ERG of ADOA participants was subtracted from the group averaged ERG of the controls to obtain a difference ERG. The time-to-peak of the greatest discrepancy between the two was identified for the PhNR-ON and PhNR-OFF responses and was used as the fixed time point for all measurements. This method of measuring the PhNR was adapted from a previous study by Viswanathan et al (Viswanathan et al., 2001). The fixed times at which the PhNR amplitudes were measured are shown in Table 5.3. When assessing the other components of the flash and pattern ERGs, the identification of all peaks and troughs was determined objectively using Microsoft Excel i.e. as the minimum/maximum voltage within a fixed time window.

Table 5.3. Fixed time points for measuring the PhNR components

ERG Type	PhNR-ON, msec	PhNR-OFF, msec
Focal long duration		
• Central macula	95	347
• Nasal macula	122	395
• Temporal macula	98	354
Full-field long duration	83	352
Brief flash	72	NA

NA – not applicable

5.3.14 Statistical Analysis

The distribution of the ERG data was checked for normality using the Shapiro-Wilk test. Where data were normally distributed, independent samples t-tests (2-tailed) were used to compare controls and participants with ADOA; the Mann-Whitney U test was used where data were non-normally distributed. In order to minimise Type 1 errors due to the number of comparisons made, observations were reported as significant when $p \leq 0.01$, unless otherwise specified. Where data were normally distributed, comparisons between ERGs recorded from the central, nasal and temporal macula from each participant in either the ADOA or control cohort were conducted using one-way repeated measures analysis of variance (ANOVA) with Bonferonni adjustment for multiple comparisons; otherwise a Friedman test (with post-hoc Wilcoxon Signed Ranked tests for post-hoc pairwise comparisons) was conducted. Receiver Operating Characteristic (ROC) curve analysis was used to calculate the area under the curve (AUC) to assess the discriminatory ability of the various ERG

components. The comparisons between AUCs were made using the method described by Hanley and McNeil (Hanley and McNeil, 1983).

5.4 Results

5.4.1 Demographical Results of Participants

The twelve participants recruited for this study comprised nine females and three males aged 18 to 61 years (mean = 43.75 $\pm$ 14.03 years) from five families (see Table 5.4 for characteristics of all 12 participants). Detailed information about the clinical characteristics of nine of the participants with ADOA (1010 – 1015, 1018 and 1019) have been reported elsewhere (Votruba et al., 1998a). The control group was made up sixteen participants comprising seven females and nine males aged 19 to 61 years (mean = 39.13 $\pm$ 14.06 years). The difference in the mean ages of the groups was not statistically significant ($p = 0.40$). The range of refractive errors for all participants (control and ADOA) included in the study ranged from +4.00 to -7.00 D with cylinders of up to -2.00 D.

5.4.2 Psychophysical Assessment

The BCVA, CS and VFS results were significantly worse in the participants with ADOA compared to controls ($p < 0.05$) (Figure 5.6). The BCVA for participants with ADOA ranged from 0.00 logMAR (normal) to 1.64 logMAR (severe visual impairment) with a median of 0.88 logMAR (Figure 5.6A). Contrast sensitivity was also reduced in participants with ADOA. CS scores ranged from 1.65 (near normal) to 0.00 (severe loss) log units. The median CS score was 1.15 log units. (Figure 5.7B).

All participants with ADOA presented with various visual field defects (Figure 5.7) except one participant (EM-1021) who had normal visual fields (Figure 5.7B). The mean deviation scores of the central 18^o x 18^o field ranged from -1.35 dB (normal) to -15.52 dB (severe visual loss) with a median value of -6.56 dB. Colour vision was abnormal in all participants with ADOA who were tested. The colour vision defects were variable, but participants from the same family had similar defects (Table 5.4).

Table 5.4. Characteristics of Participants with ADOA

Participant ID/Gender	Family	Age	Visual Acuity, logMAR		Contrast Sensitivity, log units		Mean Deviation, dB		Mean Deviation (18º x 18º), dB	Color Vision	*OPA1* Mutation	*ADOA+*
			RE	LE	RE	LE	RE	LE	Test Eye			
1010/F	A	49	1.34	1.32	0.35	0.40	-27.03	-25.15	-15.52	Mixed	c.1202G>A	Atx, Df, Myp
1011/F	B	55	1.64	1.62	0.00	0.00	-17.65	-19.58	-15.51	Mixed	C1508A	Df
1012/F	C	58	0.80	1.00	1.15	1.05	-8.68	-10.39	-5.39	Mixed	IVS8+5G>A	None
1013/F	C	61	1.10	0.64	NA	NA	-12.47	-9.06	-7.05	Mixed	IVS8+5G>A	None
1014/M	D	33	1.40	1.32	0.30	0.45	-13.84	-11.89	-11.40	Protan/Deutan	NA	Nystagmus
1015/F	D	31	1.02	0.98	1.05	1.05	-13.98	-13.20	-13.78	Protan/Deutan	NA	KD
1016/F	E	18	0.80	0.80	1.65	1.35	-7.08	-8.15	-6.45	Tritan	IVS9+3A>T	None
1017/F	E	27	0.82	0.80	1.65	1.65	-5.14	-5.82	-3.70	Tritan	IVS9+3A>T	None
1018/F	E	59	0.86	0.96	0.90	0.75	-9.55	-7.03	-6.21	Tritan	IVS9+3A>T	Df, Myp
1019/F	E	49	0.72	1.20	1.50	1.50	-5.99	-6.79	-6.67	Tritan	IVS9+3A>T	None
1020/M	E	46	0.98	1.20	1.65	1.20	-10.15	-8.21	-5.35	Tritan	IVS9+3A>T	None
1021/M	F	39	0.02	0.00	1.65	1.65	-1.31	-2.25	-1.35	NA	c.357delT	None

NA – not available. Atx – Ataxia (poor gait). Df – Deafness. Myp – Myopathy. KD – Kidney disease.

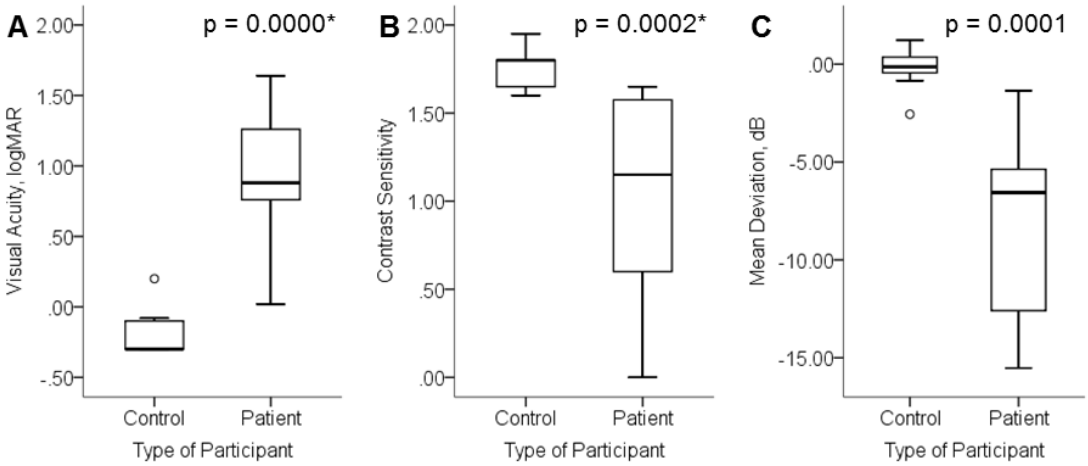

Figure 5.6. Comparison of results for controls and participants with ADOA for (A) BCVA, (B) CS and (C) mean deviation of VFS. The p-values are displayed on top of each plot. * - data were not normally distributed

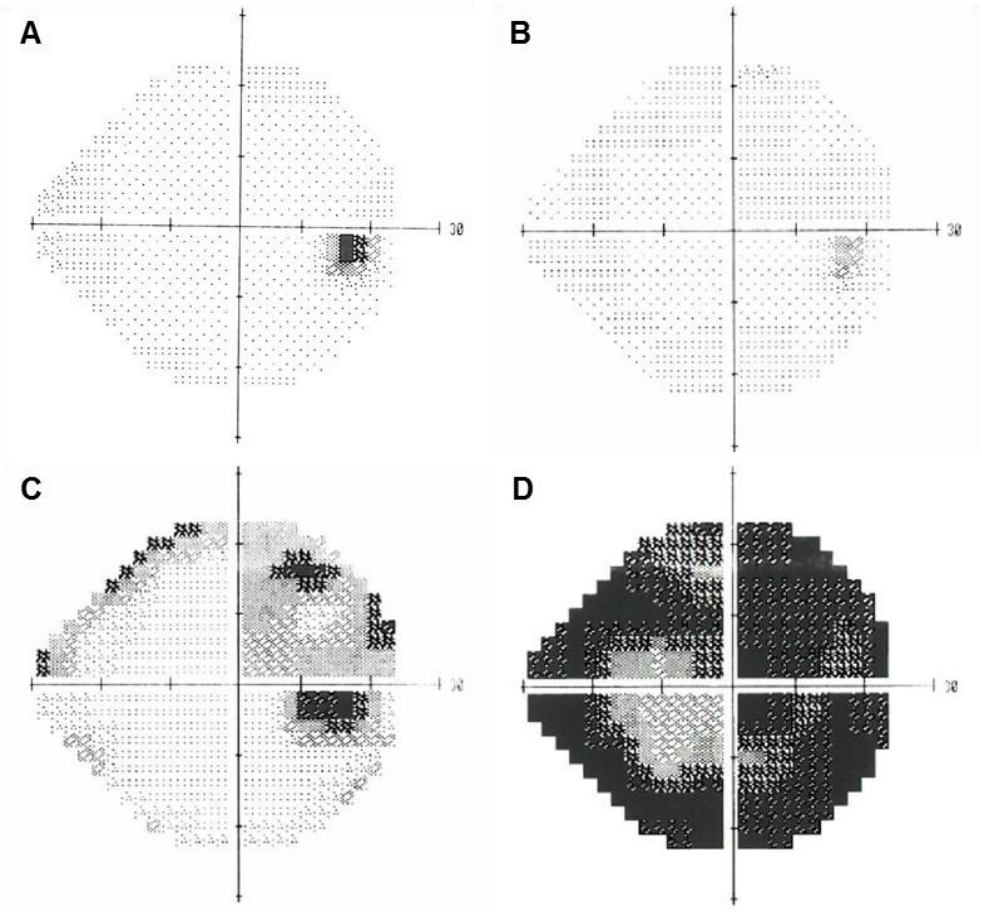

Figure 5.7. Visual field plots from study participants Displayed plots are from one control participant EM-241 (A) and three participants with ADOA (B - D). B = 1021; C = 1012 and D = 1010

5.4.3 Effect of Age on Psychophysical Measures

In participants with ADOA, VA, CS and mean deviation worsened with age, however, this trend was not significant (Figure 5.8, Table 5.5). In controls, VA and CS declined with age (significant for CS) while mean deviation improved significantly with age (Table 5.5).

Table 5.5. Regression analysis for the effect of age on the psychophysical measures

Parameter		Equation	R^2	p-value
Visual Acuity	ADOA	0.0038x + 0.7684	0.0163	0.6928
	Control	-0.0036x – 0.0822	0.2215	0.0658
Contrast Sensitivity	ADOA	-0.0205x + 1.9061	0.2353	0.1305
	Control	**-0.0037x + 1.9169**	**0.2632**	**0.0421**
Mean Deviation	ADOA	-0.0152x – 7.5311	0.0021	0.8881
	Control	**0.0316x – 1.3863**	**0.3885**	**0.0099**

Regressions significant at $p \leq 0.05$ are shown in bold fonts in shaded cells

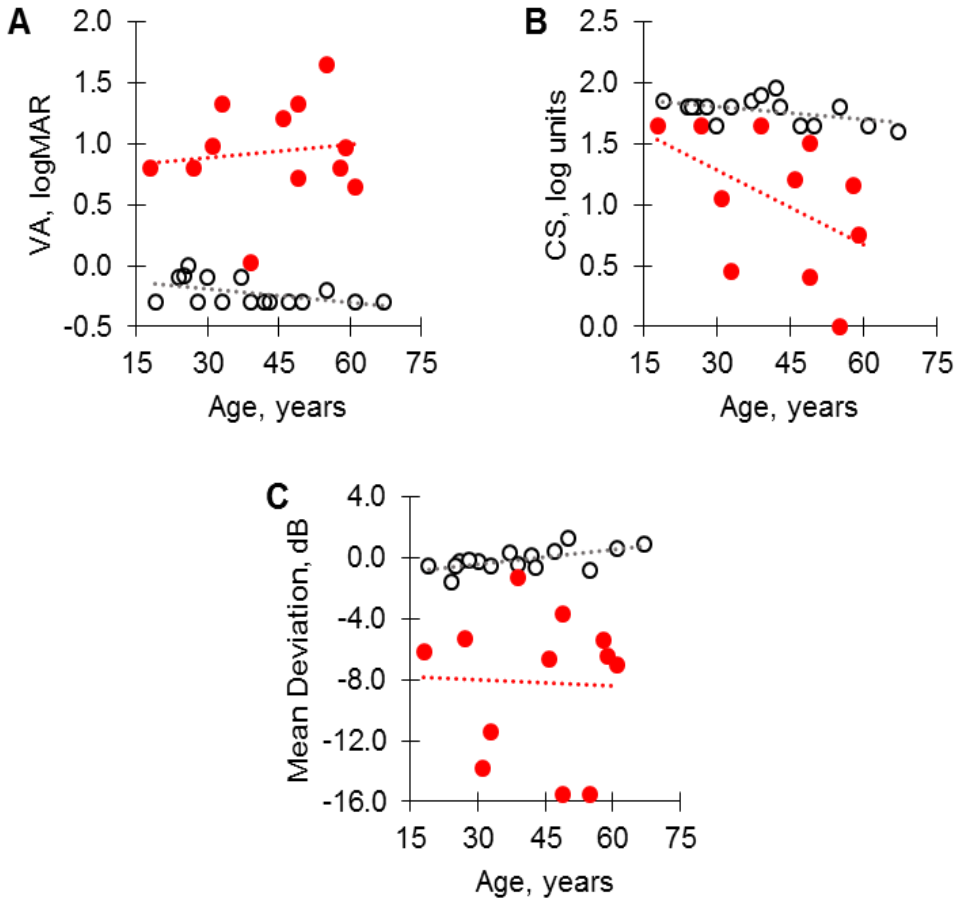

Figure 5.8. Scatter plots showing the relationship between age and (A) BCVA, (B) CS, and (C) mean deviation score. Data for participants with ADOA are shown as red dots and controls as open black circles. The dotted lines represent the lines of regression. The equation of the regression lines are provided in Table 5.5.

5.4.4 Macular Retinal Thickness

Figure 5.9 shows the horizontal OCT scans taken from the six participants with ADOA and one control. The foveal pits are shallower in the participants with ADOA, especially in 1011, 1013 and 1020, compared to the control, which indicates a reduction in the thickness of the inner retinal layers of the OCT scan. The mean thicknesses of each retinal layer in the macula are shown for each patient in Table 5.6. The total retinal thicknesses, i.e. from the RNFL to the RPE, are also shown. There was a significant reduction in the RNFL, GCL and IPL in the ADOA group compared to controls. There was however no significant difference between the two groups for the INL, OPL and photoreceptor layers. The RNFL and IPL in participants with ADOA were reduced to about 60% of the mean thickness in controls while the GCL was reduced to about 35% of the mean thickness in controls, making the GCL the most severely affected layer of the retina in ADOA participants.

5.4.5 Peripapillary RNFL Thickness

The thicknesses of the peripapillary RNFL in each quadrant at the optic nerve head for the participants with ADOA and controls are displayed in Table 5.6. The mean total thickness was 44.03 $\pm$ 13.50 µm in participants with ADOA and 95.86 $\pm$ 12.26 µm in controls (Table 5.6). The comparison of the mean RNFL thicknesses between participants with ADOA and controls are provided in Table 5.7. The RNFL thickness was significantly reduced in all four quadrants in ADOA participants. The average RNFL in ADOA participants was significantly reduced by nearly 50% in comparison with controls. The greatest loss in RNFL thickness in ADOA was recorded in the temporal sector (~70% loss) and the least in the superior quadrant (~30% loss).

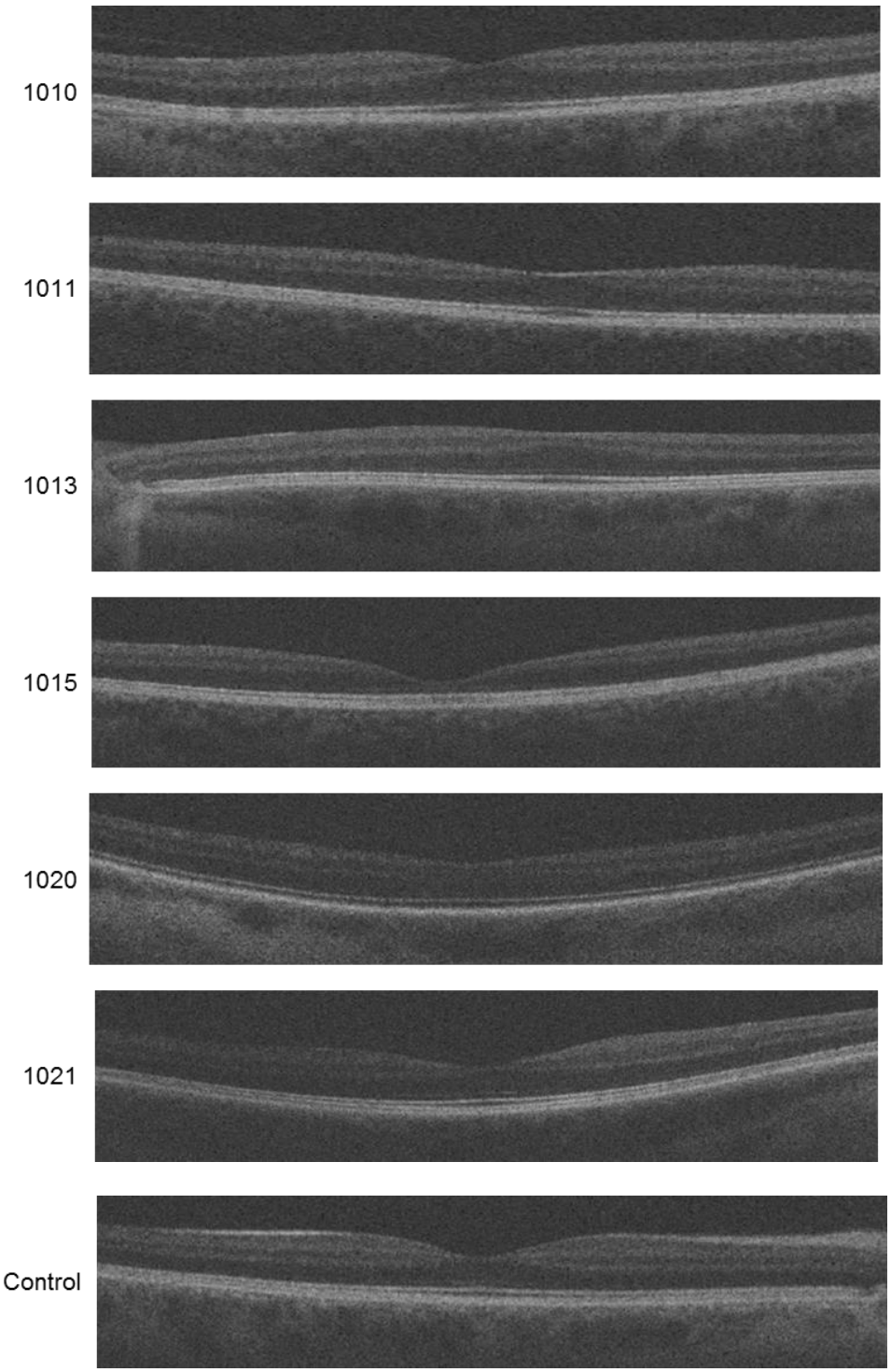

Figure 5.9. OCT images showing horizontal scans of the macula of the six participants with ADOA (numbered) and one control. Each scan was centred at the fovea. The foveal pit is notably shallow for patients 1011, 1013 and 1020.

Table 5.6. Thicknesses of the retinal layers at the macula and the peripapillary RNFL in participants with ADOA

Participant ID/Gender	Age	Macula Thickness								Peripapillary RNFL				
		RNFL	GCL	IPL	INL	OPL	Photo	RPE	Total Mean[a]	Sup	Tem	Inf	Nas	Total Mean
1010/F	49	18.48	14.86	25.39	35.77	30.07	153.49	17.86	295.92	42.41	20.18	60.12	29.34	38.01
1011/F	55	21.42	8.70	21.01	29.63	22.93	146.71	15.38	265.77	44.67	18.13	47.31	48.69	39.70
1013/F	61	21.47	10.98	24.95	34.62	32.93	126.25	17.30	268.50	86.14	24.54	51.09	34.11	48.97
1015/F	31	23.51	10.02	20.92	17.37	23.37	122.65	15.74	233.59	23.10	14.31	35.14	24.50	24.26
1017/F	27	25.55	7.00	18.81	21.69	25.53	115.34	18.92	232.85	87.05	14.99	55.4	37.65	48.77
1021/M	39	21.26	18.35	28.12	28.05	26.21	133.00	18.08	273.07	100.21	28.52	85.21	44.06	64.50

a – Total mean macula thickness includes RPE thickness

Table 5.7. Comparison of mean retinal layer thickness at the macula for ADOA participants and controls

	Macula								Peripapillary RNFL				
	RNFL[a]	GCL[a]	IPL	INL	OPL	Photo	RPE	Total[b]	Sup	Tem	Inf	Nas	Total
ADOA Group Mean ±Standard Deviation	21.95 ±2.38	11.65 ±4.21	23.20 ±3.50	27.86 ±7.20	26.84 ±3.92	132.91 ±14.64	17.22 ±1.39	261.62 ±24.44	63.93 ±31.13	20.11 ±5.55	55.71 ±16.76	36.39 ±9.03	44.04 ±13.50
Control Group Mean ±Standard Deviation	33.95 ±3.46	35.08 ±4.74	37.59 ±2.58	29.16 ±2.46	28.00 ±2.38	129.81 ±7.67	18.67 ±1.52	312.26 ±15.18	116.51 ±14.42	70.16 ±26.19	121.90 ±27.30	74.86 ±19.22	95.86 ±12.96
p-value	0.0000*	0.0000*	0.0000*	0.6805	0.4025	0.6393	0.1048	0.0000*	0.0006*	0.0005*	0.0006*	0.0011*	0.0005*

a - RNFL and GCL thicknesses exclude central zone. b - Total mean macula thickness includes RPE thickness. * - significant difference at $p < 0.05$

5.4.6 Effect of Age on OCT measures

To assess the effect of age on the retinal structure, regression analysis were conducted for age and peripariliary RNFL (Figure 5.10A) and age and total macula thickness (Figure 5.10B). The layers of the macula were further grouped into the RNFL – IPL layer and the INL – RPE layer and their respective relationship with age determined (Figure 5.10C-D). This grouping of the retina was employed to separate the ganglion cell rich layers from the rest of the retina. There were no significant relationships between age and any of these parameters in either the ADOA or control group. However, in the ADOA group the R^2 values for age and total macula thickness was 0.47 while that for age and outer macula thickness was 0.55. All other R^2 values were below 0.1.

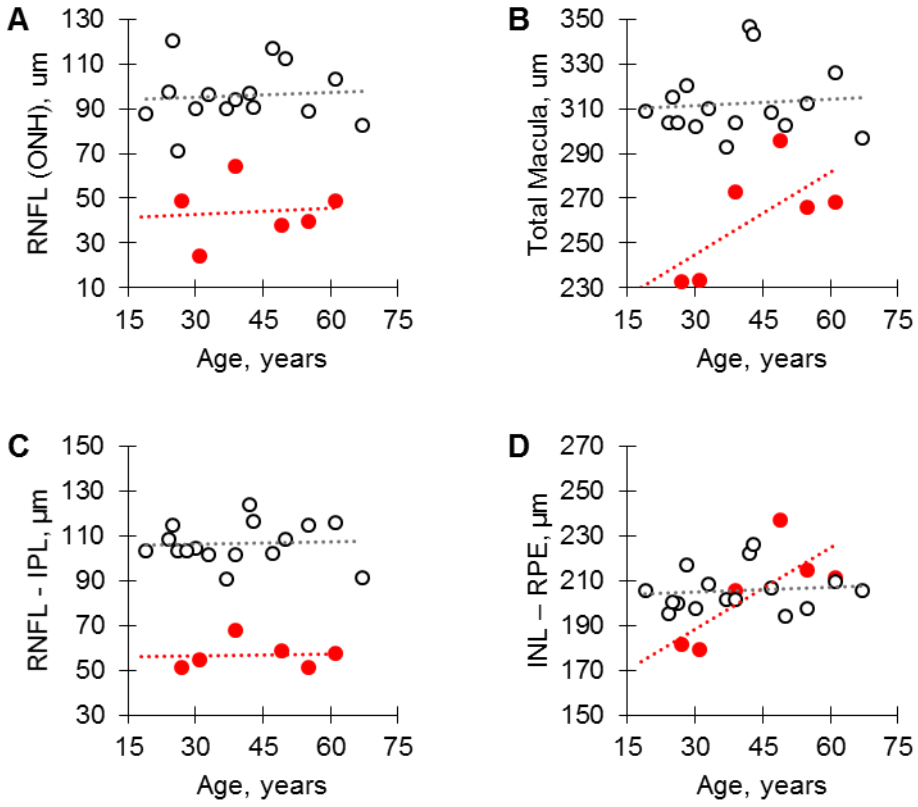

Figure 5.10. Scatter plots showing the relationship between age and OCT measures. (A) peripapillary RNFL, (B) total macula thickness, (C) RNFL – IPL layers and (D) INL – RPE layers.

Table 5.8. Regression analysis for the effect of age on OCT measures

Parameter		Equation	R^2	p-value
RNFL (ONH)	ADOA	0.0876x + 40.2107	0.0077	0.8686
	Control	0.0652x + 93.2596	0.0051	0.7999
Total Macula Thickness	ADOA	1.2326x + 207.7898	0.4667	0.1347
	Control	0.0973x + 308.4475	0.0081	0.7400
Macula RNFL – IPL Thickness	ADOA	0.0282x + 55.5690	0.0038	0.9074
	Control	0.0291x + 105.4675	0.0021	0.8678
Macula INL – RPE Thickness	ADOA	1.2044x + 152.2208	0.5571	0.0883
	Control	0.0683x + 202.9771	0.0104	0.7071

5.5 Discussion

5.5.1 Psychophysical Tests

The results of the psychophysical tests showed that visual function in participants with ADOA was significantly poorer than in controls. However, there was a wide variation in the results of in the ADOA cohort. For example, visual acuity results ranged from normal to severe visual impairment (Table 5.4; Figure 5.6 and 5.7). The wide range of visual acuities seen in this study follows similar previous reports in which visual acuities ranged from -0.1 logMAR to hand-motion (Holder et al., 1998; Votruba et al., 1998a; Cohn et al., 2007; Yu-Wai-Man et al., 2010a; Yu-Wai-Man et al., 2010b). The median BCVA in participants with ADOA of 0.88 logMAR (~6/48 on the Snellen chart) in this study is similar to results obtained in other studies (Eliott et al., 1993; Votruba et al., 1998a; Yu-Wai-Man et al., 2010a; Yu-Wai-Man et al., 2010b). These wide variations were also reflected in the results for CS, VFS and colour vision tests and are consistent with results from other studies which reported variable degrees of visual field loss in ADOA (Berninger et al., 1991; Votruba et al., 1998a).

Although genotype-phenotype correlations are difficult to establish, disease severity appears linked to the type and site of the mutation on the *OPA1* gene (Thiselton et al., 2002; Barboni et al., 2010; Yu-Wai-Man et al., 2010b). For example, missense mutations are often associated with worse visual dysfunction and carry greater odd ratios for developing ADOA+ phenotypes (Table 5.9) (Yu-Wai-Man et al., 2010b; Barboni et al., 2014). The type and location of mutations in the ADOA cohort in this study is provided in Table 5.10. Due to the inadequate number of members in each family, a reliable association

between the mutation and severity of visual impairment could not be computed. However, an observation of Table 5.4 shows that as may be predicted by Yu-Wai Man et al (2010b), Patient 1021 with a deletion occurring in the basic domain had only mild visual impairment (VA = 0.02 logMAR, VFS = -1.35), while Patient 1011, who carried a missense mutation occurring in the GTPase domain, had severe visual impairment (VA = 1.64 logMAR, VFS = -15.51). This patient also self-reported a 30% loss in hearing.

Nonetheless, other studies have shown that wide phenotype variations exist in homogenous ADOA populations, which, are not correlated with age (Almind et al., 2012; Ronnback et al., 2013). For example, Ronnback et al. (2013) reported a two-fold variation in GCL-IPL thickness as well as variations in visual acuity from 20/20 – 20/700 in a homogeneous ADOA population (n = 49) carrying the 2826delT *OPA1* mutation. The phenotype variations were not correlated with age, thus suggesting that other environmental or genetic factors other than the patient's specific mutation may impact largely on the phenotype (Ronnback et al., 2013; Bonifert et al., 2014).

Table 5.9. Odd ratios for developing ADOA+ phenotype based on *OPA1* mutation type and domain. (Yu-Wai-Man et al., 2010b)

***OPA1* mutations**		**Odd ratio**	**95% CI**	**p-value**
Type	Missense	3.06	1.44 – 6.49	0.0027*
	Nonsense	0.31	0.07 – 1.34	0.0975
	Substitution	0.81	0.35 – 1.92	0.6378
	Deletion	0.50	0.18 – 1.38	0.1745
Domain	GTPase	2.29	1.08 – 4.82	0.0271*
	Dynamin	0.28	0.10 – 0.84	0.0159*
	Others	1.02	0.46 – 2.27	0.9628

CI = confidence interval; * significant p value at 0.05

Table 5.10. Type and location of *OPA1* mutations in the cohort of participants with ADOA

Family (no. of members)	***OPA1* mutation**	**Type**	**Location (Domain)**
A (n = 1)	c.1202G>A	Substitution	Exon 12, GTPase
B (n = 1)	C1508A	Missense	Exon 15, GTPase
C (n = 2)	IVS8+5G>A	Substitution	Intron 8; GTPase
E (n = 5)	IVS9+3A>T	Substitution	Intron 9, GTPase
F (n = 1)	c.357delT	Deletion	Exon 3; Basic

There were variable colour vision defects in participants with ADOA, however members of the same family had similar colour vision defects (Table 5.4).

Tritanopic defects were the commonest finding in the ADOA cohort, similar to some previous studies (Kjer, 1959; Holder et al., 1998; Almind et al., 2012). It has been suggested that the preponderance of tritanopic defects is related to the fewer cells of the short-wavelength (S)-cone pathway compared to the long (L-) and medium (M-) cone pathways in the retina (Jaeger, 1988; Johnston et al., 1997). In this hypothesis, the different pathways are equally vulnerable, but the loss of RGCs in the S-cone pathway has a greater effect due to their scarcity. Tritanopic defects are therefore seen early in the course of the disease, but progress to protanopic and/or mixed defects at later stages.

Although the percentage of tritanopic defects in the ADOA cohort was the highest and may appear to support this notion, all these participants belonged to one family and were therefore associated with one *OPA1* mutation. Therefore, while the S-cone pathway scarcity theory remained probable, the findings of this study raised the possibility that the colour vision defects may be mutation specific. Earlier studies have however reported variable colour vision defects between and within families with the same mutations (Holder et al., 1998; Simunovic et al., 1998; Votruba et al., 1998a; Johnston et al., 1999), thus implying that the heterogeneity in colour vision is not fully explained by genetic heterogeneity (Simunovic et al., 1998).

5.5.2 Retinal Thickness Measures

At the outset, it was hypothesised that the peripapillary RNFL thickness and retinal thickness would be significantly reduced in participants with ADOA compared to controls. The results of this study confirm this hypothesis. The peripapillary RNFL thickness was significantly reduced in all quadrants with the temporal quadrant being the most affected. This is consistent with previous studies showing that the papillomacular bundle subserving central vision is the most affected part of the retina in ADOA (Johnston et al., 1979; Kjer et al., 1983; Milea et al., 2010; Barboni et al., 2011; Carbonelli et al., 2015). Total macular thickness was significantly reduced in participants with ADOA compared to controls. This was caused by a selective reduction in the RNFL - IPL layer with a relative sparing of the INL - RPE layer. This agrees with other studies which show that ADOA is essentially a disease that targets RGC and their axons (Ito et al., 2007; Milea et al., 2010; Ronnback et al., 2013).

It is not clear why RGCs are the primary target of ADOA since *OPA1* is present in all body tissues (Aijaz et al., 2004; Davies and Votruba, 2006; Sarzi et al., 2012). Several hypotheses have been advanced for this super-selectivity of the RGCs and the major views are summarised in Section 1.2.5 (See also Carelli et al. 2009 and Yu Wai Man et al. 2011). The most supported explanation, however, relates to the peculiar distribution of mitochondria in RGCs (Yu Wai Man et al., 2005; Carelli et al., 2009; Yu-Wai-Man et al., 2009; Yu-Wai-Man et al., 2011b). They are accumulated in the cell bodies and in the intra retinal unmyelinated axons to support the higher energy demands of unmyelinated nerve conduction, but scarce in the myelinated part of axons after the lamina cribosa. It is therefore likely that a delicate cytoskeletal architecture is needed to maintain this sharp mitochondrial gradient (Bristow et al., 2002; Barron et al., 2004). Since the majority of the macula RGCs have small, unmyelinated fibres and with high firing rates, pathological mechanisms which disrupt this unique structural feature would lead to impaired axonal transport and set up a vicious cycle with fragmentation of the mitochondrial network at the lamina cribrosa exacerbating even subtle mitochondrial energy deficits and eventually precipitating apoptotic cell death of RGCs (Yu-Wai-Man et al., 2009).

The changes in the RNFL corresponds to those in the inner macula. Although macula thickness is significantly reduced in ADOA participants, there was a tendency towards increasing thickness.

5.5.3 Effect of Age on Psychophysical and Structural Measures

In this study, there were no significant relationships between age and any of the psychophysical tests in the ADOA cohort. This agrees with previous studies which did not find a significant effect of age on disease severity or progression (Votruba et al. 1998a; Cohn et al. 2008; Almind et al. 2012; Ronnback et al. 2013) and may suggest that disease severity is determined by a combination of factors such as the type of *OPA1* mutation (Yu-Wai-Man et al., 2010b; Barboni et al., 2014), environmental and genetic factors (Almind et al., 2012; Ronnback et al., 2013; Bonifert et al., 2014). In comparison, there was a significant effect of age on contrast sensitivity and mean deviation in the control group. While contrast sensitivity in the control group decreased with age as expected

(Owsley, 2011), mean deviation improved with age contrary to previous reports (Johnson et al., 1989). Since the majority of participants in the control group were staff and students of the School of Optometry, it is possible that the older participants having more experience with the test performed better than the younger participants.

The results from the six participants with ADOA in this study showed that there was no significant correlation between age and periparpillary RNFL or macula thickness. This was also the case in the control cohort. It was observed that while the variances were similar in the ADOA and control groups for the peripapillary RNFL (<1%), the variances of the total macular thickness in the ADOA and control group differed substantially, i.e. 47% in ADOA compared to <1% in controls. When the macula was segregated into the RNFL – IPL and INL – RPE layers, it was noted that the INL – RPE layer was the major contributor for this variance (Figure 5.10D, Table 5.8). An increase in the INL was recently reported in a group of ADOA participants (Carbonelli et al., 2015) They proposed that the firm vitreo-retinal adhesions holding the retina in place most likely caused the retina to expand or split to form empty cystic spaces as the RNFL and GCL become thinner in ADOA. Furthermore, rod inner segments are known to increase with age (Gao and Hollyfield, 1992; Curcio et al., 1993) while the INL is relatively preserved in ageing (Lei et al., 2011). These factors may contribute to the observation of thickening of the INL – RPE layer with age in this study.

5.6 Conclusion

The results of the baseline tests showed that the participants with ADOA recruited in this study exhibited features which were consistent with those reported in previous studies. The participants with ADOA typically presented with reduced visual acuity and contrast sensitivity as well as visual field scotomas and colour vision defects. Participants with ADOA also showed significant reduction in the peripapillary RNFL thickness as well as a selective reduction in the thickness of the RNFL – IPL layer, pointing to the RGCs and their axons as the primary site of assault in ADOA.

6 CHAPTER SIX – ELECTROPHYSIOLOGICAL ASSESSMENT OF RETINAL FUNCTION IN AUTOSOMAL DOMINANT OPTIC ATROPHY - II: RESULTS OF ELECTROPHYSIOLOGICAL TESTS

6.1 Preamble

This chapter is a continuation of the previous chapter. The methods, participant characteristics and baseline results were presented in the previous chapter. Here the results of the electrophysiological assessment of participants with ADOA are presented and discussed.

6.2 Electrophysiological Results

6.2.1 Pattern ERGs

PERGs were successfully recorded from the central, nasal and temporal macula of participants with ADOA and controls. The individual PERG responses for the nine participants with ADOA are displayed in Figure 6.1. The PERGs for three participants (1016, 107 and 1019) which were recorded at the City site were not included as they were contaminated by extraneous noise arising from construction works outside the recording room. In participants with ADOA, the P50 component was typically more discernible than the N95 component in all three retinal locations. However, in two participants (1014 and 1015), the PERG responses were nearly flat.

The PERG responses from the nasal macula of participants with ADOA and controls (middle columns of Figures 6.1 and 6.2) were different in waveform compared to those from the central and temporal macula. In participants with ADOA, the N95 component could not be determined for nearly half the participants, and even where it was present, the N95 had a shallow trough. In controls, the N95 had a wide and shallow trough.

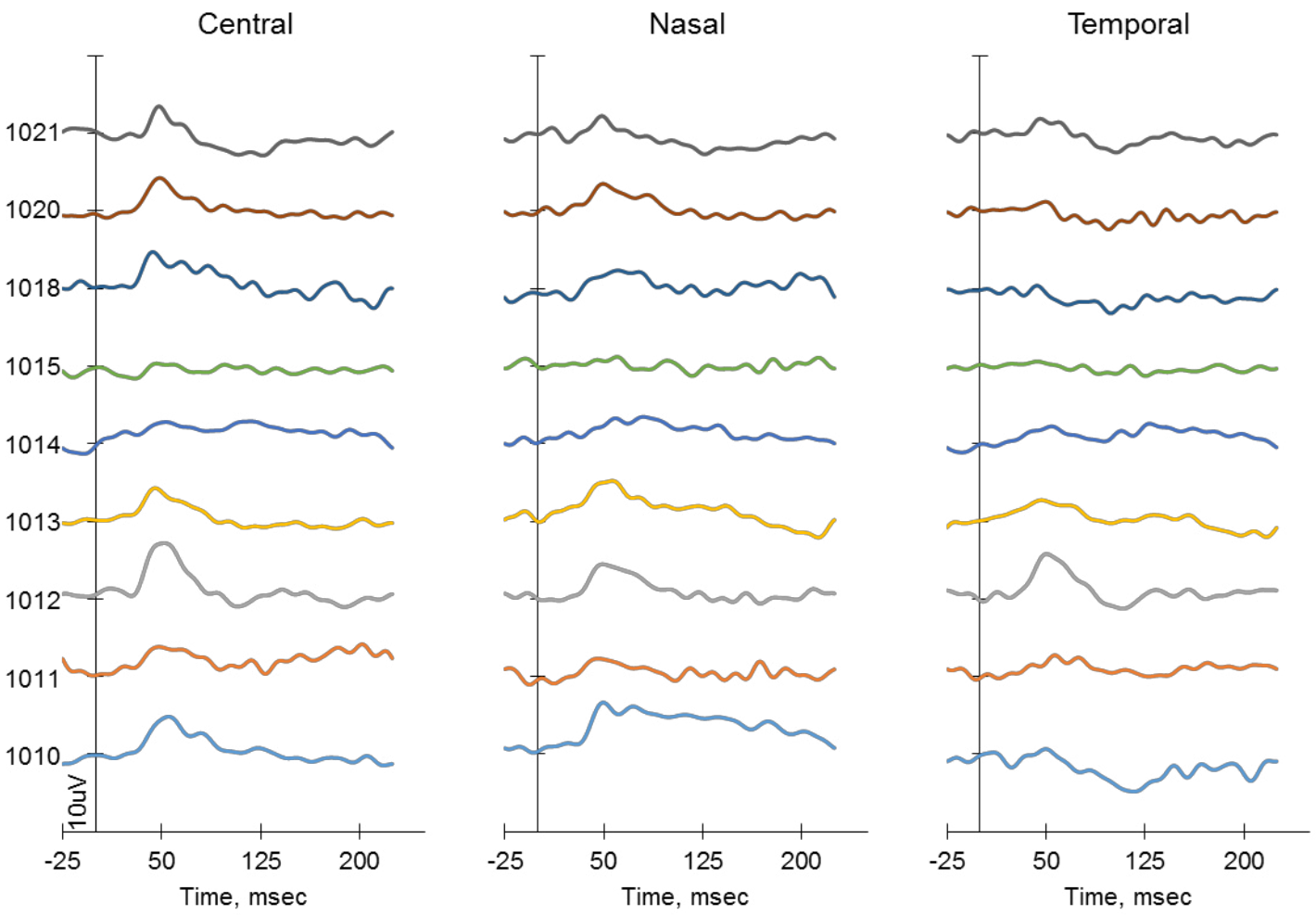

Figure 6.1. Individual PERGs recorded from participants with ADOA from the central, nasal and temporal macula.

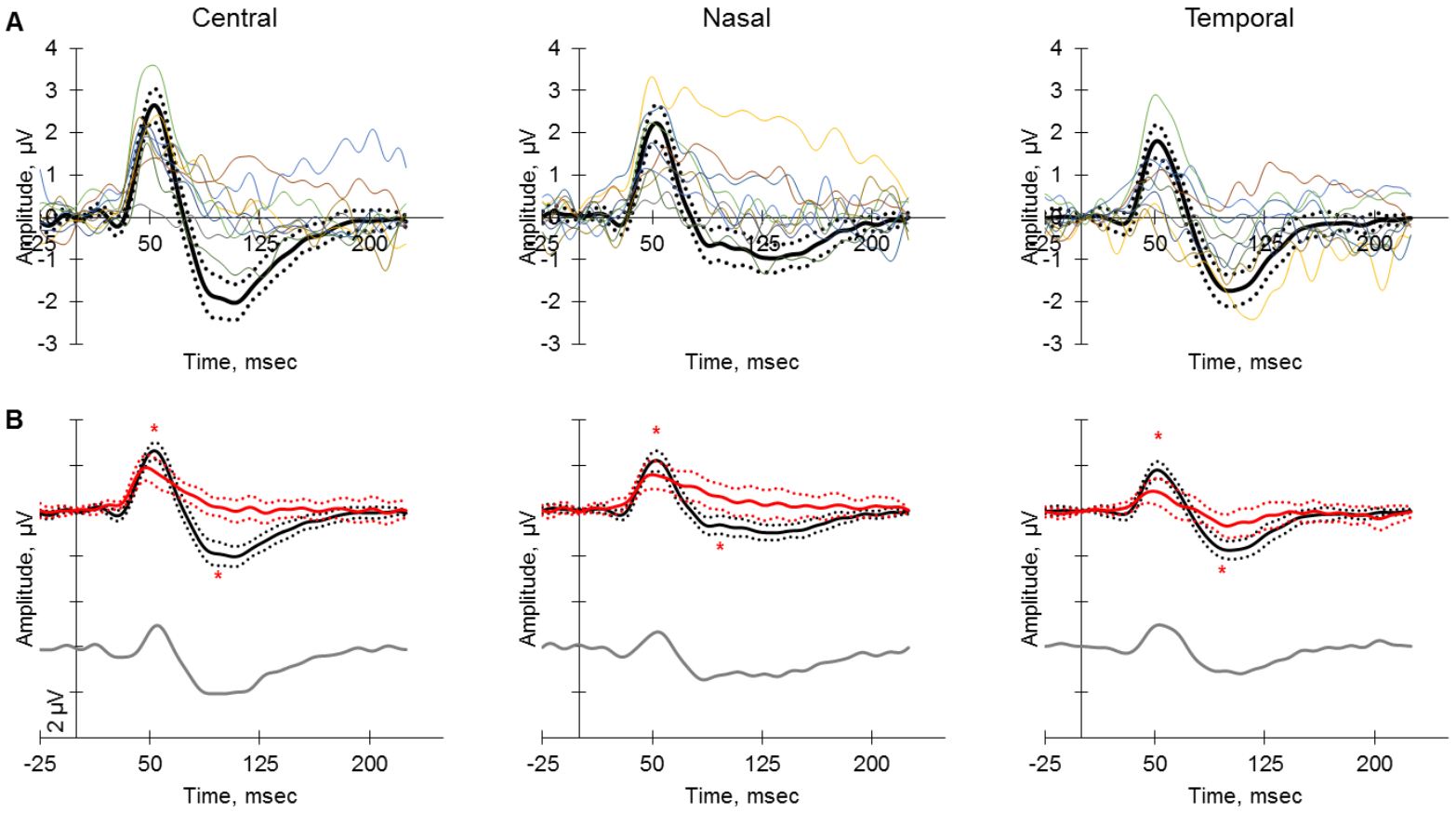

Figure 6.2. (A) Individual PERG responses (thin coloured lines) recorded from the central, nasal and temporal macula of participants with ADOA and superimposed on group-averaged PERG traces of controls. (B) Comparison between group-averaged PERGs of participants with ADOA (thick red line) and controls (thick black lines) recorded from the central, nasal and temporal retina. Dotted lines represent 95% confidence intervals. Grey line represents the difference ERG for each paired comparison. * - Significant difference, p < 0.01.

In Figure 6.2A, the individual PERG responses from the ADOA cohort are superimposed on the corresponding group-averaged PERG response for controls for each location. Notably, the P50 and N95 components in the central (left column) and temporal (right column) macula were reduced in amplitude for nearly all participants with ADOA beyond the 95% confidence intervals for the control data.

There was evidence of a significant P50 and N95 loss in people with ADOA compared to controls in all locations (Figure 6.2B, Table 6.1). However, the difference plot of the central retina (grey line in Figure 6.2B, left column) was dominated by a negative going signal corresponding to the loss of the N95 component. The difference between the groups was greatest in the central macula (2.97 µV) and approximately equal in the nasal (1.75µV) and temporal macula (1.91 µV).

Table 6.1. Mean values of amplitudes and times-to-peak of PERG components in participants with ADOA and in controls.

Location	Component		ADOA	Control	P-value
Central	P50	A, µV	1.90 ± 0.79	3.11 ± 0.88	0.0020*
		T, msec	48.83 ± 3.95	53.41 + 3.16	0.0042*
	N95	A, µV	2.13 ± 1.13	5.10 ± 0.96	0.0000*
		T, msec	102.00 ± 11.53	101.95 ± 7.44	0.4788†
	N95:P50 Ratio		1.07 ± 0.32	1.73 ± 0.47	0.0008*†
Nasal PERG	P50	A, µV	1.60 ± 0.52	2.62 ± 0.63	0.0010*
		T, msec	53.11 ± 5.82	53.23 ± 4.06	0.9574
	N95	A, µV	1.55 ± 0.52	3.30 ± 1.04	0.0001*
		T, msec	108.89 ± 6.56	97.05 ± 9.62	0.0041*
	N95:P50 Ratio		1.12 ± 0.57	1.27 ± 0.28	0.4034
Temporal	P50	A, µV	1.02 ± 0.73	2.08 ± 0.53	0.0016*†
		T, msec	48.89 ± 4.62	52.21 ± 3.17	0.0528
	N95	A, µV	1.83 ± 0.87	3.74 ± 0.94	0.0001*
		T, msec	103.08 ± 10.06	102.11 ± 7.32	0.7899
	N95:P50 Ratio		2.28 ± 1.14	1.84 ± 0.40	0.3049

Data are expressed as mean ± standard deviation. A – Amplitude; T – Time-to-peak from stimulus onset. * – Value is significant at $p \leq 0.01$ level; † – data was non-uniformly distributed and Mann-Whitney U test was used for statistical comparison.

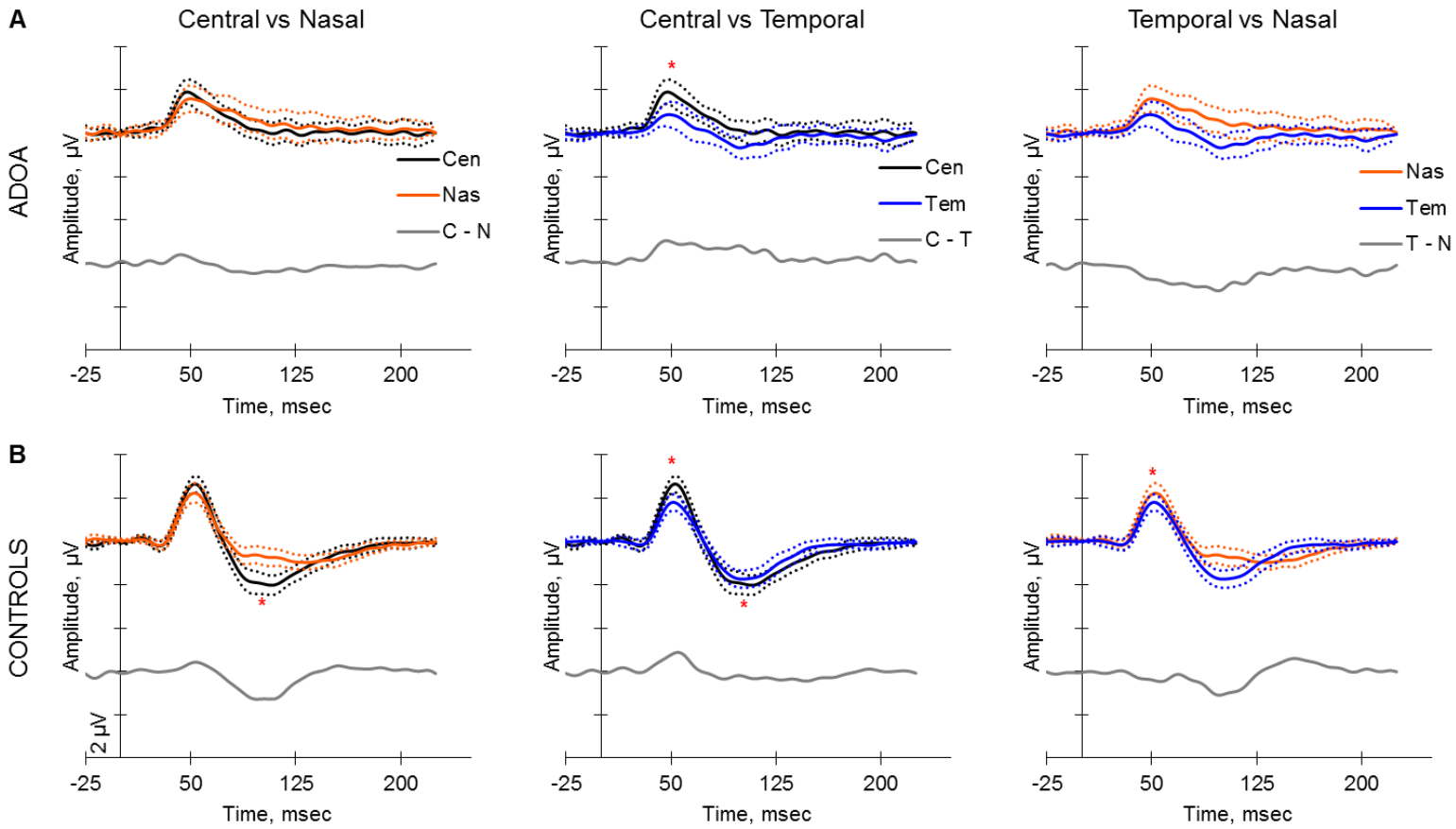

Figure 6.3. A pair-wise comparison of group-averaged PERGs recorded from the central, nasal and temporal retina for participants with (A) ADOA and (B) controls. The legend in A applies to B. Dotted lines represent 95% confidence intervals. Grey line represents the difference ERG for each paired comparison. Cen/C – Central retina; Nas/N – Nasal retina; Tem/T – Temporal. * - Significant difference, $p < 0.01$.

The PERGs recorded from the different locations were also compared within individuals in each cohort to determine regional variations in the PERG (Figure 6.3; Table 6.2). In both the ADOA and control groups, there was a significant effect of location on the P50 amplitudes. The mean P50 amplitude was greatest in the central retina, followed by the nasal and temporal macula in decreasing order. However this difference was significant ($p < 0.01$) for comparisons between the central and temporal macula (ADOA and control group) and between the nasal and temporal macula (control group only).

The mean N95 amplitudes in both groups were greatest in the central macula, followed by the temporal and nasal macula. However, the difference was only significant between the central and nasal macula and between the temporal and nasal macula (Figure 6.2). There was no significant difference in mean time-to-peak of either the P50 or N95 component across the three locations.

Table 6.2. Summary of results for intra-individual comparisons (repeated measures)

Component		ADOA	Controls
P50	Amp	Significant† ($p = 0.0124$) Pairwise: Cen > Tem ($p = 0.0065$)	Significant ($p = 0.0002$; $P.Eta^2 = 0.76$) Pairwise: Cen > Tem ($p=0.0003$); Nas > Tem ($p = 0.0013$)
	Time	Not significant ($p = 0.3950$; $P.Eta^2 = 0.23$)	Not significant ($p = 0.2446$; $P.Eta^2 = 0.21$)
N95	Amp	Not significant ($p = 0.1650$; $P.Eta^2 = 0.40$)	Significant ($p = 0.0000$; $P.Eta^2 = 0.83$) Pairwise: Cen > Nas ($p = 0.0010$); Cen > Tem ($p = 0.0000$)
	Time	Not significant† ($p = 0.4594$)	Not significant ($p = 0.3783$; $P.Eta^2 = 0.15$)
N95:P50		Significant† ($p = 0.0131$) Pairwise: Cen > Tem ($p = 0.0109$)	Significant† ($p = 0.0025$) Pairwise: Cen > Nas ($p = 0.0028$) Nas < Tem ($p = 0.0015$)

† – data were non-normally distributed and Friedman test was used. $P.Eta^2$ = partial Eta^2 are given for parametric tests. Pairwise comparisons are given only for significant comparisons. The significant value of $p < 0.05$ is Bonferroni adjusted

6.2.2 Focal Long Duration Cone ERGs

Focal long duration cone ERGs were successfully recorded from the central, nasal and temporal retina of 12 participants with ADOA and are displayed for each participant in Figure 6.4. The typical ERG responses were characterised by the a-wave, b-wave, PhNR-ON, d-wave and PhNR-OFF. In Figure 6.5A, the

individual traces of ADOA participants are superimposed on the group-averaged traces of controls for each location. These showed that in the central and temporal macula, the PhNR-ON and PhNR-OFF amplitudes were significantly reduced in amplitude below the 95% confidence limit of control data in most ADOA participants. This was reflected in the difference plots in Figure 6.5B (left and right columns) which were dominated by two negative going waves representing the PhNR-ON and PhNR-OFF components affected by ADOA. There was however no significant difference between ADOA and control participants in the PhNR-ON or PhNR-OFF amplitudes recorded from the nasal macula (Figure 6.5, middle column; Table 6.3).

Notably, the waveform after stimulus offset varied considerably between ADOA participants for the central and temporal macula (Figure 6.5B). For instance, in participants with ADOA, the most prominent positive peak after stimulus offset, assumed to be the d-wave, was delayed and had a broad peak whose maximum amplitude occurred at highly variable times (Figure 6.5B, left and right column). In comparison, this prominent peak was highly consistent among control participants with respect to time-to-peak and was reflected in the much smaller SD of the d-wave time-to-peak in contrast to data from participants with ADOA (Table 6.3). In addition, the PhNR-OFF components of the central and temporal group-averaged traces of the ADOA group were practically eliminated and the d-wave peak extended over the place where the PhNR-OFF trough was expected to be when compared to the control traces.

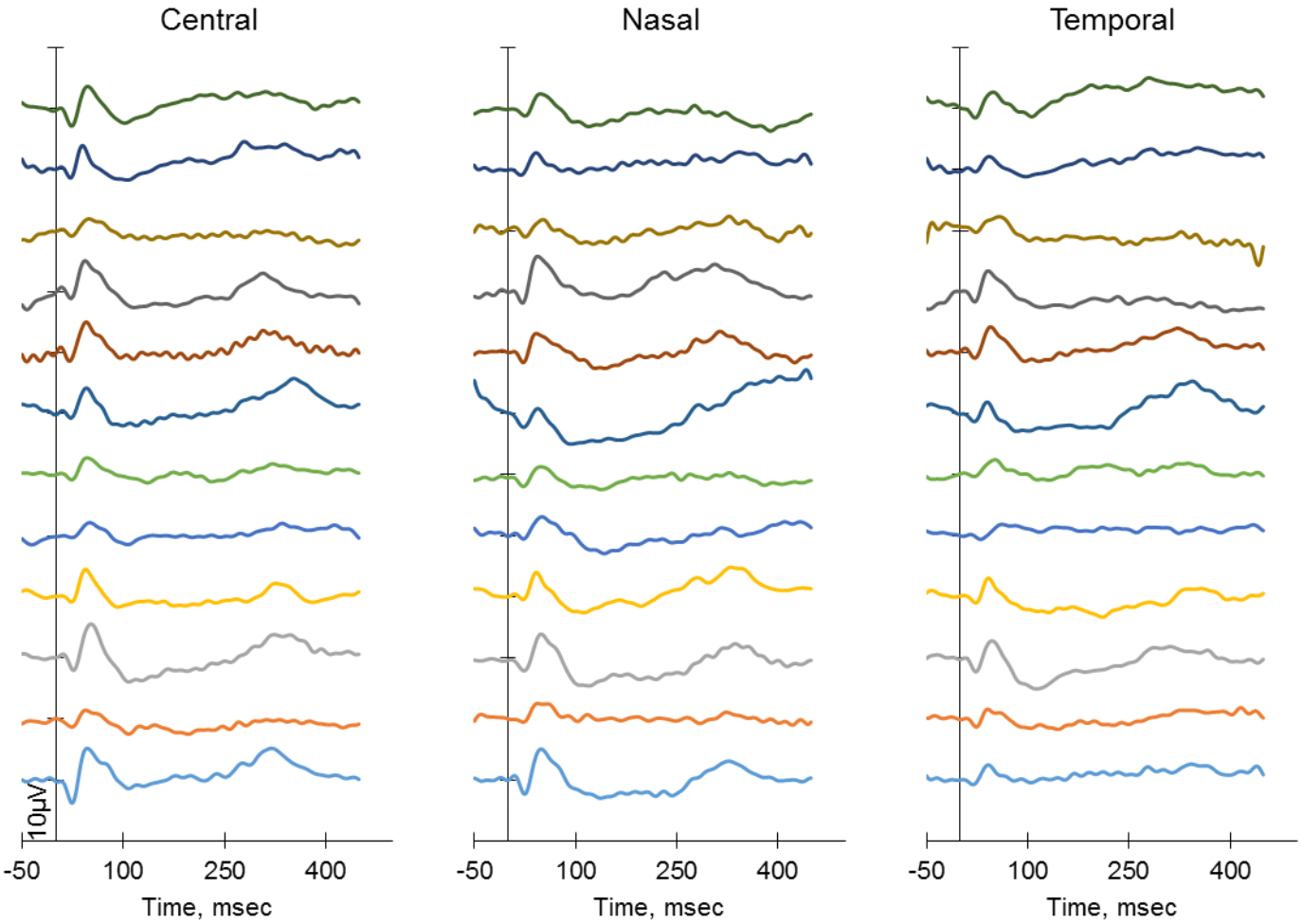

Figure 6.4. Focal long-duration ERGs recorded from (left to right) the central, nasal and temporal macula in participants with ADOA. Traces in the same row were recorded from the same participant

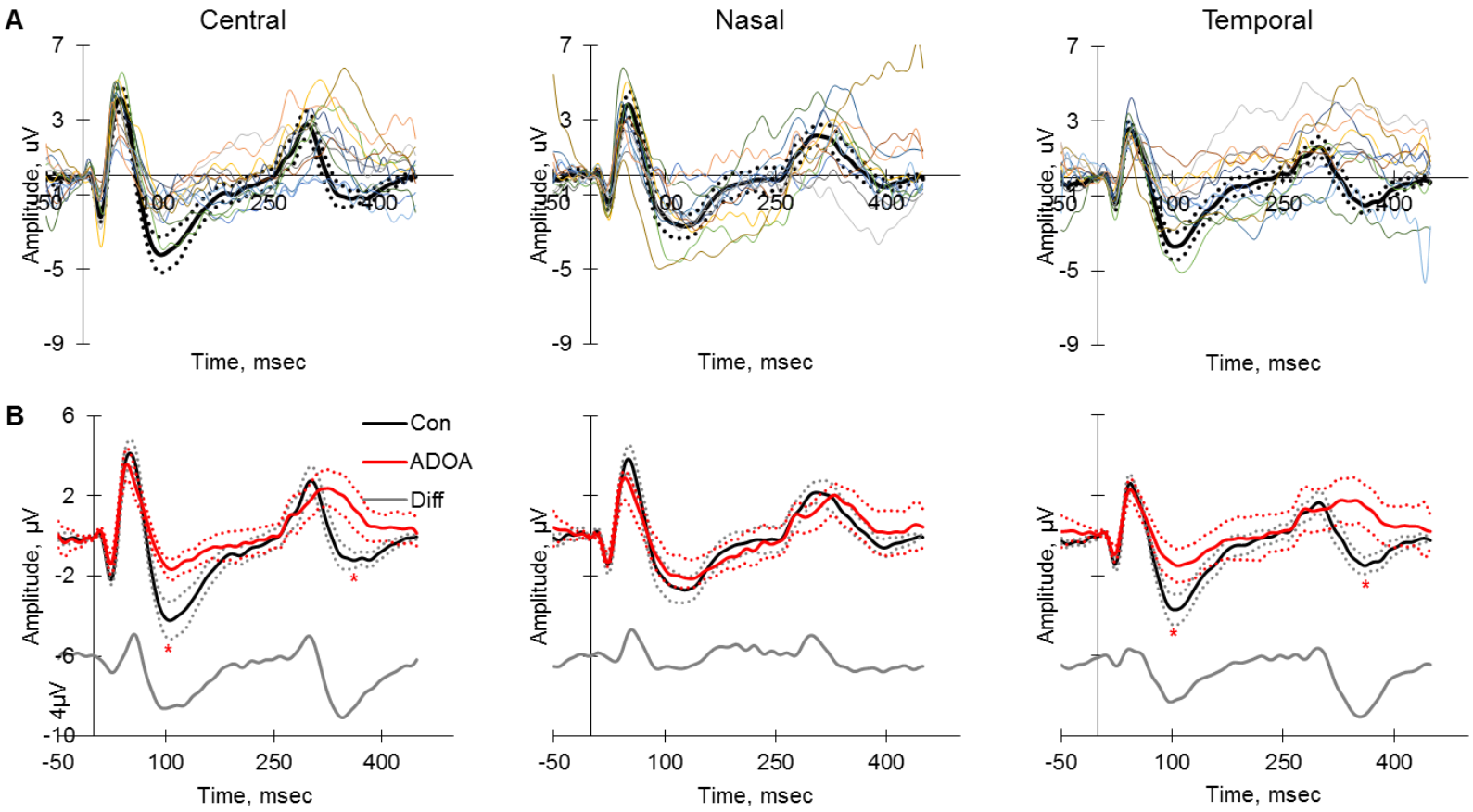

Figure 6.5. (A) Individual focal long duration ERGs responses (thin coloured lines) recorded from the central, nasal and temporal macula of participants with ADOA and superimposed on group-averaged traces of controls (thick lines). (B) Comparison between group-averaged focal ERGs of participants with ADOA (thick red lines) and controls (thick black lines) recorded from the three retinal locations. Dotted lines represent 95% confidence intervals. Grey lines represent the difference ERG for each paired comparison.

Table 6.3. Mean values of amplitude and time-to-peak of long duration focal ERGs recorded from central, nasal and temporal macula in ADOA and control participants.

Location	Component		ADOA	Control	p-value
Central Focal ERG	a-wave	A, µV	1.76 ± 0.94	2.22 ± 0.61	0.0069*
		T, msec	23.00 ± 1.72	23.75 + 1.74	0.2454
	b-wave	A, µV	5.29 ± 2.08	6.76 ± 1.74	0.0529
		T, msec	46.25 + 3.14	49.81 + 4.88	0.0349
	PhNR-ON	A, µV	1.02 ± 0.97	3.81 ± 1.74	0.0000*
		T, msec	109.25 ± 7.16	104.50 ± 8.49	0.0554
	d-wave	A, µV	2.81 ± 1.52	3.12 ± 1.04	0.2045
		T, msec	321.92 ± 13.80	302.41 ± 5.92	0.0000*
	PhNR-OFF	A, µV	-1.97 ± 1.52	0.93 ± 1.23	0.0000*
		T, msec	422.08 ± 26.51	369.00 ± 21.29	0.0000*
Nasal Focal ERG	a-wave	A, µV	1.31 + 0.97	1.40 + 0.76	0.7715
		T, msec	23.08 + 1.88	23.33 + 1.67	0.7339
	b-wave	A, µV	4.44 + 1.69	5.55 + 1.16	0.1488†
		T, msec	46.25 + 3.60	50.00 + 4.16	0.0273
	PhNR-ON	A, µV	2.03 + 1.55	2.21 + 1.31	0.4529†
		T, msec	112.67 + 8.82	111.83 + 9.80	0.9763†
	d-wave	A, µV	2.23 + 1.70	2.44 + 0.69	0.8847
		T, msec	317.67 + 8.81	306.42 + 10.27	0.0087*
	PhNR-OFF	A, µV	-0.55 + 2.75	-1.07 + 1.29	0.3026
		T, msec	396.08 + 39.73	403.50 + 19.75	0.7948†
Temporal Focal ERG	a-wave	A, µV	1.05 + 0.57	1.44 + 0.64	0.1460
		T, msec	22.50 + 2.71	22.83 + 1.64	0.3592†
	b-wave	A, µV	3.59 + 1.06	4.23 + 0.82	0.1060†
		T, msec	43. 75 + 8.73	43.75 + 4.05	0.9073†
	PhNR-ON	A, µV	1.18 + 1.09	3.57 + 1.33	0.0001*
		T, msec	101.17 + 26.73	103.17 + 5.80	0.1741†
	d-wave	A, µV	1.74 + 1.03	1.59 + 0.84	0.5371
		T, msec	288.92 + 84.78	298.58 + 5.40	0.0426†
	PhNR-OFF	A, µV	-1.48 + 1.14	1.58 + 0.93	0.0000*
		T, msec	410.67 ± 50.62	361.92 + 11.66	0.0372†

Data are expressed as mean ± standard deviation. A – Amplitude; T – Time-to-peak from stimulus onset. * – Value is significant at $p \leq 0.01$ level; † – data were non-normally distributed.

The focal ERGs recorded from the different locations were again compared within individuals in each cohort (Figure 6.6). In participants with ADOA, there was no observable difference when the group-averaged ERGs were compared pairwise between the locations. On the other hand, in controls, there difference plots showed prominent differences in the negative components (PhNR-ON and PhNR-OFF) for comparisons between the central and nasal macula and between the temporal and nasal macula. The comparison between the central and temporal macula showed a prominent difference in the positive components (b-wave and d-wave). A summary of the statistical comparisons is shown in Table 6.4.

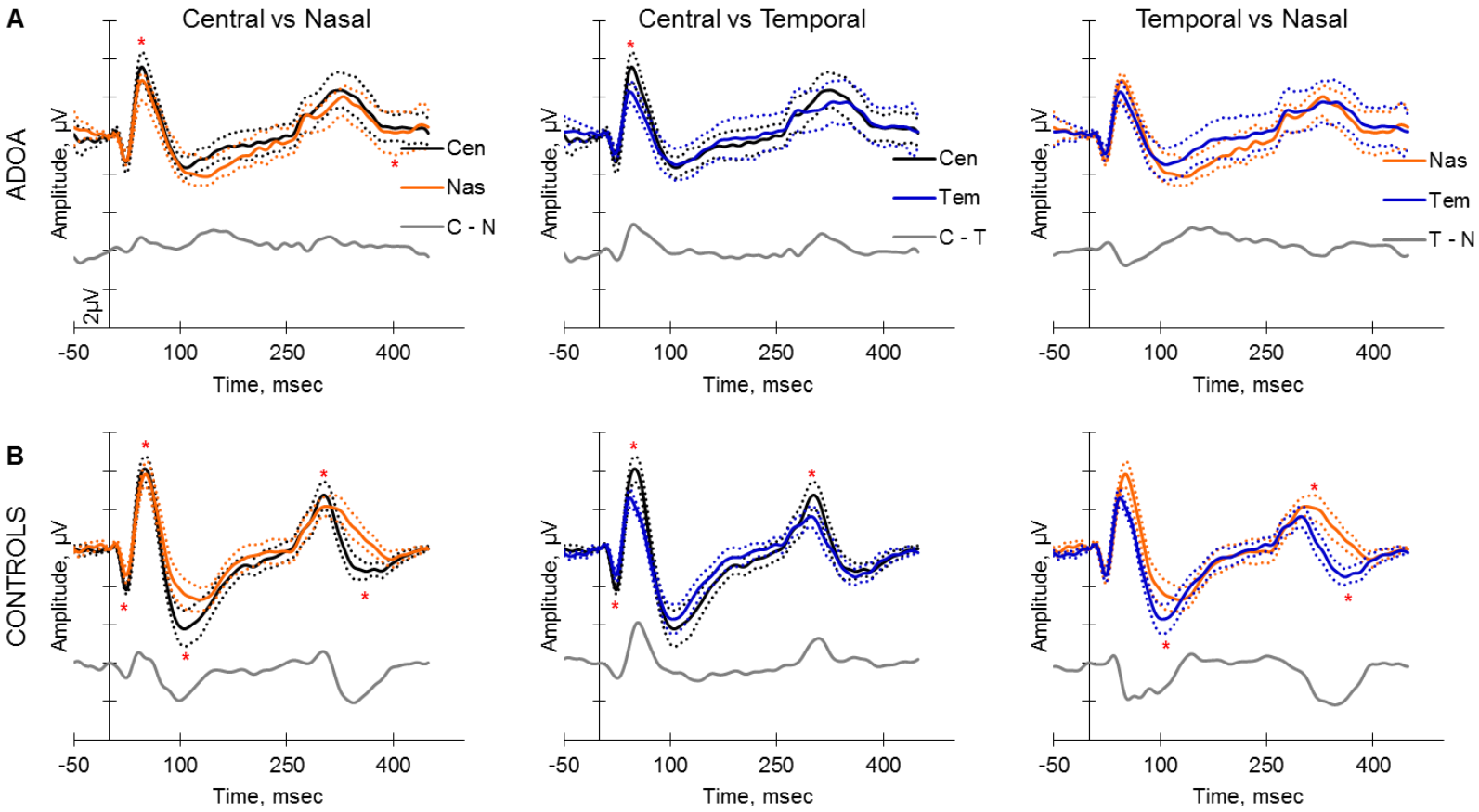

Figure 6.6. A pair-wise comparison of group-averaged focal ERGs recorded from the central, nasal and temporal retina for participants with (A) ADOA and (B) controls. The legend in A applies to B. Dotted lines represent 95% confidence intervals. Grey line represents the difference ERG for each paired comparison. Cen/C – Central retina; Nas/N – Nasal retina; Tem/T - Temporal

Table 6.4. Summary of comparisons between ERGs recorded from different locations within individual (repeated measures comparisons)

Component		ADOA	Controls
a-wave	Amp	Not significant ($p = 0.4924$; $P.Eta^2 = 0.13$)	Significant ($p = 0.0001$); $P.Eta^2 = 0.86$ Pairwise: Cen > Nas ($p = 0.0001$); Cen > Tem ($p = 0.0014$)
	Time	Not significant† ($p = 0.4966$)	Not significant † ($p = 0.1870$)
b-wave	Amp	Significant† ($p = 0.0087$) Pairwise: Cen > Tem ($p = 0.0037$)	Significant ($p = 0.0003$; $P.Eta^2 = 0.81$ Pairwise: Cen > Nas ($p = 0.0002$) Cen > Tem ($p = 0.0001$)
	Time	Not significant ($p = 0.6547$; $P.Eta^2 = 0.08$)	Significant† ($p = 0.0000$) Pairwise: Cen > Tem ($p = 0.0022$); Nas > Tem ($p = 0.0022$)
PhNR-ON	Amp	Not significant ($p = 0.2328$; $P.Eta^2 = 0.25$)	Significant† ($p = 0.0003$) Pairwise: Cen >Nas ($p = 0.0022$); Tem > Nas ($p = 0.0022$)
	Time	Not significant† ($p = 0.4723$)	Significant† ($p = 0.0077$) Pairwise: Cen < Nas ($p = 0.0183$); Nas > Tem ($p = 0.0150$)
d-wave	Amp	Not significant ($p = 0.2531$; $P.Eta^2 = 0.24$)	Significant ($p = 0.0028$; $P.Eta^2 = 0.69$) Pairwise: Cen > Nas ($p = 0.0183$); Cen > Tem ($p = 0.0016$); Nas > Tem ($p = 0.0018$)
	Time	Not significant† ($p = 0.3878$)	Significant ($p = 0.0338$; $P.Eta^2 = 0.49$) Pairwise: Nas > Tem ($p = 0.0099$)
PhNR-OFF	Amp	Significant ($p = 0.0319$; $P.Eta^2 = 0.50$) Pairwise: Cen > Nas ($p = 0.0500$)	Significant ($p = 0.0336$; $P.Eta^2 = 0.49$) Tem > Nas ($p = 0.0242$)
	Time	Not significant† ($p = 0.2636$)	Significant† ($p = 0.0005$) Pairwise: Cen > Nas ($p = 0.0120$); Tem > Nas ($p = 0.0022$)

† – data were non-normally distributed. $P.Eta^2$ = partial Eta^2 are given for parametric tests. Pairwise comparisons are given only for significant comparisons. The significant value of $p \leq 0.05$ is Bonferonni adjusted

6.2.3 Long Duration Full-field Cone ERG

The individual long duration full-field cone ERGs recorded from the twelve participants with ADOA are displayed in Figure 6.7A and again in Figure 6.7B, where they (thin coloured lines) are superimposed on the group-averaged trace of the 16 age matched controls (thick black line).

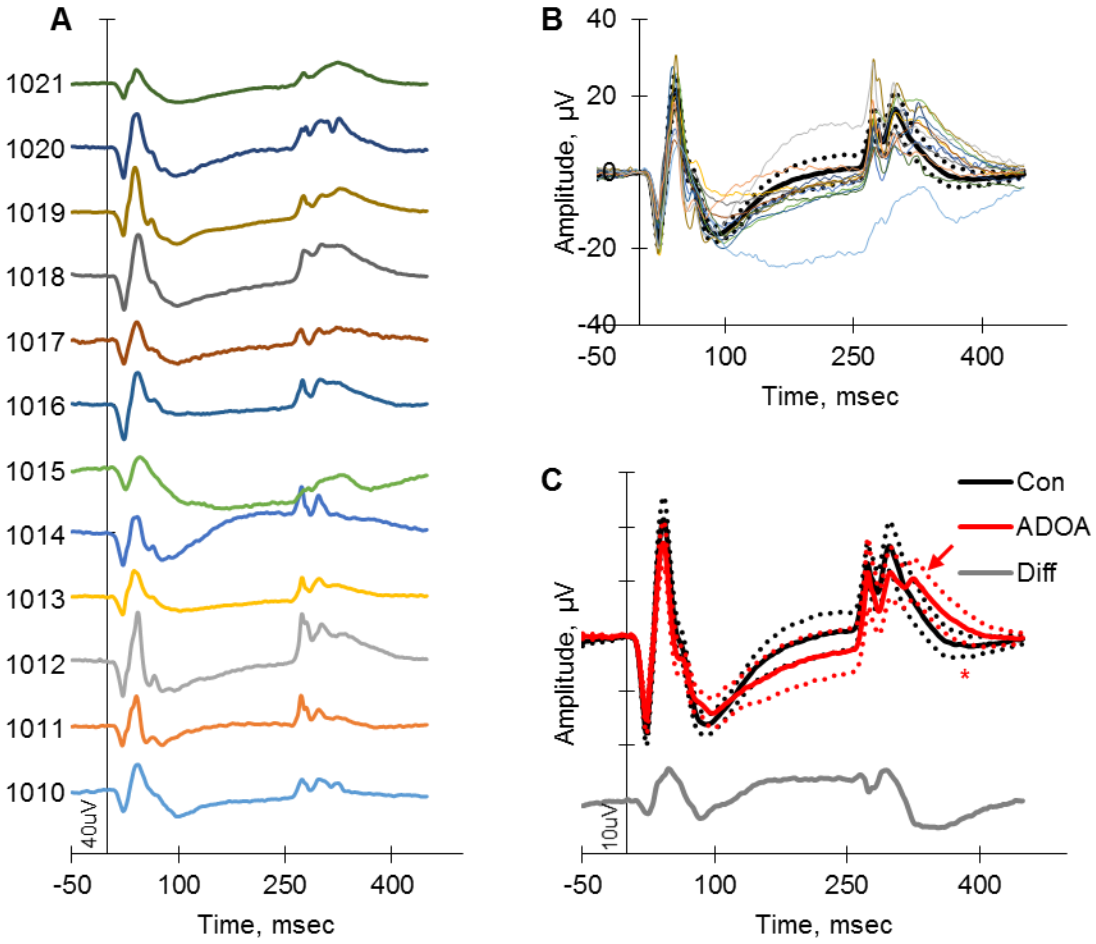

Figure 6.7. (A) Individual long duration full-field ERG recorded from the ADOA participants. (B) Individual ERGs (thin coloured lines) superimposed on group averaged ERG of controls (black line). (C) Comparison of group-averaged traces of ADOA participants (red thick line) and controls (thick black line). Thick grey line represents the difference ERG between the ADOA and control trace. Red arrow shows a third positive peak (3PP) after light offset in ADOA participants. Dotted lines represent 95% CI. * - Significant difference at p ≤ 0.01

Table 6.5. Mean values of amplitudes and times-to-peak of long full-field long duration ERG

Component		ADOA	Controls	p-value
a-wave	A, µV	15.87 ± 4.44	18.84 ± 4.45	0.0927
	T, msec	22.50 ± 1.09	23.16 ± 1.70	0.2537
b-wave	A, µV	33.57 ± 10.67	41.29 ± 11.18	0.0768
	T, msec	41.83 ± 2.86	42.16 ± 2.47	0.7515
PhNR-ON	A, µV	12.26 ± 3.95	15.68 ± 4.36	0.0430
	T, msec	96.18 + 9.16	92.72 + 4.15	0.2472
d-wave	A, µV	15.11 ± 6.20	12.84 ± 4.89	0.2866
	T, msec	274.67 ± 1.15	273.47 ± 1.02	0.0172†
2nd positive peak	A, µV	15.48 ± 4.87	16.10 ± 7.55	0.8064
	T, msec	302.50 ± 8.35	298.19 ± 2.00	0.1360†
PhNR-OFF	A, µV	-8.31 ± 5.69	0.45 ± 5.74	0.0005*
	T, msec	178.33 + 27.02	132.19 + 17.30	0.0000*†

The form of the long duration ERG was similar under focal and full-field conditions with one exception. There were at least two positive peaks immediately after light offset in the full-field ERG; the first being the d-wave (Evers and Gouras, 1986; Viswanathan et al., 1999). The mean amplitude of the PhNR-OFF, but not the PhNR-ON, was significantly reduced in participants with ADOA (Table 6.5). On the difference plot (Figure 6.7C) the amplitude of the PhNR-OFF difference (8.76 µV) was more than twice the amplitude of the PhNR-ON difference (3.42 µV) when measured.

Once again, the OFF components showed greater variability than ON components for participants with ADOA. In fact, in at least 6 participants with ADOA, there was a third positive peak (3PP) after light offset not seen in controls (Figure 6.7C, arrowed). There was no obvious pattern to the presence or absence of the 3PP in ADOA participants. The amplitude and time-to-peak of the 3PP measured from the ADOA group averaged trace was 13.34 µV and 75 msec after light offset respectively. Comparatively, none of the control traces displayed the 3PP prominently, although on close visual inspection, a kink corresponding in time with the 3PP was observed in some individual control traces.

6.2.4 Comparison of Focal and Full-field Long Duration ERGs

The waveforms of the central retina focal and full-field long duration ERGs were further compared by normalising the group averaged ERGs to their respective b-wave amplitudes (Figure 6.8). The focal and full-field ERGs of controls (Figure 6.8A) and participants with ADOA (Figure 6.8B) had similar profiles although times-to-peak of the b-wave, PhNR-ON and d-wave were significantly delayed in the focal ERG ($p \leq 0.01$, data not shown). The most prominent positive peak of the focal ERG after light offset coincided with the 2PP of the full-field ERG in the control traces while in the ADOA group, the broad peak of the focal ERG after offset described a curve that roughly matched the profile of the 2PP and 3PP of the full-field ERG.

In controls, the PhNRs were proportionally greater in the focal ERG than in the full-field ERG (Figure 6.8A). The losses in amplitudes of the PhNRs were also

greater in the focal ERG than the full-field ERG in participants with ADOA (Figure 6.8B and 6.8C).

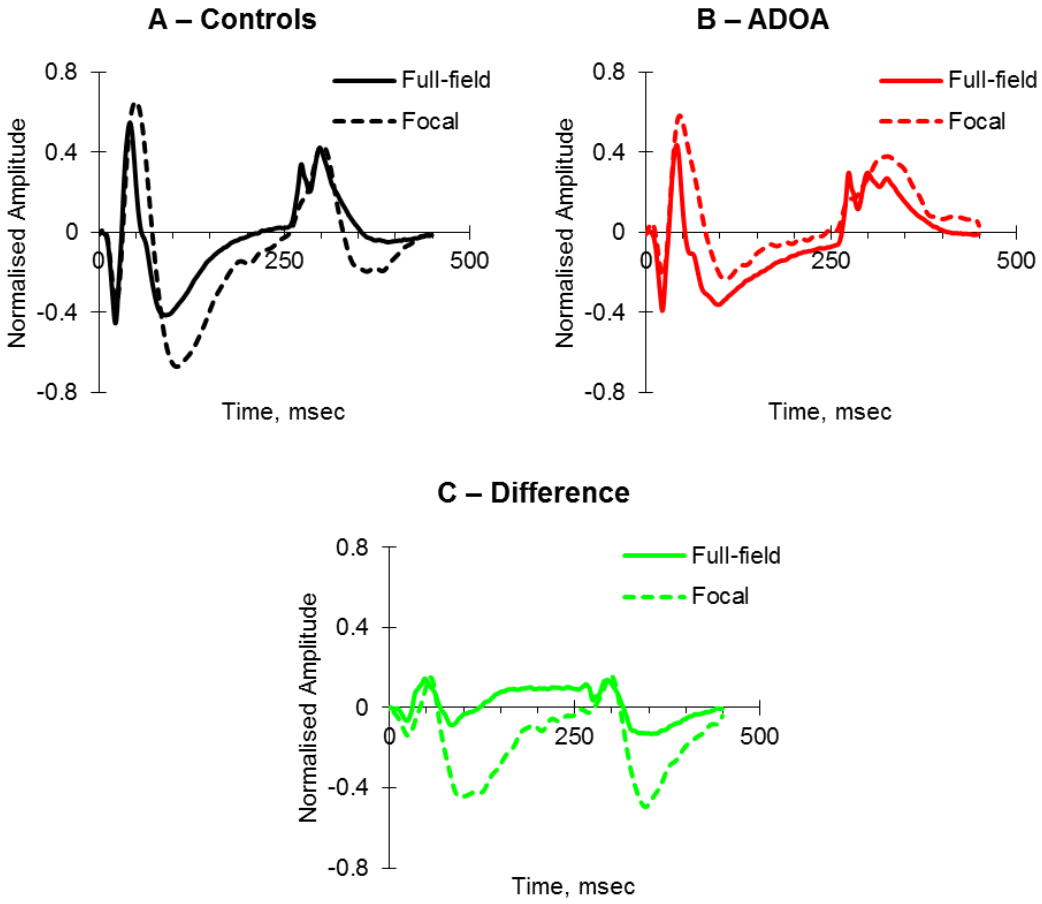

Figure 6.8. A comparison of the focal (dashed lines) and full field (solid lines) long duration group-averaged ERGs for (A) controls, (B) participants with ADOA and (C) difference plots (i.e. Control – ADOA). ERGs have been normalised to the b-wave amplitude of their respective control group-averaged ERG.

6.2.5 The Brief Full-field ERG

Brief full-field ERGs recorded from 7 ADOA participants are shown in Figure 6.9A. Typical ERG responses had a-wave, b-wave, i-wave and PhNR components. The PhNR amplitude was reduced significantly in people with ADOA compared to controls (Figure 6.9B and Table 6.6). The difference plot in Figure 6.9C indicates that the greatest deficit in ADOA corresponds to the timing of the b-wave and the PhNR. An i-wave was recorded for all participants (controls and ADOA). Although it appeared more prominent in ADOA participants, there was no statistical difference in amplitude or time-to-peak between control and ADOA participants (Table 6.6).

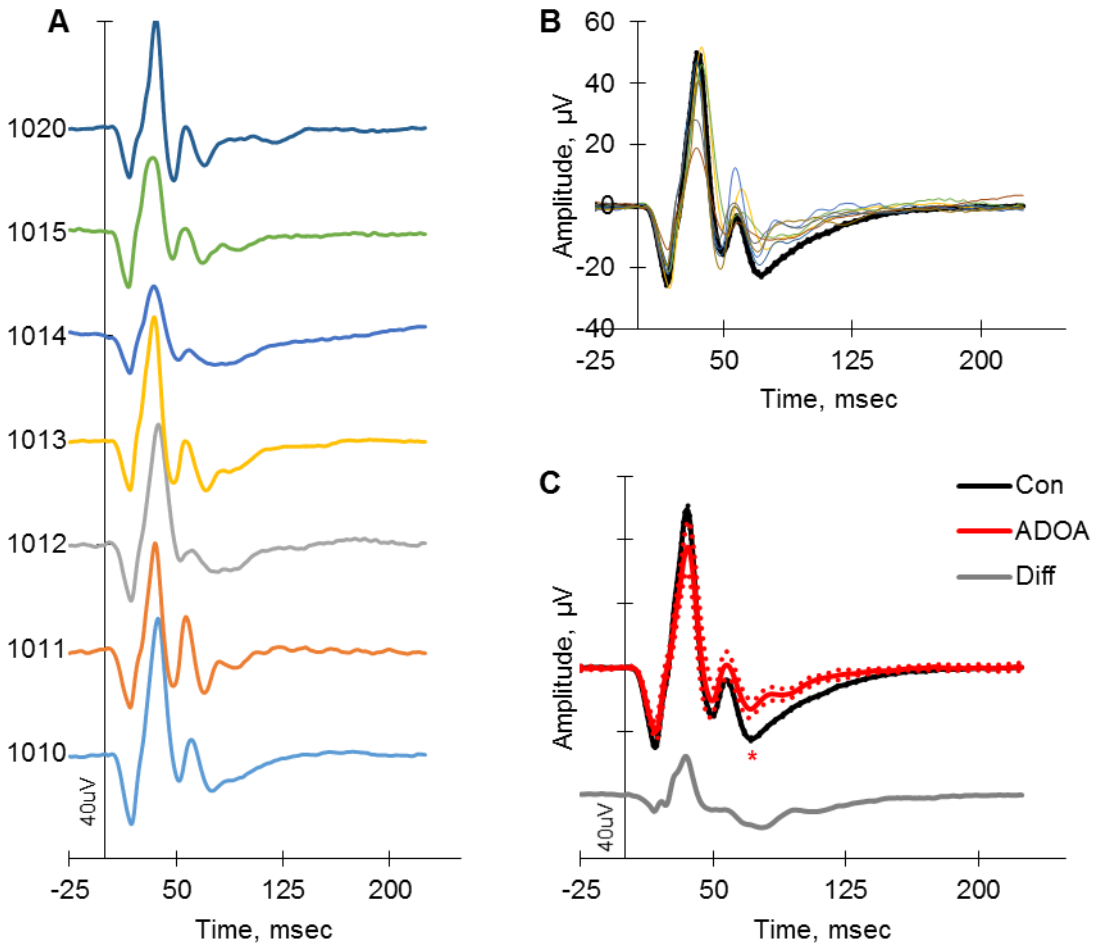

Figure 6.9. (A) Individual full-field brief ERGs recorded from 7 participants with ADOA. (B) Individual ERGs (thin coloured lines) superimposed on group averaged ERG of controls (black line). (C) Comparison of group-averaged traces of ADOA participants (red thick line) and controls (thick black line). Thick grey line represents the difference ERG between the ADOA and control trace. Dotted lines represent 95% CI. * - Significant difference at p ≤ 0.01

Table 6.6. Mean amplitude and implicit values for the full-field brief ERG

Component		ADOA	Controls	p-value
a-wave	A, µV	20.60 ± 3.79	25.73 ± 5.91	0.0422†
	T, msec	17.50 ± 0.69	17.22 ± 0.76	0.4133
b-wave	A, µV	59.75 + 14.58	77.88 ± 18.17	0.0302
	T, msec	35.39 ± 1.51	35.38 ± 1.26	0.9768
i-wave	A, µV	14.00 ± 8.37	16.19 ± 7.58	0.5420
	T, msec	58.04 ± 2.04	57.61 ± 2.37	0.6844
PhNR	A, µV	12.93 ± 3.38	22.39 ± 6.17	0.0001*
	T, msec	72.75 + 4.13	70.59 + 6.40	0.6390†

6.2.6 Specificity and Sensitivity of the Different ERGs

Receiver operating characteristics (ROC) curves were used to determine the effectiveness of the N95 and long duration focal and full-field PhNRs at discriminating participants with ADOA from controls for 9 participants with

ADOA and 16 controls for whom PERG and long duration focal and full-field ERG data were available. The AUC, sensitivity, specificity and cut off value which produced an optimal sensitivity while maintaining minimum specificity of ~90% are shown in Table 6.7. The N95 amplitude had the greatest diagnostic power. However, a comparison of the AUCs of the focal and full field PhNRs with the N95 amplitude, using the method described by Hanley and McNeil (1983)(Hanley and McNeil, 1983) showed that the N95 amplitude was only significantly more sensitive than the full-field PhNR-ON amplitude ($z = 2.12$). Therefore, considered in terms of their diagnostic ability, the focal PhNRs were equivalent to the N95 amplitude.

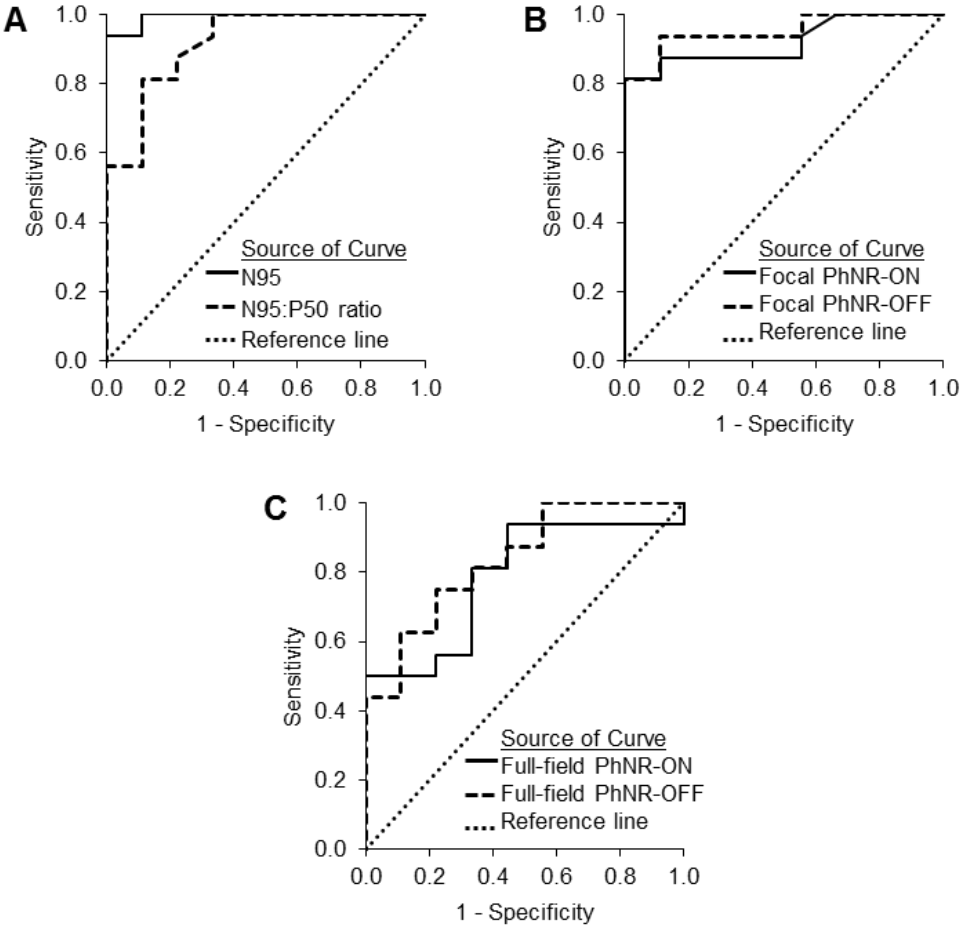

Figure 6.10. Receiver Operating Characteristic (ROC) curves for ERG components. (A) N95 component and N95:P50 ratio of the PERG, (B) focal PhNR-ON and PhNR-OFF amplitudes and (C) full-field PhNR-ON and PhNR-OFF amplitudes.

Table 6.7. Sensitivity, specificity and Area Under Curve of ROC analysis for ERG components

Test Variable	Area (95% CI)	Sensitivity	Specificity	Cut Off Value
N95	0.993 (0.971 – 1.000)	93.8	100	4.12 µV
N95:P50	0.920 (0.809 – 1.000)	81.3	89.9	1.44
Focal PhNR-ON	0.920 (0.834 – 1. 000)	81.3	100	2.62 µV
Focal PhNR-OFF	0.951 (0.871 – 1.000)	81.3	100	0.24 µV
Full-field PhNR-ON	0.785 (0.599 – 0.970)	50.0	100	16.99 µV
Full-field PhNR-OFF	0.833 (0.731 – 0.995)	62.5	89.9	0.35 µV

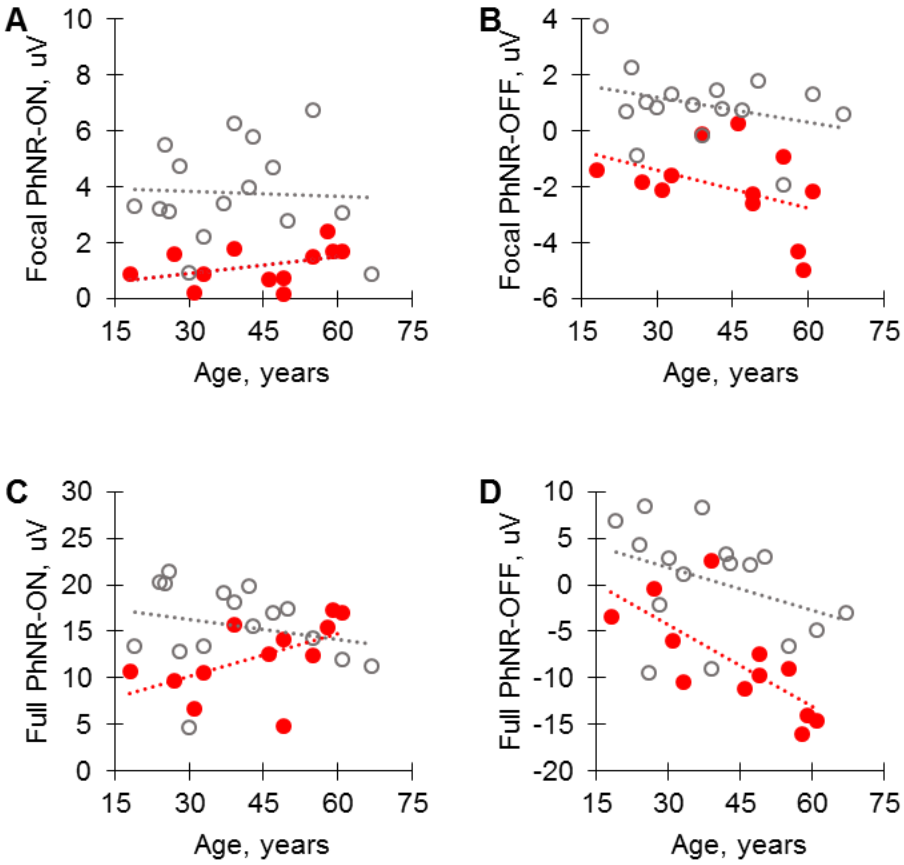

Figure 6.11 Scatter plot of long duration focal (A – B) and full-field (C – D) PhNRs as a function of age for participants with ADOA (red dots) and controls (grey dots). The dotted lines represent the regression line. Equations and R^2 of the lines are provided in Table 6.8.

6.2.7 Effect of Age on Electrophysiological Measures

Separate regression analyses were carried out for focal PhNR-ON and PhNR-OFF and full-field PhNR-ON and PhNR-OFF, each as a function of age, within ADOA and control groups. Their scatter plots are shown in Figure 6.11.. These were selected since they were the parameters for which data were available for all participants. There was no significant relationship between age (independent

variable) and any of the dependent variables except the full-field PhNR-OFF amplitude in the ADOA group, which declined with age (Table 6.8). The R^2 values were low for each parameter's comparison with age ($R^2 \leq 0.3$) except for the PhNR-OFF which had an R^2 of 0.52 in the ADOA participants.

Table 6.8. Linear regression equations for the relationship between age (independent variable) and selected parameters (dependent variables)

Parameter		Equation	R^2	p-value
Focal PhNR-ON	ADOA	0.0199x + 0.3198	0.16	0.1912
	Control	-0.0057x + 4.0293	0.00	0.8655
Focal PhNR-OFF	ADOA	-0.0452x – 0.0193	0.18	0.1728
	Control	-0.0300x + 2.0995	0.11	0.2057
Full-field PhNR-ON	ADOA	0.1530x + 5.5611	0.30	0.0674
	Control	-0.0716x + 18.4777	0.05	0.3925
Full-field PhNR-OFF	ADOA	-0.2938x + 4.5390	0.52	0.0078*
	Control	-0.1524x + 6.4139	0.14	0.1540

* - Significant at $p < 0.05$

6.3 Discussion

6.3.1 Effect of ADOA on ON and OFF RGCs

In this section and section 6.3.3, only the focal ERG from the central retina is considered. This study sought to determine whether the PhNR-ON was preferentially affected in ADOA as might be predicted based on the study by Williams et al (2010). The findings of the present study, however, suggested that in patients with ADOA the PhNR-ON and PhNR-OFF amplitudes were equally reduced in the focal ERG, while in the full-field ERG, there was a greater reduction in the PhNR-OFF amplitude than the PhNR-ON amplitude. What then might explain this apparent contradiction?

In the study by William et al (2010), evidence for the preferential loss of ON-RGCs was based on mouse retinal flat mounts showing significant dendritic pruning of ON-, but not OFF-centre RGCs. The experiment reported here, however, assessed the effect of ADOA on the ON and OFF RGCs by evaluating the PhNR amplitude of the human ERG, a functional measure. The role of the RGCs as primary originators of the PhNR has been demonstrated in previous studies (Viswanathan et al., 1999; Viswanathan et al., 2000; Viswanathan et al., 2001; Rangaswamy et al., 2007; Luo and Frishman, 2011). In experiments

using long duration full-field ERGs, they showed that that PhNR-ON and PhNR-OFF components were both reduced or eliminated after experimental glaucoma and intravitreal injection of tetrodotoxin (TTX) (an agent that blocks generation of sodium dependent spikes in retinal neurons) in macaque, as well as in patients with glaucoma. Furthermore, Luo and Frishman (Luo and Frishman, 2011) showed that the PhNR-ON (and b-wave) component, but not the PhNR-OFF (or d-wave) was eliminated after injecting 2-amino-4-phosphonobutyric acid (APB) into the macaque retina to block synaptic transmission from photoreceptors to ON-bipolar cells and hence ON-RGCs. Injecting TTX after APB then removed the PhNR-OFF thereby linking the PhNR-ON and PhNR-OFF components to the ON and OFF pathways respectively (Figure 6.12).

Previous human (Gotoh et al., 2004; Machida et al., 2011; Nakamura et al., 2011b) and animal (Viswanathan et al., 1999; Barnard et al., 2011) studies (including our mouse model) have shown that the PhNR amplitude is very susceptible to RGC damage with severe attenuation of PhNR amplitude recorded even when morphologic and other functional parameters were within normal range i.e. in early stage disease. It is possible that the PhNR-ON pathways may be selectively compromised at an earlier stage of the disease process than that studied here. In addition, it is important to consider the timing of the onset of ON-RGC dendropathy and visual loss in mice in relation to the age at which symptoms are reported in ADOA patients. In the mouse model, preferential ON-RGC dendropathy was detected in 10 – 15-month-old mutant mice and become pronounced in >20-month mutant old mice (Williams et al., 2010; Williams et al., 2012). One human year is equivalent to 9 mouse days (Dutta and Sengupta, 2016); hence the equivalent human age of the 10 – 15-month and 20-month old mice would be 33.3 – 50 years and 66.6 years respectively. Furthermore, a decline in visual function was detected in 12-month-old mutant mice (~ 40 human years) (Davies et al., 2007) and a significant reduction in the PhNR amplitude was detected in 11-month-old mutant mice (~ 37 human years) (Barnard et al., 2011).

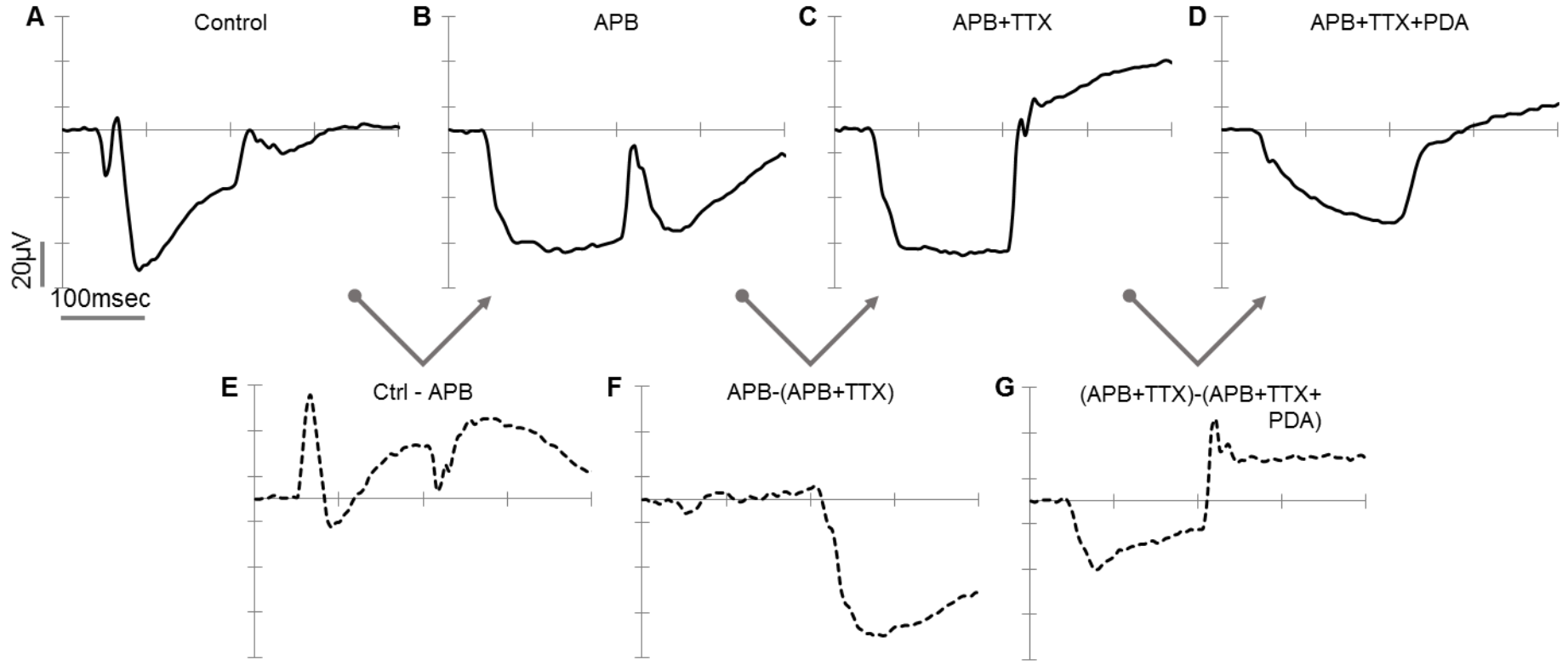

Figure 6.12. Full-field long duration ERGs (200 msec white-on-white flash) recorded from a macaque monkey before and after serial injection of APB, TTX and PDA showing the contributions of the various retinal cells to the long duration ERG. The top row shows ERG traces recorded before (A) and after drug administration (B – D), while the bottom row (E – G) shows the ERG components lost as a result of the drug administration. (A) Control ERG showing the sum of all retinal cells. (B) Photoreceptor, OFF-bipolar and OFF inner retinal cell (RGC and amacrine) activity. (C) Photoreceptor and OFF bipolar cell activity. (D) Photoreceptor activity. (E) Contribution from ON-Bipolar, and ON inner retinal cells (RGCs and amacrine). (F) Contribution from OFF inner retinal cells (OFF RGC and amacrine). (G) Contribution of OFF-bipolar cells. After APB, the ERG trace represents the photoreceptors and OFF responses. (Digitised and modified from Luo and Frishman 2011, Figure 4, using ImageJ 1.49u).

Per these estimates, the mean age of the ADOA cohort in this study (44 ± 14 years) fell within the predicted age range in which a selective effect of ON-RGC dendropathy would be detected in humans (i.e. 10 – 15 month mice = 33.3 – 50 year humans). However, the onset of a decline in visual function in ADOA patients is much earlier (usually before 10 years) (Votruba et al., 1998a; Johnston et al., 1999; Yu-Wai-Man et al., 2010a) than was predicted by the mouse model. Therefore, if as suggested by the mouse model, the selective ON-RGC dendropathy preceded or coincided with the decline in visual signs, then in humans such a selective effect of ON-RGC would be detected before the first decade of life and with time, the OFF-RGCs may also be compromised by the disease. Thus, the age range of the ADOA cohort in this study may have precluded the detection of a selective effect of ON-RGC dysfunction. A similar study in pre-symptomatic people with the *OPA1* mutations or in people with ADOA at a much earlier stage of the disease (e.g. <10-year-old children with ADOA) could provide additional insights.

The findings of this study may also be a reflection of the heterogeneous nature of ADOA (Votruba et al., 1998a; Votruba et al., 1998b; Ferre et al., 2005; Amati-Bonneau et al., 2009; Ferre et al., 2009; Yu-Wai-Man et al., 2010a; Yu-Wai-Man et al., 2010b). There are over 200 *OPA1* mutations (Ferre et al., 2005; Ferre et al., 2009) which cause ADOA with wide phenotypic variations both within and between affected families (Votruba et al., 1998a; Granse et al., 2003). In the mouse model, the mutant mice (>10 months old) were genetically homogenous and disease severity correlated with age. Participants studied here were from 6 families, with a different mutation in each family, and at different stages of the disease. This may have diluted observations that would have been made from a homogenous cohort.

6.3.2 Comparison of ERGs from Different Retinal Locations in ADOA and Control Participants

PERGs and focal ERGs were recorded from the central, nasal and temporal retinas in both participants with ADOA and controls to assess whether ADOA showed a preferential locus of damage to the retina. The amplitude of the N95 was significantly reduced in the ADOA group compared to controls in all

locations while in the case of the focal PhNRs, the difference between the ADOA and control group was significant in the central and temporal macula, but not the nasal macula. In cases of both the N95 and focal PhNR amplitudes, the greatest difference between the ADOA and control group was recorded in the central macula. This was consistent with the hypothesis that the greatest difference between participants with ADOA and controls would be recorded from the central macula since ADOA was characterised by central scotomas.

It was also expected that the difference in the nasal macula would be greater than that in the temporal macula since centrocoecal scotomas also characterise ADOA. However, the amplitude difference between the ADOA and control groups for the N95 amplitude was approximately equal for the nasal and temporal macula while the focal PhNRs reported a significant difference in the temporal, but not the nasal. This could be explained by the variable visual field defects present in the ADOA cohort in this study. Centrocoecal scotomas are frequently reported in ADOA, however scotomas in other locations are also common (Votruba et al., 1998a). With regards to the focal PhNRs, the lack of statistical difference between the ADOA and control groups in the nasal macula could be related to the factors that caused the waveform of the ERGs from the nasal macula to be different to those recorded from the central and temporal retina. These factors are discussed below where the ERGs recorded from the three locations within each cohort are compared.

In healthy individuals, the nasal retina has a greater RGC density than the temporal retina at similar eccentricities (Curcio and Allen, 1990; Silveira and Perry, 1991; Dacey, 1993b). It was therefore expected that in controls, the N95 and focal PhNR amplitudes from the nasal retina would be greater than those from the temporal retina as shown in previous studies (Kurimoto et al., 2009). However, in both the focal PERG and focal ERG, responses initially recorded from the nasal macula had smaller N95 and PhNR amplitudes than those from the temporal macula. It was assumed that this reduction in the nasal retina was due to the optic nerve head being present within the stimulated area when the 20^{o} stimulus was moved to the nasal side of the fovea. Since ERGs amplitudes are directly proportional to retinal cell numbers (Murray et al., 2004), the nasal ERG were multiplied by a factor of 1.11 (for PERGs) and 1.14 (for focal ERG) to

account for the loss in signal due to the optic nerve head (assuming an angular radius of 3.5° (Curcio and Allen, 1990)). This however did not result in the nasal N95 and focal PhNRs becoming significantly greater than their counterparts from the temporal macula. The temporal PhNR-ON, for example, remained significantly greater than the nasal PhNR-ON (Figure 6.6, right column).

In both the PERG and focal ERGs, the control group-averaged traces from the nasal macula were different in waveform compared to those from the central and temporal retina (Figure 6.3B and 6.6B) as observed previously in Chapter 3 (compare Figure 3.2). As explained in section 3.4, the reasons for this could be due to the luminance imbalance caused by the presence of the ONH when the nasal retina was stimulated and/or the intrusion of components associated with the optic nerve head (Sutter and Bearse Jr, 1999).

Interestingly, the ADOA group-averaged waveforms of the PERG and focal ERGs from the three locations (Figure 6.3A and 6.6B) were more similar to each other than the control group-averaged waveforms (Figure 6.3B and 6.6B); the difference plots (grey traces) for comparisons in the ADOA group were less remarkable (appeared flatter) than for comparisons in the control group. This suggested that the factors contributing to the waveform differences in the control ERGs recorded from the three retinal locations may have been removed or diminished by the disease. It was further observed that the waveforms of the ADOA group-averaged focal ERGs from all three locations (red traces in Figure 6.5B) were closely similar in shape to the control group-averaged trace from the nasal retina. The waveform similarity is shown for the comparison between the nasal records of the ADOA and control group-averaged traces in the middle column of Figure 6.5B. In addition, the waveform difference between the nasal trace and the central/temporal trace in controls was most obviously observed in the OFF responses. This particular difference in the OFF responses in controls was similar to the differences observed in the OFF responses between the ADOA and control group for the central and temporal macula (Figure 6.5B). These observations suggested that the ERGs recorded from controls may have contained a component whose amplitude and/or time-to-peak were/was influenced by proximity to the optic nerve head (or eccentricity away from the fovea). This potential will be called the late-potential (LP).

In light of the fact that the ERG recorded at the cornea is the resultant wave produced by the superimposition of several component waves arising from different retinal cells (as explained for example by Granit's classical analysis (Granit, 1933) or Sieving's push-pull model (Sieving, 1993; Sieving et al., 1994)), it was difficult to establish the true nature of the LP without further evidence. Such evidence could have been procured from a pharmacological study into the nature and origin of the LP, however, this was beyond the scope of this study. Nevertheless, the following inferences may be made about the LP.

1. It was a slow component with a time-to-peak either coinciding with or occurring close to the time-to-peak of the PhNR-OFF component
2. Its amplitude and/or time-to-peak were/was influenced by proximity to the optic nerve head (or eccentricity away from the fovea)
3. It was susceptible to the dysfunction of RGC bodies, RGC axons or the optic nerve, and further suggesting that it may have been generated by or related to these elements.

Although the proposal about the LP is drawn from the results of the focal ERGs, the results of the transient PERG are also consistent with the submission. The transient PERG generated in this study (using ISCEV standards) does not discriminate between ON and OFF components, they overlap. However, pharmacological interventions which selectively block ON or OFF pathways have shown that the P50 component of the transient PERG originates from both spiking and non-spiking activity of ON and OFF pathways, while the N95 originates solely from the spiking activity of the two pathways (Viswanathan et al., 2000; Luo and Frishman, 2011). If as proposed, the LP exerts its greatest influence in the nasal macula and at a time coinciding with the activities of the OFF-RGCs, then one would expect that, at least in the control group, any differences in the PERG waveforms between the nasal and central/temporal macula would be seen prominently in the N95 component. This was the case as seen in Figure 6.3, thereby lending credence to the LP theory. It was earlier suggested that luminance imbalance may be responsible for the difference in the nasal PERG. The current proposal about the LP is not necessarily in contradiction with that since both luminance imbalance and the LP may together be responsible for the differences observed.

A discrepancy was noticed between the quantitative comparison of the ERG components and the qualitative (graphical) comparisons of the group-averaged ERGs in the comparison of ERGs from different locations within the groups (repeated measures comparisons). For example, in Figure 6.3B (middle column), the most negative point of the N95 trough for both central and temporal PERGs occur at the same point (~ -2uV) and an overlap of the 95% confidence intervals may be observed. However, since the N95 amplitude was quantitatively measured from the peak of P50 (as recommended by ISCEV), which was reduced in the temporal macula, the N95 amplitude of the temporal macula was also reported to be significantly reduced when analysed with SPSS (Table 6.2). Conversely, in Figure 6.3 (right column), a separation of the 95% confidence intervals for the N95 components of the nasal and temporal macula was observed, yet quantitative analysis reported no significant difference between the two locations. The presence of the discrepancy between the quantitative and graphical comparisons therefore supports a different approach for measuring the N95 amplitude (e.g. from baseline).

A similar phenomenon was observed for the focal ERGs (Figure 6.6A, left column). The PhNR-OFF components in the graph overlap, yet quantitative analysis showed them to be significantly different. This was also due to the method of measuring the PhNR components. The PhNR-OFF was measured from the d-wave to a fixed time point which was determined as the time point marking the greatest difference between the ADOA and control groups. This fixed time point was different for the two locations (Table 5.3) and hence the amplitudes for the two locations were also different. This discrepancy again supports alternative methods of measuring the ERG components which do not rely solely on peaks and troughs (Gauvin et al., 2014; Wood et al., 2014).

6.3.3 Comparison of Focal and Full-field PhNRs

The long duration focal and full-field ERGs in this study were recorded using the same stimulus parameters, which were comparable to the parameters recommended by Kondo et al (Kondo et al., 2008a) for eliciting focal responses. This enabled a comparison of the long duration focal (central macula only) and

the full-field ERG to determine the effect of ADOA on them. Although the waveforms of the focal and full field ERGs were similar within the ADOA and control groups, they were not identical (Figure 6.8A-B). In the control group, there was a greater contribution of PhNR-ON and PhNR-OFF components to the focal ERG than to the full-field ERG (Figure 6.8A) which reflects the decreasing proportion of RGCs with eccentricity (Curcio and Allen, 1990). The focal PhNRs were more severely affected than their full-field counterparts by ADOA and this was reflected in the larger normalised difference plot (Figure 6.8C) and AUCs (Table 6.8) found for the focal signals. In addition, whereas the focal ON- and OFF-PhNRs were both significantly reduced ($p<0.001$), only the full-field PhNR-OFF was significantly reduced in the full-field ERG (Table 2). These findings were consistent with the central field defects recorded in ADOA participants in this study and in others (Votruba et al., 1998a; Votruba et al., 1998b; Fuhrmann et al., 2010).

The symmetrical loss in the focal PhNR-ON and PhNR-OFF amplitudes (Figure 6.5B, left column and 6.8C) may reflect the 1:1 ratio of ON- to OFF-RGCs in the macula, while the greater loss in the full-field PhNR-OFF amplitude than the PhNR-ON amplitude (Figure 6.7C and 6.8C) reflects the nearly 1:2 (Dacey and Petersen, 1992; Dacey, 1993b; Drasdo et al., 2007) ratio of ON- to OFF- RGCs in the peripheral retina. The broadening of the d-wave peak in the focal ERG and the presence of the 3PP in the full-field long ERG in participants with ADOA may be due to contributions from the cone receptor potential (CRP) and/or depolarising OFF-bipolar cell responses after light offset which were unmasked in the relative absence of the negative going PhNR-OFF (Bush and Sieving, 1994; Sieving et al., 1994). The 3PP in the full-field ERG could also be due to the unmasking of the late positive potential originating from the optic nerve as proposed earlier. The 2PP may be the i_{OFF}-wave described by Horn et al (2011), although in contrast to their results, this study did not record a significant difference in amplitude between controls and participants with ADOA in this component.

6.3.4 Comparison to other Electrophysiological Studies in ADOA

Miyata et al (2007) reported a significant reduction in the full-field brief PhNR, but none in the a- or b-wave amplitude, in ADOA patients using white-on-white stimulus. Similar results were obtained by Barnard et al (Barnard et al., 2011) in the mouse model. This present study found similar results using a red on blue stimulus. The flash luminance used in this study was adopted from a previous study in this laboratory (Mortlock et al., 2010) and was comparable to the flash luminance used by Miyata et al (2007). This supports findings that the red-on blue stimulus is effective for clinical evaluation of RGC function.

Holder et al reported a significant reduction in N95 amplitude and the N95:P50 ratio of the PERG participants with ADOA (Holder et al., 1998). Similar results were obtained and showed that the performance of the focal PhNRs and N95 amplitude at discriminating controls from participants with ADOA were not significantly different. The focal ERG could therefore be used as an alternative to the PERG, and has the advantage of not relying on clear optical media or refractive error correction (as is the case for the PERG). Although the N95 and focal PhNR amplitudes were highly diagnostic for ADOA, it should be noted that the participants in this study had relatively late stage disease. The better performance of the N95 (although not significant) could therefore imply an advantage of the PERG over the focal PhNRs in the detection of early or subclinical stages of the disease as has been reported for comparisons between the PERG and full-field PhNRs (North et al., 2010; Preiser et al., 2013).

In this study, as well as in the study by Holder et al (1998), the P50 amplitude was significantly reduced. Since bipolar cells are involved in generating the P50, this may indicate that bipolar cell function is compromised as well in ADOA. In fact, Reis et al reported a significant reduction in the N1 and P1 of the multifocal ERG in participants with ADOA indicating bipolar cell dysfunction which they attributed to retrograde degeneration of bipolar cells subsequent to RGC dysfunction in ADOA (Reis et al., 2013). However, a significant reduction in the amplitudes of the b- or d-wave, which also originate from ON- and OFF-bipolar cells respectively, was not found.

6.3.5 Effect of Age of Long Duration PhNR

One of the objectives of this study was to find out whether age significantly affected the amplitudes of the PhNR components. Some previous studies had found that visual function in ADOA measured by VA or VFS deteriorated with age (Berninger et al. 1991; Yu-Wai-Man et al. 2010a; Reis et al. 2013). Some other studies, however, did not find any significant decline in visual function with age in ADOA patients (Votruba et al. 1998a; Cohn et al. 2008; Almind et al. 2012; Ronnback et al. 2013). In this study, there was no significant effect of age on the ERG amplitudes except for the PhNR-OFF amplitude which decreased with age (Table 6.8). Age accounted for ~50% of the variance observed in the PhNR-OFF amplitude in participants with ADOA compared to 14% in controls. This finding could imply that the full-field PhNR-OFF amplitude may be a better indicator of disease progression (or severity) than the other ERG parameters, although the reason for this could not be determined. Alternatively, it could be due to an interaction of other OFF components; e.g. an age-related delay in d-wave time-to-peak may be impacting on the PhNR-OFF component.

Apart from the heightened effect of age on the PhNR-OFF amplitude in participants with ADOA, the results presented here and the earlier results of no significant effect of age on the psychophysical or structural defects in ADOA (section 5.4.3 and 5.4.6), agree with the proposal other environmental and/genetic factors other than age impact largely on the severity of visual dysfunction (Ronnback et al., 2013).

6.4 Conclusion

The following conclusions are drawn from this study.

1. The ON- and OFF-RGCs are equally affected in patients with symptomatic ADOA, as evidenced by the symmetrical reduction in amplitude of the focal PhNR-ON and PhNR-OFF in participants with ADOA across a range of disease severity.

2. The central retina is primarily affected in ADOA as demonstrated by the fact that the central macula produced the greatest differences in the focal PhNR and N95 amplitudes between the ADOA and control groups. In addition, the focal PhNRs were superior to the full-field responses at discriminating participants with ADOA from controls.
3. The focal PhNR and N95 components have similar diagnostic power and are similarly effective at discriminating between participants with ADOA and controls.
4. With the exception of the full-field PhNR-OFF amplitude, disease severity determined by electrophysiology was not significantly affected by age in ADOA.

7 CHAPTER SEVEN - ELECTROPHYSIOLOGICAL ASSESSMENT OF RETINAL FUNCTION IN AUTOSOMAL DOMINANT OPTIC ATROPHY – III: RELATIONSHIP BETWEEN ELECTROPHYSIOLOGICAL, PSYCHOPHYSICAL AND STRUCTURAL MEASURES

7.1 Preamble

The results of the baseline tests and the electrophysiological assessment of the participants were presented in Chapters 5 and 6 respectively. This chapter explores the relationship between the psychophysical, structural and electrophysiological results using correlation coefficients and linear regression analysis.

7.2 Introduction

ADOA causes losses in visual function which have been measured using a variety of psychophysical tests namely visual acuity, visual fields, contrast sensitivity and colour vision tests (Kjer, 1959; Krill et al., 1970; Kline and Glaser, 1979; Hoyt, 1980; Kjer et al., 1983; Berninger et al., 1991; Eliott et al., 1993; Kjer et al., 1996; Brown et al., 1997; Johnston et al., 1997; Simunovic et al., 1998; Votruba et al., 1998a; Votruba et al., 1998b; Johnston et al., 1999; Thiselton et al., 2002; Votruba et al., 2003a; Nakamura et al., 2006; Walters et al., 2006; Cohn et al., 2008; Yu-Wai-Man et al., 2010a; Yu-Wai-Man et al., 2010b; Almind et al., 2012; Reis et al., 2013; Ronnback et al., 2013). These studies showed that visual dysfunction in participants with ADOA was characterised by reduced visual acuity and contrast sensitivity as well as visual field defects and colour vision anomalies. They also reported however, wide inter- and intra-family variations in the results of these tests, which ranged from normal to severe loss.

Histological examination of post-mortem tissue in humans and murine models shows that the RGCs and their axons are selectively affected in ADOA

(Johnston et al., 1979; Kjer et al., 1983; Williams et al., 2010; Sarzi et al., 2012; Williams et al., 2012). These findings have been confirmed in studies using optical coherence tomography (OCT) which provides a means of measuring the thickness of the retina in-vivo (Ito et al., 2007; Barboni et al., 2010; Milea et al., 2010; Barboni et al., 2011; Gocho et al., 2013; Russo et al., 2013; Carbonelli et al., 2015). The parapapillary retinal nerve fibre layer (RNFL), especially the temporal quadrant, is significantly reduced in ADOA compared to healthy controls or mutation-free first degree relatives of patients with ADOA (Ronnback et al., 2013). The macula is also thinner in people with ADOA than healthy controls (Ito et al., 2007). Current advances in OCT technology which allow layer by layer segmentation of the retina and analysis have been used in a number of studies (Ito et al., 2007; Gocho et al., 2013; Ronnback et al., 2013; Russo et al., 2013; Carbonelli et al., 2015) and show that the thickness of the inner retina comprising the RNFL, ganglion cell layer (GCL), and inner plexiform layer (IPL), is significantly reduced in participants with ADOA compared to controls, while the outer retinal layers are spared.

Electrophysiological tests of retinal function in participants with ADOA also show a reduction in the amplitude of the photopic negative response (PhNR) component of the flash ERG (Miyata et al., 2007; Morny et al., 2015), the PERG and PVEP (Holder et al., 1998; Russo et al., 2013); findings which are consistent with RGC dysfunction.

The psychophysical, structural and electrophysiological test results point to defects consistent with RGC damage. The purpose of this part of the study was therefore to determine the relationship between these tests in participants with ADOA and to find out whether the electrophysiological tests (the main instrument of this study) could be used to predict results of the psychophysical or structural tests. Since there were more than two measurement variables under consideration, it would have been ideal to perform multiple regression analysis. Multiple regressions provide an equation that best predicts the Y (dependent) variable as a linear function of the X (independent) variables. However, as a rule of thumb, there should be at least 10 observations per independent variable (Altman, 1991). This implied that for the six electrophysiological variables to be used as the independent variables, 60

cases per group would be required. As there were not enough cases in this study to satisfy this criteria, linear correlation and linear regression analysis were used instead.

7.3 Methods

The methods for recording the baseline measures and electrophysiological tests are described in Chapter 5.

7.3.1 Statistical Analysis

Correlations within the ADOA dataset were explored using Spearman's rank correlation test (2 tailed) since the distribution of the data was not always normal. Statistical significance was set at $p< 0.05$ (with no Bonferroni correction). Linear regression analysis were later performed on comparisons for which the correlation coefficients were significant. With regards to the PERG and focal ERG data, only results from the central retina were used in these analyses. Cohen's convention was adopted in categorising the strength of the correlation coefficient where 0 – 0.29 was classified as weak, 0.30 – 0.49 as moderate and $\geq$0.5 as strong (Cohen, 1988).

7.4 Results

The characteristics of the twelve participants with ADOA as well as the results of their baseline and electrophysiological assessments have been reported in Chapters 5 and 6.

7.4.1 Correlation between Psychophysical and Electrophysiological Measures

Figure 7.1 shows the scatter plots for comparisons between the electrophysiological (N95 of the PERG, focal and full-field PhNR-ON and PhNR-OFF and brief flash PhNR) and the psychophysical (VA, CS, VFS) tests in participants with ADOA. The corresponding correlation coefficients for the comparisons are shown in Table 7.2 for participants with ADOA.

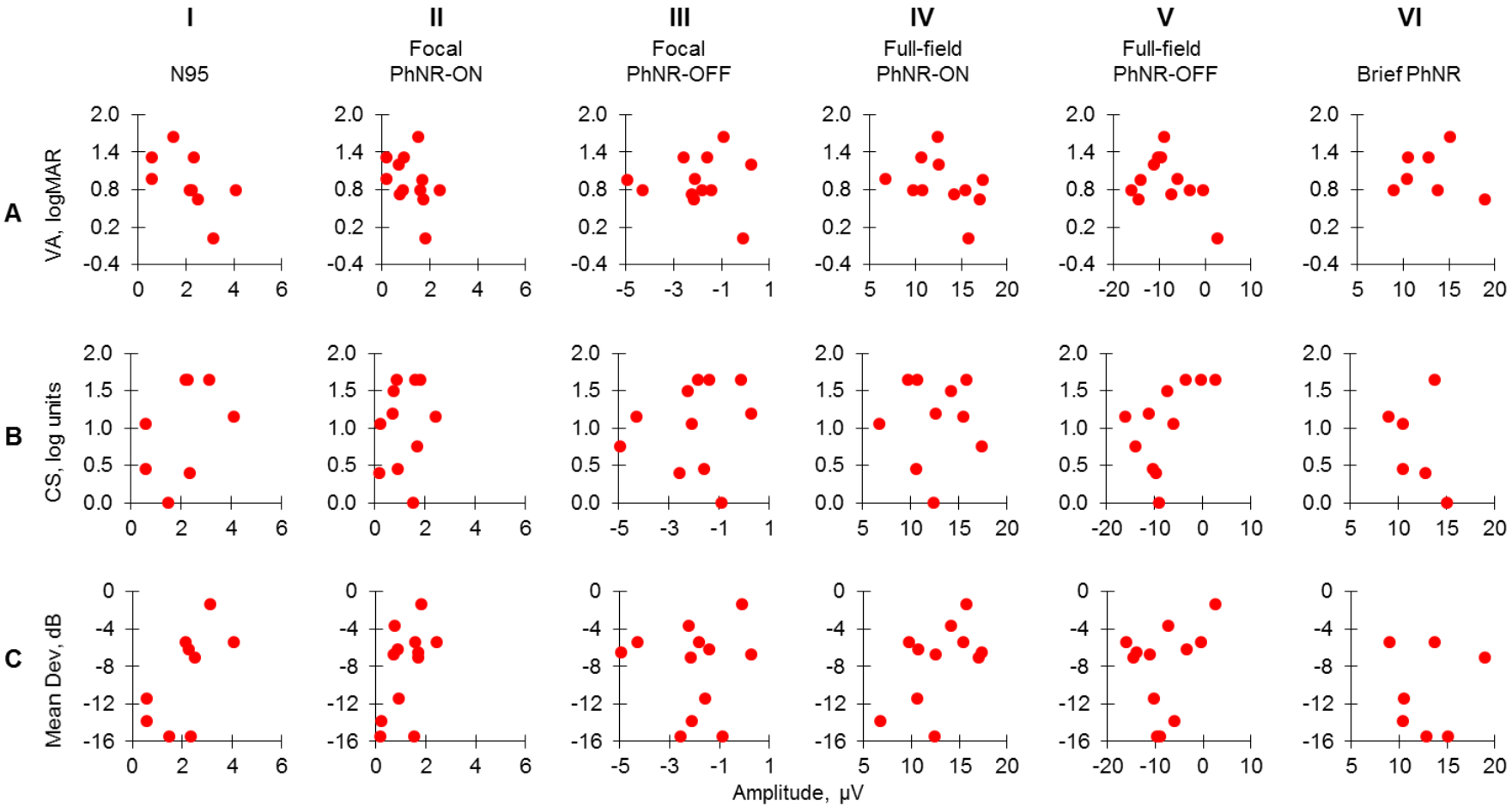

Figure 7.1. Scatter plots of ERG components and psychophysical measures in participants with ADOA. The amplitude of the ERG components (shown as headings on the columns) are plotted on the horizontal (x-) axis against the vertical (y-) axis of (A) visual acuity in logMAR; (B) contrast sensitivity (CS) in log units and (C) mean deviation in dB.

Table 7.1. Correlations between psychophysical (vertical axis) and electrophysiological (horizontal axis) assessments in participants with ADOA

Parameter	*Cor*	N95	Focal PhNR-ON	Focal PhNR-OFF	Full-field PhNR-ON	Full-field PhNR-OFF	Brief PhNR
VA, logMAR	*r* =	-0.65	-0.53	0.10	-0.55	-0.20	-0.06
	p =	0.06	0.08	0.75	0.06	0.53	0.91
CS, log units	*r* =	0.42	0.22	0.26	0.22	0.58	-0.41
	p =	0.30	0.52	0.45	0.52	0.06	0.43
VFS (18^o x 18^o), dB	*r* =	0.50	0.51	0.04	0.48	0.32	-0.07
	p =	0.17	0.09	0.90	0.12	0.31	0.88

Cor – Spearman's correlations test (2-tailed); *r* – correlation value; *p* – p-value of significance. Size of ADOA group, n = 12, except for comparisons with N95 (n = 9) and brief PhNR (n = 7). None of the correlations were statistically significant (p>0.05).

In participants with ADOA, there were moderate inverse correlations between VA and the N95, focal PhNR-ON and full-field PhNR-ON amplitudes; that is, better VA was associated with higher ERG amplitudes. The VFS showed a moderate correlation with the N95, focal and full field PhNR-ON amplitude. The correlations between the psychophysical tests and the focal or full-field PhNR-OFF amplitudes were weak, except between CS and full-field PhNR-OFF amplitude. However, none of the correlations reached statistical significance.

7.4.2 Correlation between Structural and Electrophysiological Measures

The correlations between structural and the electrophysiological measures are shown in Table 7.2 and Figure 7.2. The peripapillary RNFL, inner macula layer and total retinal thickness were selected for analysis because they were the parameters which were significantly reduced in ADOA compared to controls. In participants with ADOA, the total peripapillary RNFL thickness showed strong correlations with the N95 (r = 0.94), focal PhNR-ON (r = 0.83) and full-field PhNR-ON (r = 0.66) as well as with the brief PhNR (r = 0.7). However, these correlations were significant only for the N95 and focal PhNR-ON amplitude. The equation of the regression analysis for N95 amplitude (x-axis) and peripapillary RNFL thickness (y-axis) was $y = 13.80x + 16.09$, $R^2 = 0.83$, $p = 0.01$, while that for the PhNR-ON amplitude (x-axis) and peripapillary RNFL thickness (y-axis) was $y = 14.25x + 27.48$, $R^2 = 0.64$, $p = 0.06$.

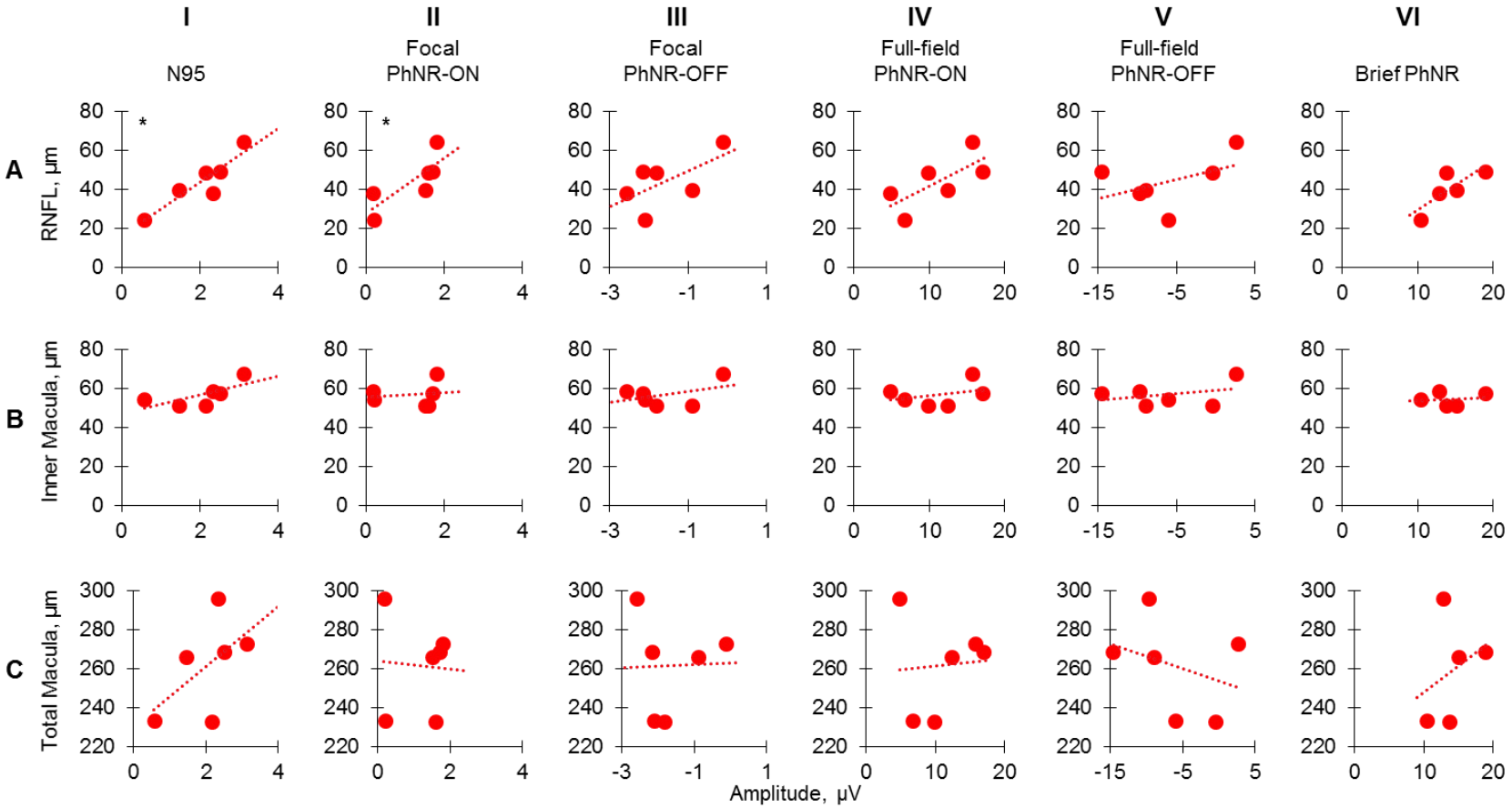

Figure 7.2. Scatter plots of OCT measures and ERG amplitudes in participants with ADOA. The amplitude of the ERG components (shown as headings on the columns) are plotted on the horizontal (x-) axis against the vertical (y-) axis of (A) peripapillary RNFL; (B); inner macular (RNFL+GCL+IPL) thickness and (C) total macular thickness. * - Correlation was significant at $p < 0.05$. Dotted lines represent regression lines

Table 7.2 Correlations between structural (vertical axis) and electrophysiological (horizontal axis) assessments in participants with ADOA.

Parameter	*Cor*	N95	Focal PhNR-ON	Focal PhNR-OFF	Full-field PhNR-ON	Full-field PhNR-OFF	Brief PhNR
Total peripapillary RNFL, um	*r* =	**0.94**	**0.83**	0.26	0.66	0.20	0.70
	p =	**0.01**	**0.04**	0.62	0.16	0.70	0.19
Inner Macula Thickness, um	*r* =	0.77	0.26	-0.14	0.09	0.09	-0.20
	p =	0.07	0.62	0.79	0.87	0.87	0.75
Total Macular Thickness, um	*r* =	0.66	-0.03	-0.26	0.03	-0.31	0.20
	p =	0.16	0.96	0.62	0.96	0.54	0.75

Par't – participant type; AD – ADOA; C – Control; Cor – Spearman's correlations test (2-tailed); r – correlation value; p – p-value of significance. Significant correlations at $p < 0.05$ are shown in bold fonts in shaded cells. Size of ADOA group, n = 6, except for comparisons with brief flash, where n = 5.

7.5 Discussion

This chapter explored the relationship between the electrophysiological, psychophysical and structural measures in participants with ADOA in order to determine whether the psychophysical and structural results could be predicted from the electrophysiological results. Correlations between the psychophysical and electrophysiological tests did not attain statistical significance in this study, although previous studies have shown correlations between psychophysical tests (VA and mean deviation) and ERG amplitudes (N95 and PhNR) in glaucoma studies (Colotto et al., 2000; Viswanathan et al., 2001; Garway-Heath et al., 2002; Harwerth et al., 2002). For example, Colotto et al. (2000) found a significant correlation ($r = 0.60$, $p < 0.05$) between the N95 amplitude and the mean deviation of the VFT in 11 glaucoma patients while Viswanathan et al. (2001) also found a significant correlation ($r = 0.59$, $p < 0.01$) between the brief PhNR amplitude and the mean deviation in 18 glaucoma patients. In this study, some of the correlations showing large effects approached statistical significance (e.g. VA vs N95, VA vs focal PhNR-ON and CS vs full-field PhNR-OFF in Table 7.1) and a significant effect might have been found if a larger sample size had been used. Using Cohen's convention (Cohen, 1988), the reported r values in the previous literature (Colotto et al. 2000; Viswanathan et al. 2001) suggested a large effect ($r \geq 0.5$) for the association between the ERG and psychophysical parameters. To detect such an effect at a significant value of 0.05 and power of 80% in the ADOA cohort, a minimum sample size of 29

was required for the bivariate correlation (Hulley et al., 2013) (see Appendix V for calculation).

It is, however, important to note that though the psychophysical and electrophysiological tests both assess related aspects of visual function, and were expected to be significantly correlated, the two categories of tests differ in their nature (Garway-Heath et al., 2002). The ERGs are objective measures of massed retinal responses to a suprathreshold stimulus, whereas the psychophysical tests depend on subjective responses to a threshold stimulus. The fact that these sets of results were not correlated suggest that the information provided by the two types of test are independent and complementary. The combination of subjective and objective functional tests could thus improve disease detection and staging of progression (Garway-Heath et al., 2002).

Table 7.3. Comparison of the correlation coefficient between RNFL thickness and ERG (N95 and PhNR) amplitudes obtained in previous studies

Study	Variables	Sample Size	Correlation coefficient, r	p-value
Parisi et al. (2001)	N95 vs RNFL	30 (OAG)	0.69	< 0.0001
Toffoli et al (2002)	N95 vs RNFL	112 (OAG+OHT+C)	0.31	< 0.05
North et al. (2010)	N95 vs RNFL	23 (OHT)	0.26	0.020
Machida et al. (2008)	PhNR vs RNFL	99 (OAG)	0.53	<0.001
Horn et al. (2011)	PhNR-ON vs RNFL	53 (OAG+OHT+C)	-0.46#	0.001

Initials in brackets indicate sample group used in analysis. POAG = open angle glaucoma; OHT = ocular hypertensive patients; ADOA = autosomal dominant optic atrophy; C = controls. # = The PhNR-ON amplitude was defined by the deepest negative point after following the b-wave.

The correlations between the OCT and the electrophysiological results were mostly not significant (Table 7.2). Significant correlations were found only for the peripapillary RNFL and N95 amplitude ($r = 0.94$, $p < 0.01$) and the peripapillary RNFL and focal PhNR-ON amplitude ($r = 0.83$, $p < 0.05$). Regression analysis showed that the N95 amplitude accounted for more than 80% of the variance in RNFL thickness, implying a good model fit for predicting peripapillary RNFL thickness. Similar significant relationships have been shown in previous studies (Table 7.3) (Parisi et al., 2001; Toffoli et al., 2002; Parisi, 2003; Ventura et al., 2006; North et al., 2010), which, highlight the fact that the N95 of the PERG reflects the activities of the RGCs (Arden et al., 1982; Bach et al., 1992; Thompson and Drasdo, 1994; Holder et al., 1998; Holder, 2001; Bach

and Hoffmann, 2008). Although the correlation coefficient between the PhNR-ON and RNFL was strong and significant (r = 0.83, p = 0.04), the relationship failed to reach statistical significance in regression analysis. Considering that the R^2 value for the relationship was ~60%, it is possible that the lack of statistical significance was due to the small sample size in this study.

In this study, the correlation between the PhNR-OFF amplitude and RNFL thickness was weak and not statistically significant. Only one previous study was found to have reported on the correlation between the PhNR-OFF amplitude and the RNFL thickness (Horn et al., 2011). They found a significant correlation between the PhNR-OFF and RNFL thickness (Figure 7.3). A critical appraisal of their data, however, showed that controls and glaucoma patients were analysed together, with the controls clustering to one side and the glaucoma patients to another side. If the data from the glaucoma patients (filled circles) were isolated, their reported significant relationship would likely breakdown.

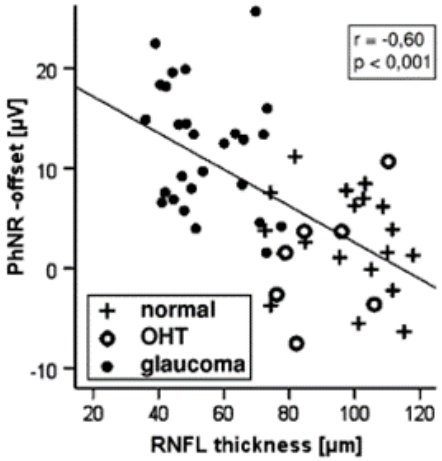

Figure 7.3. Correlation between the full-field PhNR-OFF amplitude and peripapillary RNFL thickness a combined group of participants with glaucoma (filled circles) and ocular hypertension (open circles) as well as controls (crosses). The diagonal line is the line of regression. r = Pearson's correlation. p = p-value of significance. (Horn et al., 2011)

The scarcity of such reports is due to the high variability in measuring the PhNR-OFF (Viswanathan et al., 1999; Colotto et al., 2000; Horn et al., 2011). Although the ADOA cohort in this study was comparatively small, the large variability was present in the control group as well. Furthermore, the experiment correlating the PhNR-ON and –OFF with RGC distribution (Chapter 4) showed

that the PhNR-OFF had the poorest fit to published OFF-centre RGC distributions.

7.6 Conclusion

In this study, there were no significant correlations between the electrophysiological and psychophysical tests of visual function in ADOA participants. This implies that the two classes of tests assess different aspect of visual function. In addition, the correlation between electrophysiological and structural measures assessed using the OCT were significant only for correlations between the N95 amplitude and the RNFL thickness as well as the PhNR-ON amplitude and RNFL thickness. The results of this study supports the view that disease detection and staging of disease progression may be improved when electrophysiological, psychophysical and structural tests are combined. However, given the small sample size included here the results should be treated cautiously.

8 CHAPTER EIGHT – GENERAL DISCUSSION AND CONCLUSION

8.1 Discussion and Conclusion

The primary aim of this thesis was to assess the effect of ADOA on the PhNR-ON and PhNR-OFF components of the photopic ERG in order to determine whether the ON pathway was selectively susceptible to the disease. In order to achieve the main aim of this study, a series of studies was conducted in Chapter 2 using control participants to develop a suitable protocol for recording the focal long duration PhNR. A 250 msec red flash of luminance 55cd/m^2 with an angular diameter of 20^o flashing at 2Hz on a rod saturating blue background of luminance 100 scot cd/m^2 was found to be optimal for eliciting the PhNR-ON and –OFF components of the photopic ERG. Previous studies which recorded focal ERGs used stimulus sizes ranging from 5 – 15 degrees (Kondo et al., 2008a; Machida et al., 2008b; Kurimoto et al., 2009; Tamada et al., 2009; Tamada et al., 2010; Nakamura et al., 2011a; Nakamura et al., 2011b). However, a 20^o stimulus size was chosen for this study to encompass as much of the central field as possible while avoiding the optic disc, which starts approximately 12^o to 15^o nasal to the fovea.

It has been hypothesised that the tritanopic defects often associated with ADOA may be due to preferential damage to the S-cone pathway caused by the disease (Johnston et al., 1999). Since the red-on-blue stimulus produces L and M cone dominated ERGs (Viswanathan et al., 1999; Rangaswamy et al., 2007; Sustar et al., 2009), it was initially desired to also assess the S-cone pathway by eliciting S-cone dominated ERGs using a blue flash (luminance = 55 cd/m^2) on a rod saturating amber background (luminance = 115 scot cd/m^2). Although the S-cone ERGs successfully recorded in some control participants and in two ADOA participants, this extended the entire duration of the experiments and increased patient fatigue. This aspect of the study was therefore discontinued. The parameters of the focal ERG were later used to record full field ERGs in order for the focal and full-field ERGs to be directly comparable.

As the PhNR of the flash ERG and the N95 of the PERG have been previously reported to share similar retinal origins (Viswanathan et al., 2000; Luo and Frishman, 2011), the retinotopic characteristics of the focal ERG and PERG were compared in Chapter 3. It was found that the focal ERG and PERG exhibited certain similar retinotopic characteristics. In both the focal ERG and PERG, the ERG waveforms recorded from the nasal macula were different from those recorded from the central and temporal macula. In addition, the amplitudes of their respective subcomponents recorded from the central macula were significantly larger than amplitudes from the nasal and temporal retinal. This agreed with histological data showing that neuronal densities in the central macula are greater than in the nasal or temporal macula (Curcio and Allen, 1990; Curcio et al., 1990). However, while the positive components of the focal ERG (b- and d-waves) and PERG (P50) in the nasal macula were significantly greater than in the temporal retina, the negative going components of the focal ERG (a-wave, PhNR-ON and PhNR-OFF) and PERG (N95) did not show significant differences. This was contrary to expectations as histological data shows that the neuronal density is significantly greater in the nasal macula than in the temporal macula. The identification of a new ERG component, the late component (LC), in addition to other factors such as luminance imbalance of the PERG stimulus and the intrusion of the optic nerve head component may have contributed to this discrepancy.

In spite of the similarities in the focal ERG and PERG, linear regression analysis found no significant relationship between the amplitudes of the focal long duration PhNRs (measured using peak-to-trough method) and the N95. This implied that the retinal origins of these components are not identical. This is a clinically relevant finding as it shows that the ERG subcomponents may assess different aspects of RGC function (Preiser et al. 2013)

In Chapter 4, the relationship between the PhNR (elicited by brief and long stimuli) and RGC density obtained from published data (Curcio and Allen, 1990; Watson, 2014) was evaluated. Linear regression analysis established a significant relationship between the PhNRs and RGC density. This showed that the PhNR reflected the distribution of RGCs in the retina and could therefore be used as a reliable measure of RGC function.

Chapters 5 – 7 constituted the main study of this thesis where the main aims presented in section 1.7 were addressed. Retinal function in twelve participants with ADOA and sixteen healthy age matched controls was assessed using focal (20°) and full-field ERGs produced in response to a long duration red flash (55 cd/m^2, 2Hz) on a rod saturating blue background (100 scot cd/m^2). Additional electrophysiological assessment included the PERG and the full-field ERG in response to a brief red flash on a rod saturating blue background. Baseline tests of visual function (VA, CS and VFT and colour vision) and structure (OCT) were also carried out.

The results of the studies carried out in this thesis demonstrated that ADOA affects both the ON and OFF RGC pathways. There was no evidence of a preferential effect on ON-RGCs as had been hypothesised based on previous findings in a mouse model of the disease. As noted previously in section 6.3.1, the evidence for the preferential loss of ON-RGCs in the mouse model was based on histological data showing significant dendritic pruning of ON-, but not OFF-centre RGCs, while this study assessed the effect of ADOA on the ON- and OFF-RGCs using the PhNR amplitude of the human ERG, a functional measure. The susceptibility of the PhNR amplitude to functional damage even when other functional and morphologic parameters remain normal makes it plausible that the PhNR-ON amplitudes may be selectively compromised at an earlier stage of the disease process than that studied here. A longitudinal study in pre-symptomatic people with the *OPA1* mutations or in people with ADOA at a much earlier stage of the disease (e.g. children with ADOA) could provide additional insights.

This thesis further demonstrated that the largest difference between participants in ADOA and controls was recorded in the central macula, followed by the temporal macula with the least difference being in the nasal macula. This confirmed that the central macula is the most susceptible part of the retina to ADOA. If the paracentral areas of the retina are relatively spared in ADOA as suggested by the results of this study, patients with ADOA may benefit from vision rehabilitation strategies that enhance the use of eccentric viewing training (Gaffney et al. 2014).

Differences in the ERGs between ADOA and control groups were not only observed in the amplitudes and times-to-peak of subcomponents, but also in the waveform of the ERG. The broadening of the d-wave peak in the focal ERG and the emergence of the late positive peak (2PP) in the full field ERG seen in the ADOA are examples of these waveform changes. When the waveform differences between ADOA and control groups are coupled with the waveform differences of the nasal and central/temporal macula, the method of using amplitude and time-to-peak to evaluate ERG components prove inadequate. Other methods of waveform analysis (e.g. principal component analysis, Fourier analysis, are required in assessing the ERG waveform in order capture more of the information contained therein. Such novel approaches to evaluating the ERG are currently being tried (Gauvin et al., 2014; Wood et al., 2014).

In light of ongoing studies to find a treatment for a number of hereditary optic neuropathies, of which ADOA is part (Yu-Wai-Man et al., 2014), the establishment of robust early biomarkers of disease and the quantification of RGC dysfunction is an essential prerequisite for human treatment trials. This thesis is important to the extent that it shows that the brief and long duration PhNRs are reliable and robust parameters for assessing RGC function in controls and dysfunction in diseases that compromise the integrity of RGCs. Furthermore, although the results of this study as well as a previous study in glaucoma (Preiser et al. 2014) indicated that the N95 amplitude of the PERG performed better than the PhNR amplitude at discriminating between disease and non-disease states, the difference was not statistically significant. The choice of one over the other can therefore be currently guided by practical considerations, namely PhNR requiring mydriasis and the PERG requiring an optimal retinal image (i.e., clear optics and adequate refractive correction) (Preiser et al 2014).

8.2 Study Limitations

A major limitation in this study was the small sample size of participants with ADOA and incomplete data for some participants. Nearly 70 individuals with known *OPA1* mutations were contacted from a nationwide database of about 200 patients who had been studied over the last 20 years by the primary

supervisor of this project (MV). However, many declined to participate in the study due to travel distance. Many of them were living between 100 – 200 miles of Cardiff. The group of five members in Family E expressed interest in the study, but were unwilling to come to Cardiff. This led to the setting up of a second site in City University, London. However, the use of an additional site led to the following technical challenges which prevented the collection of a complete dataset for some participants.

1. The monitors used for generating the PERG stimuli at the Cardiff and City sites were different. Although the luminance and check sizes at the City site were calibrated to match that of the Cardiff site, the PERG traces from City were different in form to those from Cardiff.
2. The Ganzfeld stimulator available at City was an Epsion Colour Dome while the one used at Cardiff, was an Electronica model. The properties of the brief flashes produced by the two systems were not identical.
3. As explained in the methods, the Topcon 2000 OCT available at the City site did not have the same data storage settings as the Topcon 1000 OCT in Cardiff. It was not, therefore, possible to analyse the data collected from the City site using the OCT Explorer.

Another limitation to this study relates to the different methods of measuring the PhNR amplitudes (Mortlock et al., 2010). This study used the peak to trough (Chapter 2 and 4), peak to fixed time (Chapter 3) and the baseline to trough (Chapter 5, 6 and 7) methods. It is possible that using a different method of assessing the PhNR amplitude (e.g. PhNR/b-wave ratio) could have produced different outcomes.

In spite of these limitations, the results of this research were consistent with previous reports indicating that the findings were not spurious. At the start of the study, an initial sample size of 14 participants (7 per group) was calculated based on the results reported by Miyata et al (2007). This gave a standardised difference of 1.48 with 80% power at a significance level of 0.05. The revised standardised difference calculated from the focal PhNR-ON amplitude in this present study is 1.60, giving a power of 98% at a significance level of 0.05 (or 90% at $p = 0.01$).

Previous studies of visual acuity loss, visual field loss and colour vision changes (Kjer, 1959; Krill et al., 1970; Kline and Glaser, 1979; Hoyt, 1980; Kjer et al., 1983; Berninger et al., 1991; Eliott et al., 1993; Kjer et al., 1996; Brown et al., 1997; Johnston et al., 1997; Simunovic et al., 1998; Votruba et al., 1998a; Votruba et al., 1998b; Johnston et al., 1999; Thiselton et al., 2002; Votruba et al., 2003a; Nakamura et al., 2006; Walters et al., 2006; Cohn et al., 2008; Yu-Wai-Man et al., 2010a; Yu-Wai-Man et al., 2010b; Almind et al., 2012; Reis et al., 2013; Ronnback et al., 2013) as well as thinning of the retina (Ito et al., 2007; Barboni et al., 2010; Milea et al., 2010; Barboni et al., 2011; Gocho et al., 2013; Russo et al., 2013; Carbonelli et al., 2015) have shown changes associated with ADOA which are in keeping with the findings of this research. Furthermore, these studies have shown a similar wide phenotypic variability between individuals, which may be attributable to genetic heterogeneity. This corroboration of previous studies again supports the validity of the findings of this PhD.

8.3 Future Directions

ERG components have been traditionally assessed by measuring their amplitudes and times-to-peak. However, the weaknesses in this approach are becoming increasingly evident. Further research into developing a new paradigm of evaluating the ERG response which does not rely on amplitude and time-to-peak would therefore be highly valuable in future.

The ERG provides a reliable and robust objective assessment of retinal function. The long duration ERG especially provides the unique opportunity to dissect ON and OFF pathways in vivo and has been used in assessing diseases of the visual system that preferentially affect one pathway or the other (e.g. congenital stationary night blindness). However, its clinical use is limited by the longer recording times, especially for the low amplitude focal response. For example, it took an average of one hour to record focal ERGs from the central, nasal and temporal macula (i.e. at least 20 mins per location). It would therefore be of interest to develop recording protocols that cut recording times at least in half. This may involve improvements in the hardware for ERG

recordings; for example, developing better amplifiers or more sensitive electrodes to improve the signal to noise ratio so that fewer responses are required for averaging or the development of more sensitive electrodes. Alternatively, more cost-effective approaches which would look into optimising recording techniques could be investigated (e.g. investigations into optimum electrode placement and minimum duration of stimulus flash required to obtain an optimum separation of ON and OFF components).

In Chapter 7, the significant relationship between the PhNR-OFF and ageing in participants with ADOA was interesting and would require further probing. A longitudinal study or a cross sectional study with sufficient numbers in appropriate age bins could be conducted in future to look into this.

REFERENCES

Aguilar, M. and Stiles, W. S. (1954). Saturation of the rod mechanism of the retina at high levels of stimulation. *Optica Acta* **1:**59-65.

Aijaz, S., Erskine, L., Jeffery, G., Bbattacharya, S. S. and Votruba, M. (2004). Developmental expression profile of the optic atrophy gene product: OPA1 is not localized exclusively in the mammalian retinal ganglion cell layer. *Investigative Ophthalmology and Visual Science* **45:**1667-1673.

Alavi, M. V., Bette, S., Schimpf, S., Schuettauf, F., Schraermeyer, U., Wehrl, H. F., Ruttiger, L., et al. (2007). A splice site mutation in the murine Opa1 gene features pathology of autosomal dominant optic atrophy. *Brain* **130:**1029-1042.

Alexander, C., Votruba, M., Pesch, U. E. A., Thiselton, D. L., Mayer, S., Moore, A., Rodriguez, M., et al. (2000). OPA1, encoding a dynamin-related GTPase, is mutated in autosomal dominant optic atrophy linked to chromosome 3q28. *Nature Genetics* **26:**211-215.

Almind, G. J., Ek, J., Rosenberg, T., Eiberg, H., Larsen, M., LuCamp, L., Brondum-Nielsen, K., et al. (2012). Dominant optic atrophy in Denmark - report of 15 novel mutations in OPA1, using a strategy with a detection rate of 90%. *BMC Medical Genetics* **13:**1-7.

Altman, D. G. 1991. *Practical statistics for medical research*, London: Chapman and Hall.

Amati-Bonneau, P., Guichet, A., Olichon, A., Chevrollier, A., Viala, F., Miot, S., Ayuso, C., et al. (2005). OPA1 R445H mutation in optic atrophy associated with sensorineural deafness. *Annals of Neurology* **58:**958-963.

Amati-Bonneau, P., Milea, D., Bonneau, D., Chevrollier, A., Ferre, M., Guillet, V., Gueguen, N., et al. (2009). OPA1-associated disorders: phenotypes and pathophysiology. *International Journal of Biochemistry and Cell Biology* **41:**1855-1865.

Amati-Bonneau, P., Valentino, M. L., Reynier, P., Gallardo, M. E., Bornstein, B., Boissiere, A., Campos, Y., et al. (2008). OPA1 mutations induce mitochondrial DNA instability and optic atrophy 'plus' phenotypes. *Brain* **131:**338-351.

Anikster, Y., Kleta, R., Shaag, A., Gahl, W. A. and Elpeleg, O. (2001). Type III 3-methylglutaconic aciduria (optic atrophy plus syndrome, or Costeff optic atrophy syndrome): Identification of the OPA3 gene and its founder mutation in Iraqi Jews. *American Journal of Human Genetics* **69:**1218-1224.

Arden, G., Wolf, J., Berninger, T., Hogg, C. R., Tzekov, R. and Holder, G. E. (1999). S-cone ERGs elicited by a simple technique in normals and in tritanopes. *Vision Research* **39:**641-650.

Arden, G. B., Vaegan and Hogg, C. R. (1982). Clinical and experimental evidence that the pattern electroretinogram (PERG) is generated in more proximal retinal layers than the focal electroretinogram (FERG). *Annals of the New York Academy of Sciences* **388:**580-607.

Asi, H. and Perlman, I. (1992). Relationships between the electroretinogram a-wave, b-wave and oscillatory potentials and their application to clinical-diagnosis. *Documenta Ophthalmologica* **79:**125-139.

Assink, J. J. M., Tijmes, N. T., tenBrink, J. B., Oostra, R. J., Riemslag, F. C., deJong, P. and Bergen, A. A. B. (1997). A gene for X-linked optic atrophy is closely linked to the Xp11.4-Xp11.2 region of the X chromosome. *American Journal of Human Genetics* **61:**934-939.

Bach, M., Brigell, M. G., Hawlina, M., Holder, G. E., Johnson, M. A., McCulloch, D. L., Meigen, T., et al. (2013). ISCEV standard for clinical pattern electroretinography (PERG): 2012 update. *Documenta Ophthalmologica* **126:**1-7.

Bach, M., Gerling, J. and Geiger, K. (1992). Optic atrophy reduces the pattern-electroretinogram for both fine and coarse stimulus patterns. *Clinical Vision Sciences* **7:**327-333.

Bach, M. and Hoffmann, M. B. 2006. The origin of the pattern electroretinogram. *In:* Heckenlively, J. R. and Arden, G. B. (eds.) *Principles and practice of clinical electrophysiology of vision.* Cambridge, London: The MIT Press.

Bach, M. and Hoffmann, M. B. (2008). Update on the pattern electroretinogram in glaucoma. *Optometry and Vision Science* **85:**386-395.

Bach, M. and Poloschek, C. M. (2013). Electrophysiology and glaucoma: current status and future challenges. *Cell and Tissue Research* **353:**287-296.

Bailey, I. L. and Lovie, J. E. (1976). New design principles for visual acuity letter charts. *American Journal of Optometry and Physiological Optics* **53:**740-745.

Baker, C. L., Jr., Hess, R. R., Olsen, B. T. and Zrenner, E. (1988). Current source density analysis of linear and non-linear components of the primate electroretinogram. *Journal of Physiology* **407:**155-176.

Baker, M. R., Fisher, K. M., Whittaker, R. G., Griffiths, P. G., Yu-Wai-Man, P. and Chinnery, P. F. (2011). Subclinical multisystem neurologic disease in "pure" OPA1 autosomal dominant optic atrophy. *Neurology* **77:**1309-1312.

Barbet, F., Gerber, S., Hakiki, S., Perrault, I., Hanein, S., Ducroq, D., Tanguy, G., et al. (2003). A first locus for isolated autosomal recessive optic atrophy (ROA1) maps to chromosome 8q. *European Journal of Human Genetics* **11:**966-971.

Barbet, F., Hakiki, S., Orssaud, C., Gerber, S., Perrault, I., Hanein, S., Ducroq, D., et al. 2005. A third locus for dominant optic atrophy on chromosome 22q. *Journal of Medical Genetics.* England.

Barboni, P., Carbonelli, M., Savini, G., Foscarini, B., Parisi, V., Valentino, M. L., Carta, A., et al. (2010). OPA1 mutations associated with dominant optic atrophy influence optic nerve head size. *Ophthalmology* **117:**1547-1553.

Barboni, P., Savini, G., Cascavilla, M. L., Caporali, L., Milesi, J., Borrelli, E., La Morgia, C., et al. (2014). Early macular retinal ganglion cell loss in dominant optic atrophy: genotype-phenotype correlation. *American Journal of Ophthalmology* **158:**628-636.e623.

Barboni, P., Savini, G., Parisi, V., Carbonelli, M., La Morgia, C., Maresca, A., Sadun, F., et al. (2011). Retinal nerve fiber layer thickness in dominant optic atrophy: measurements by optical coherence tomography and correlation with age. *Ophthalmology* **118:**2076-2080.

Barboni, P., Valentino, M. L., La Morgia, C., Carbonelli, M., Savini, G., De Negri, A., Simonelli, F., et al. 2013. Idebenone treatment in patients with OPA1-mutant dominant optic atrophy. *Brain.* England.

Barlow, H. B. (1953). Summation and inhibition in the frog's retina. *Journal of Physiology* **119:**69-88.

Barnard, A. R., Issa, P. C., Perganta, G., Williams, P. A., Davies, V. J., Sekaran, S., Votruba, M., et al. (2011). Specific deficits in visual electrophysiology in a mouse model of dominant optic atrophy. *Experimental Eye Research* **93:**771-777.

Barron, M. J., Griffiths, P., Turnbull, D. M., Bates, D. and Nichols, P. (2004). The distributions of mitochondria and sodium channels reflect the specific energy requirements and conduction properties of the human optic nerve head. *British Journal of Ophthalmology* **88:**286-290.

Batten, B. (1896). A family suffering hereditary optic atrophy. *Transactions of the Ophthalmological Societies of the United Kingdom* **16**.

Berninger, T. A., Jaeger, W. and Krastel, H. (1991). Electrophysiology and color perimetry in dominant infantile optic atrophy. *British Journal of Ophthalmology* **75:**49-52.

Binns, A. M., Mortlock, K. E. and North, R. V. (2011). The relationship between stimulus intensity and response amplitude for the photopic negative response of the flash electroretinogram. *Documenta Ophthalmologica* **122:**39-52.

Birch, J. (2008). Pass rates for the Farnsworth D15 colour vision test. *Ophthalmic and Physiological Optics* **28:**259-264.

Bonifert, T., Karle, K. N., Tonagel, F., Batra, M., Wilhelm, C., Theurer, Y., Schoenfeld, C., et al. (2014). Pure and syndromic optic atrophy explained by deep intronic OPA1 mutations and an intralocus modifier. *Brain* **137:**2164-2177.

Bonneau, D., Souied, E., Gerber, S., Rozet, J. M., D'Haens, E., Journel, H., Plessis, G., et al. (1995). No evidence of genetic heterogeneity in dominant optic atrophy. *Journal of Medical Genetics* **32:**951-953.

Bowmaker, J. K. and Dartnall, H. J. (1980). Visual pigments of rods and cones in a human retina. *Journal of Physiology* **298:**501-511.

Bowmaker, J. K., Dartnall, H. J. and Mollon, J. D. (1980). Microspectrophotometric demonstration of four classes of photoreceptor in an old world primate, Macaca fascicularis. *Journal of Physiology* **298:**131-143.

Boycott, B. B. and Wassle, H. (1991). Morphological classification of bipolar cells of the primate retina. *European Journal of Neuroscience* **3:**1069-1088.

Bremner, F. D., Tomlin, E. A., Shallo-Hoffmann, J., Votruba, M. and Smith, S. E. (2001). The pupil in dominant optic atrophy. *Investigative Ophthalmology and Visual Science* **42:**675-678.

Brigell, M., Bach, M., Barber, C., Moskowitz, A. and Robson, J. (2003). Guidelines for calibration of stimulus and recording parameters used in clinical electrophysiology of vision. *Documenta Ophthalmologica* **107:**185-193.

Brindley, G. S. and Westheimer, G. (1965). The spatial properties of the human electroretinogram. *Journal of Physiology* **179:**518-537.

Bristow, E. A., Griffiths, P. G., Andrews, R. M., Johnson, M. A. and Turnbull, D. M. (2002). The distribution of mitochondrial activity in relation to optic nerve structure. *Archives of Ophthalmology* **120:**791-796.

Brown, J., Jr., Fingert, J. H., Taylor, C. M., Lake, M., Sheffield, V. C. and Stone, E. M. (1997). Clinical and genetic analysis of a family affected with dominant optic atrophy (OPA1). *Archives of Ophthalmology* **115:**95-99.

Brown, K. T. (1968). The electroretinogram: Its components and their origins. *Vision Research* **8:**633-IN636.

Brown, K. T., Watanabe, K. and Murakami, M. (1965). Early and late receptor potentials of monkey cones and rods. *Cold Spring Harbor Symposia on Quantitative Biology* **30:**457-482.

Brown, K. T. and Wiesel, T. N. (1961a). Analysis of intraretinal electroretinogram in intact cat eye. *Journal of Physiology-London* **158:**229-256.

Brown, K. T. and Wiesel, T. N. (1961b). Localization of origins of electroretinogram components by intraretinal recording in intact cat eye. *Journal of Physiology-London* **158:**257-280.

Bui, B. V. and Fortune, B. (2004). Ganglion cell contributions to the rat full-field electroretinogram. *Journal of Physiology-London* **555:**153-173.

Bush, R. A. and Sieving, P. A. (1994). A proximal retinal component in the primate photopic ERG a-wave. *Investigative Ophthalmology and Visual Science* **35:**635-645.

Calkins, D. J. (2001). Seeing with S cones. *Progress in Retinal and Eye Research* **20:**255-287.

Callaway, E. M. (2005). Structure and function of parallel pathways in the primate early visual system. *Journal of Physiology* **566:**13-19.

Carbonelli, M., La Morgia, C., Savini, G., Cascavilla, M. L., Borrelli, E., Chicani, F., do V. F. Ramos, C., et al. (2015). Macular microcysts in mitochondrial optic neuropathies: prevalence and retinal layer thickness measurements. *PloS One* **10:**e0127906.

Carelli, V., La Morgia, C., Valentino, M. L., Barboni, P., Ross-Cisneros, F. N. and Sadun, A. A. (2009). Retinal ganglion cell neurodegeneration in mitochondrial inherited disorders. *Biochimica et Biophysica Acta (BBA) - Bioenergetics* **1787:**518-528.

Carelli, V., Ross-Cisneros, F. N. and Sadun, A. A. (2004). Mitochondrial dysfunction as a cause of optic neuropathies. *Progress in Retinal and Eye Research* **23:**53-89.

Carelli, V., Schimpf, S., Fuhrmann, N., Valentino, M. L., Zanna, C., Iommarini, L., Papke, M., et al. (2011). A clinically complex form of dominant optic atrophy (OPA8) maps on chromosome 16. *Human Molecular Genetics* **20:**1893-1905.

Carkeet, A. (2001). Modeling logMAR visual acuity scores: Effects of termination rules and alternative forced-choice options. *Optometry and Vision Science* **78:**529-538.

Casagrande, V. A., Yazar, F., Jones, K. D. and Ding, Y. (2007). The morphology of the koniocellular axon pathway in the macaque monkey. *Cerebral Cortex* **17:**2334-2345.

Chen, H., Wu, D., Huang, S. and Yan, H. (2006). The photopic negative response of the flash electroretinogram in retinal vein occlusion. *Documenta Ophthalmologica* **113:**53-59.

Chen, H., Zhang, M., Huang, S. and Wu, D. (2008). The photopic negative response of flash ERG in nonproliferative diabetic retinopathy. *Documenta Ophthalmologica* **117:**129-135.

Chen, H. C. and Chan, D. C. (2005). Emerging functions of mammalian mitochondrial fusion and fission. *Human Molecular Genetics* **14:**R283-R289.

Chen, Y., Jia, X., Wang, P., Xiao, X., Li, S., Guo, X. and Zhang, Q. (2013). Mutation survey of the optic atrophy 1 gene in 193 Chinese families with suspected hereditary optic neuropathy. *Molecular Vision* **19:**292-302.

Chichilnisky, E. J. and Kalmar, R. S. (2002). Functional asymmetries in ON and OFF ganglion cells of primate retina. *Journal of Neuroscience* **22:**2737-2747.

Chylack, L. T. J., Wolfe, J. K., Singer, D. M., C., L. M., A, B. M., L, B. I., J., F., et al. (1993). The lens opacities classification system III. *Archives of Ophthalmology* **111:**831-836.

Cohen, J. 1988. *Statistical power analysis for the behavioral sciences*, 2nd, Hillsdale, NJ: Lawrence Erlbaum Associates.

Cohn, A. C., Toomes, C., Hewitt, A. W., Kearns, L. S., Inglehearn, C. F., Craig, J. E. and Mackey, D. A. (2008). The natural history of OPA1-related autosomal dominant optic atrophy. *British Journal of Ophthalmology* **92:**1333-1336.

Cohn, A. C., Toomes, C., Potter, C., Towns, K. V., Hewitt, A. W., Inglehearn, C. F., Craig, J. E., et al. (2007). Autosomal dominant optic atrophy: penetrance and expressivity in patients with OPA1 mutations. *American Journal of Ophthalmology* **143:**656-662.

Colotto, A., Falsini, B., Salgarello, T., Iarossi, G., Galan, M. E. and Scullica, L. (2000). Photopic negative response of the human ERG: losses associated with glaucomatous damage. *Investigative Ophthalmology and Visual Science* **41:**2205-2211.

Coupland, S. G. 2006. Electrodes for visual testing. *In:* Heckenlively, J. R. and Arden, G. B. (eds.) *Principles and practice of clinical electrophysiology of vision.* 2 ed. London: MIT Press.

Croner, L. J. and Kaplan, E. (1995). Receptive-fields of p-ganglion and m-ganglion cells across the primate retina. *Vision Research* **35:**7-24.

Curcio, C. A. and Allen, K. A. (1990). Topography of ganglion-cells in human retina. *Journal of Comparative Neurology* **300:**5-25.

Curcio, C. A., Millican, C. L., Allen, K. A. and Kalina, R. E. (1993). Aging of the human photoreceptor mosaic: evidence for selective vulnerability of rods in central retina. *Investigative Ophthalmology and Visual Science* **34:**3278-3296.

Curcio, C. A., Sloan, K. R., Kalina, R. E. and Hendrickson, A. E. (1990). Human photoreceptor topography. *Journal of Comparative Neurology* **292:**497-523.

Dacey, D. 2004. Origins of perception: retinal ganglion cell diversity and the creation of parallel visual pathways. *In:* Gazzaniga, M. S. (ed.) *The cognitive neurosciences.* 3 ed. Cambridge, MA: MIT.

Dacey, D., Packer, O. S., Diller, L., Brainard, D., Peterson, B. and Lee, B. (2000). Center surround receptive field structure of cone bipolar cells in primate retina. *Vision Research* **40:**1801-1811.

Dacey, D. M. (1993a). Morphology of a small-field bistratified ganglion cell type in the macaque and human retina. *Visual Neuroscience* **10:**1081-1098.

Dacey, D. M. (1993b). The mosaic of midget ganglion cells in the human retina. *Journal of Neuroscience* **13:**5334-5355.

Dacey, D. M. (1996). Circuitry for color coding in the primate retina. *Proceedings of the National Academy of Sciences of the United States of America* **93:**582-588.

Dacey, D. M. and Lee, B. B. (1994). The 'blue-on' opponent pathway in primate retina originates from a distinct bistratified ganglion cell type. *Nature* **367:**731-735.

Dacey, D. M. and Petersen, M. R. (1992). Dendritic field size and morphology of midget and parasol ganglion-cells of the human retina. *Proceedings of the National Academy of Sciences of the United States of America* **89:**9666-9670.

Dacey, D. M., Peterson, B. B., Robinson, F. R. and Gamlin, P. D. (2003). Fireworks in the primate retina: in vitro photodynamics reveals diverse LGN-projecting ganglion cell types. *Neuron* **37:**15-27.

Davies, V. and Votruba, M. (2006). Focus on molecules: The OPA1 protein. *Experimental Eye Research* **83:**1003-1004.

Davies, V. J., Hollins, A. J., Piechota, M. J., Yip, W., Davies, J. R., White, K. E., Nicols, P. P., et al. (2007). Opa1 deficiency in a mouse model of autosomal dominant optic atrophy impairs mitochondrial morphology, optic nerve structure and visual function. *Human Molecular Genetics* **16:**1307-1318.

Delettre, C., Griffoin, J. M., Kaplan, J., Dollfus, H., Lorenz, B., Faivre, L., Lenaers, G., et al. (2001). Mutation spectrum and splicing variants in the OPA1 gene. *Human Genetics* **109:**584-591.

Delettre, C., Lenaers, G., Griffoin, J. M., Gigarel, N., Lorenzo, C., Belenguer, P., Pelloquin, L., et al. (2000). Nuclear gene OPA1, encoding a mitochondrial

dynamin-related protein, is mutated in dominant optic atrophy. *Nature Genetics* **26:**207-210.

Delettre, C., Lenaers, G., Pelloquin, L., Belenguer, P. and Hamel, C. P. (2002). OPA1 (Kjer type) dominant optic atrophy: A novel mitochondrial disease. *Molecular Genetics and Metabolism* **75:**97-107.

Desir, J., Coppieters, F., van Regemorter, N., De Baere, E., Abramowicz, M. and Cordonnier, M. (2012). TMEM126A mutation in a Moroccan family with autosomal recessive optic atrophy. *Molecular Vision* **18:**1849-1857.

Desmet, K. D., Paz, D. A., Corry, J. J., Eells, J. T., Wong-Riley, M. T., Henry, M. M., Buchmann, E. V., et al. (2006). Clinical and experimental applications of NIR-LED photobiomodulation. *Photomedicine and Laser Surgery* **24:**121-128.

Drasdo, N., Aldebasi, Y. H., Chiti, Z., Mortlock, K. E., Morgan, J. E. and North, R. V. (2001). The S-cone PhNR and pattern ERG in primary open angle glaucoma. *Investigative Ophthalmology and Visual Science* **42:**1266-1272.

Drasdo, N. and Fowler, C. W. (1974). Non-linear projection of the retinal image in a wide-angle schematic eye. *The British Journal of Ophthalmology* **58:**709-714.

Drasdo, N., Millican, C. L., Katholi, C. R. and Curcio, C. A. (2007). The length of Henle fibers in the human retina and a model of ganglion receptive field density in the visual field. *Vision Research* **47:**2901-2911.

Drasdo, N., Thompson, D. A., Thompson, C. M. and Edwards, L. (1987). Complementary components and local variations of the pattern electroretinogram. *Investigative Ophthalmology and Visual Science* **28:**158-162.

Dutta, S. and Sengupta, P. (2016). Men and mice: Relating their ages. *Life Sciences* **152:**244-248.

Efron, N. (1998). Efron grading scales for contact lens complications. *Ophthalmic and Physiological Optics* **18:**182-186.

Eiberg, H., Kjer, B., Kjer, P. and Rosenberg, T. (1994). Dominant optic atrophy (OPA1) mapped to chromosome 3q region. I. Linkage analysis. *Human Molecular Genetics* **3:**977-980.

Elachouri, G., Vidoni, S., Zanna, C., Pattyn, A., Boukhaddaoui, H., Gaget, K., Yu-Wai-Man, P., et al. (2011). OPA1 links human mitochondrial genome maintenance to mtDNA replication and distribution. *Genome Research* **21:**12-20.

Eliott, D., Traboulsi, E. I. and Maumenee, I. H. (1993). Visual prognosis in autosomal dominant optic atrophy (Kjer type). *American Journal of Ophthalmology* **115:**360-367.

Elliot, D. 2006. Contrast sensitivity and glare testing. *In:* Benjamin, W. J. (ed.) *Borish's Clinical Refraction.* 2 ed.: Butterworth-Heinemann.

Elliot, D. 2007. *Clinical procedures in primary eye care*, 3: Elsevier.

Errico, P., Falsini, B., Porciatti, V. and Cefala, F. M. (1990). The human focal electroretinogram as a function of stimulus area. *Documenta Ophthalmologica* **75:**41-48.

Euler, T., Haverkamp, S., Schubert, T. and Baden, T. (2014). Retinal bipolar cells: elementary building blocks of vision. *Nature Reviews: Neuroscience* **15:**507-519.

Evers, H. U. and Gouras, P. (1986). Three cone mechanisms in the primate electroretinogram: two with, one without off-center bipolar responses. *Vision Research* **26:**245-254.

Ferre, M., Amati-Bonneau, P., Tourmen, Y., Malthiery, Y. and Reynier, P. (2005). eOPA1: An online database for OPA1 mutations. *Human Mutation* **25:**423-428.

Ferre, M., Bonneau, D., Milea, D., Chevrollier, A., Verny, C., Dollfus, H., Ayuso, C., et al. (2009). Molecular Screening of 980 Cases of Suspected Hereditary Optic Neuropathy with a Report on 77 Novel OPA1 Mutations. *Human Mutation* **30:**692-705.

Ferre, M., Caignard, A., Milea, D., Leruez, S., Cassereau, J., Chevrollier, A., Amati-Bonneau, P., et al. (2015). Improved locus-specific database for OPA1 mutations allows inclusion of advanced clinical data. *Human Mutation* **36:**20-25.

Ferris, F. L., 3rd and Bailey, I. (1996). Standardizing the measurement of visual acuity for clinical research studies: Guidelines from the Eye Care Technology Forum. *Ophthalmology* **103:**181-182.

Ferris, F. L., 3rd, Kassoff, A., Bresnick, G. H. and Bailey, I. (1982). New visual acuity charts for clinical research. *American Journal of Ophthalmology* **94:**91-96.

Ferris, F. L., Davis, M. D., Clemons, T. E., Lee, L. Y., Chew, E. Y., Lindblad, A. S., Milton, R. C., et al. (2005). A simplified severity scale for age-related macular degeneration - AREDS report no. 18. *Archives of Ophthalmology* **123:**1570-1574.

Fishman, G. A. 2001. The Electroretinogram. *Ophthalmology monograph 2, Electrophysiologic testing in the retina, optic nerve and visual pathway.* 2nd ed.

Fortune, B., Bui, B. V., Cull, G., Wang, L. and Cioffi, G. A. (2004). Inter-ocular and inter-session reliability of the electroretinogram photopic negative response (PhNR) in non-human primates. *Experimental Eye Research* **78:**83-93.

Frishman, L. J. 2006. Origins of the electroretinogram. *In:* Heckenlively, J. R. and Arden, G. B. (eds.) *Principles and practice of clinical electrophysiology of vision.* London, England.

Frishman, L. J., Reddy, M. G. and Robson, J. G. (1996). Effects of background light on the human dark-adapted electroretinogram and psychophysical threshold. *Journal of the Optical Society of America A: Optics and Image Science* **13:**601-612.

Frishman, L. J., Robson, J. G. and Du, L. (1993). Contributions of the positive and negative scotopic threshold responses to the scotopic cat. *Investigative Ophthalmology and Visual Science* **34:**1273-1273.

Fuhrmann, N., Schimpf, S., Kamenisch, Y., Leo-Kottler, B., Alexander, C., Auburger, G., Zrenner, E., et al. (2010). Solving a 50 year mystery of a missing OPA1 mutation: more insights from the first family diagnosed with autosomal dominant optic atrophy. *Molecular Neurodegeneration* **5**.

Gallus, G. N., Cardaioli, E., Rufa, A., Collura, M., Da Pozzo, P., Pretegiani, E., Tumino, M., et al. (2012). High frequency of OPA1 mutations causing high ADOA prevalence in south-eastern Sicily, Italy. *Clinical Genetics* **82:**277-282.

Gao, H. and Hollyfield, J. G. (1992). Aging of the human retina. Differential loss of neurons and retinal pigment epithelial cells. *Investigative Ophthalmology and Visual Science* **33:**1-17.

Garvin, M. K., Abramoff, M. D., Kardon, R., Russell, S. R., Wu, X. and Sonka, M. (2008). Intraretinal layer segmentation of macular optical coherence tomography images using optimal 3-D graph search. *IEEE Transactions on Medical Imaging* **27:**1495-1505.

Garvin, M. K., Abramoff, M. D., Wu, X., Russell, S. R., Burns, T. L. and Sonka, M. (2009). Automated 3-D intraretinal layer segmentation of macular spectral-domain optical coherence tomography images. *IEEE Transactions on Medical Imaging* **28:**1436-1447.

Garway-Heath, D. F., Holder, G. E., Fitzke, F. W. and Hitchings, R. A. (2002). Relationship between electrophysiological, psychophysical, and anatomical measurements in glaucoma. *Investigative Ophthalmology and Visual Science* **43:**2213-2220.

Gauvin, M., Lina, J. M. and Lachapelle, P. (2014). Advance in ERG analysis: from peak time and amplitude to frequency, power, and energy. *BioMed research international* **2014:**246096.

Gocho, K., Kikuchi, S., Kabuto, T., Kameya, S., Shinoda, K., Mizota, A., Yamaki, K., et al. (2013). High-Resolution En Face Images of Microcystic Macular Edema in Patients with Autosomal Dominant Optic Atrophy. *BioMed Research International* **2013:**676803.

Gotoh, Y., Machida, S. and Tazawa, Y. (2004). Selective loss of the photopic negative response in patients with optic nerve atrophy. *Archives of Ophthalmology* **122:**341-346.

Gouras, P., MacKay, C. J. and Yamamoto, S. (1993). The human S-cone electroretinogram and its variation among subjects with and without L and M-cone function. *Investigative Ophthalmology and Visual Science* **34:**2437-2442.

Granit, R. (1933). The components of the retinal action potential in mammals and their relation to the discharge in the optic nerve. *Journal of Physiology (London)* **77:**207-240.

Granse, L., Bergstrand, I., Thiselton, D., Ponjavic, V., Heijl, A., Votruba, M. and Andreasson, S. (2003). Electrophysiology and ocular blood flow in a family with dominant optic nerve atrophy and a mutation in the OPA1 gene. *Ophthalmic Genetics* **24:**233-245.

Grosvenor, T. 2007. *Primary care optometry*, 5th, St. Louis, Missouri: Butteworth-Heinemann/Elsevier.

Guedes, V., Schuman, J. S., Hertzmark, E., Wollstein, G., Correnti, A., Mancini, R., Lederer, D., et al. (2003). Optical coherence tomography measurement of macular and nerve fiber layer thickness in normal and glaucomatous human eyes. *Ophthalmology* **110:**177-189.

Hack, I., Peichl, L. and Brandstatter, J. H. (1999). An alternative pathway for rod signals in the rodent retina: rod photoreceptors, cone bipolar cells, and the localization of glutamate receptors. *Proceedings of the National Academy of Sciences of the United States of America* **96:**14130-14135.

Hanein, S., Garcia, M., Fares-Taie, L., Serre, V., De Keyzer, Y., Delaveau, T., Perrault, I., et al. (2013). TMEM126A is a mitochondrial located mRNA (MLR) protein of the mitochondrial inner membrane. *Biochimica et Biophysica Acta* **1830:**3719-3733.

Hanein, S., Perrault, I., Roche, O., Gerber, S., Khadom, N., Rio, M., Boddaert, N., et al. (2009). TMEM126A, encoding a mitochondrial protein, is mutated in autosomal-recessive nonsyndromic optic atrophy. *American Journal of Human Genetics* **84:**493-498.

Hanley, J. A. and McNeil, B. J. (1983). A method of comparing the areas under receiver operating characteristic curves derived from the same cases. *Radiology* **148:**839-843.

Harrison, J. M., O'Connor, P. S., Young, R. S., Kincaid, M. and Bentley, R. (1987). The pattern ERG in man following surgical resection of the optic nerve. *Investigative Ophthalmology and Visual Science* **28:**492-499.

Harrison, W. W., Viswanathan, S. and Malinovsky, V. E. (2006). Multifocal pattern electroretinogram: Cellular origins and clinical implications. *Optometry and Vision Science* **83:**473-485.

Hartline, H. K. (1938). The response of single optic nerve fibers of the vertebrate eye to illumination of the retina. *American Journal of Physiology* **121:**400-415.

Harwerth, R. S., Crawford, M. L. J., Frishman, L. J., Viswanathan, S., Smith Iii, E. L. and Carter-Dawson, L. (2002). Visual field defects and neural losses from experimental glaucoma. *Progress in Retinal and Eye Research* **21:**91-125.

Hashemi, H., Khabazkhoob, M., Miraftab, M., Emamian, M. H., Shariati, M., Abdolahinia, T. and Fotouhi, A. (2012). The distribution of axial length, anterior chamber depth, lens thickness, and vitreous chamber depth in an adult population of Shahroud, Iran. *BMC Ophthalmology* **12:**50.

Hebert, M., Vaegan and Lachapelle, P. (1999). Reproducibility of ERG responses obtained with the DTL electrode. *Vision Research* **39:**1069-1070.

Hendry, S. H. C. and Reid, R. C. (2000). The koniocellular pathway in primate vision. *Annual Review of Neuroscience* **23:**127-153.

Heymann, J. A. W. and Hinshaw, J. E. (2009). Dynamins at a glance. *Journal of Cell Science* **122:**3427-3431.

Heynen, H. and van Norren, D. (1985). Origin of the electroretinogram in the intact macaque eye--II. Current source-density analysis. *Vision Research* **25:**709-715.

Holder, G. E. (1997). The pattern electroretinogram in anterior visual pathway dysfunction and its relationship to the pattern visual evoked potential: A personal clinical review of 743 eyes. *Eye* **11:**924-934.

Holder, G. E. (2001). Pattern electroretinography (PERG) and an integrated approach to visual pathway diagnosis. *Progress in Retinal and Eye Research* **20:**531-561.

Holder, G. E., Gale, R. P., Acheson, J. F. and Robson, A. G. (2009). Electrodiagnostic assessment in optic nerve disease. *Current Opinion in Neurology* **22:**3.

Holder, G. E., Votruba, M., Carter, A. C., Bhattacharya, S. S., Fitzke, F. W. and Moore, A. T. (1998). Electrophysiological findings in dominant optic atrophy (DOA) linking to the OPA1 locus on chromosome 3q 28-qter. *Documenta Ophthalmologica* **95:**217-228.

Hood, D. C., Anderson, S. C., Wall, M., Raza, A. S. and Kardon, R. H. (2009). A test of a linear model of glaucomatous structure-function loss reveals sources of variability in retinal nerve fiber and visual field measurements. *Investigative Ophthalmology and Visual Science* **50:**4254-4266.

Hood, D. C., Bach, M., Brigell, M., Keating, D., Kondo, M., Lyons, J. S., Marmor, M. F., et al. (2012). ISCEV standard for clinical multifocal electroretinography (mfERG) (2011 edition). *Documenta Ophthalmologica* **124:**1-13.

Hood, D. C. and Birch, D. G. (1993). Human cone receptor activity: the leading edge of the a-wave and models of receptor activity. *Visual Neuroscience* **10:**857-871.

Hood, D. C., Frishman, L. J., Saszik, S. and Viswanathan, S. (2002). Retinal origins of the primate multifocal ERG: Implications for the human response. *Investigative Ophthalmology and Visual Science* **43:**1673-1685.

Hood, D. C., Greenstein, V., Frishman, L., Holopigian, K., Viswanathan, S., Seiple, W., Ahmed, J., et al. (1999). Identifying inner retinal contributions to the human multifocal ERG. *Vision Research* **39:**2285-2291.

Hood, D. C. and Kardon, R. H. (2007). A framework for comparing structural and functional measures of glaucomatous damage. *Progress in Retinal and Eye Research* **26:**688-710.

Horn, F. K., Gottschalk, K., Mardin, C. Y., Pangeni, G., Junemann, A. G. and Kremers, J. (2011). On and off responses of the photopic fullfield ERG in normal subjects and glaucoma patients. *Documenta Ophthalmologica* **122:**53-62.

Hoyt, C. S. (1980). Autosomal dominant optic atrophy - a spectrum of disability. *Ophthalmology* **87:**245-251.

Huang, T., Santarelli, R. and Starr, A. (2009). Mutation of OPA1 gene causes deafness by affecting function of auditory nerve terminals. *Brain Research* **1300:**97-104.

Hudson, G., Amati-Bonneau, P., Blakely, E. L., Stewart, J. D., He, L., Schaefer, A. M., Griffiths, P. G., et al. (2008). Mutation of OPA1 causes dominant optic atrophy with external ophthalmoplegia, ataxia, deafness and multiple mitochondrial DNA deletions: a novel disorder of mtDNA maintenance. *Brain* **131:**329-337.

Huizing, M., Dorward, H., Ly, L., Klootwijk, E., Kleta, R., Skovby, F., Pei, W., et al. (2010). OPA3, mutated in 3-methylglutaconic aciduria type III, encodes two transcripts targeted primarily to mitochondria. *Molecular Genetics and Metabolism* **100:**149-154.

Hulley, S. B., Cummings, S. R., Browner, W. S., Grady, D. and B., N. T. 2013. *Designing clinical research: an epidemiologic approach*, Philadelphia, PA: Lippincott Williams and Wilkins.

Ito, Y., Nakamura, M., Yamakoshi, T., Lin, J., Yatsuya, H. and Terasaki, H. (2007). Reduction of inner retinal thickness in patients with autosomal dominant optic atrophy associated with OPA1 mutations. *Investigative Ophthalmology and Visual Science* **48:**4079-4086.

Iverson, H. A. (1958). Hereditary optic atrophy. *A.M.A. Archives of Ophthalmology* **59:**850-853.

Jacob, M. M., Pangeni, G., Gomes, B. D., Souza, G. S., da Silva Filho, M., Silveira, L. C., Maguire, J., et al. (2015). The spatial properties of L- and M-cone inputs to electroretinograms that reflect different types of post-receptoral processing. *PloS One* **10:**1-15.

Jaeger, W. (1954). [Hereditary optic atrophy with dominant transmission; with special reference to the associated color-sense disorder]. *Albrecht Von Graefes Arch Ophthalmol* **155:**457-484.

Jaeger, W. (1988). Diagnosis of dominant infantile optic atrophy in early childhood. *Ophthalmic Paediatrics and Genetics* **9:**7-11.

Jaissle, G. B., May, C. A., Reinhard, J., Kohler, K., Fauser, S., Lütjen–Drecoll, E., Zrenner, E., et al. (2001). Evaluation of the rhodopsin knockout mouse as a model of pure cone function. *Investigative Ophthalmology and Visual Science* **42:**506-513.

Janaky, M., Goupland, S. G. and Benedek, G. (1996). Human oscillatory potentials: Components of rod origin. *Ophthalmologica* **210:**315-318.

Johnson, C. A., Adams, A. J. and Lewis, R. A. (1989). Evidence for a neural basis of age-related visual field loss in normal observers. *Investigative Ophthalmology and Visual Science* **30:**2056-2064.

Johnston, P. B., Gaster, R. N., Smith, V. C. and Tripathi, R. C. (1979). A clinicopathologic study of autosomal dominant optic atrophy. *American Journal of Ophthalmology* **88:**868-875.

Johnston, R. L., Burdon, M. A., Spalton, D. J., Bryant, S. P., Behnam, J. T. and Seller, M. J. (1997). Dominant optic atrophy, Kjer type. Linkage analysis and clinical features in a large British pedigree. *Archives of Ophthalmology* **115:**100-103.

Johnston, R. L., Seller, M. J., Behnam, J. T., Burdon, M. A. and Spalton, D. J. (1999). Dominant optic atrophy. Refining the clinical diagnostic criteria in light of genetic linkage studies. *Ophthalmology* **106:**123-128.

Jonas, J. B., Schmidt, A. M., Muller-Bergh, J. A., Schlotzer-Schrehardt, U. M. and Naumann, G. O. (1992). Human optic nerve fiber count and optic disc size. *Investigative Ophthalmology and Visual Science* **33:**2012-2018.

Junghardt, A., Wildberger, H., Robert, Y. and Torok, B. (1993). Pattern electroretinogram and visual evoked potential amplitudes are influenced by different stimulus field sizes and scotomata. *Documenta Ophthalmologica* **83:**139-149.

Kamei, S., Chen-Kuo-Chang, M., Cazevieille, C., Lenaers, G., Olichon, A., Belenguer, P., Roussignol, G., et al. (2005). Expression of the Opa1 mitochondrial protein in retinal ganglion cells: Its downregulation causes aggregation of the mitochondrial network. *Investigative Ophthalmology and Visual Science* **46:**4288-4294.

Karwoski, C. J. and Xu, X. (1999). Current source-density analysis of light-evoked field potentials in rabbit retina. *Visual Neuroscience* **16:**369-377.

Kelly, J., Kniffin, C. L., O'Neill, M. J. F., McKusick, V. A. and Hamosh, A. 2012. *Optic atrophy, OPA1* [Online]. Johns Hopkins University. Available: http://omim.org/entry/165500?search=dominant%20optic%20atrophy&highlight=atrophy%20dominant%20optic#reference18 [Accessed 17 May 2013.

Kerrison, J. B., Arnould, V. J., Sallum, J. M. F., Vagefi, M. R., Barmada, M. M., Li, Y. Y., Zhu, D. P., et al. (1999). Genetic heterogeneity of dominant optic atrophy, Kjer type - Identification of a second locus on chromosome 18q12.2-12.3. *Archives of Ophthalmology* **117:**805-810.

Kiszkielis, M., Lubinski, W. and Penkala, K. (2012). The photopic negative response as a promising diagnostic tool in glaucoma. A review. *Klinika Oczna* **114:**138-142.

Kizawa, J., Machida, S., Kobayashi, T., Gotoh, Y. and Kurosaka, D. (2006). Changes of oscillatory potentials and photopic negative response in patients with early diabetic retinopathy. *Japanese Journal of Ophthalmology* **50:**367-373.

Kjer, B., Eiberg, H., Kjer, P. and Rosenberg, T. (1996). Dominant optic atrophy mapped to chromosome 3q region .2. Clinical and epidemiological aspects. *Acta Ophthalmologica Scandinavica* **74:**3-7.

Kjer, P. (1959). Infantile optic atrophy with dominant mode of inheritance: a clinical and genetic study of 19 Danish families. *Acta Ophthalmologica. Supplement* **164:**1-147.

Kjer, P., Jensen, O. A. and Klinken, L. (1983). Histopathology of eye, optic-nerve and brain in a case of dominant optic atrophy. *Acta Ophthalmologica* **61:**300-312.

Kline, L. B. and Glaser, J. S. (1979). Dominant optic atrophy: The clinical profile. *Archives of Ophthalmology* **97:**1680-1686.

Klopstock, T., Metz, G., Yu-Wai-Man, P., Büchner, B., Gallenmüller, C., Bailie, M., Nwali, N., et al. (2013). Persistence of the treatment effect of idebenone in Leber's hereditary optic neuropathy. *Brain* **136:**e230-e230.

Klopstock, T., Yu-Wai-Man, P., Dimitriadis, K., Rouleau, J., Heck, S., Bailie, M., Atawan, A., et al. (2011). A randomized placebo-controlled trial of idebenone in Leber's hereditary optic neuropathy. *Brain* **134:**2677-2686.

Kolb, H. (2003). How the retina works. *American Scientist* **91:**28-35.

Kolb, H. 2011. Simple anatomy of the retina. *In:* Kolb, H., Nelson, R., Fernandez, E., et al. (eds.) *Webvision: The organisation of the retina and visual system.* Salt Lake City.

Kolloniatis, M. and Luu, C. 2007. Temporal Resolution. *In:* Kolb, H., Nelson, R., Fernandez, E., et al. (eds.) *Webvision: The organisation of the retina and visual system.* Salt Lake City.

Kondo, M., Kurimoto, Y., Sakai, T., Koyasu, T., Miyata, K., Ueno, S. and Terasaki, H. (2008a). Recording focal macular photopic negative response (PhNR) from monkeys. *Investigative Ophthalmology and Visual Science* **49:**3544-3550.

Kondo, M., Miyake, Y., Horiguchi, M., Suzuki, S. and Tanikawa, A. (1998). Recording multifocal electroretinogram on and off responses in humans. *Investigative Ophthalmology and Visual Science* **39:**574-580.

Kondo, M., Piao, C.-H., Tanikawa, A., Horiguchi, M., Terasaki, H. and Miyake, Y. (2000). Amplitude Decrease of Photopic ERG b-Wave at Higher Stimulus Intensities in Humans. *Japanese Journal of Ophthalmology* **44:**20-28.

Kondo, M., Ueno, S., Piao, C.-H., Miyake, Y. and Terasaki, H. (2008b). Comparison of focal macular cone ERGs in complete-type congenital stationary night blindness and APB-treated monkeys. *Vision Research* **48:**273-280.

Kouyama, N. and Marshak, D. W. (1992). Bipolar cells specific for blue cones in the macaque retina. *Journal of Neuroscience* **12:**1233-1252.

Kremers, J., Jertila, M., Link, B., Pangeni, G. and Horn, F. K. (2012). Spectral characteristics of the PhNR in the full-field flash electroretinogram of normals and glaucoma patients. *Documenta Ophthalmologica* **124:**79-90.

Krill, A. E., Smith, V. C. and Pokorny, J. (1970). Similarities between congenital tritan defects and dominant optic-nerve atrophy - coincidence or identity. *Journal of the Optical Society of America* **60:**1132-1139.

Krill, A. E., Smith, V. C. and Pokorny, J. (1971). Further studies supporting identitiy of congenital tritanopia and hereditary dominant optic atrophy. *Investigative Ophthalmology* **10:**457-465.

Kuffler, S. W. (1953). Discharge patterns and functional organization of mammalian retina. *Journal of Neurophysiology* **16:**37-68.

Kurimoto, Y., Kondo, M., Ueno, S., Sakai, T., Machida, S. and Terasaki, H. (2009). Asymmetry of focal macular photopic negative responses (PhNRs) in monkeys. *Experimental Eye Research* **88:**92-98.

Lee, B. B. (1996). Receptive field structure in the primate retina. *Vision Research* **36:**631-644.

Lee, B. B., Kremers, J. and Yeh, T. (1998). Receptive fields of primate retinal ganglion cells studied with a novel technique. *Visual Neuroscience* **15:**161-175.

Lee, K., Niemeijer, M., Garvin, M. K., Kwon, Y. H., Sonka, M. and Abramoff, M. D. (2010). Segmentation of the optic disc in 3-D OCT scans of the optic nerve head. *IEEE Transactions on Medical Imaging* **29:**159-168.

Lei, Y., Garrahan, N., Hermann, B., Fautsch, M. P., Johnson, D. H., Hernandez, M. R., Boulton, M., et al. (2011). Transretinal degeneration in ageing human retina: a multiphoton microscopy analysis. *British Journal of Ophthalmology* **95:**727-730.

Lenaers, G., Hamel, C., Delettre, C., Amati-Bonneau, P., Procaccio, V., Bonneau, D., Reynier, P., et al. (2012). Dominant optic atrophy. *Orphanet Journal of Rare Diseases* **7**.

Lennie, P. (2003). Receptive fields. *Current Biology* **13:**R216-R219.

Leventhal, A. G., Rodieck, R. W. and Dreher, B. (1981). Retinal ganglion cell classes in the Old World monkey: morphology and central projections. *Science* **213:**1139-1142.

Lodi, R., Tonon, C., Valentino, M. L., Lotti, S., Clementi, V., Malucelli, E., Barboni, P., et al. (2004). Deficit of in vivo mitochondrial ATP production in OPA1-related dominant optic atrophy. *Annals of Neurology* **56:**719-723.

Lodi, R., Tonon, C., Valentino, M. L., Manners, D., Testa, C., Malucelli, E., La Morgia, C., et al. (2011). Defective mitochondrial adenosine triphosphate production in skeletal muscle from patients with dominant optic atrophy due to OPA1 mutations. *Archives of Neurology* **68:**67-73.

Luo, X. and Frishman, L. J. (2011). Retinal Pathway Origins of the Pattern Electroretinogram (PERG). *Investigative Ophthalmology and Visual Science* **52:**8571-8584.

Machida, S. (2012). Clinical applications of the photopic negative response to optic nerve and retinal diseases. *Journal of ophthalmology* **2012:**397178-397178.

Machida, S., Gotoh, Y., Tanaka, M. and Tazawa, Y. (2004). Predominant loss of the photopic negative response in central retinal artery occlusion. *American Journal of Ophthalmology* **137:**938-940.

Machida, S., Raz-Prag, D., Fariss, R. N., Sieving, P. A. and Bush, R. A. (2008a). Photopic ERG negative response from amacrine cell signaling in RCS rat retinal degeneration. *Investigative Ophthalmology and Visual Science* **49:**442-452.

Machida, S., Tamada, K., Oikawa, T., Gotoh, Y., Nishimura, T., Kaneko, M. and Kurosaka, D. (2011). Comparison of photopic negative response of full-field and focal electroretinograms in detecting glaucomatous eyes. *Journal of ophthalmology* **2011**.

Machida, S., Toba, Y., Ohtaki, A., Gotoh, Y., Kaneko, M. and Kurosaka, D. (2008b). Photopic negative response of focal electoretinograms in

glaucomatous eyes. *Investigative Ophthalmology and Visual Science* **49:**5636-5644.

Mafei, L. and Fiorentini, A. (1981). Electroretinographic responses to alternating gratings before and after section of the optic nerve. *Science* **211:**953-955.

Maffei, L., Fiorentini, A., Bisti, S. and Hollander, H. (1985). Pattern ERG in the monkey after section of the optic nerve. *Experimental Brain Research* **59:**423-425.

Man, P. Y. W., Turnbull, D. M. and Chinnery, P. F. (2002). Leber hereditary optic neuropathy. *Journal of Medical Genetics* **39:**162-169.

Marmor, M. F., Fulton, A. B., Holder, G. E., Miyake, Y., Brigell, M. and Bach, M. (2009). ISCEV Standard for full-field clinical electroretinography (2008 update). *Documenta Ophthalmologica* **118:**69-77.

Marmor, M. F., Holder, G. E., Seeliger, M. W. and Yamamoto, S. (2004). Standard for clinical electroretinography (2004 update). *Documenta Ophthalmologica* **108:**107-114.

Marmor, M. F. and Zrenner, E. 2006. Introduction to the ISCEV Standards. *In:* Heckenlively, J. R. and Arden, G. B. (eds.) *Principles and practice of clinical electrophysiology of vision.* London, England: The MIT Press.

Martin, P. R., White, A. J. R., Goodchild, A. K., Wilder, H. D. and Sefton, A. E. (1997). Evidence that blue-on cells are part of the third geniculocortical pathway in primates. *European Journal of Neuroscience* **9:**1536-1541.

Massey, S. C. (1990). Cell types using glutamate as a neurotransmitter in the vertebrate retina. *Progress in retinal research* **9:**399-425.

Matsumoto, C. S., Shinoda, K. and Nakatsuka, K. (2011). High correlation of scotopic and photopic electroretinogram components with severity of central retinal artery occlusion. *Clinical Ophthalmology (Auckland, N.Z.)* **5:**115-121.

Matsumoto, C. S., Shinoda, K., Yamada, K. and Nakatsuka, K. 2009. Photopic negative response reflects severity of ocular circulatory damage after central retinal artery occlusion. *Ophthalmologica.* Switzerland: 2009 S. Karger AG, Basel.

Maturana, M. I., Kameneva, T., Burkitt, A. N., Meffin, H. and Grayden, D. B. (2014). The effect of morphology upon electrophysiological responses of retinal ganglion cells: simulation results. *Journal of Computational Neuroscience* **36:**157-175.

McCulloch, D. L., Marmor, M. F., Brigell, M. G., Hamilton, R., Holder, G. E., Tzekov, R. and Bach, M. (2015). ISCEV standard for full-field clinical electroretinography (2015 update). *Documenta Ophthalmologica* **130:**1-12.

Milea, D., Sander, B., Wegener, M., Jensen, H., Kjer, B., Jorgensen, T. M., Lund-Andersen, H., et al. (2010). Axonal loss occurs early in dominant optic atrophy. *Acta Ophthalmologica* **88:**342-346.

Miller, R. F. and Dowling, J. E. (1970). Intracellular responses of the Muller (glial) cells of mudpuppy retina: their relation to b-wave of the electroretinogram. *Journal of Neurophysiology* **33:**323-341.

Miura, G., Wang, M. H., Ivers, K. M. and Frishman, L. J. (2009). Retinal pathway origins of the pattern ERG of the mouse. *Experimental Eye Research* **89:**49-62.

Miyata, K., Nakamura, M., Kondo, M., Lin, J., Ueno, S., Miyake, Y. and Terasaki, H. (2007). Reduction of oscillatory potentials and photopic negative response in patients with autosomal dominant optic atrophy with OPA1 mutations. *Investigative Ophthalmology and Visual Science* **48:**820-824.

Miyata, K., Ueno, S., Kondo, M., Koyasu, T. and Terasaki, H. (2008). Comparison of photopic negative responses elicited by red and white xenon flashes in monkeys. *Japanese Journal of Ophthalmology* **52:**327-330.

Moon, C. H., Hwang, S. C., Kim, B. T., Ohn, Y. H. and Park, T. K. 2011. Visual prognostic value of optical coherence tomography and photopic negative response in chiasmal compression. *Investigative Ophthalmology and Visual Science.* United States.

Morny, E. K. A., Margrain, T. H., Binns, A. M. and Votruba, M. (2015). Electrophysiological ON and OFF responses in autosomal dominant optic atrophy. *Investigative Ophthalmology and Visual Science* **56:**7629-7637.

Mortlock, K. E., Binns, A. M., Aldebasi, Y. H. and North, R. V. (2010). Inter-subject, inter-ocular and inter-session repeatability of the photopic negative response of the electroretinogram recorded using DTL and skin electrodes. *Documenta Ophthalmologica* **121:**123-134.

Movassat, M. 2012. Diagnostic Values of Electrophysiology in Ophthalmology. *In:* Oraii, D. s. (ed.) *Electrophysiology - from plants to heart.* InTech.

Murakami, M. and Kaneko, A. (1966). Subcomponents of P3 in cold-blooded vertebrate retinae. *Nature* **210:**103-104.

Murray, I. J., Parry, N. R., Kremers, J., Stepien, M. and Schild, A. (2004). Photoreceptor topography and cone-specific electroretinograms. *Visual Neuroscience* **21:**231-235.

Nakamura, H., Hangai, M., Mori, S., Hirose, F. and Yoshimura, N. (2011a). Hemispherical focal macular photopic negative response and macular inner retinal thickness in open-angle glaucoma. *American Journal of Ophthalmology* **151:**494-506 e491.

Nakamura, H., Miyamoto, K., Yokota, S., Ogino, K. and Yoshimura, N. (2011b). Focal macular photopic negative response in patients with optic neuritis. *Eye (London, England)* **25:**358-364.

Nakamura, M., Lin, J., Ueno, S., Asaoka, R., Hirai, T., Hotta, Y., Miyake, Y., et al. (2006). Novel mutations in the OPA1 gene and associated clinical features in Japanese patients with optic atrophy. *Ophthalmology* **113:**483-488.

Newman, N. J. and Biousse, V. (2004). Hereditary optic neuropathies. *Eye* **18:**1144-1160.

Nochez, Y., Arsene, S., Gueguen, N., Chevrollier, A., Ferre, M., Guillet, V., Desquiret, V., et al. (2009). Acute and late-onset optic atrophy due to a novel OPA1 mutation leading to a mitochondrial coupling defect. *Molecular Vision* **15:**598-608.

North, R. V., Jones, A. L., Drasdo, N., Wild, J. M. and Morgan, J. E. (2010). Electrophysiological evidence of early functional damage in glaucoma and ocular hypertension. *Investigative Ophthalmology and Visual Science* **51:**1216-1222.

Olichon, A., Baricault, L., Gas, N., Guillou, E., Valette, A., Belenguer, P. and Lenaers, G. (2003). Loss of OPA1 perturbates the mitochondrial inner membrane structure and integrity, leading to cytochrome c release and apoptosis. *Journal of Biological Chemistry* **278:**7743-7746.

Olichon, A., Landes, T., Arnaune-Pelloquin, L., Emorine, L. J., Mils, V., Guichet, A., Delettre, C., et al. (2007). Effects of OPA1 mutations on mitochondrial

morphology and apoptosis: relevance to ADOA pathogenesis. *Journal of Cellular Physiology* **211:**423-430.

Osborne, N. N., Li, G. Y., Ji, D., Mortiboys, H. J. and Jackson, S. (2008). Light affects mitochondria to cause apoptosis to cultured cells: possible relevance to ganglion cell death in certain optic neuropathies. *Journal of Neurochemistry* **105:**2013-2028.

Osterberg, G. (1935). Topography of the layer of rods and cones in the human retina. *Acta Ophthalmologica. Supplement* **6:**1-103.

Owsley, C. (2011). Aging and vision. *Vision Research* **51:**1610-1622.

Pangeni, G., Lammer, R., Tornow, R. P., Horn, F. K. and Kremers, J. (2012). On- and off-response ERGs elicited by sawtooth stimuli in normal subjects and glaucoma patients. *Documenta Ophthalmologica* **124:**237-248.

Parisi, V. (2003). Correlation between morphological and functional retinal impairment in patients affected by ocular hypertension, glaucoma, demyelinating optic neuritis and Alzheimer's disease. *Seminars in Ophthalmology* **18:**50-57.

Parisi, V., Manni, G., Centofanti, M., Gandolfi, S. A., Olzi, D. and Bucci, M. G. (2001). Correlation between optical coherence tomography, pattern electroretinogram, and visual evoked potentials in open-angle glaucoma patients. *Ophthalmology* **108:**905-912.

Payne, M., Yang, Z. L., Katz, B. J., Warner, J. E. A., Weight, C. J., Zhao, Y., Pearson, E. D., et al. (2004). Dominant optic atrophy, sensorineural hearing loss, ptosis, and ophthalmoplegia: A syndrome caused by a missense mutation in OPA1. *American Journal of Ophthalmology* **138:**749-755.

Pearson, R. M. (2003). Optometric grading scales for use in everyday practice. *Optometry Today* **40:**39-42.

Pelli, D. G., Robson, J. G. and Wilkins, A. J. (1988). The design of a new letter chart for measuring contrast sensitivity. *Clinical Vision Sciences* **2:**187-199

Perganta, G., Barnard, A. R., Katti, C., Vachtsevanos, A., Douglas, R. H., MacLaren, R. E., Votruba, M., et al. (2013). Non-image-forming light driven functions are preserved in a mouse model of autosomal dominant optic atrophy. *PloS One* **8**.

Perlman, I. 2001. The Electroretinogram: ERG. *In:* Kolb, H., Nelson, R., Fernandez, E., et al. (eds.) *Webvision: The organisation of the retina and visual system.* Salt Lake City (UT): University of Utah Health Sciences Center.

Perry, V. H. and Cowey, A. (1981). The morphological correlates of X- and Y-like retinal ganglion cells in the retina of monkeys. *Experimental Brain Research* **43:**226-228.

Perry, V. H. and Cowey, A. (1984). Retinal ganglion cells that project to the superior colliculus and pretectum in the macaque monkey. *Neuroscience* **12:**1125-1137.

Perry, V. H. and Cowey, A. (1985). The ganglion-cell and cone distributions in the monkeys retina - implications for central magnification factors. *Vision Research* **25:**1795-1810.

Perry, V. H., Oehler, R. and Cowey, A. (1984). Retinal ganglion cells that project to the dorsal lateral geniculate nucleus in the macaque monkey. *Neuroscience* **12:**1101-1123.

Pesch, U. E. A., Fries, J. E., Bette, S., Kalbacber, H., Wissinger, B., Alexander, C. and Kohler, K. (2004). OPA1, the disease gene for autosomal dominant optic atrophy, is specifically expressed in ganglion cells and intrinsic neurons of the retina. *Investigative Ophthalmology and Visual Science* **45:**4217-4225.

Polyak, S. L. 1941. *The retina*. Chicago: University of Chicago Press.

Porciatti, V. (1987). Non-linearities in the focal ERG evoked by pattern and uniform-field stimulation. Their variation in retinal and optic nerve dysfunction. *Investigative Ophthalmology and Visual Science* **28:**1306-1313.

Preiser, D., Lagreze, W. A., Bach, M. and Poloschek, C. M. (2013). Photopic negative response versus pattern electroretinogram in early glaucoma. *Investigative Ophthalmology and Visual Science* **54:**1182-1191.

Puomila, A., Huoponen, K., Mantyjarvi, M., Hamalainen, P., Paananen, R., Sankila, E. M., Savontaus, M. L., et al. (2005). Dominant optic atrophy: correlation between clinical and molecular genetic studies. *Acta Ophthalmologica Scandinavica* **83:**337-346.

Quigley, H. A., Addicks, E. M. and Green, W. R. (1982). Optic nerve damage in human glaucoma. III. Quantitative correlation of nerve fiber loss and visual field

defect in glaucoma, ischemic neuropathy, papilledema, and toxic neuropathy. *Archives of Ophthalmology* **100:**135-146.

Quigley, H. A., Brown, A. E., Morrison, J. D. and Drance, S. M. (1990). The size and shape of the optic disc in normal human eyes. *Archives of Ophthalmology* **108:**51-57.

Rangaswamy, N. V., Frishman, L. J., Dorotheo, E. U., Schiffman, J. S., Bahrani, H. M. and Tang, R. A. (2004). Photopic ERGs in patients with optic neuropathies: comparison with primate ERGs after pharmacologic blockade of inner retina. *Investigative Ophthalmology and Visual Science* **45:**3827-3837.

Rangaswamy, N. V., Shirato, S., Kaneko, M., Digby, B. I., Robson, J. G. and Frishman, L. J. (2007). Effects of spectral characteristics of ganzfeld stimuli on the photopic negative response (PhNR) of the ERG. *Investigative Ophthalmology and Visual Science* **48:**4818-4828.

Rangaswamy, N. V., Zhou, W., Harwerth, R. S. and Frishman, L. J. (2006). Effect of experimental glaucoma in primates on oscillatory potentials of the slow-sequence mfERG. *Investigative Ophthalmology and Visual Science* **47:**753-767.

Read, S. A., Collins, M. J. and Iskander, D. R. (2008). Diurnal Variation of Axial Length, Intraocular Pressure, and Anterior Eye Biometrics. *Investigative Ophthalmology and Visual Science* **49:**2911-2918.

Reis, A., Mateus, C., Viegas, T., Florijn, R., Bergen, A., Silva, E. and Castelo-Branco, M. (2013). Physiological evidence for impairment in autosomal dominant optic atrophy at the pre-ganglion level. *Graefes Archive for Clinical and Experimental Ophthalmology* **251:**221-234.

Remington, L. A. 2005. *Clinical anatomy of the visual system*, 2, St. Louis, Missouri: Elsevier/Butterworth-Heinemann.

Reynier, P., Amati-Bonneau, P., Verny, C., Olichon, A., Simard, G., Guichet, A., Bonnemains, C., et al. (2004). OPA3 gene mutations responsible for autosomal dominant optic atrophy and cataract. *Journal of Medical Genetics* **41**.

Robson, J. G. and Frishman, L. J. (1998). Dissecting the dark-adapted electroretinogram. *Documenta Ophthalmologica* **95:**187-215.

Rodieck, R. W., Binmoeller, K. F. and Dineen, J. (1985). Parasol and midget ganglion cells of the human retina. *The Journal of Comparative Neurology* **233:**115-132.

Ronnback, C., Milea, D. and Larsen, M. (2013). Imaging of the macula indicates early completion of structural deficit in autosomal-dominant optic atrophy. *Ophthalmology* **120:**2672-2677.

Rowling, J. E. 1987. *The retina: an approachable part of the brain*, London, England: The Belknap Press of Harvard Univerisity Press.

Russo, A., Delcassi, L., Marchina, E. and Semeraro, F. (2013). Correlation between visual acuity and OCT-measured retinal nerve fiber layer thickness in a family with ADOA and an OPA1 mutation. *Ophthalmic Genetics* **34:**69-74.

Sarzi, E., Angebault, C., Seveno, M., Gueguen, N., Chaix, B., Bielicki, G., Boddaert, N., et al. (2012). The human OPA1delTTAG mutation induces premature age-related systemic neurodegeneration in mouse. *Brain* **135:**3599-3613.

Schaaf, C. P., Blazo, M., Lewis, R. A., Tonini, R. E., Takei, H., Wang, J., Wong, L.-J., et al. (2011). Early-onset severe neuromuscular phenotype associated with compound heterozygosity for OPA1 mutations. *Molecular Genetics and Metabolism* **103:**383-387.

Seiple, W., Greenstein, V., Holopigian, K. and Carr, R. (1988). Changes in the focal electroretinogram with retinal eccentricity. *Documenta Ophthalmologica* **70:**29-36.

Seiple, W. H., Siegel, I. M., Carr, R. E. and Mayron, C. (1986). Evaluating macular function using the focal ERG. *Investigative Ophthalmology and Visual Science* **27:**1123-1130.

Seller, M. J., Behnam, J. T., Lewis, C. M., Johnston, R. L., Burdon, M. A. and Spalton, D. J. (1997). Linkage studies in dominant optic atrophy, Kjer type: possible evidence for heterogeneity. *Journal of Medical Genetics* **34:**967-972.

Sharpe, L. T. and Stockman, A. (1999). Rod pathways: the importance of seeing nothing. *Trends in Neurosciences* **22:**497-504.

Shimizu, S., Mori, N., Kishi, M., Sugata, H., Tsuda, A. and Kubota, N. (2003). A novel mutation in the OPA1Gene in a Japanese patient with optic atrophy. *American Journal of Ophthalmology* **135:**256-257.

Sieving, P. A. (1993). Photopic ON- and OFF-pathway abnormalities in retinal dystrophies. *Transactions of the American Ophthalmological Society* **91:**701-773.

Sieving, P. A., Frishman, L. J. and Steinberg, R. H. (1986). Scotopic threshold response of proximal retina in cat. *Journal of Neurophysiology* **56:**1049-1061.

Sieving, P. A., Murayama, K. and Naarendorp, F. (1994). Push-pull model of the primate photopic electroretinogram: a role for hyperpolarizing neurons in shaping the b-wave. *Visual Neuroscience* **11:**519-532.

Sieving, P. A. and Nino, C. (1988). Scotopic threshold response (str) of the human electroretinogram. *Investigative Ophthalmology and Visual Science* **29:**1608-1614.

Sieving, P. A. and Steinberg, R. H. (1987). Proximal retinal contribution to the intraretinal 8-Hz pattern ERG of cat. *Journal of Neurophysiology* **57:**104-120.

Sillman, A. J., Ito, H. and Tomita, T. (1969). Studies on the mass receptor potential of the isolated frog retina. I. General properties of the response. *Vision Research* **9:**1435-1442.

Silveira, L. C., Saito, C. A., Lee, B. B., Kremers, J., da Silva Filho, M., Kilavik, B. E., Yamada, E. S., et al. (2004). Morphology and physiology of primate M- and P-cells. *Progress in Brain Research* **144:**21-46.

Silveira, L. C. L. and Perry, V. H. (1991). The topography of magnocellular projecting ganglion cells (M-ganglion cells) in the primate retina. *Neuroscience* **40:**217-237.

Simunovic, M. P., Votruba, M., Regan, B. C. and Mollon, J. D. (1998). Colour discrimination ellipses in patients with dominant optic atrophy. *Vision Research* **38:**3413-3419.

Slaughter, M. M. and Miller, R. F. (1981). 2-amino-4-phosphonobutyric acid - a new pharmacological tool for retina research. *Science* **211:**182-185.

Slaughter, M. M. and Miller, R. F. (1983). An excitatory amino acid antagonist blocks cone input to sign-conserving second-order retinal neurons. *Science* **219:**1230-1232.

Smith, B. J., Wang, X., Chauhan, B. C., Cote, P. D. and Tremblay, F. (2014). Contribution of retinal ganglion cells to the mouse electroretinogram. *Documenta Ophthalmologica* **128:**155-168.

Smith, N. P. and Lamb, T. D. (1997). The a-wave of the human electroretinogram recorded with a minimally invasive technique. *Vision Research* **37:**2943-2952.

Smith, R. S., Joh, S. W. M., Nishina, P. M. and Sundberg, J. P. 2002. *Systematic evaluation of the mouse eye: anatomy, pathology and biomethods.*, Boca Raton, Florida: CRC Press.

Snell, S. (1897). Disease of the optic nerve I: hereditary or congenital optic atrophy and allied cases. *Transactions of the Ophthalmological Societies of the United Kingdom* **17:**66-81.

Spileers, W., Falcaoreis, F., Smith, R., Hogg, C. and Arden, G. B. (1993). The human ERG evoked by a ganzfeld stimulator powered by red and green light-emitting-diodes. *Clinical Vision Sciences* **8:**21-39.

Spillmann, L. (2014). Receptive fields of visual neurons: the early years. *Perception* **43:**1145-1176.

Stroud, K. A. 1986. *Further engineering mathematics: programmes and problems*, Basingstoke, United Kingdom: Palgrave Macmillan.

Sustar, M., Cvenkel, B. and Brecelj, J. (2009). The effect of broadband and monochromatic stimuli on the photopic negative response of the electroretinogram in normal subjects and in open-angle glaucoma patients. *Documenta Ophthalmologica* **118:**167-177.

Sustar, M., Hawlina, M. and Brecelj, J. (2006). ON- and OFF-response of the photopic electroretinogram in relation to stimulus characteristics. *Documenta Ophthalmologica* **113:**43-52.

Sutter, E. (2000). The interpretation of multifocal binary kernels. *Documenta Ophthalmologica* **100:**49-75.

Sutter, E. E. and Bearse Jr, M. A. (1999). The optic nerve head component of the human ERG. *Vision Research* **39:**419-436.

Sutter, E. E. and Tran, D. (1992). The field topography of ERG components in man--I. The photopic luminance response. *Vision Research* **32:**433-446.

Szmajda, B. A., Grünert, U. and Martin, P. R. (2008). Retinal ganglion cell inputs to the koniocellular pathway. *The Journal of Comparative Neurology* **510:**251-268.

Tamada, K., Machida, S., Oikawa, T., Miyamoto, H., Nishimura, T. and Kurosaka, D. (2010). Correlation between photopic negative response of focal electroretinograms and local loss of retinal neurons in glaucoma. *Current Eye Research* **35:**155-164.

Tamada, K., Machida, S., Yokoyama, D. and Kurosaka, D. (2009). Photopic negative response of full-field and focal macular electroretinograms in patients with optic nerve atrophy. *Japanese Journal of Ophthalmology* **53:**608-614.

Thiselton, D. L., Alexander, C., Taanman, J. W., Brooks, S., Rosenberg, T., Eiberg, H., Andreasson, S., et al. (2002). A comprehensive survey of mutations in the OPA1 gene in patients with autosomal dominant optic atrophy. *Investigative Ophthalmology and Visual Science* **43:**1715-1724.

Thompson, D. and Drasdo, N. (1989). The effect of stimulus contrast on the latency and amplitude of the pattern electroretinogram. *Vision Research* **29:**309-313.

Thompson, D. A. and Drasdo, N. (1994). The origins of luminance and pattern responses of the pattern electroretinogram. *International Journal of Psychophysiology* **16:**219-227.

Thompson, D. A., Feather, S., Stanescu, H. C., Freudenthal, B., Zdebik, A. A., Warth, R., Ognjanovic, M., et al. (2011). Altered electroretinograms in patients with KCNJ10 mutations and EAST syndrome. *Journal of Physiology* **589:**1681-1689.

Toffoli, G., Vattovani, O., Cecchini, P., Pastori, G., Rinaldi, G. and Ravalico, G. (2002). Correlation between the retinal nerve fiber layer thickness and the pattern electroretinogram amplitude. *Ophthalmologica* **216:**159-163.

Tsukamoto, Y., Morigiwa, K., Ueda, M. and Sterling, P. (2001). Microcircuits for night vision in mouse retina. *Journal of Neuroscience* **21:**8616-8623.

Ueno, S., Kondo, M., Piao, C. H., Ikenoya, K., Miyake, Y. and Terasaki, H. (2006a). Selective amplitude reduction of the PhNR after macular hole surgery:

ganglion cell damage related to ICG-assisted ILM peeling and gas tamponade. *Investigative Ophthalmology and Visual Science* **47:**3545-3549.

Ueno, S., Kondo, M., Ueno, M., Miyata, K., Terasaki, H. and Miyake, Y. (2006b). Contribution of retinal neurons to d-wave of primate photopic electroretinograms. *Vision Research* **46:**658-664.

Ventura, L. M., Sorokac, N., Santos, R. D. L., Feuer, W. J. and Porciatti, V. (2006). The relationship between retinal ganglion cell function and retinal nerve fiber thickness in early glaucoma. *Investigative Ophthalmology and Visual Science* **47:**3904-3911.

Vincent, A., Robson, A. G. and Holder, G. E. 2013. Pathognomonic (diagnostic) ERGs. A review and update. *Retina.* United States.

Viswanathan, S. and Frishman, L. J. (1997). Evidence that negative potentials in the photopic electroretinograms of cats and primates depend upon spiking activity of retinal ganglion cell axons. *Society for Neuroscience Abstracts* **23:**1024-1024.

Viswanathan, S., Frishman, L. J. and Robson, J. G. (2000). The uniform field and pattern ERG in macaques with experimental glaucoma: removal of spiking activity. *Investigative Ophthalmology and Visual Science* **41:**2797-2810.

Viswanathan, S., Frishman, L. J., Robson, J. G., Harwerth, R. S. and Smith, E. L., 3rd (1999). The photopic negative response of the macaque electroretinogram: reduction by experimental glaucoma. *Investigative Ophthalmology and Visual Science* **40:**1124-1136.

Viswanathan, S., Frishman, L. J., Robson, J. G. and Walters, J. W. (2001). The photopic negative response of the flash electroretinogram in primary open angle glaucoma. *Invest Ophthalmol Vis Sci* **42:**514-522.

Votruba, M., Aijaz, S. and Moore, A. T. (2003a). A review of primary hereditary optic neuropathies. *Journal of Inherited Metabolic Disease* **26:**209-227.

Votruba, M., Fitzke, F. W., Holder, G. E., Carter, A., Bhattacharya, S. S. and Moore, A. T. (1998a). Clinical features in affected individuals from 21 pedigrees with dominant optic atrophy. *Archives of Ophthalmology* **116:**351-358.

Votruba, M., Moore, A. T. and Bhattacharya, S. S. (1998b). Clinical features, molecular genetics, and pathophysiology of dominant optic atrophy. *Journal of Medical Genetics* **35:**793-800.

Votruba, M., Thiselton, D. and Bhattacharya, S. S. (2003b). Optic disc morphology of patients with OPA1 autosomal dominant optic atrophy. *British Journal of Ophthalmology* **87:**48-53.

Wachtmeister, L. (1998). Oscillatory potentials in the retina: what do they reveal. *Progress in Retinal and Eye Research* **17:**485-521.

Wakabayashi, K. and Sieving, P. A. (1988). Scotopic threshold response a comparison for cat monkey and man. *Investigative Ophthalmology and Visual Science* **29:**103-103.

Wali, N. and Leguire, L. E. (1992). The photopic hill: a new phenomenon of the light adapted electroretinogram. *Documenta Ophthalmologica* **80:**335-345.

Walters, J. W., Gaume, A. and Pate, L. (2006). Short wavelength-automated perimetry compared with standard achromatic perimetry in autosomal dominant optic atrophy. *British Journal of Ophthalmology* **90:**1267-1270.

Wang, J., Cheng, H., Hu, Y. S., Tang, R. A. and Frishman, L. J. 2012. The photopic negative response of the flash electroretinogram in multiple sclerosis. *Investigative Ophthalmology and Visual Science.* United States.

Warrant, E. J. (1999). Seeing better at night: life style, eye design and the optimum strategy of spatial and temporal summation. *Vision Research* **39:**1611-1630.

Wassle, H. (2004). Parallel processing in the mammalian retina. *Nature Reviews: Neuroscience* **5:**747-757.

Wassle, H., Peichl, L. and Boycott, B. B. (1983). A spatial analysis of on- and off-ganglion cells in the cat retina. *Vision Research* **23:**1151-1160.

Watanabe, M. and Rodieck, R. W. (1989). Parasol and midget ganglion cells of the primate retina. *Journal of Comparative Neurology* **289:**434-454.

Watson, A. B. (2014). A formula for human retinal ganglion cell receptive field density as a function of visual field location. *J Vis* **14**.

Weisinger, H. S., Vingrys, A. J. and Sinclair, A. J. (1996). Review: electrodiagnostic methods in vision part 1. clinical application and measurement. *Clinical and experimental optometry* **79**.

White, K. E., Davies, V. J., Hogan, V. E., Piechota, M. J., Nichols, P. P., Turnbull, D. M. and Votruba, M. (2009). OPA1 deficiency associated with increased autophagy in retinal ganglion cells in a murine model of dominant optic atrophy. *Investigative Ophthalmology and Visual Science* **50:**2567-2571.

Williams, P. A., Morgan, J. E. and Votruba, M. (2010). Opa1 deficiency in a mouse model of dominant optic atrophy leads to retinal ganglion cell dendropathy. *Brain* **133:**2942-2951.

Williams, P. A., Morgan, J. E. and Votruba, M. (2011). Mouse models of dominant optic atrophy: What do they tell us about the pathophysiology of visual loss? *Vision Research* **51:**229-234.

Williams, P. A., Piechota, M., von Ruhland, C., Taylor, E., Morgan, J. E. and Votruba, M. (2012). Opa1 is essential for retinal ganglion cell synaptic architecture and connectivity. *Brain* **135:**493-505.

Witkovsky, P., Dudek, F. E. and Ripps, H. (1975). Slow PIII component of the carp electroretinogram. *Journal of General Physiology* **65:**119-134.

Wolpert, K. and Tsang, S. 2011. Electroretinography. *In:* Belusic, G. (ed.) *Electroretinograms.* Intech.

Wood, A., Margrain, T. and Binns, A. M. (2014). Detection of early age-related macular degeneration using novel functional parameters of the focal cone electroretinogram. *PloS One* **9:**e96742.

Xu, X. and Karwoski, C. (1995). Current source density analysis of the electroretinographic d wave of frog retina. *Journal of Neurophysiology* **73:**2459-2469.

Xu, X. and Karwoski, C. J. (1994). Current source density analysis of retinal field potentials. II. Pharmacological analysis of the b-wave and M-wave. *Journal of Neurophysiology* **72:**96-105.

Xu, X. and Karwoski, C. J. (1997). The origin of slow PIII in frog retina: current source density analysis in the eyecup and isolated retina. *Visual Neuroscience* **14:**827-833.

Xu, X. M., Bonds, A. B. and Casagrande, V. A. (2002). Modeling receptive-field structure of koniocellular, magnocellular, and parvocellular LGN cells in the owl monkey (Aotus trivigatus). *Visual Neuroscience* **19:**703-711.

Yamada, E. S., Silveira, L. C. L. and Perry, V. H. (1996). Morphology, dendritic field size, somal size, density, and coverage of M and P retinal ganglion cells of dichromatic Cebus monkeys. *Visual Neuroscience* **13:**1011-1029.

Yu-Wai-Man, P., Bailie, M., Atawan, A., Chinnery, P. F. and Griffiths, P. G. (2011a). Pattern of retinal ganglion cell loss in dominant optic atrophy due to OPA1 mutations. *Eye* **25:**597-601.

Yu-Wai-Man, P., Griffiths, P. G., Burke, A., Sellar, P. W., Clarke, M. P., Gnanaraj, L., Ah-Kine, D., et al. (2010a). The prevalence and natural history of dominant optic atrophy due to OPA1 mutations. *Ophthalmology* **117:**1538-1546, 1546.e1531.

Yu-Wai-Man, P., Griffiths, P. G. and Chinnery, P. F. (2011b). Mitochondrial optic neuropathies - Disease mechanisms and therapeutic strategies. *Progress in Retinal and Eye Research* **30:**81-114.

Yu-Wai-Man, P., Griffiths, P. G., Gorman, G. S., Lourenco, C. M., Wright, A. F., Auer-Grumbach, M., Toscano, A., et al. (2010b). Multi-system neurological disease is common in patients with OPA1 mutations. *Brain* **133:**771-786.

Yu-Wai-Man, P., Griffiths, P. G., Hudson, G. and Chinnery, P. F. (2009). Inherited mitochondrial optic neuropathies. *Journal of Medical Genetics* **46:**145-158.

Yu-Wai-Man, P., Shankar, S. P., Biousse, V., Miller, N. R., Bean, L. J., Coffee, B., Hegde, M., et al. (2011c). Genetic screening for OPA1 and OPA3 mutations in patients with suspected inherited optic neuropathies. *Ophthalmology* **118:**558-563.

Yu-Wai-Man, P., Votruba, M., Moore, A. T. and Chinnery, P. F. (2014). Treatment strategies for inherited optic neuropathies: past, present and future. *Eye* **28:**521-537.

Yu Wai Man, C. Y., Chinnery, P. F. and Griffiths, P. G. (2005). Optic neuropathies--importance of spatial distribution of mitochondria as well as function. *Medical Hypotheses* **65:**1038-1042.

APPENDIX I – CALIBRATION OF LIGHT SOURCES USED IN THIS STUDY

The miniature Ganzfeld stimulator used in this study contained four LEDs which were individually controlled by an analogue dial. The change in luminance of the four LEDs with the dial settings are shown in Figure 1.

At the start of the study, the maximum luminance of the red LED was 35.10 cd/m^2, which was lower than required for this study. The original configuration of diffusers in the tube of the miniature Ganzfeld included a semi-spherical diffuser cap. In order to increase the luminance of the red LED, the diffuser cap removed and replaced with a series of diffusing sheets at different stages during the pilot studies. The LEDs were therefore re-calibrated (i.e. dial settings were changed) after each change of diffusers to ensure the required luminances were obtained. The dial settings and corresponding luminances of the light sources are provided in Tables A1 – A8. Note however, that the configuration used at the start of the main study was maintained throughout the study.

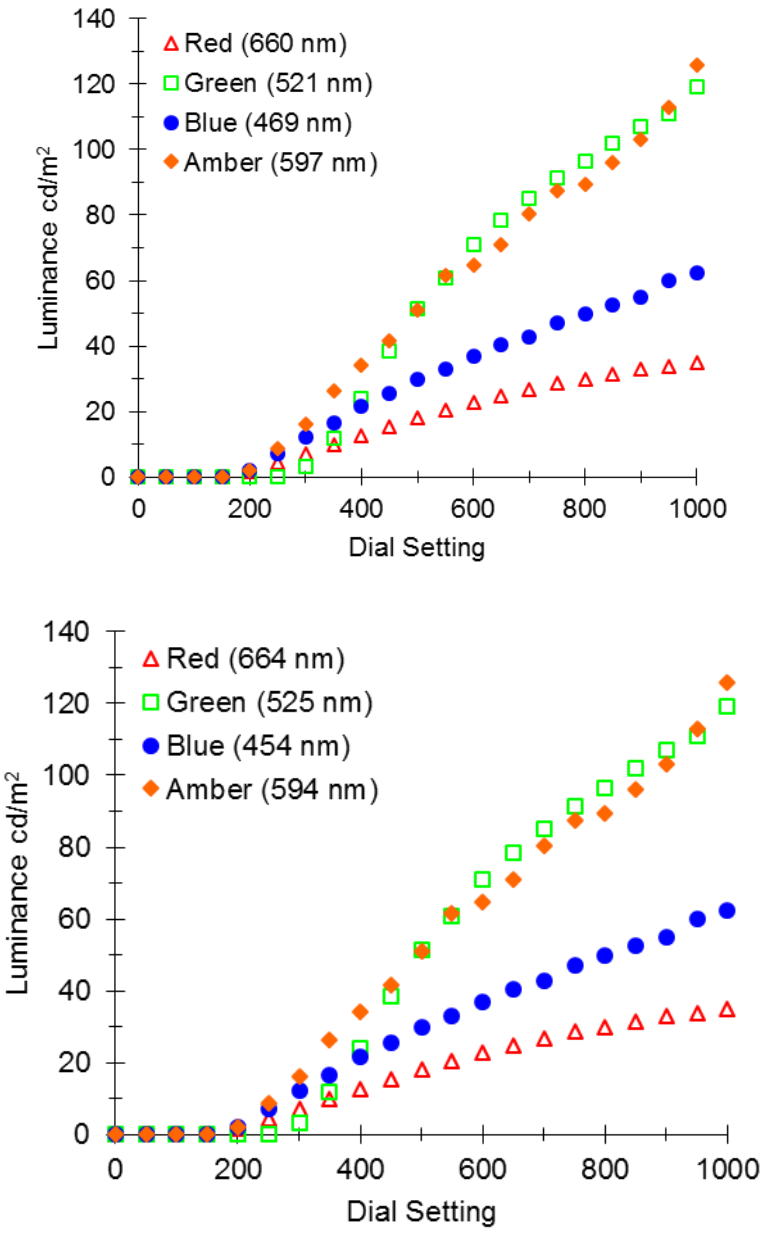

Figure A.1. Graph showing the change in luminance of the four LEDs in the miniature Ganzfeld to the dial settings. Luminance were measured using Minolta CS-100 on 21/02/2013.

Table A.1. Maximum luminance for the LEDs after diffuser cap was replaced with diffusion sheets (26-06-2016)

LED	Dial Setting	Luminance
Red	1000	61.93
Green	1000	341.30
Blue	1000	168.03
Amber	1000	228.36

Table A.2. Settings used for experiment to determine optimum stimulus duration for eliciting the long duration focal PhNR in Section 2.3. (29/07/2013)

Light Source	Dial Settings	Luminance, cd/m^2	
		Photopic	Scotopic
Red LED flash	710	55	NA
Blue LED background	195	3.75	67.35
Blue Surround	8.5V, 0.08 Amp	5.65	113.10

Table A.3. Settings used for the red LED flash in experiment to determine optimum luminance for eliciting the long duration focal PhNR in Section 2.4. (12-04-2013)

Luminance, cd/m^2 (Red LED flash)	2	4	7	12	17	26	40	55
Dial Setting	198	230	272	339	412	556	772	989

Table A.4. Settings used for background light sources in experiment to determine optimal luminance for eliciting the long duration focal PhNR in Section 2.4. Date - 12-04-2013

Light Source	Dial Settings	Luminance, cd/m^2	
		Photopic	Scotopic
Blue LED	199	3.75	67.35
Blue Surround	8.5V, 0.08 Amp#	5.65	113.10

- The blue surround background was controlled by a voltage controller

Table A.7. Settings for experiment to determine optimum stimulus wavelength for eliciting the long duration focal PhNR in section 2.5. (26/07/2013 to 09/08/2013)

LED	Type	Dial Setting	Luminance, cd/m^2	
			Photopic	Scotopic
Red	Flash	710	57.18	NA
Green	Flash	385	53.12	NA
Blue	Flash	400	60.68	NA
Amber	Flash	310	56.86	NA
Green	Background	372	35.59	143.42
Blue	Background	198	3.75	67.35
Amber	Background	Max	300.58	104.70

Table A.8. Settings used for main study. Calibrated using ILT 1700 (Able Instruments and Controls, Reading, UK). (20/01/2014 to 24/01/2014)

ERG	Light Source	Type	Dial Setting	Luminance, cd/m^2	
				Photopic	Scotopic
Focal	Red	Flash	600	55.10	NA
	Blue	Flash	300	56.50	NA
	Blue	Background	180	4.47	80.27
	Blue	Surround	0.85 V, 0.09 amps	7.00	139.94
Full-field	Red	Flash	870	53.00	NA
	Blue	Background	186	4.31	77.40

Table A.9. Ganzfeld bowl settings for brief full-field ERG. Calibrated using ILT1700 (Able Instruments and Controls, Reading, UK). (14/01/2014)

Flash Settings	Colour	Red
	Flash Strength	20
	Measured luminance	1.51 cd.s/m^2
	Neutral density filter	0.3
	Duration	300
	Flash frequency	2 Hz
Background Settings	Colour	Blue
	Background luminance setting	300
	Measured luminance	2.92 cd/m^2 (63.95 scot cd/m^2)

APPENDIX II – CALCULATION OF DENSITIES AND CUMULATIVE COUNTS OF THE RECEPTIVE FIELDS OF RGCS

1. The receptive field densities of all RGCs, d_{gf}, in deg^2, at a given eccentricity, r_x, in each of the four meridians were calculated based on the formula Watson 2014 (Equation I.1). A data table of receptive field densities was generated for values of *r*, ranging from 0 to 70^o in 0.01^o steps using Microsoft Excel.

$$d_{gf}(r,k) = d_{gf}(0) * \left[a_k \left(1 + \frac{r}{r_{2,k}}\right)^{-2} + (1 - a_k)\exp\left(-\frac{r}{r_{e,k}}\right)\right]$$

Equation II.1

where $d_{gf}(r, k)$ is the density of RGCfs at eccentricity, *r,* in degrees along meridian, *k;* $d_{gf}(0)$ is the density receptive fields at the centre of the fovea (33,163.2 RGCf/deg^2), a_k is the weighting function of the first term, r_2 is the eccentricity at which RGC receptive field density is reduced by a factor of 4 (and spacing is doubled) and $r_{e,k}$ is the scale factor by the index *k*. The values of the constants are provided in Table II.1.

Table II.1. The values of constants for Equation 1 in four meridians (Watson, 2014)

Meridian (*k*)*	***a***	***r_2***	***r_e***
Temporal	0.9851	1.058	22.14
Superior	0.9935	1.035	16.35
Nasal	0.9729	1.084	7.633
Inferior	0.9960	0.9932	12.13

* Meridians refer to visual field locations

2. Since a circular stimulus was used in this study, the mean density, d_{av}, in deg^2, was calculated as the average of the densities of the four meridians and plotted as a function of eccentricity (Figure 1A). The dimensions of the stimuli used in the study are provided in Table 2. The mean receptive field densities are shown in Table 3 for the eccentricities used in this study. Note that the density in temporal visual field from 12^o – 17^o = 0 because of optic nerve head.

3. The number of all RGCfs, *T*, at a given eccentricity, r_x, was calculated by integrating the mean density, d_{av}, at eccentricity, r_x, using the trapezoid rule and multiplying this by 2πr to account for the increasing area (Equation 2), as required by Watson (2014).

$$T = (r_x - r_0) * \left(\frac{d_{avx} - d_{av0}}{2}\right) * 2\pi r_x$$

Equation 2

where *T* is the total number of RGC receptive fields, r_x is the given eccentricity, r_o is the previous adjacent eccentricity, d_{avx} and d_{avo} are the mean RGCf densities at r_x and r_o respectively.

4. The cumulative count of all RGCfs at a given eccentricity, r_x, was calculated as the cumulative sum of *T* from $r = 0$, to r_x. This was plotted in Figure 1B.
5. The number of RGCfs in each annulus was then calculated as the sum of T for from the inner radius to the outer radius of the annulus (see Table 4)

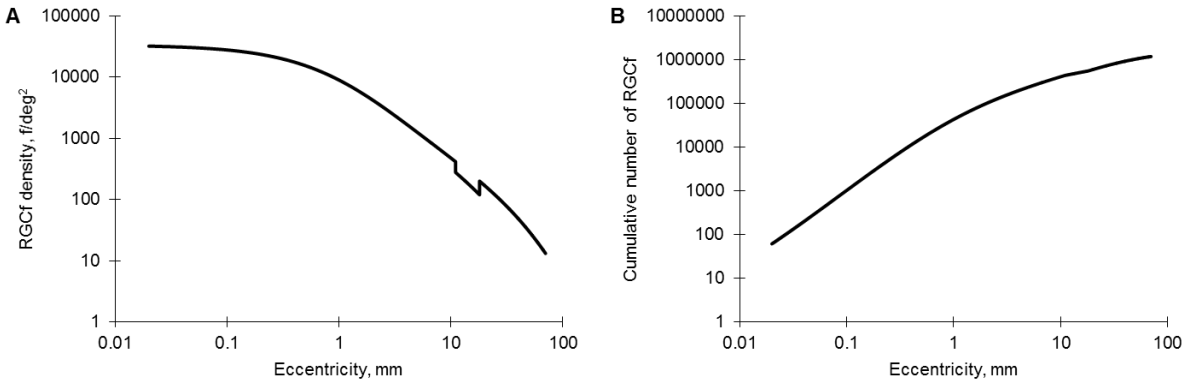

Figure II.1. A – Mean density of midget ganglion cell receptive fields as a function of eccentricity computed from the formula provided by Watson (2014). The "valley" in the curve corresponds to the blind spot. B – Cumulative number of midget ganglion cell receptive fields as a function of eccentricity. Graphs are plotted on a log scale

Calculation of densities and cumulative counts of the receptive fields of ON and OFF RGCs

For the long duration stimulus, the densities and cumulative counts of the receptive fields of ON and OFF RGCs were required in order to compare them respectively to the PhNR-ON and PhNR-OFF parameters. For this, the distribution of ON and OFF

cell of all RGC types was needed. As there are many different RGC types in the retina, the two major morphological types, the midget and parasol RGCs, were settled on. A third group, which was called “others” was added to include all the other RGCs in the retina.

The receptive field density of midget cells (mRGCf) at a given eccentricity, r, in a meridian, *k*, was given by Watson (2014) as,

$$d_{mf}\,(r,k) = 2d_c\,(0)(1+\frac{r}{r_m})^{-1} * [a_k(+\frac{r}{r_{2,k}})^{-2} + (1-\ a_k)\exp(-\frac{r}{r_{ek}})$$

Equation II.3

where d_{mf} is the density of midget RGC receptive fields, d_c is the density of foveal cones (= 14,804.6 cones/deg^2); r is the eccentricity of interest, r_m = 41.03º, r_2 = eccentricity is the eccentricity at which RGC receptive field density is reduced by a factor of 4 (and spacing is doubled), a_k is the weighting function of the first term, $r_{e,k}$ is the scale factor by the index, k, and k is the index of the meridian.

Calculations for ON and OFF mRGCs were based on the ratio of ON:OFF mRGCs from 0 – 5º = 1:1; from 5 – 25º = 1:1 to 1:1.69; and beyond 25º = 1:1.69 (Drasdo et al., 2007). Explicit details of the distribution of the parasol RGCs (pRGCs) in humans were not available in the searched literature. Therefore, they were assumed to constitute 10% of the RGC population at all eccentricities based on the 8 – 12% reported by Silveiro et al (2004) for macaque. The ON:OFF ratio of parasol RGCs was then computed to be 0.4:0.6 based on the dendritic field size differences between ON and OFF pRGCs (Dacey and Petersen, 1992). The proportion of RGCs in the “others” group was calculated by subtracting the sum of the midget and parasol RGCs from the total number of RGCs at each eccentricity. The ON:OFF ratio for the others group was assumed to be 1:1.

Table II.2. Dimensions of stimulus sizes used in the study.

Stimulus Angular Size (Diameter), deg	Viewing distance, cm	Angular radius, deg	Stimulus Angular Area, deg^2	Annulus Area, deg^2	Annulus Dimension (Inner - outer radius), deg	Eccentricity (midpoint of stimulus), mm
5	66.42	2.5	19.63	19.63	0.00 – 2.5	1.25
5.5	(60.37)	2.75	(23.76)	(23.76)	0.00 – 2.75	(1.38)
10	33.15	5.00	78.54	58.90 (54.78)	2.51 – 5.00 (2.76 – 5.00)	3.75 (3.88)
15	22.03	7.50	176.71	98.17	5.51 – 7.50	6.25
20	16.45	10.00	314.16	137.44	7.51 – 10.00	8.75
30	10.82	15.00	668.37	392.70	10.01 – 15.00	12.50
(45)	7.00	(22.50)	(1590.43)	(883.57)	(15.01 – 22.50)	(18.75)
60	5.02	30.00	2788.95	2120.58 (1237.00)	15.01 – 30.00 (22.51 – 30.00)	22.50 (26.25)
110	NA	55.00	9464.83	6675.88	30.01 – 55.00	42.50

Values in brackets apply to long duration stimulus used in Experiment 1. NA – not applicable. NB – The area of the optic nerve head (38.48 deg^2; assuming a diameter of 7^o and beginning at 11^o from the fovea (Watson, 2014)) has been subtracted from angular areas of stimuli $\geq$30^o.

Table II.3. Mean receptive field density and counts of RGCfs for eccentricities used in this study

Stimulus Size, deg	Eccentricity, deg	RGCf Density, /deg^2	RGCf Cumulative Count, n	No. of RGCfs in Annulus
5	1.25	7211.95	56245.41	123728.93
(5.5)	(1.38)	6491.82	63560.24	136063.34
10	3.75 (3.88)	1857.47 (1779.49)	182196.35 (187425.19)	110293.66 (97959.25)
15	6.25	917.72	281056.76	90485.39
20	8.75	573.29	365148.74	78977.70
30	12.50	224.88	460348.69	98368.63
(45)	(18.75)	(187.41)	(561932.51)	(138541.34)
60	22.50 (26.25)	139.60 (107.43)	640198.36 (710322.80)	271687.79 (133146.45)
110	42.50	42.77	942631.07	291422.63

Table II.4. Table for calculating the proportion of receptive fields of ON and OFF cells of all RGC types, midget RGCs, parasol RGCs and other RGCs

Stimulus Size (Diameter), deg	Annulus (Inner - outer radius), deg	No. of all RGCf in Annulus (A)	No. of Midget RGCfs in Annulus#			No. of Parasol RGCfs in Annulus			No. of Other RGCfs in Annulus		
			Total mRGCf (B)	ON mRGCf (C)	OFF mRGCf (D)	Total pRGCf (E = A – B)	ON pRGCf (F= E*0.4)	OFF pRGCf (G= E*0.6)	Total oRGCf (H = A – B – E)	ON oRGCfs (I= H*0.5)	OFF oRGCFs (J= H*0.5)
5.5	0.00 – 2.75	136063.34	117354.34	58677.17	58677.17	13606.33	5442.53	8163.80	5102.67	2551.33	2551.33
10	2.76 – 5.00	97959.25	80001.69	40000.85	40000.85	9795.92	3918.37	5877.55	8161.63	4080.82	4080.82
15	5.51 – 7.50	90485.39	70174.28	34534.80	35639.48	9048.54	3619.42	5429.12	11262.57	5631.29	5631.29
20	7.51 – 10.00	78977.70	58160.09	27673.66	30486.43	7897.77	3159.11	4738.66	12919.83	6459.92	6459.92
30	10.01 – 15.00	98368.63	67740.56	30712.75	37027.80	9836.86	3934.75	5902.12	20791.21	10395.61	10395.61
45	15.01 – 22.50	138541.34	84613.43	34631.23	49982.20	13854.13	5541.65	8312.48	40073.78	20036.89	20036.89
60	22.51 – 30.00	133146.45	72714.80	27126.28	45588.52	13314.65	5325.86	7988.79	47117.01	23558.50	23558.50
110	30.01 – 55.00	291263.11	130815.36	48401.68	82413.67	29126.31	11650.52	17475.79	131321.44	65660.72	65660.72
Total		1064805.21	681574.54	301758.42	379816.12	106480.52	42592.21	63888.31	276750.15	138375.07	138375.07

- Total number of mRGCf was calculated from Equation 3. Calculations for ON and OFF mRGCs were based on the ratio of ON:OFF mRGCs from 0 – 5^{o} = 1:1; from 5 – 25^{o} = 1:1 to 1:1.69; and beyond 25^{o} = 1:1.69 (Drasdo et al., 2007)

Table II.4. (continued)

Stimulus Size (Diameter), deg	Annulus (Inner - outer radius), deg	No. of all RGCf in Annulus (A)	Total No. of ON RGCfs (K = C + F + I)	Total No. of OFF RGCfs (L = D + G + I)	ON-RGCfs Fraction (M = K/A)	OFF-RGCfs Fraction (N = L/A)	RGC Density, /deg^2 (O)	All ON-RGCf Density (P = M*O)	All OFF-RGCf density (Q = N*O)
5.5	0.00 – 2.75	136063.34	66671.04	69392.30	0.49	0.51	6491.82	3180.99	3310.83
10	2.76 – 5.00	97959.25	48000.03	49959.22	0.49	0.51	1779.49	871.95	907.54
15	5.51 – 7.50	90485.39	43785.50	46699.89	0.48	0.52	917.72	444.08	473.64
20	7.51 – 10.00	78977.70	37292.69	41685.01	0.47	0.53	573.29	270.70	302.59
30	10.01 – 15.00	98368.63	45043.10	53325.53	0.46	0.54	22.4.88	102.97	121.91
45	15.01 – 22.50	138541.34	60209.77	78331.57	0.43	0.57	187.41	81.45	105.96
60	22.51 – 30.00	133146.45	56010.64	77135.81	0.42	0.58	107.43	45.19	62.24
110	30.01 – 55.00	291263.11	125712.93	165550.18	0.43	0.57	42.77	18.46	24.31
Total		1064805.21	482725.70	582079.51	-	-	-	-	-

Table II.5. Table of values for number of RGCf in annuli used to calculate PhNR density using the brief flash

Stimulus Angular Size (Diameter), deg	Eccentricity (Midpoint of Annulus), deg	Annulus Dimension (Inner - outer radius), deg	Number of RGCf in Annulus
5	1.25	0.00 – 2.50	123728.93
10	3.75	2.51 – 5.00	110293.66
15	6.25	5.51 – 7.50	90485.39
20	8.75	7.51 – 10.00	78977.70
30	12.50	10.01 – 15.00	98368.63
60	22.50	15.01 – 30.00	271687.79
110	42.50	30.01 – 55.00	291422.63

APPENDIX III – SAMPLE SIZE CALCULATION FOR INDEPENDENT SAMPLES T-TEST

Sample size calculated using Altman Nomogram (Figure 1) based on standardised difference = 1.5 (see Equation III.1), power of the study = 80% and significance level of 5%.

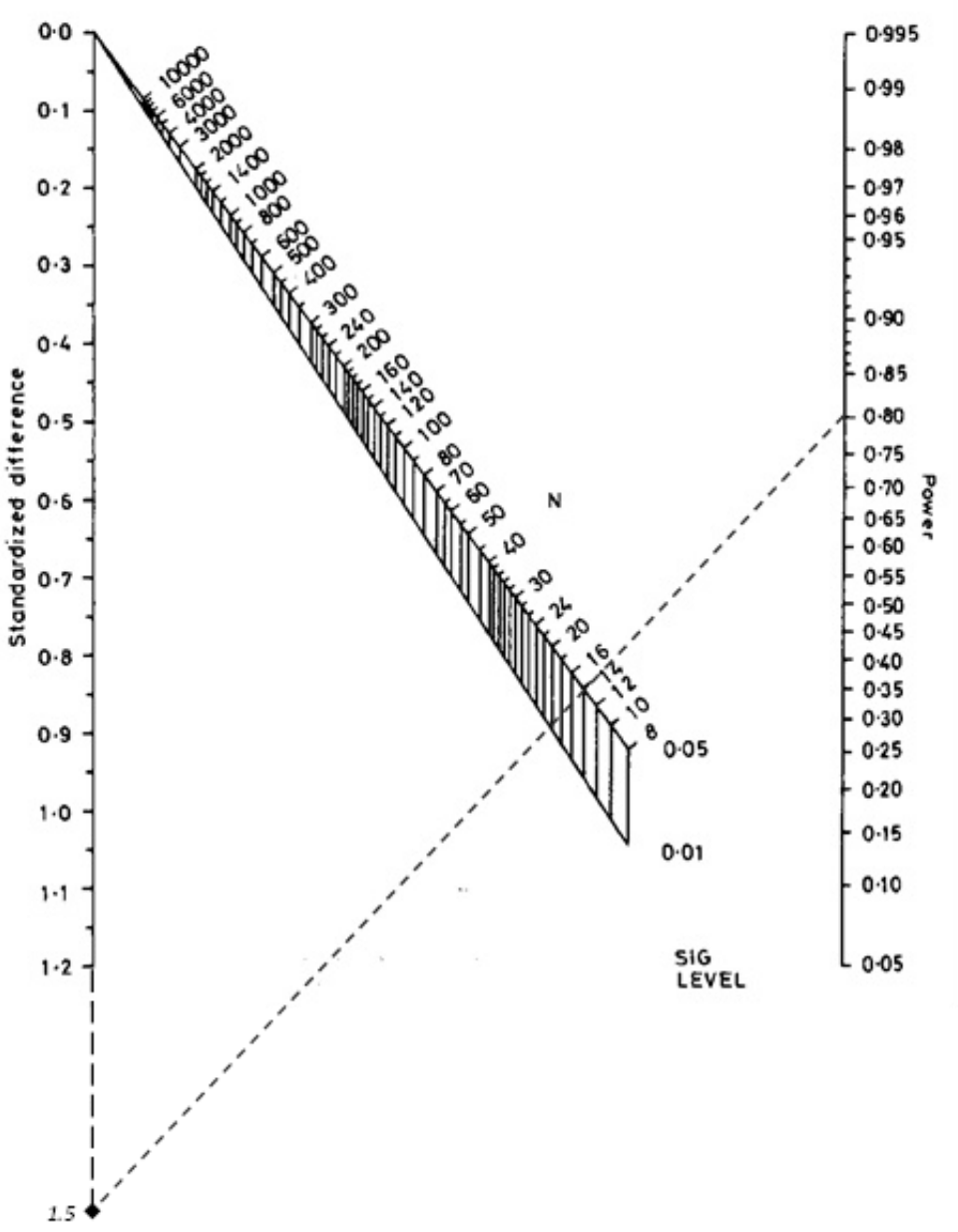

Figure III.1 Nomogram for calculating sample size, given Power = 80% and standardised difference = 1.5 (rounded up for simplicity). (Modified from Altman, 1991)

Equation III.1:

$$Standardised\ Difference = \frac{difference\ between\ groups}{standard\ deviation}$$

Based on Miyata et al. 2007:

Mean PhNR amplitude in controls (± standard deviation) = 34.3 (± 9.0)

Mean PhNR amplitude in ADOA (± standard deviation) = 21.0 (± 2.4)

$$Standardised\ Difference = \frac{(34.3 - 21.0)\mu V}{(9.0)\mu V}$$

$$Standardised\ Difference = 1.48$$

APPENDIX IV – STUDY PROTOCOL

PARAMETER	EQUIPMENT	IMPLEMENTATION
OBJECTIVE REFRACTIVE ERROR	Topcon KR – 7500 Auto-kerato-refractometer	Record mean of three readings If patient has uncorrected refractive error $\geq$ +/- 0.50 DS, perform subjective refraction for best corrected visual acuity (BCVA) If objective prescription is within +/- 0.50 D (best vision sphere) of patient's current spectacle prescription, then proceed; if not, then refract for BCVA BCVA should be better than or equal to 1.0 logMAR in the better seeing eye for inclusion into study
PRESENTING DISTANCE VISUAL ACUITY	Early treatment diabetic retinopathy study (ETDRS) Chart	Test distance VA: 4m Room illumination: Well lit (60-120 cd/m^2) Check VA with near addition if required Patient is encouraged to read/guess until more than half the letters on line are missed Record VA in logMAR
PRESENTING READING ABILITY	Near logMAR chart (N-notation)	Test distance: 40 cm Room illumination: Well lit (60-120 cd/m^2) Check VA with current prescription if available Record near VA in N-notation
CONTRAST SENSITIVITY	Pelli-Robson Chart	Test distance: 1 metre Room Illumination: Well lit Record contrast sensitivity in log units (Score 0.05 log CS per letter. Per letter recording is more repeatable than the line recording (Elliot, 2006)
VISUAL FIELDS	Humphrey Field Analyzer – 720i	Protocol: 24-2 SITA Fast Perform two sessions. First session is for training and second session results will be recorded for study Record the following indices Fixation losses (should be <30% for reliability) False negative (should be <20% for reliability) False positive (should be <20% for reliability)

		Mean deviation (dB) If “a” AND either “b” or “c” are unreliable, repeat test to confirm Save and print out field plot data
INTRAOCULAR PRESSURE	Nidek Auto non-contact tonometer, NT-2000	Record the mean of 3 readings per eye (mmHg)
COLOUR VISION	Farnsworth-Munsell D-15 desaturated colour vision kit	Illumination: Well Lit Plot score (arrangement of discs) on score sheet Determine axis of defect if present (protanopia, deutranopia, tritanopia) otherwise record “Normal”
ANTERIOR SEGMENT OCULAR HEALTH	Keeler SL-16 Slit lamp biomicroscope	Assess Eyelids*, Conjunctiva*, Sclera*, Cornea*, Anterior chamber angle#, Pupils (shape, size, reflex), Lens# *: Based on Efron Grading Scales for Contact Lens Complications (Efron, 1998) #: Based on Optometric Grading Scales (Pearson, 2003)
RETINAL GANGLION LAYER FUNCTION	Electrodes: DTL fibre Electronic recording system: Medelec Synergy System Visual stimulation PERG: Computer monitor, ViewSonic G70fm Full field ERG: Ganzfeld full field stimulator, GS2000, LACE Elettronica, Italy Focal ERG: LED miniature Ganzfeld Stimulator, CH Electronics, Bromley, Kent, UK	Pattern electroretinogram (PERG) Check size: $0.8^o \pm 0.2^o$ (=5mm)* Repetition rate: 4 reversals per second* Field size: 20^o x 20^o Viewing distance: 36 cm Contrast = 98.5%* Mean luminance: 46.7 cd/m^2 Amplitude of P50: measured from trough of N35 to peak of P50* Amplitude of N95: measured from peak of P50 to trough of N95* Calculate P50:N95 ratio Brief flash full field ERG#+ Red flash duration = 300µsec Red flash luminance = 1.69 cd.s/m^2 Flash repetition rate = 4 Hz

		Blue background luminance = 3.9 log scot td (206 scot cd/m^2) Long duration full field ERG+ Red flash duration = 250msec Flash luminance = 55 cd/m^2 Flash repetition rate = 2Hz Blue background luminance = 100 scot cd/m^2 Measurement of components: a-wave: Amplitude: pre-stimulus baseline to trough of a-wave Time-to-peak: stimulus onset to trough of a-wave b-wave Amplitude: trough of a-wave to peak of b-wave Time-to-peak: stimulus onset to peak of b-wave PhNR-ON Amplitude: peak of b-wave to trough of PhNR-on Time-to-peak: d-wave Amplitude: time point of stimulus offset to peak of d-wave Time-to-peak: stimulus offset to peak of d-wave PhNR-OFF Amplitude: peak of d-wave to trough of PhNR-OFF Time-to-peak: stimulus offset to trough of PhNR-OFF Long duration focal ERG+ Red on Blue Red flash duration = 250msec Flash luminance = 55 cd/m^2 Flash repetition rate = 2Hz Blue background luminance = 100 scot cd/m^2 Stimulus size = 20^o

		Test area: Central, nasal, temporal macula Blue on Amber (focal) Blue flash duration = 250msec Flash luminance = 55 cd/m^2 Flash repetition rate = 2Hz Amber background = 100 scot cd/m^2 Stimulus size = 20^o Test area: Central, nasal, temporal macula Measurement of components: See “3.e.” above (*: ISCEV protocol; #: Settings adopted from (Binns et al., 2011); +: Test requires pupil dilation with 1% Tropicamide)
POSTERIOR SEGMENT OCULAR HEALTH AND FUNDUS EXAMINATION	Direct ophthalmoscope (Keeler Professional) Fundus camera (Topcon 3D 1000 OCT)	Ophthalmoscopy: Assess Vitreous, Optic nerve head, Cup to disc ratio, Pallor, Disc contours, Macula Fundus photography: Peripheral retina Field angle: 45^o Take photograph with macula centred Assess central retina and optic nerve head features (cup to disc ratio and disc pallor)
RETINAL NERVE FIBRE LAYER THICKNESS	Topcon 3D OCT 1000	Scan type: B-scan of Macula B-scan of Optic nerve Record average mean (360^o) thickness (µm) and mean thickness of temporal, superior, nasal, inferior quadrants

APPENDIX V – SAMPLE SIZE CALCULATION FOR A BIVARIATE CORRELATION

The total sample size required for a bivariate correlation, N, is given by:

$$N = \left(\frac{Z_\alpha + Z_\beta}{C}\right)^2 + 3$$

Where Z_α is the z-score for α (2-tailed) and Z_β is the z-score for β. α is the level of significance (p-value) and β $=1 - \frac{power}{100}$. C $=0.5\times \ln(\frac{1+r}{1-r})$ **, w**here r is the correlation coefficient.

Based on previous studies, the correlation between the retinal nerve fibre layer and ERG amplitude shows a large effect ($r \geq 0.5$). To determine the required sample size for this study using r = 0.5, p = 0.05 and power = 80%,

$$C = 0.5\times \ln\left(\frac{1 + 0.5}{1 - 0.5}\right)$$

$$C = 0.549$$

Given that $Z_\alpha = 1.960$ and $Z_\beta = 0.842$, then

$$N = \left(\frac{1.960 + 0.842}{0.549}\right)^2 + 3$$

$$N = 29.05$$

APPENDIX VI – POWER SPECTRUM OF FOCAL AND PATTERN ELECTRORETINOGRAM

Focal and pattern ERGs were Fourier analysed offline to remove high frequency signals. The Fourier analysis was based on the approach (derived from first principles) by Stroud (1986). A visual inspection of the power spectrum (generated offline) of the focal ERGs showed that most of the power was concentrated in the first 20 harmonics (40 Hz) (Figure II.1). In the case of the PERG, the power was concentrated in the first 10 harmonics (20 Hz) (Figure II.2). However, the cut-off was increased to 25 harmonics (50Hz) for the focal ERG and 15 harmonics (30 Hz) for the PERG as these were points at which the power had levelled off.

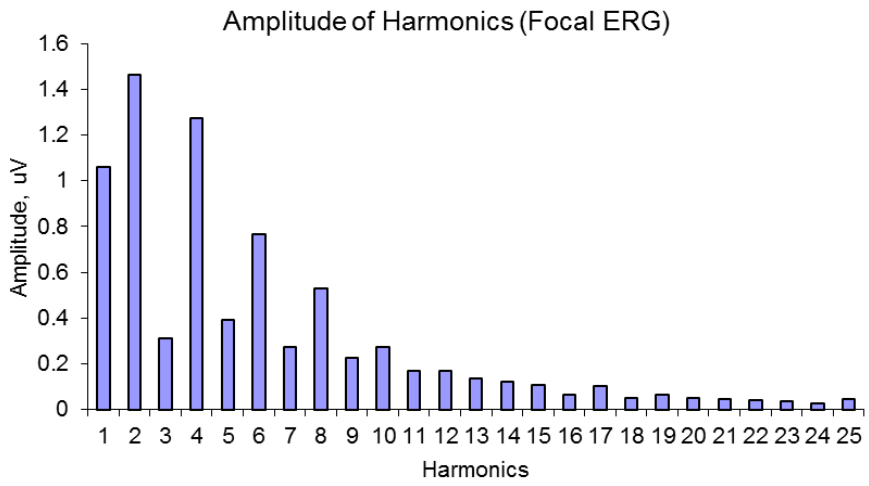

Figure II.1. Power spectrum for grouped average focal ERG of 12 control participants.

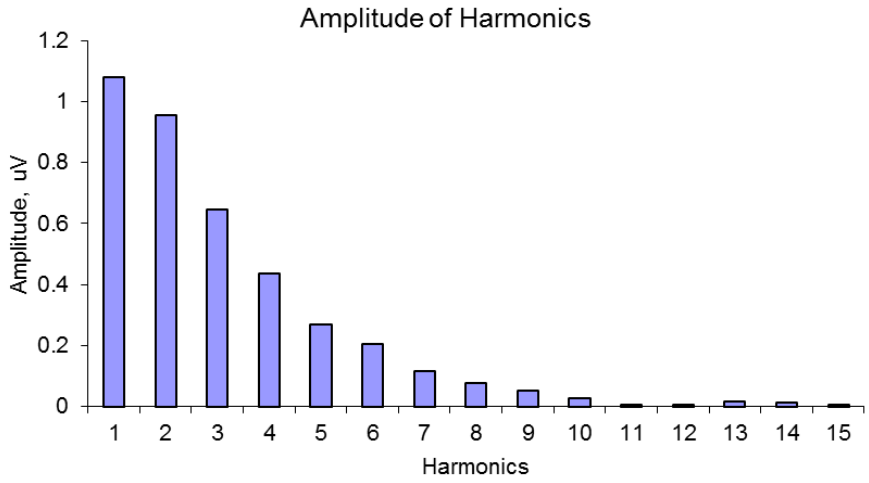

Figure II.2. Power spectrum for grouped average PERG of 12 control participants.

APPENDIX VI – PEER REVIEWED PUBLICATION

Please turn over to next page.

Retina

Electrophysiological ON and OFF Responses in Autosomal Dominant Optic Atrophy

Enyam Komla A. Morny,[1] Tom H. Margrain,[1] Alison M. Binns,[2] and Marcela Votruba[1,3]

[1]School of Optometry and Vision Sciences, Cardiff University, Cardiff, United Kingdom
[2]Division of Optometry and Visual Sciences, City University, London, United Kingdom
[3]Eye Unit, University Hospital of Wales, Cardiff, United Kingdom

Correspondence: Marcela Votruba, School of Optometry and Vision Sciences, Cardiff University, Maindy Road, Cardiff CF24 4HQ, UK; votrubaM@cardiff.ac.uk.

Submitted: August 14, 2015
Accepted: October 21, 2015

Citation: Morny EKA, Margrain TH, Binns AM, Votruba M. Electrophysiological ON and OFF responses in autosomal dominant optic atrophy. *Invest Ophthalmol Vis Sci*. 2015;56:7629–7637. DOI:10.1167/iovs.15-17951

Purpose. To assess the effect of autosomal dominant optic atrophy (ADOA) on ON and OFF retinal ganglion cell (RGC) function by evaluating the ON and OFF components of the photopic negative response (PhNR).

Methods. Twelve participants from six families with *OPA1* ADOA and 16 age-matched controls were recruited. Electrophysiological assessment involved pattern ERGs (PERGs), focal (20°) and full-field long-duration (250 ms) flash ERGs using a red light-emitting diode flash on a rod-saturating blue background, and full-field brief (300 μs) xenon flash ERGs using a red filter over a continuous rod saturating blue background. Amplitudes and implicit times of the ERG components were analyzed and the diagnostic potential of each electrophysiological technique was determined by generating receiver operating characteristic (ROC) curves.

Results. Mean amplitudes of the N95 and all PhNRs, except the full-field $PhNR_{ON}$, were significantly reduced in participants with ADOA ($P < 0.01$). Subtraction of the group-averaged focal ERG of ADOA participants from that of controls showed an equal loss in the focal $PhNR_{ON}$ and $PhNR_{OFF}$ components, whereas in the full-field ERG the loss in the $PhNR_{OFF}$ was greater than that in the $PhNR_{ON}$ component. The areas under the ROC curve (AUC) for the focal $PhNR_{ON}$ (0.92), focal $PhNR_{OFF}$ (0.95), and full-field $PhNR_{OFF}$ (0.83), were not significantly different from that of the PERG N95 (0.99).

Conclusions. In patients with ADOA, the $PhNR_{ON}$ and $PhNR_{OFF}$ components are nearly symmetrically reduced in the long-duration ERG, suggesting that ON- and OFF-RGC pathways may be equally affected.

Keywords: autosomal dominant optic atrophy, photopic negative response, PhNR

Autosomal dominant optic atrophy (ADOA) is a hereditary optic neuropathy characterized by variable bilateral loss of vision in early childhood, optic nerve pallor, centrocecal visual field scotoma, and color vision defects.[1–5] It is the commonest hereditary optic neuropathy with a prevalence between 1 in 50,000 and 1 in 8000.[6–11]

Autosomal dominant optic atrophy is caused primarily by mutations in the autosomal nuclear gene, *OPA1*,[9,12–15] a key player in mitochondrial dynamics, controlling mitochondrial fusion, among other key roles. Histopathologic studies in humans[16,17] and mouse models[18–21] show that ADOA is principally characterized by the degeneration of the RGCs.

In a mouse model of ADOA, generated in our laboratory,[21] the defect is first evident as a dendritic pruning of RGCs in B6:C3-*Opa1*^{Q285STOP} *Opa1* mutant mouse, which appears to be ON-center specific.[18,22] This selective vulnerability of ON-center RGCs may reflect their higher energy demands in comparison with their OFF-center counterparts, as *OPA1* mutations are thought to curtail mitochondrial energy output.[18,22] This new finding has, however, not been investigated in humans with ADOA.

The functional integrity of RGCs can be evaluated by assessing the photopic negative response (PhNR) of the flash ERG. The PhNR is a negative potential seen after the b-wave in a photopic ERG elicited by a brief flash. The PhNR is believed to primarily originate from spiking activity in RGCs and their axons with contributions from amacrine cells and possible involvement of associated glial cells/astrocytes of the retina.[23–26] When a long-duration flash is used to evoke the ERG, the PhNR is seen once after the b-wave ($PhNR_{ON}$) and again as a negative going potential after the d-wave ($PhNR_{OFF}$). Furthermore, it has been demonstrated that the ERG obtained in response to a long-duration red flash of moderate intensity provides optimal delineation of the $PhNR_{ON}$ and $PhNR_{OFF}$ components.[23,26,27]

The brief-flash PhNR is attenuated in patients with ADOA[28] and in the *Opa1*^{Q285STOP} mutant mouse.[29] In the mouse model, the defect is seen before any changes in visual acuity on optokinetic drum testing and before morphologic changes on retinal histology. This suggests that retinal connectivity may be affected before RGC somal loss affects RGC function.[22] Thus, the PhNR deficit could serve as a marker for early disease. These early changes in RGC function may be reversible and need to be defined as markers for targeted therapies in any forthcoming therapeutic trials.

Miyata et al.[28] and Barnard et al.[29] highlight the diagnostic potential of the PhNR in ADOA; however, the investigators used a brief white flash (broadband stimulus) to evoke the PhNR,

Copyright 2015 The Association for Research in Vision and Ophthalmology, Inc.

TABLE 1. Clinical Characteristics of Participants With ADOA

Participant ID/Sex	Family	Age	Visual Acuity, logMAR		Contrast Sensitivity, log Units		Mean Deviation, dB		Color Vision	*OPA1* Mutation
			RE	LE	RE	LE	RE	LE		
1010/F	A	49	1.34	1.32	0.35	0.40	−27.03	−25.15	Mixed	c.1202G>A
1011/F	B	55	1.64	1.62	0.00	0.00	−17.65	−19.58	Mixed	C1508A
1012/F	C	58	0.80	1.00	1.15	1.05	−8.68	−10.39	Mixed	IVS8+5G>A
1013/F	C	61	1.10	0.64	NA	NA	−12.47	−9.06	Mixed	IVS8+5G>A
1014/M	D	33	1.40	1.32	0.30	0.45	−13.84	−11.89	Protan/deutan	NA
1015/F	D	31	1.02	0.98	1.05	1.05	−13.98	−13.20	Protan/deutan	NA
1016/F	E	18	0.80	0.80	1.65	1.35	−7.08	−8.15	Tritan	IVS9+3A>T
1017/F	E	27	0.82	0.80	1.65	1.65	−5.14	−5.82	Tritan	IVS9+3A>T
1018/F	E	59	0.86	0.96	0.90	0.75	−9.55	−7.03	Tritan	IVS9+3A>T
1019/F	E	49	0.72	1.20	1.50	1.50	−5.99	−6.79	Tritan	IVS9+3A>T
1020/M	E	46	0.98	1.20	1.65	1.20	−10.15	−8.21	Tritan	IVS9+3A>T
1021/M	F	39	0.02	0.00	1.65	1.65	−1.31	−2.25	NA	c.357delT

RE, right eye; LE, left eye; NA, not available.

which provides a poor signal-to-noise ratio compared with monochromatic stimuli,[26] and cannot distinguish ON and OFF components. Furthermore, the studies elicited full-field (global) PhNRs that, in contrast to the focal PhNR, are less sensitive in detecting focal retinal lesions, such as those seen in early to moderate glaucoma.[30,31] As ADOA results in localized centrocecal visual field defects,[1] it might be expected that a focal stimulus presented to this region would enhance the sensitivity of the PhNR to early disease-related changes.

The aim of this study was to assess the relative effect of ADOA on the $PhNR_{ON}$ and $PhNR_{OFF}$ components elicited using focal and full-field long-duration red flashes on a rod-suppressing blue background. An additional aim was to compare the diagnostic potential of the long-duration PhNRs to responses that have previously been shown to be affected by ADOA; the full-field brief-flash PhNR[28,29] and the N95 amplitude of the pattern ERG (PERG),[32] which also reflects spiking activity of the RGCs.[33]

METHODS

Participants

Twelve participants (aged 18–61 years) from six families with documented *OPA1* mutations and 16 healthy age-matched controls (aged 19–61 years) were recruited for the study (see Table 1 for characteristics of all 12 participants). Detailed information about the clinical characteristics of nine of the participants have been reported elsewhere.[1] The study conformed to the Declaration of Helsinki and was approved by the National Health Service Research Ethics Committee for Wales, as well as the ethics committees of the School of Optometry and Vision Sciences, Cardiff University, and the Division of Optometry and Visual Science, City University, London. All participants provided their written consent after receiving a participant information sheet and having the opportunity to ask questions. Nine participants with ADOA (ID numbers 1010–1017, 1021) were examined in Cardiff and the rest at City University London by the same investigator.

Electroretinograms

All ERGs were recorded monocularly using a DTL fiber active electrode (Unimed Electrode Supplies, Ltd., Surrey, UK) and a contralateral reference. The DTL fiber was placed in the lower fornix to maximize stability during recording and the loose end fastened using medical tape at the inner canthus (Blenderm; Viasys Healthcare, Ltd., Warwick, UK). A silver–silver chloride 10-mm diameter touch-proof skin electrode (Unimed Electrode Supplies, Ltd.), placed at the midfrontal forehead position was used as ground electrode.

Electroretinogram responses were obtained using an evoked potential monitoring system (Medelec EP; Oxford Instruments PLC, Surrey, UK [Cardiff site]; Espion; Diagnosys LLC, Cambridge, UK [City University site]). Responses were bandpass filtered from 1 to 100 Hz and digitally averaged. Signals were recorded in blocks of 10 to 20 responses, with a total of 40 to 60 averaged per trace. Between four and six traces were obtained for each stimulus condition. The traces were superimposed to confirm signal repeatability and averaged off-line into a single averaged trace containing 160 to 300 responses. An automatic artifact rejection system removed signals contaminated by large eye movements and blinks.

Transient PERG stimuli (four reversals per second; check size = 1°) were generated on a computer monitor at 98% contrast. The screen was masked with a black opaque cardboard with a 13 × 13-cm square cut-out at the center so that it produced a 20° × 20° field at a viewing distance of 36 cm.

Long-duration ERGs were recorded using a red flash stimulus (peak output 660 nm, 250-ms duration, 3.33 log phot td, 2 Hz) on a rod-saturating blue background (peak output 469 nm, 3.49 scot log td) produced by a handheld miniature Ganzfeld light-emitting diode (LED) stimulator (CH Electronics, Kent, UK). Focal stimulation was produced by mounting the miniature Ganzfeld LED tube into the middle of a light box (44 × 44 × 10 cm) such that the circular stimulus subtended 20° diameter at a viewing distance of 15.6 cm. The 20° stimulus size was chosen to encompass as much of the central field as possible while avoiding the optic disc, which starts approximately 12° to 15° nasal to the fovea. To minimize the effect of stray light stimulating the peripheral retina (i.e., the area outside the stimulus area), the light box contained a strip of white LEDs (color temperature > 7000K) passed through a blue filter (Lee Filter 068 Sky Blue; Lee Filters, Hampshire, UK) to produce a desensitizing blue surround of 3.73 scot log td (field size = 109° × 109° field). Cross hairs centered in the middle of the stimulus served as the fixation target. Full-field ERGs were recorded by holding the stimulator head, fitted with a diffusing cap, directly to the eye.

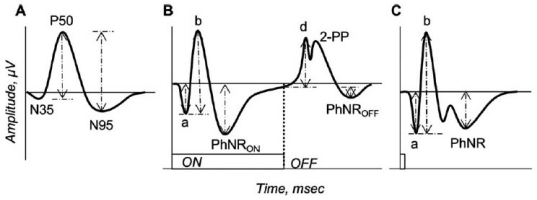

Figure 1. Representative ERG traces of the (**A**) PERG, (**B**) full-field long-duration ERG, and (**C**) full-field brief-flash ERG showing their components and how their amplitudes were measured (*double-headed arrows*). The amplitudes of the P50, N95 (**A**), a-wave (*a*) and b-wave (*b*) (**B**, **C**) were measured as recommended by the International Society of Clinical Electrophysiology of Vision.[35] The d-wave (*d*) amplitude was measured from the point of light offset to the peak of the d-wave. The PhNR$_{ON}$ (PhNR in brief flash) and PhNR$_{OFF}$ amplitudes were measured from the prestimulus baseline and voltage at stimulus offset respectively to a fixed time point in their respective troughs (see main text for details). The focal long-duration ERG had the same profile as the full-field long duration except that in the focal ERG there was only one prominent positive peak after light offset, the d-wave.

Full-field brief (flash) ERGs were elicited by a Ganzfeld stimulator (GS2000; LACE Elettronica, Rome, Italy) presenting a xenon flash stimulus (1.76 log td.s, 300 μs maximum flash duration, 4 Hz). Filters were used to obtain a red stimulus (Lee Filter "Terry Red"; Lee Filters, Hampshire, UK, transmittance $< 5\%$ at wavelengths shorter than 575 nm, and above 85% from 625–700 nm) over a continuous rod-saturating 3.39 scot log td blue background (Schott Glass filter BG28; Schott AG, Mainz, Germany, peak transmittance 454 nm). All stimulus backgrounds were of sufficient scotopic illuminance to saturate the rods.[34]

All ERGs were recorded by the same investigator using the same protocol at both sites. Long-duration ERGs (focal and full-field) were generated by the same miniature Ganzfeld LED stimulator at both sites. Pattern ERG and full-field brief flash data were obtained only from participants attending Cardiff University, so as to ensure consistency. All stimuli were calibrated using an ILT 1700 radiometer with SED033/Y/R luminance detector (Able Instruments and Controls, Reading, UK) assuming a 7-mm pupil with no correction for the Stiles-Crawford effect. The wavelengths of the light sources were measured using a Specbos 1201 spectro-radiometer (Horiba Jobin Yvon Ltd., Middlesex, UK).

Procedures

All participants underwent a comprehensive ophthalmic examination that included best corrected visual acuity (ETDRS), contrast sensitivity (Pelli-Robson), visual field assessment (24-2 SITA-FAST, Humphrey Visual Field Analyzer, Carl Zeiss Meditec, Inc., Dublin, CA, USA), slit lamp biomicroscopy, optical coherence tomography (OCT; Topcon 3D-OCT 1000; Topcon Medical Systems, Inc., Tokyo, Japan), fundus photography, color vision (D-15 desaturated test) and auto-refraction. To target earlier-stage ADOA, the eye with the better visual field mean deviation score was selected for ERG recording, with the dominant eye chosen in the case of equal scores between the two eyes.

Pattern ERGs were always recorded first with natural pupils and near refractive correction when necessary. Pupils were then dilated using 1% tropicamide to a minimum of 7 mm and flash ERGs were recorded in the following order: focal long-duration, full-field long-duration, and full-field brief-flash ERG.

Signal Analysis

Pattern ERGs and focal ERGs were Fourier analyzed to remove high-frequency noise above 30 Hz and 50 Hz, respectively. The method for measuring the amplitude of the various subcomponents is described in Figure 1. The PhNR$_{ON}$ (PhNR for brief-flash ERG) and PhNR$_{OFF}$ amplitudes were measured from the prestimulus baseline and voltage at stimulus offset, respectively, to a fixed time point in their respective troughs. When determining the most appropriate fixed time point at which to measure the PhNR$_{ON}$ and PhNR$_{OFF}$ responses, the group-averaged ERG of ADOA participants was subtracted from the group-averaged ERG of the controls to obtain a difference ERG. The implicit time of the greatest discrepancy between the two was identified for the PhNR$_{ON}$ and PhNR$_{OFF}$ responses and was used as the fixed time point for all measurements. The fixed times at which the PhNR amplitudes were measured were as follows: focal PhNR$_{ON}$ at 95 ms after onset, focal PhNR$_{OFF}$ at 97 ms after offset, full-field PhNR$_{ON}$ at 83 ms after onset, full-field PhNR$_{OFF}$ at 102 ms after offset and full-field brief PhNR at 72 ms after onset. The identification of all peaks and troughs was determined objectively using Microsoft Excel (Microsoft Corp., Redmond, WA, USA) (i.e., as the minimum/maximum voltage within a fixed time window).

Statistical Analysis

Data expressed on a logarithmic scale (i.e., visual acuity, contrast sensitivity, and visual field mean deviation) were converted (antilogged) into a linear scale to calculate mean and SD values. The mean and SD values were then converted back to log units. The distribution of the ERG data was checked for normality using the Shapiro-Wilk test. Where data were normally distributed, independent sample *t*-tests (2-tailed) were used to compare controls and participants with ADOA; the Mann-Whitney *U* test was used where data were non-normally distributed. To minimize Type 1 errors due to the number of comparisons made ($n = 35$), we applied a Bonferroni adjustment to the α level (0.05) and report observations as significant when $P < 0.0014$. Receiver operating characteristic (ROC) curve analysis was used to calculate the area under the curve (AUC) to assess the diagnostic potential of the various ERG components. The comparison between AUCs was made using the method described by Hanley and McNeil.[36]

Results

The clinical characteristics of all 12 ADOA participants from six families are shown in Table 1. The means and SDs for visual acuity, contrast sensitivity, and mean deviation were 1.10 ± 1.07 logMAR, 1.30 ± 1.26 log units, and −7.39 ± 7.09 dB, respectively. The visual field defects were mostly central or centrocecal and color vision defects were variable, but participants from the same family had similar defects. More details regarding the relationship between the clinical characteristics and ERG data in ADOA participants is to be the subject of a future manuscript.

Pattern ERGs

Pattern ERGs recorded from nine ADOA participants are shown superimposed on the group-averaged trace of 16 controls in the left column of Figure 2A. It shows that the negative N95 component is reduced in amplitude for all participants with ADOA, beyond the 95% confidence intervals (CIs) for the control data. The P50 amplitudes in ADOA participants were also below the lower 95% CIs except for one

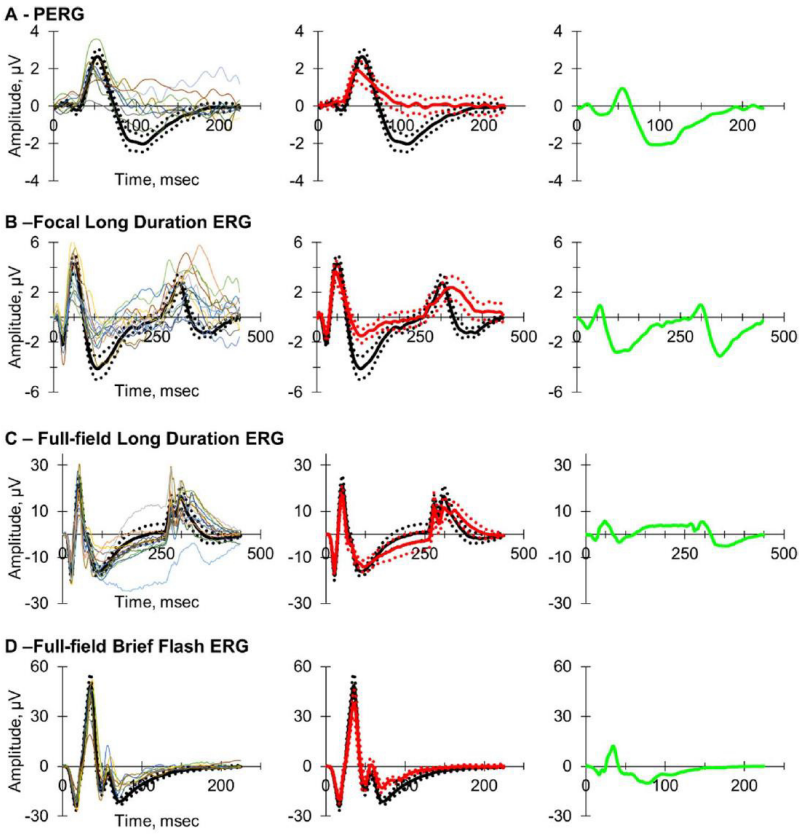

FIGURE 2. Electroretinogram traces of the (**A**) PERG, (**B**) focal long-duration ERG, (**C**) full-field long-duration ERG, and (**D**) full-field brief-flash ERG recorded from participants in this study. *Left column*: Individual traces of participants with ADOA (*thin lines*) superimposed on the group averaged ERG of 16 controls (*thick lines*) for each type of ERG recorded. The number of participants with ADOA are 9 (**A**), 12 (**B**), 12 (**C**), and 7 (**D**). *Dotted lines* represent 95% CIs. *Middle column*: Comparison between group-averaged traces of controls (*thick black line*) and ADOA participants (*thick red line*). *Right column*: Difference plots generated by subtracting the group-averaged ADOA ERG from the control ERG.

participant. The middle column of Figure 2A and the data in Table 2 demonstrate that the mean P50 and N95 amplitudes were significantly reduced in ADOA participants compared with controls. The mean N95:P50 ratio in ADOA participants of 1.05 was significantly reduced compared with 1.73 in controls (Table 2). Although there was evidence of P50 and N95 loss in people with ADOA, the difference plot in the right column of Figure 2A is dominated by a negative going signal corresponding to the loss of the N95 component.

Focal Long-Duration Cone ERGs

Focal long-duration cone ERGs recorded from 12 participants with ADOA are shown superimposed on the group-averaged trace of 16 controls in the left column of Figure 2B. The typical ERG responses were characterized by the a-wave, b-wave, $PhNR_{ON}$, d-wave, and $PhNR_{OFF}$. The $PhNR_{ON}$ was reduced in amplitude below the lower 95% confidence limit of the control data in almost all ADOA participants except one. Notably, the waveform after stimulus offset varied considerably among ADOA participants. For instance, in participants with ADOA, the most prominent positive peak after stimulus offset, assumed to be the d-wave, was delayed and had a broad peak whose maximum amplitude occurred at highly variable times (Fig. 2B, right and middle columns). In comparison, this prominent peak was highly consistent among control participants with respect to implicit time and was reflected in the much smaller SD of the d-wave implicit time in controls than in participants with ADOA (Table 2).

The difference plot (Fig. 2B, right) was dominated by two negative going waves representing the $PhNR_{ON}$ and $PhNR_{OFF}$ components affected by ADOA. The difference plots of the ON and OFF components had similar profiles and amplitudes of 2.80 µV and 2.88 µV, respectively.

Long-Duration Full-Field Cone ERG

The long duration full-field cone ERGs in Figure 2C were recorded from the same ADOA participants (thin lines) and controls (group-averaged thick black line) as the focal cone ERGs in Figure 2B. The form of the long-duration ERG was similar under focal and full-field conditions with one exception. There were two positive peaks immediately after light offset in the full-field ERG; the first being the d-wave.[23,37] The

Table 2. Means of Amplitudes and Implicit Times in Controls and Participants With ADOA

ERG Type	Component		ADOA Mean Values	Control Mean Values	*P* Value
PERG	P50	A, μV	1.92 ± 0.81	3.18 ± 0.81	0.0011*
		T, ms	49.03 ± 3.67	53.16 ± 3.28	0.0082
	N95	A, μV	2.12 ± 1.31	5.20 ± 0.87	0.0000*
		T, ms	101.67 ± 11.21	99.77 ± 7.76	0.6212†
	N95:P50 ratio		1.05 ± 0.31	1.73 ± 0.47	0.0009*†
Focal ERG	a-wave	A, μV	1.76 ± 0.94	2.22 ± 0.61	0.1301
		T, ms	23.00 ± 1.72	23.75 ± 1.74	0.2534
	b-wave	A, μV	5.29 ± 2.08	6.76 ± 1.74	0.0524
		T, ms	46.25 ± 3.14	49.81 ± 4.88	0.0271
	$PhNR_{ON}$	A, μV	1.02 ± 0.97	3.81 ± 1.74	0.0000*
		T, ms	109.25 ± 7.16	104.50 ± 8.49	0.1299
	d-wave	A, μV	2.81 ± 1.52	3.12 ± 1.04	0.5290
		T, ms	321.92 ± 13.80	302.41 ± 5.92	0.0004*
	$PhNR_{OFF}$	A, μV	−1.97 ± 1.52	0.93 ± 1.23	0.0000*
		T, ms	138.08 ± 9.94	113.09 + 14.64	0.0000*†
Full-field long ERG	a-wave	A, μV	15.87 ± 4.44	18.84 ± 4.45	0.0917
		T, ms	22.50 ± 1.09	23.16 ± 1.70	0.2537
	b-wave	A, μV	33.57 ± 10.67	41.29 ± 11.18	0.0768
		T, ms	41.83 ± 2.86	42.16 ± 2.47	0.7515
	$PhNR_{ON}$	A, μV	12.26 ± 3.95	15.68 ± 4.36	0.0430
		T, ms	96.18 ± 9.16	92.72 ± 4.15	0.2471
	d-wave	A, μV	15.11 ± 6.20	12.84 ± 4.89	0.2866
		T, ms	274.67 ± 1.15	273.47 ± 1.02	0.0075†
	Second positive peak	A, μV	15.48 ± 4.87	16.10 ± 7.55	0.8064
		T, ms	302.50 ± 8.35	298.19 ± 2.00	0.1054†
	$PhNR_{OFF}$	A, μV	−8.31 ± 5.69	0.45 ± 5.74	0.0005*
		T, ms	178.33 ± 27.02	132.19 ± 17.30	0.0000*†
Full-field brief ERG	a-wave	A, μV	20.60 ± 3.79	25.73 ± 5.91	0.0480†
		T, ms	17.50 ± 0.69	17.22 ± 0.76	0.4133
	b-wave	A, μV	59.75 ± 14.58	77.88 ± 18.17	0.0302
		T, ms	35.39 ± 1.51	35.38 ± 1.26	0.9767
	i-wave	A, μV	14.00 ± 8.37	16.19 ± 7.58	0.5420
		T, ms	58.04 ± 2.04	57.61 ± 2.37	0.6844
	PhNR	A, μV	12.93 ± 3.38	22.39 ± 6.17	0.0011*
		T, ms	72.75 ± 4.13	70.59 ± 6.40	0.4244†

Data are expressed as mean ± SD. A, amplitude; T, implicit time from stimulus onset.
* Value is significant at $P \leq 0.0014$ level.
† Data were nonuniformly distributed and Mann-Whitney *U* test was used for statistical comparison.

mean amplitude of the $PhNR_{OFF}$, but not the $PhNR_{ON}$, was significantly reduced in participants with ADOA (Table 2). On the difference plot (Fig. 2C, right) the amplitude of the $PhNR_{OFF}$ difference (8.76 μV) was more than twice the amplitude of the $PhNR_{ON}$ difference (3.42 μV) when measured.

Once again, the OFF components showed greater variability than ON components for participants with ADOA. In fact, in at least six participants with ADOA, there was a third positive peak (3PP) after light offset not seen in controls (Fig. 2C, left). There was no obvious pattern to the presence or absence of the 3PP in ADOA participants. The amplitude and implicit time of the 3PP measured from the ADOA group-averaged trace was 13.34 μV and 75 ms after light offset, respectively. Comparatively, none of the control traces displayed the 3PP prominently, although on close visual inspection, a kink corresponding in time with the 3PP was observed in some individual control traces.

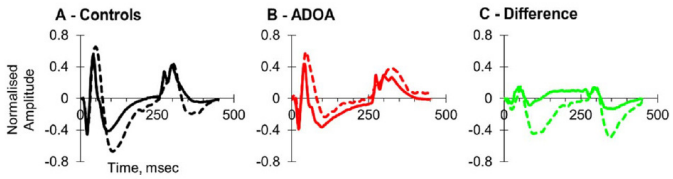

Figure 3. A comparison of the long-duration focal (*dashed lines*) and full-field (*solid lines*) group-averaged ERGs for (**A**) controls, (**B**) participants with ADOA, and (**C**) difference plots. Electroretinograms have been normalized to the b-wave amplitude of their respective control group–averaged ERG.

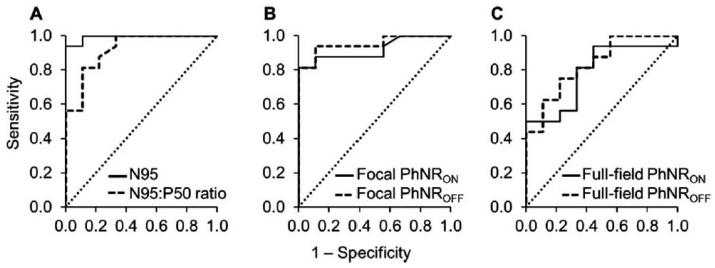

FIGURE 4. Receiver operating characteristic curves derived using (**A**) N95 component and N95:P50 ratio of the PERG, (**B**) focal PhNR$_{ON}$ and PhNR$_{OFF}$ amplitudes, and (**C**) full-field PhNR$_{ON}$ and PhNR$_{OFF}$ amplitudes. *Diagonal dashed line* is the reference line.

Comparison of Focal and Full-Field Long-Duration ERGs

The waveform of the focal and full-field long-duration ERGs was further compared by normalizing the group-averaged ERGs to their respective b-wave amplitudes (Fig. 3). The focal and full-field ERGs of controls (Fig. 3A) and participants with ADOA (Fig. 3B) had similar profiles, although implicit times of the b-wave, PhNR$_{ON}$, and d-wave were significantly delayed in the focal ERG ($P \leq 0.01$, data not shown). The most prominent positive peak of the focal ERG after light offset coincided with the 2PP of the full-field ERG in the control traces, whereas in the ADOA group, the broad peak of the focal ERG after offset described a curve that roughly matched the profile of the 2PP and 3PP of the full-field ERG.

In controls, the PhNRs are proportionally greater in the focal ERG than in the full-field ERG (Fig. 3A). The losses in amplitudes of the PhNRs were also greater in the focal ERG than the full-field ERG in participants with ADOA (Figs. 3B, 3C).

The Brief Full-Field ERG

Brief full-field ERGs recorded from seven ADOA participants are shown in Figure 2D. Typical ERG responses had a-wave, b-wave, i-wave, and PhNR components. The PhNR amplitude was reduced significantly in people with ADOA compared with controls (Fig. 2D; Table 2). The difference plot in the right column of Figure 2D indicates that the greatest deficit in ADOA corresponds to the timing of the b-wave and the PhNR. An i-wave was recorded for all participants (controls and ADOA). Although it appeared more prominent in ADOA participants, there was no statistical difference in amplitude or implicit time between control and ADOA participants (Table 2).

TABLE 3. Sensitivity, Specificity, and Area Under Curve of ROC Analysis for ERG Components

Test Variable	Area (95% CI)	Sensitivity	Specificity	Cutoff Value, μV
N95	0.99 (0.97–1.00)	93.80	100.00	4.12
N95:P50	0.92 (0.81–1.00)	81.30	89.90	1.44
Focal PhNR$_{ON}$	0.92 (0.81–1.00)	81.30	100.00	2.62
Focal PhNR$_{OFF}$	0.95 (0.87–1.00)	81.30	100.00	0.24
Full-field PhNR$_{ON}$	0.78 (0.60–0.97)	50.00	100.00	16.99
Full-field PhNR$_{OFF}$	0.83 (0.73–0.99)	62.50	89.90	0.35

Specificity and Sensitivity of the Different ERGs

Receiver operating characteristic curves were used to determine the effectiveness of the N95 and long-duration focal and full-field PhNRs at discriminating participants with ADOA from controls for nine participants with ADOA and 16 controls for whom PERG and long-duration focal and full-field ERG data were available (Fig. 4). The AUC, sensitivity, specificity, and cutoff value, which produced an optimal sensitivity while maintaining minimum specificity of approximately 90%, are shown in Table 3. The N95 amplitude had the greatest diagnostic power. However, a comparison of the AUCs of the focal and full-field PhNRs with the N95 amplitude, using the method described by Hanley and McNeil[36] showed that the N95 amplitude was only significantly more sensitive than the full-field PhNR$_{ON}$ amplitude ($z = 2.12$). Therefore, considered in terms of their diagnostic ability, the focal PhNRs and N95 component were not significantly different.

DISCUSSION

Effect of ADOA on ON and OFF RGCs

In this study, we sought to determine whether the PhNR$_{ON}$ was preferentially affected in ADOA as might be predicted based on the study by Williams et al.[18] Our findings, however, showed that in human patients, the PhNR$_{ON}$ and PhNR$_{OFF}$ amplitudes were equally reduced in the focal ERG, whereas in the full-field ERG, there was a greater reduction in the PhNR$_{OFF}$ amplitude than the PhNR$_{ON}$ amplitude. What then might explain this apparent contradiction?

In the study by Williams et al.,[18] evidence for the preferential loss of ON-RGCs was based on mouse retinal flat mounts showing significant dendritic pruning of ON- but not OFF-RGCs. The experiment reported here, however, assessed the effect of ADOA on the ON- and OFF-RGCs by evaluating the PhNR amplitude of the human ERG, a functional measure. The role of RGCs as primary originators of the PhNR has been demonstrated in previous studies.[23–26,33] In experiments using long-duration full-field ERGs, they showed that that PhNR$_{ON}$ and PhNR$_{OFF}$ components were both reduced or eliminated after experimental glaucoma and intravitreal injection of tetrodotoxin (TTX) (an agent that blocks generation of sodium-dependent spikes in retinal neurons) in macaques, as well as in patients with glaucoma. Although the origins of the PhNR$_{ON}$ and PhNR$_{OFF}$ have not been conclusively traced to the ON- and OFF-RGCs respectively, Luo and Frishman[33] showed that the PhNR$_{ON}$ (and b-wave) component but not the PhNR$_{OFF}$ (or d-wave) was eliminated after injecting 2-amino-4-phosphonobutyric acid (APB) into the macaque retina to

block synaptic transmission from photoreceptors to ON-bipolar cells and hence ON-RGCs. Injecting TTX after APB then removed the $PhNR_{OFF}$ but not the d-wave, thereby linking the $PhNR_{ON}$ and $PhNR_{OFF}$ components (although indirectly) to the ON and OFF pathways, respectively.

Previous human[30,38,39] and animal[23,29] studies (including our mouse model) have shown that the PhNR amplitude is very susceptible to RGC damage with severe attenuation of PhNR amplitude recorded even when morphologic and other functional parameters were within normal range (i.e., in early-stage disease). It is possible that the $PhNR_{ON}$ pathways may be selectively compromised at an earlier stage of the disease process than that studied here. A similar study in presymptomatic people with the *OPA1* mutations or in people with ADOA at a much earlier stage of the disease (e.g., children with ADOA) could provide additional insights.

Our findings also may be a reflection of the heterogeneous nature of ADOA. There are more than 200 *OPA1* mutations[14,15] that cause ADOA, with wide phenotypic variations both within and between affected families.[1,40] Genotype–phenotype correlations have been difficult to establish in previous studies,[2,41] and the number of patients in each family of *OPA1* mutations (except family E) was insufficient to reliably explore such correlations. In the mouse model, the mutant mice (>10 months old) were genetically homogeneous and disease severity correlated with age. Participants studied here were from six families, with a different mutation in each family (Table 1), and at different stages of the disease. This may have diluted observations that would have been made from a homogeneous cohort.

Comparison of Focal and Full-Field PhNRs

The long-duration focal and full-field ERGs in this study were recorded using the same stimulus parameters, which were comparable to the parameters recommended by Kondo et al.[42] for eliciting focal responses. Although the waveforms of the focal and full-field ERGs were similar, they were not identical (Figs. 3A, 3B). There was a greater contribution of $PhNR_{ON}$ and $PhNR_{OFF}$ components to the focal ERG than to the full-field ERG (Fig. 3A), which reflects the decreasing proportion of RGCs to other retinal cells with eccentricity.[43] The focal PhNRs were more severely affected than their full-field counterparts by ADOA, and this was reflected in the larger AUCs found for the focal signals. These findings were consistent with the central field defects recorded in ADOA participants in this study and in others.[1,5,44] In addition, whereas the focal PhNRs were both significantly reduced ($P < 0.001$), only the full-field $PhNR_{OFF}$ was significantly reduced in the full-field ERG (Table 2). Although the N95 and focal PhNR amplitudes were highly discriminatory for ADOA, it should be noted that the participants in this study had relatively late-stage disease.

The symmetrical loss in the focal $PhNR_{ON}$ and $PhNR_{OFF}$ amplitudes (Fig. 2B, right column; Fig. 3C) may reflect the 1:1 ratio of ON- to OFF-RGCs in the macula, whereas the greater loss in the full-field $PhNR_{OFF}$ amplitude than the $PhNR_{ON}$ amplitude (Fig. 2C, right column; Fig. 3C) may reflect the nearly 1:2 ratio of ON- to OFF-RGCs in the peripheral retina.[45–47] The broadening of the d-wave peak in the focal ERG and the presence of the 3PP in the full-field long ERG in participants with ADOA may be due to contributions from the cone receptor potential and/or depolarizing OFF-bipolar cell responses after light offset, which were unmasked in the relative absence of the negative going $PhNR_{OFF}$.[48–50] The 2PP may be the i_{OFF}-wave described by Horn et al.,[51] although in contrast to their results, this study did not record a significant difference in amplitude between controls and participants with ADOA.

Comparison With Other Electrophysiological Studies in ADOA

Miyata et al.[28] reported a significant reduction in the full-field brief PhNR, but none in the a- or b-wave amplitude, in ADOA patients using white-on-white stimulus. Similar results were obtained by Barnard et al.[29] in the mouse model. In this present study, we show similar results using a red-on-blue stimulus. The flash luminance used in this study was adopted from a previous study in this laboratory[52] and was comparable to the flash luminance used by Miyata et al.[28] This supports findings that the red-on-blue stimulus is effective for clinical evaluation of RGC function.

Holder et al.[33] reported a significant reduction in N95 amplitude and the N95:P50 ratio of the PERG participants with ADOA. We obtained similar results and showed that the focal PhNRs and N95 amplitude were equally effective at discriminating controls from participants with ADOA. The focal ERG could therefore be used as an alternative to the PERG.

In this study, as well as in that of Holder et al.,[32] the P50 amplitude was significantly reduced. This may indicate that bipolar cell function is compromised in ADOA, as has been put forward by Reis et al.[53] However, a reduction in P50 amplitude is also seen when only RGCs are compromised[33]; therefore, the P50 reduction observed in this study could be due to dysfunction of bipolar cells, RGCs, or both.

Conclusions

This study showed there was a nearly symmetrical reduction in the $PhNR_{ON}$ and $PhNR_{OFF}$ amplitudes in participants with ADOA with no evidence of a preferential ON-pathway loss. This suggests that ON- and OFF-RGCs may be equally affected in patients. In addition, in terms of their diagnostic potential, the focal PhNR-ON and -OFF amplitudes were better than their full-field counterparts and were not significantly different from the N95 amplitude of the PERG.

Acknowledgments

Supported by the Ghana Education Trust Fund (EKAM). We acknowledge Fight for Sight Small Grants Award (MV) for their contribution to genotyping.

Disclosure: **E.K.A. Morny**, None; **T.H. Margrain**, None; **A.M. Binns**, None; **M. Votruba**, None

References

1. Votruba M, Fitzke FW, Holder GE, Carter A, Bhattacharya SS, Moore AT. Clinical features in affected individuals from 21 pedigrees with dominant optic atrophy. *Arch Ophthalmol*. 1998;116:351–358.
2. Votruba M, Thiselton D, Bhattacharya SS. Optic disc morphology of patients with OPA1 autosomal dominant optic atrophy. *Br J Ophthalmol*. 2003;87:48–53.
3. Newman NJ, Biousse V. Hereditary optic neuropathies. *Eye*. 2004;18:1144–1160.
4. Yu-Wai-Man P, Griffiths PG, Hudson G, Chinnery PF. Inherited mitochondrial optic neuropathies. *J Med Genet*. 2009;46:145–158.
5. Votruba M, Moore AT, Bhattacharya SS. Clinical features, molecular genetics, and pathophysiology of dominant optic atrophy. *J Med Genet*. 1998;35:793–800.

6. Krill AE, Smith VC, Pokorny J. Similarities between congenital tritan defects and dominant optic-nerve atrophy: coincidence or identity. *J Opt Soc Am*. 1970;60:1132–1139.
7. Kjer B, Eiberg H, Kjer P, Rosenberg T. Dominant optic atrophy mapped to chromosome 3q region. II. Clinical and epidemiological aspects. *Acta Ophthalmol Scand*. 1996;74:3–7.
8. Votruba M, Aijaz S, Moore AT. A review of primary hereditary optic neuropathies. *J Inherit Metab Dis*. 2003;26:209–227.
9. Yu-Wai-Man P, Griffiths PG, Burke A, et al. The prevalence and natural history of dominant optic atrophy due to OPA1 mutations. *Ophthalmology*. 2010;117:1538–1546.e1.
10. Gallus GN, Cardaioli E, Rufa A, et al. High frequency of OPA1 mutations causing high ADOA prevalence in south-eastern Sicily, Italy. *Clin Genet*. 2012;82:277–282.
11. Lenaers G, Hamel C, Delettre C, et al. Dominant optic atrophy. *Orphanet J Rare Dis*. 2012;7:46.
12. Alexander C, Votruba M, Pesch UEA, et al. OPA1, encoding a dynamin-related GTPase, is mutated in autosomal dominant optic atrophy linked to chromosome 3q28. *Nat Genet*. 2000; 26:211–215.
13. Delettre C, Lenaers G, Griffoin JM, et al. Nuclear gene OPA1, encoding a mitochondrial dynamin-related protein, is mutated in dominant optic atrophy. *Nat Genet*. 2000;26:207–210.
14. Ferre M, Bonneau D, Milea D, et al. Molecular screening of 980 cases of suspected hereditary optic neuropathy with a report on 77 novel OPA1 mutations. *Hum Mutat*. 2009;30:E692–E705.
15. Ferre M, Amati-Bonneau P, Tourmen Y, Malthiery Y, Reynier P. eOPA1: an online database for OPA1 mutations. *Hum Mutat*. 2005;25:423–428.
16. Johnston PB, Gaster RN, Smith VC, Tripathi RC. A clinicopathologic study of autosomal dominant optic atrophy. *Am J Ophthalmol*. 1979;88:868–875.
17. Kjer P, Jensen OA, Klinken L. Histopathology of eye, optic-nerve and brain in a case of dominant optic atrophy. *Acta Ophthalmol (Copenh)*. 1983;61:300–312.
18. Williams PA, Morgan JE, Votruba M. Opa1 deficiency in a mouse model of dominant optic atrophy leads to retinal ganglion cell dendropathy. *Brain*. 2010;133:2942–2951.
19. Sarzi E, Angebault C, Seveno M, et al. The human OPA1delTTAG mutation induces premature age-related systemic neurodegeneration in mouse. *Brain*. 2012;135:3599–3613.
20. Alavi MV, Bette S, Schimpf S, et al. A splice site mutation in the murine Opa1 gene features pathology of autosomal dominant optic atrophy. *Brain*. 2007;130:1029–1042.
21. Davies VJ, Hollins AJ, Piechota MJ, et al. Opa1 deficiency in a mouse model of autosomal dominant optic atrophy impairs mitochondrial morphology, optic nerve structure and visual function. *Hum Mol Genet*. 2007;16:1307–1318.
22. Williams PA, Piechota M, von Ruhland C, Taylor E, Morgan JE, Votruba M. Opa1 is essential for retinal ganglion cell synaptic architecture and connectivity. *Brain*. 2012;135:493–505.
23. Viswanathan S, Frishman LJ, Robson JG, Harwerth RS, Smith EL III. The photopic negative response of the macaque electroretinogram: reduction by experimental glaucoma. *Invest Ophthalmol Vis Sci*. 1999;40:1124–1136.
24. Viswanathan S, Frishman LJ, Robson JG. The uniform field and pattern ERG in macaques with experimental glaucoma: removal of spiking activity. *Invest Ophthalmol Vis Sci*. 2000; 41:2797–2810.
25. Viswanathan S, Frishman LJ, Robson JG, Walters JW. The photopic negative response of the flash electroretinogram in primary open angle glaucoma. *Invest Ophthalmol Vis Sci*. 2001;42:514–522.
26. Rangaswamy NV, Shirato S, Kaneko M, Digby BI, Robson JG, Frishman LJ. Effects of spectral characteristics of ganzfeld stimuli on the photopic negative response (PhNR) of the ERG. *Invest Ophthalmol Vis Sci*. 2007;48:4818–4828.
27. Sustar M, Hawlina M, Brecelj J. ON- and OFF-response of the photopic electroretinogram in relation to stimulus characteristics. *Doc Ophthalmol*. 2006;113:43–52.
28. Miyata K, Nakamura M, Kondo M, et al. Reduction of oscillatory potentials and photopic negative response in patients with autosomal dominant optic atrophy with OPA1 mutations. *Invest Ophthalmol Vis Sci*. 2007;48:820–824.
29. Barnard AR, Issa PC, Perganta G, et al. Specific deficits in visual electrophysiology in a mouse model of dominant optic atrophy. *Exp Eye Res*. 2011;93:771–777.
30. Machida S, Tamada K, Oikawa T, et al. Comparison of photopic negative response of full-field and focal electroretinograms in detecting glaucomatous eyes. *J Ophthalmol*. 2011;1–11.
31. Tamada K, Machida S, Yokoyama D, Kurosaka D. Photopic negative response of full-field and focal macular electroretinograms in patients with optic nerve atrophy. *Jpn J Ophthalmol*. 2009;53:608–614.
32. Holder GE, Votruba M, Carter AC, Bhattacharya SS, Fitzke FW, Moore AT. Electrophysiological findings in dominant optic atrophy (DOA) linking to the OPA1 locus on chromosome 3q 28-qter. *Doc Ophthalmol*. 1998;95:217–228.
33. Luo X, Frishman LJ. Retinal pathway origins of the pattern electroretinogram (PERG). *Invest Ophthalmol Vis Sci*. 2011; 52:8571–8584.
34. Aguilar M, Stiles WS. Saturation of the rod mechanism of the retina at high levels of stimulation. *Opt Acta (Lond)*. 1954;1: 59–65.
35. Marmor MF, Brigell MG, McCulloch DL, Westall CA, Bach M. ISCEV standard for clinical electro-oculography (2010 update). *Doc Ophthalmol*. 2011;122:1–7.
36. Hanley JA, McNeil BJ. A method of comparing the areas under receiver operating characteristic curves derived from the same cases. *Radiology*. 1983;148:839–843.
37. Evers HU, Gouras P. Three cone mechanisms in the primate electroretinogram: two with, one without off-center bipolar responses. *Vision Res*. 1986;26:245–254.
38. Nakamura H, Miyamoto K, Yokota S, Ogino K, Yoshimura N. Focal macular photopic negative response in patients with optic neuritis. *Eye (Lond)*. 2011;25:358–364.
39. Gotoh Y, Machida S, Tazawa Y. Selective loss of the photopic negative response in patients with optic nerve atrophy. *Arch Ophthalmol*. 2004;122:341–346.
40. Granse L, Bergstrand I, Thiselton D, et al. Electrophysiology and ocular blood flow in a family with dominant optic nerve atrophy and a mutation in the OPA1 gene. *Ophthalmic Genet*. 2003;24:233–245.
41. Yu-Wai-Man P, Griffiths PG, Gorman GS, et al. Multi-system neurological disease is common in patients with OPA1 mutations. *Brain*. 2010;133:771–786.
42. Kondo M, Kurimoto Y, Sakai T, et al. Recording focal macular photopic negative response (PhNR) from monkeys. *Invest Ophthalmol Vis Sci*. 2008;49:3544–3550.
43. Curcio CA, Allen KA. Topography of ganglion-cells in human retina. *J Comp Neurol*. 1990;300:5–25.
44. Fuhrmann N, Schimpf S, Kamenisch Y, et al. Solving a 50 year mystery of a missing OPA1 mutation: more insights from the first family diagnosed with autosomal dominant optic atrophy. *Mol Neurodegener*. 2010;5:25.
45. Dacey DM, Petersen MR. Dendritic field size and morphology of midget and parasol ganglion-cells of the human retina. *Proc Natl Acad Sci U S A*. 1992;89:9666–9670.
46. Dacey DM. The mosaic of midget ganglion cells in the human retina. *J Neurosci*. 1993;13:5334–5355.
47. Drasdo N, Millican CL, Katholi CR, Curcio CA. The length of Henle fibers in the human retina and a model of ganglion

Investigative Ophthalmology & Visual Science

receptive field density in the visual field. *Vision Res*. 2007;47:2901–2911.

48. Bush RA, Sieving PA. A proximal retinal component in the primate photopic ERG a-wave. *Invest Ophthalmol Vis Sci*. 1994;35:635–645.
49. Ueno S, Kondo M, Ueno M, Miyata K, Terasaki H, Miyake Y. Contribution of retinal neurons to d-wave of primate photopic electroretinograms. *Vision Res*. 2006;46:658–664.
50. Sieving PA, Murayama K, Naarendorp F. Push-pull model of the primate photopic electroretinogram: a role for hyperpolarizing neurons in shaping the b-wave. *Vis Neurosci*. 1994;11:519–532.
51. Horn FK, Gottschalk K, Mardin CY, Pangeni G, Junemann AG, Kremers J. On and off responses of the photopic fullfield ERG in normal subjects and glaucoma patients. *Doc Ophthalmol*. 2011;122:53–62.
52. Mortlock KE, Binns AM, Aldebasi YH, North RV. Inter-subject, inter-ocular and inter-session repeatability of the photopic negative response of the electroretinogram recorded using DTL and skin electrodes. *Doc Ophthalmol*. 2010;121:123–134.
53. Reis A, Mateus C, Viegas T, et al. Physiological evidence for impairment in autosomal dominant optic atrophy at the preganglion level. *Graefes Arch Clin Exp Ophthalmol*. 2013;251:221–234.

Investigative Ophthalmology & Visual Science